Final Report

Unmanned Flying Cargo Delivery Van For High Value Goods

DSE Group 21

Technische Universiteit Delft

TU Delft

This page is intentionally left blank

Final Report

Unmanned Flying Cargo Delivery Van For High Value Goods

by

DSE Group 21

Student Name	Student Number
Luuk Barbian	4871979
Loek Gijzen	4880900
Vincent van Gorp	4777697
Zeyad Hisham	4680529
Jorn van Kaam	4863968
Sam Lagerwij	4658418
David Li	4872487
Nino Pérez Pérez	4644808
Stephan Schmidt	4671724
Kobi Six	4779045

Version	**Purpose/changes**	**Date**
1.0	Draft report	18/06/2021
1.1	Implement PM/SE feedback	22/06/2021
1.2	Implement tutor feedback	29/06/2021
2.0	Final report	30/06/2021

Tutor: Paul Roling
Coaches: Yanan Zhang, Nathan Eskue
Teaching Assistant: Paula Meseguer Berroy
Institution: Delft University of Technology
Place: Faculty of Aerospace Engineering, Delft

Project Duration: April, 2021 - July, 2021

TU Delft

Preface

This report was written by 10 aerospace students from the faculty of Aerospace Engineering. This final report, also called Design Synthesis Exercise, is the final step in obtaining the bachelors degree at the Delft University of Technology. After ten weeks of intensive collaboration, research and hard working this report was the final outcome.

As a group we would like to express our gratitude to our tutor ir. P.C. Roling and both coaches, ir. Y. Zhang and N.D. Eskue for giving us valuable feedback on the design and helping us out when facing difficulties related to specific topics. We also thank P. Meseguer Berroy for the feedback on the project management and systems engineering deliverables. Moreover, A. de Graaff for his valuable input during the review sessions, Dr. C.D. Rans for his insight on the structural part of the design and Prof. Dr. P.G. Simons for his input on the noise analysis. Finally we would like to thank the faculty of Aerospace Engineering of Delft University of Technology for providing us with the opportunity to participate in this design project and provide us with all the facilities and work space.

DSE Group 21
Delft, June 29, 2021

Executive Overview

The air cargo industry has been hit hard by the CoViD-19 pandemic, due to travel restrictions imposed by countries, passenger flight which accounted for nearly 50% of the cargo transportation have perished. Therefore, the idea of an unmanned cargo aircraft has come to light, intercontinental transportation of high-value and time-critical goods such as micro-chips and vaccines. A group of 10 eager aerospace student studying at the TU Delft have been designated to this assignment to come up with a viable design within 10 weeks.

After analyzing the market it became clear that no current aircraft is flying medium range distances whilst carrying small amounts of payload. The unmanned cargo aircraft (UCA) will be able to fly non-stop carrying hazardous or time-critical payloads due to the fact that is no crew is on board. Namely, this yields lower safety regulations and discards limitations by a certain time schedule for the crew. Potential routes are for example resupplying remote communities such as Saint Helena with goods or routes that are not profitable for full freighter flights, due to the small volume which needs to be transported. Possible customers are cargo delivery companies such as FedEx, DHL and UPS which are currently limited to operate large freight aircraft at hub airports. For the UCA, 7 large cargo hub airport spread across the globe are selected from where all parts of the world can be reached within the design range. Maintenance and ground control stations are located here and ground handling operations will be outsourced to companies operating at the airports already.

The final design of the UCA has a maximum take-off weight of 13250 $[kg]$ and is able to carry a maximum payload weight of 2500 $[kg]$ for a range of 2600 $[nm]$, whilst the maximum reachable range is 4900 $[nm]$. Thus, the aircraft is adaptable with respect to its design range and payload of 3000 $[nm]$ and 2000 $[kg]$ respectively. The UCA has a low wing configuration with a wing span of 21 $[m]$ and fuselage length of 18 $[m]$. Furthermore, a V-tail is implemented to account for the jet stream of the engine which is mounted on top of the fuselage. In case of engine failure, the parachute system on board is activated to slow the aircraft down for a soft landing. The cargo door is located at the nose and opens up through an upwards rotation. Moreover, the cargo is placed on pallets which can fit easily in a road accessible van, reducing (un)loading time.

An important part of the UCA are the unmanned characteristics, using ground control stations for operators to monitor and control the aircraft remotely. The UCA will be able to fly fully autonomous during take-off, cruise, and landing by following a pre-programmed flight plan. However operators can intervene whilst in flight to ensure safety or comply with orders from air traffic control. A camera system will aid the operator visually in monitoring the UCA and communications with air traffic control will be done via VHF. Lastly, for short and long range communications, 4G and SATCOM data links will be used respectively to contact the UCA.

The aircraft unit cost is estimated to be 5.9 million dollars, which includes the production and development costs, and with this in mind the selling price per unit is 7.6 million dollar. Apart from these costs, the direct operational costs amount to approximately 6200 dollars per flight, much cheaper compared to other freight aircraft. But when comparing the direct operational cost per metric tonne the costs reductions are smaller. This is because of the small payload volumes the UCA is carrying and the price of synthetic fuel since it is still in early development stages. Therefore, the aircraft shall be mostly profitable in transporting high-value goods.

Sustainability has been an important aspect which has been taken into account throughout the design of the UCA. The aircraft uses synthetic fuel instead of kerosene which allows to reduce CO_2 emissions by 51.2% compared to a B747-400F per metric tonne of payload. After decommissioning, parts of the aircraft can be re-used and up to 90% of what is left over of the structure may be recycled. Concerning economic sustainability, the UCA will be able to supply a new market contributing to economic growth and due to being unmanned and smaller in size the direct operational costs are reduced by 25% compared to the Queen of the skies. Lastly, the engine placement allows for noise shielding by the fuselage which led to lower emitted noise levels compared to a Cessna Citation II.

List of Symbols

Symbol	Definition	Units
A_i	Cell area	$[m^2]$
AR	Aspect ratio wing	$[-]$
AR_h	Horizontal stabiliser aspect ratio	$[-]$
AR_{vt}	Aspect ratio tail	$[-]$
a	Acceleration	$[m/s^2]$
a	Speed of sound	$[m/s]$
B	Bandwidth	$[bps]$
B	Boom area	$[m^2]$
B_{str}	Boom area	$[m^2]$
b	Wing span	$[m]$
bi	Inboard wing span position	$[m]$
b_{skin}	Skin length	$[m]$
b_t	Maximum tire width	$[m]$
b_t	Maximum tire width	$[m]$
b_{vt}	Tail span	$[m]$
C_a/C	Aileron to wing chord ratio	$[-]$
C_{c_0}	Airfoil zero lift drag coefficient	$[-]$
C_D	Drag coefficient	$[-]$
C_d	Airfoil drag coefficient	$[-]$
C_{D_0}	Aircraft zero lift drag coefficient	$[-]$
C_{D_i}	Induced drag coefficient	$[-]$
$C_{d_{min}}$	Minimum airfoil drag coefficient	$[-]$
C_{f_e}	Skin-friction drag	$[-]$
C_L	Lift coefficient	$[-]$
C_l	Airfoil lift coefficient	$[-]$
C_l	Rolling moment coefficient	$[-]$
C_{L_α}	Aircraft lift curve slope	$[-]$
$C_{L_{\alpha_h}}$	Tail airfoil lift curve slope	$[-]$
$C_{L_{A-h}}$	Aircraft tailless lift curve slope	$[-]$
C_{L_h}	Tail lift coefficient	$[-]$
$C_{L_{max}}$	Maximum lift coefficient	$[-]$
$C_{l_{max}}$	Maximum airfoil lift coefficient	$[-]$
$C_{Lmax,TO}$	Maximum take-off lift coefficient	$[-]$
$C_{L_{opt}}$	Optimum lift coefficient	$[-]$
C_{l_p}	Roll damping coefficient	$[-]$
$C_{L,TO}$	Take-off lift coefficient	$[-]$
$C_{l_{\delta_a}}$	Aileron roll control derivative	$[-]$
C_m	Airfoil moment coefficient	$[-]$
$C_{m_{ac}}$	Aerodynamic centre moment coefficient	$[-]$
C_p	Constant specific heat	$[J/kg \cdot K]$
c	Chord length	$[m]$
c	Speed of sound	$[m/s]$
c_j	Specific fuel consumption jet engine	$[kg/Ns]$
c_p	Specific fuel consumption propeller engine	$[kg/J]$
c_r	Root chord	$[m]$
c_t	Tip chord	$[m]$
c_T	Specific fuel consumption jet engine	$[kg/Ns]$
$\bar{c}$	Mean aerodynamic chord	$[m]$
D	Drag Force	$[N]$
D_g	Ground friction drag	$[N]$
D_t	Tire diameter	$[m]$
d	Diameter	$[m]$

Symbol	Definition	Units
$d_{f,inner}$	Fuselage inner diameter	$[m]$
$d_{f,outer}$	Fuselage outer diameter	$[m]$
$d\epsilon/d\alpha$	Downwash effect	$[-]$
E	Young's modulus	$[GPa]$
E	Energy	$[J]$
e	Oswald efficiency factor	$[-]$
FF	Form factor	$[-]$
f	Frequency	$[Hz]$
G	Shear modulus	$[GPa]$
g	Gravitational acceleration constant	$[m/s^2]$
h	Altitude	$[m]$
h_{scr}	Screen height	$[m]$
I	Intensity	$[W/m^2]$
I_{xx}	Moment of inertia about x axis	$[m^4]$
I_{yy}	Moment of inertia about y axis	$[m^4]$
I_{yy}	Moment of inertia about x-y axis	$[m^4]$
IF	Interference factor	$[-]$
K	Effort to produce first aircraft	$[-]$
K_{1C}	Fracture thoughness	$[MPa \cdot m^{1/2}]$
K_c	Buckling coefficient	$[-]$
K_{door}	Weight factor cargo door	$[-]$
K_{LG}	Weight factor landing gear	$[-]$
K_g	Mass ratio function (gust)	$[-]$
K_{ws}	Weight factor wing	$[-]$
k	Induced drag constant	$[-]$
k	Boltzmann's constant	$[J/K]$
k_1	Specific constant jet aircraft	$[kgm]$
k_2	Specific constant propeller aircraft	$[m]$
L	Lift force	$[N]$
L_A	A-weighted noise level	$[dBA]$
L/D	Lift-to-drag ratio	$[-]$
L_p	Absorptive propagation loss	$[dB]$
L_R	Receiving signal loss	$[dB]$
l_h	Tail arm	$[m]$
M	Mach number	$[-]$
M	Moment force	$[N \cdot m]$
M_x	Moment force about x axis	$[N \cdot m]$
M_y	Moment force about y axis	$[N \cdot m]$
M_{cruise}	Cruise speed mach number	$[-]$
M_{dd}	Drag divergence mach number	$[-]$
M_∞	Free stream mach number	$[-]$
$\dot{m}$	Mass Flow	$[kg/s]$
m	Mass	$[kg]$
N	Number of aircraft produced	$[-]$
N_s	Number of shocks	$[-]$
N_z	Load factor	$[-]$
n_{max}	Maximum load factor	$[-]$
n_{mw}	Number of wheels on main landing gear	$[-]$
n_{nw}	Number of wheels on nose landing gear	$[-]$
P	Roll rate	$[rad/s]$
P	Pressure	$[Pa]$
P_a	Power available	$[W]$
P_{ac}	Aircraft unit cost price	$[$]$
p_e	Effective pressure	[Pa]
P_{mw}	Static load per main gear wheel	$[N]$
P_{nw}	Static load per nose gear wheel	$[N]$
P_r	Power required	$[W]$
P_s	Maximum load gear must endure	$[W]$
p	Pressure	$[kg/ms^2]$
p_0	Reference pressure	$[Pa]$

Symbol	Definition	Units
Q	Amount of aircraft produced	$[-]$
Q	Statical moment of area	$[m^3]$
q	Dynamic pressure	$[Pa]$
q_b	Basic shear flow in skin element	$[N/m]$
q_{s_0}	Cut closing shear flow in cell	$[N/m]$
r	Distance from observer	$[m/s]$
R	Radius	$[m]$
R	Range	$[km]$
R	Specific gas constant	$[J/kgK]$
RC	Rate of climb	$[m/s]$
R_{data}	Data rate	$[j]$
RC_{steady}	Steady rate of climb	$[m/s]$
Re	Reynolds number	$[-]$
r	Fuselage radius	$[mm]$
S	Wing surface	$[m^2]$
S	Deflection of tires and shock	$[m]$
S_{csw}	Control surface area	$[m^2]$
S_f	Fuselage wetted area	$[m^2]$
S_p	Parachute surface area	$[m^2]$
S_h	Horizontal tail surface	$[m^2]$
S_t	Maximum tire deflection	$[m^2]$
S_v	Vertical tail surface	$[m^2]$
S_{vt}	V-tail surface	$[m^2]$
S_w	Trapezoidal wing area	$[m^2]$
S_{wet}	Wetted surface area	$[m^2]$
S_{wf}	Reference flapped surface area	$[m^2]$
s	Distance	$[m]$
s	Slope constant	$[-]$
T	Thrust force	$[N]$
T	Temperature	$[K]$
T_0	Ambient temperature	$[K]$
$T_{2\pi}$	Period (time)	$[s]$
TOP_{jet}	Take-off parameter	$[-]$
T_{Oper}	Operating temperature	$[C]$
T_{rev}	Reverse thrust	$[N]$
t	Skin thickness	$[mm]$
t/c	Thickness-to-chord ratio	$[-]$
T/W	Thrust-to-weight ratio	$[-]$
U	Gust speed	$[m/s]$
UP	Selling price per aircraft	[\$]
V	Aircraft airspeed	$[m/s]$
V	Shear force	$[N]$
V_x	Shear force in y-direction	$[N]$
V_y	Shear force in x-direction	$[N]$
V_1	Decision speed	$[m/s]$
V_{cruise}	Cruise speed	$[m/s]$
V_{EAS}	Equivalent airspeed	$[m/s]$
V_h/V	Tail to wing airspeed ratio	$[-]$
V_{LOF}	Lift of speed	$[m/s]$
V_{ref}	Reference aircraft cruise speed	$[m/s]$
V_{SR}	Reference stall speed	$[m/s]$
V_{TAS}	True airspeed	$[m/s]$
$\bar{V}_H$	Horizontal tail volume coefficient	$[-]$
$\bar{V}_V$	Vertical tail volume coefficient	$[-]$
W	Acoustic power	$[W]$
W	Weight	$[N]$
W_4	Begin of cruise weight	$[kg]$
W_5	End of cruise weight	$[kg]$
W_{dg}	Design gross weight	$[N]$
W_{fuel}	Fuel weight	$[kg]$

Symbol	Definition	Units
W_i	Weight of aircraft component	$[kg]$
W_{MTOW}	Maximum take-off weight	$[kg]$
W_{OEW}	Operational empty weight	$[kg]$
W_{PL}	Payload weight	$[kg]$
W_{TO}	Take-off weight	$[kg]$
w	Wing loading	$[N/m^2]$
w	Ultimate velocity of descent	$[m/s]$
x_{cg}	X-coordinate of centre of gravity from datum	$[m]$
$\bar{x}_{ac}$	Longitudinal position of the aircraft's aerodynamic centre with respect to the MAC	$[-]$
$\bar{x}_{cg}$	Longitudinal position of the aircraft's centre of gravity with respect to the MAC	$[-]$
X_{cg}	Longitudinal position of the aircraft's centre of gravity	$[m]$
X_{MLG}	Longitudinal position main landing gear	$[m]$
X_{NLG}	Longitudinal position nose landing gear	$[m]$
X_{LEMAC}	Longitudinal position mean aerodynamic chord	$[m]$
x_{climb}	Horizontal climb distance	$[m/s]$
x_i	Longitudinal position of aircraft component	$[m]$
x_{trans}	Horizontal transition distance	$[m]$
y_{cg}	Y-coordinate of centre of gravity from datum	$[m]$
Y_{MLG}	Lateral position main landing gear	$[m]$
Y_{NLG}	Lateral position nose landing gear	$[m]$
z_{cg}	Centre gravity height	$[m]$
z_t	Wing tip height	$[m]$
α	Angle of attack	$[deg]$
α_{stall}	Stall angle of attack	$[deg]$
α_{trim}	Trim angle of attack	$[deg]$
α_{0L}	Zero lift angle of attack	$[deg]$
β	Tip-back angle	$[deg]$
γ	Flight path angle	$[deg]$
γ	Specific heat ratio	$[-]$
δ_a	Aileron deflection	$[rad]$
$\delta_{a_{max}}$	Maximum aileron deflection	$[rad]$
δcg	Centre of gravity shift	$[m]$
δ_f	Flap deflection angle	$[deg]$
Δq_k	Change of shear due to boom	$[N/m]$
$(d\theta/dz)_i$	Angle of twist gradient of cell i	$[rad/m]$
η	Efficiency	$[-]$
η	Airfoil efficiency factor	$[-]$
θ	Polar directivity angle	$[deg]$
θ	Pitch angle	$[deg]$
κ	Constant specific heat ratios	$[-]$
$\Lambda_{0.25c}$	Quarter chord wing sweep	$[deg]$
$\Lambda_{0.5c}$	Half chord wing sweep	$[deg]$
λ	Wavelength	$[m]$
λ	Taper ratio	$[-]$
λ	Maximum to static load ratio	$[-]$
μ	Ground friction coefficient	$[-]$
μ	Dynamic viscosity	$[kg/ms]$
μ_s	Efficiency of shock	$[-]$
μ_t	Efficiency of tire	$[-]$
ν_{FC}	Power generation efficiency	$[-]$
ν_{PMAD}	Power delivery efficiency	$[-]$
ν_{em}	Power conversion efficiency	$[-]$
$\nu_{storage}$	Energy source storage efficiency	$[-]$
ν	Poisson's ratio	$[-]$
ν_{vol}	Energy source volumetric efficiency	$[-]$
Π	Pressure ratio	$[-]$
ρ	Density	$[kg/m^3]$
ρ_{cruise}	Density at cruise altitude	$[kg/m^3]$
ρ_{em}	Power conversion specific power	$[W/kg]$
ρ_{FC}	Power generation specific power	$[W/kg]$

Symbol	Definition	Units
ρ_{fuel}	Fuel density	$[kg/m^3]$
ρ_{PMAD}	Power delivery specific power	$[W/kg]$
ρ_{ref}	Density at reference aircraft cruise altitude	$[kg/m^3]$
σ	Density ratio	$[-]$
σ_θ	Cylindrical hoop stress	$[MPa]$
σ_1	Normal stress in boom 1	$[MPa]$
σ_2	Normal stress in boom 2	$[MPa]$
σ_θ	Cylindrical hoop stress	$[MPa]$
σ_{ult}	Ultimate tensile stress	$[MPa]$
σ_{yield}	Ultimate yield stress	$[MPa]$
σ_v	Von Mises stress	$[MPa]$
σ_z	Normal stress acting on z-direction	$[MPa]$
τ	Aileron effectiveness	$[-]$
τ	Shear stress	$[MPa]$
τ_{ult}	Ultimate shear stress	$[MPa]$
ϕ	Lateral clearance angle	$[deg]$
Φ	Bank angle	$[deg]$
ϕ	Azimuthal directivity angle	$[deg]$
Ψ	Turnover angle	$[deg]$
Ω	Angular rotation speed	$[deg/s]$
Ω	Vertical component of landing velocity	$[m/s]$

List of Abbreviations

Abbreviation	Definition
AEA	American Economic Association
ADS-B	Automatic Dependent Surveillance-Broadcast
AOA	Angle Of Attack
ATA	Actual Time of Arrival
ANOPP	Aircraft Noise Prediction Program
APU	Auxiliary Power Unit
ATC	Air Traffic Control
ATM	Available Tonne Mille
BAH	Bahrain Airport
BLOS	Beyond-Line-of-Sight
BPR	Bypass Ratio
BPSK	Binary Phase Shift Keying
C2	Command and Control
CAD	Computer-aided design
CBS	Cost Breakdown Structure
CC	Combustion Chamber
CG	Center of Gravity
CHC	Christchurch Airport
CS25	Certifications Specification 25
CTK	Cargo Tonne Kilometres
CoViD-19	Corona Virus Disease 2019
DAPCA	Development and Procurement Cost of Aircraft
DOC	Direct Operating Cost
DSE	Design Synthesis Excercise
DUR	Durban Airport
EASA	European Union Aviation Safety Agency
EIRP	Effective isotropic radiated power
EOL	End-of-Life
FAA	Federal Aviation Administration
FH	Flight Hours
FL	Flight Level
FMS	Flight Management System
FRA	Frankfurt Airport
FTK	Freight Ton Kilometer
GCS	Ground Control System
GHG	Greenhouse Gas
GPS	Global Positioning System
HPC	High Pressure Compressor
HPT	High Pressure Turbine
IFR	Instrument Flight Rules
ILS	Instrument Landing System
IMU	Inertial Measurement Unit
INS	Inertial Navigational System
IOC	Indirect Operating Cost

Abbreviation	Definition
HLD	High Lift Device
KLM	Dutch Royal Airlines
LCA	Life-Cycle Analysis
LCN	Load Classification Number
LDG	Landing Gear
LE	Leading Edge
LHV	Lower Heating Value
LOS	Line-of-Sight
LPC	Low Pressure Compressor
LPT	Low Pressure Turbine
MAC	Mean Aerodynamic Chord
MECH	Mechanical
MEM	Memphis Airport
MTBF	Mean Time Between Failures
MTBO	Mean Time Between Overhauls
MTOW	Maximum Take-Off Weight
NASA	National Aeronautics and Space Administration
NRT	Narita Airport
OEW	Operational Empty Weight
POS	Project Objective Statement
RAMS	Reliability, Availability, Maintainability & Safety
RD&T	Research, Development and Testing
ROC	Rate of Climb
ROI	Return on Investment
S.M.	Stick-fixed Static Margin
SATCOM	Satellite Communication
SCL	Santiago Airport
SFC	Specific Fuel Consumption
SNR	Signal-to-Noise Ratio
SPL	Sound Pressure Level
SPONL	Seafood Processors of Newfoundland and Labrador
SWOT	Strengths, Weaknesses, Opportunities & Threats
TBD	To Be Determined
TCAS	Traffic Collision Avoidance System
TIT	Turbine Inlet Temperature
TRU	Transformer Rectifier Unit
UA	Unmanned Aircraft
UCA	Unmanned Cargo Aircraft
USD	United States Dollar
VOL	Volume
VHF	Very High Frequency
WBS	Work Breakdown Structure
WFD	Work Flow Diagram

Contents

1 Introduction

1.1. Project Description

During the Covid-19 pandemic, it has become clear that the air transportation of cargo is largely dependent on passenger aircraft routes and schedules. Before the Covid-19 pandemic, cargo was mostly transported using the belly of passenger aircraft. As the development of the Covid crisis is far from predictable, new modes of air cargo transportation are needed to decrease the dependency on passenger aircraft. Therefore, Ir. Paul Roling has come up with the idea of an unmanned cargo aircraft which should be used to transport high value goods with a low volume. A group of 10 aerospace students studying at TU Delft are given this design assignment. They will work on this assignment for a time span of 10 weeks during the final phase of their bachelor's programme.

As new modes of air cargo transportation are needed, the following project objective statement (POS) is formulated below. Following from the objective of the project, the aim of this report is stated in the mission need statement (MNS), also stated below.

Project Objective Statement (POS)

Design an autonomous aircraft that transports a low quantity of high value and time-critical goods while being economical, sustainable and accessible to most airports.

Mission Need Statement (MNS)

A sustainable mode of air transport is needed to autonomously transport high-value payloads intercontinentally with a low turn-around time.

This project consist of four phases, which will be discussed briefly. The four phases are, Project Plan, Baseline, Midterm, and Final. In the first phase the team has been divided into organisational and technical roles. The work up till the third phase has been planned out in detail for a efficient work flow. During the baseline phase, a requirement analysis has been performed, in order to come up with all relevant requirements. The most important requirements are shown in Table 1.1. During this phase, also the design options were evaluated as well as the market itself.

Table 1.1: The driving requirements for the design

Identifier	Requirement
REQ-SYS-GRD-1.1.00	The cargo shall be unloaded from the UCA to a road capable van in less than 30 minutes.
REQ-SYS-GRD-1.1.01	The cargo shall be loaded from a road capable van into the UCA in less than 30 minutes.
REQ-SYS-MIS-3.1.00	The UCA shall have a range of at least 3000 nautical miles for maximum payload.
REQ-SYS-MIS-3.1.01	The UCA shall carry at least 2 metric tonnes of payload.
REQ-SYS-MIS-3.1.02	The UCA shall have a payload volume capacity of at least 5 $[m^3]$.
REQ-SYS-MIS-3.2.00	The UCA shall have a level of autonomy which is able to execute operations safely depending on the phase of flight.
REQ-SYS-SUS-4.1.00	The CO2 emission of the UCA shall be less than 50% per metric tonne when compared to a 747-400 freighter.
REQ-SYS-SUS-4.2.00	The noise level of the UCA shall be below that of a Cessna Citation 2.
REQ-SYS-CST-5.1.00	The UCA shall cost no more than € 5,000,000 per unit.
REQ-SYS-CST-5.2.00	The direct operational costs for the UCA shall be less than 50% per metric tonne when compared to a 747-400 freighter.

Moreover, in the midterm phase, four different concepts where introduced. They were opted for based on their variation in configuration, propulsion system, cruise speed and altitude leading to numerous considered (sub)systems for the unmanned final design. The four selected concepts are called the sustainable concept, the economical concept, the supersonic concepts and the flying wing. Literature and data was obtained for all designs in order to perform a trade-off based on the client's needs. The best option was the economical concept with some design changes. This design will be the starting point of the final phase. The design itself is shown in Figure 1.1. During the midterm phase the planning for the final stage had been performed as well.

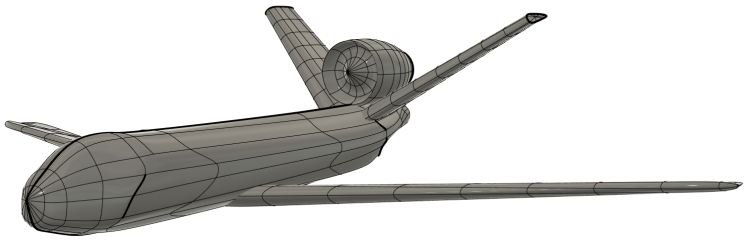

Figure 1.1: Initial design after the midterm phase, starting point final design

The overall aim of this report is to show the feasibility of an unmanned cargo aircraft, focusing on a variety of disciplines, such as aerodynamics, structures, propulsion, sustainability, etc. The report is structured as follows. Chapter 2 will discuss the market analysis, including the current and future market, potential routes and the target market. Next the design philosophy will be discussed in Chapter 3. Afterwards the technical design will be shown. Chapter 4 will discuss the preliminary design and weight estimations. Chapter 5 will discuss the aerodynamic analysis of the airfoil and wing. Chapter 6 will discuss all flight stages and its performance. Chapter 7 will discuss the chosen propulsion system. Chapter 8 will discuss the fuselage and wing structure design. Chapter 9 will discuss the chosen materials for different structural components. Chapter 10 will discuss the empennage design. Chapter 11 will examine the landing gear design. Chapter 12 will discuss the unmanned characteristics of this aircraft. The electrical systems and other relevant systems will be discussed in Chapter 13. These technical chapters will be combined in Chapter 15, where the final design is shown. Its compliance with all requirements is discussed in Chapter 16. After the design is compliant, the sustainable development strategy, as well as the noise analysis will be discussed in Chapter 14. Lastly the development, including manufacturing, operations and post-DSE planning, will be discussed in Chapter 18.

1.2. Functional Breakdown

A functional breakdown structure is made in order to obtain an overview of all the functions and associated subfunctions the UCA has to perform during its operational lifetime. The Functional breakdown, which can be seen in Figure 1.2, can be divided into three main categories, the aircraft production, operation and retirement.

The production group entails everything from finding the right materials, assembly, testing, and certifying the aircraft. Testing, certification and delivery is included for production, as production in this case entails everything up till the moment the client is able to use the aircraft. When thinking of aircraft operations, functions like taxiing, climb, cruise and landing are considered as well as certain emergency scenarios which have to be accounted for. Communicating with ATC & GCS will include aviate, navigate and communicate. This is different compared to normal aircraft as this UCA does not have a pilot. For instance visibility issues are less of a concern. Lastly, if the aircraft is retired, it will be moved to a disassembly location to be (partially) recycled and/or refurbished.

1.3. Functional Flow Diagram

The functional flow diagram for this aircraft is shown in Figure 1.3. The yellow box describes the top level functions from the design till the retirement of the aircraft, this is then further expanded into level 2 functions. In the other coloured boxes, the level 2 functions are further developed into level 3 functions. Each colour represents a level 1 function, namely, green, blue and pink are represented by the production, operation and retirement phase of the aircraft respectively.

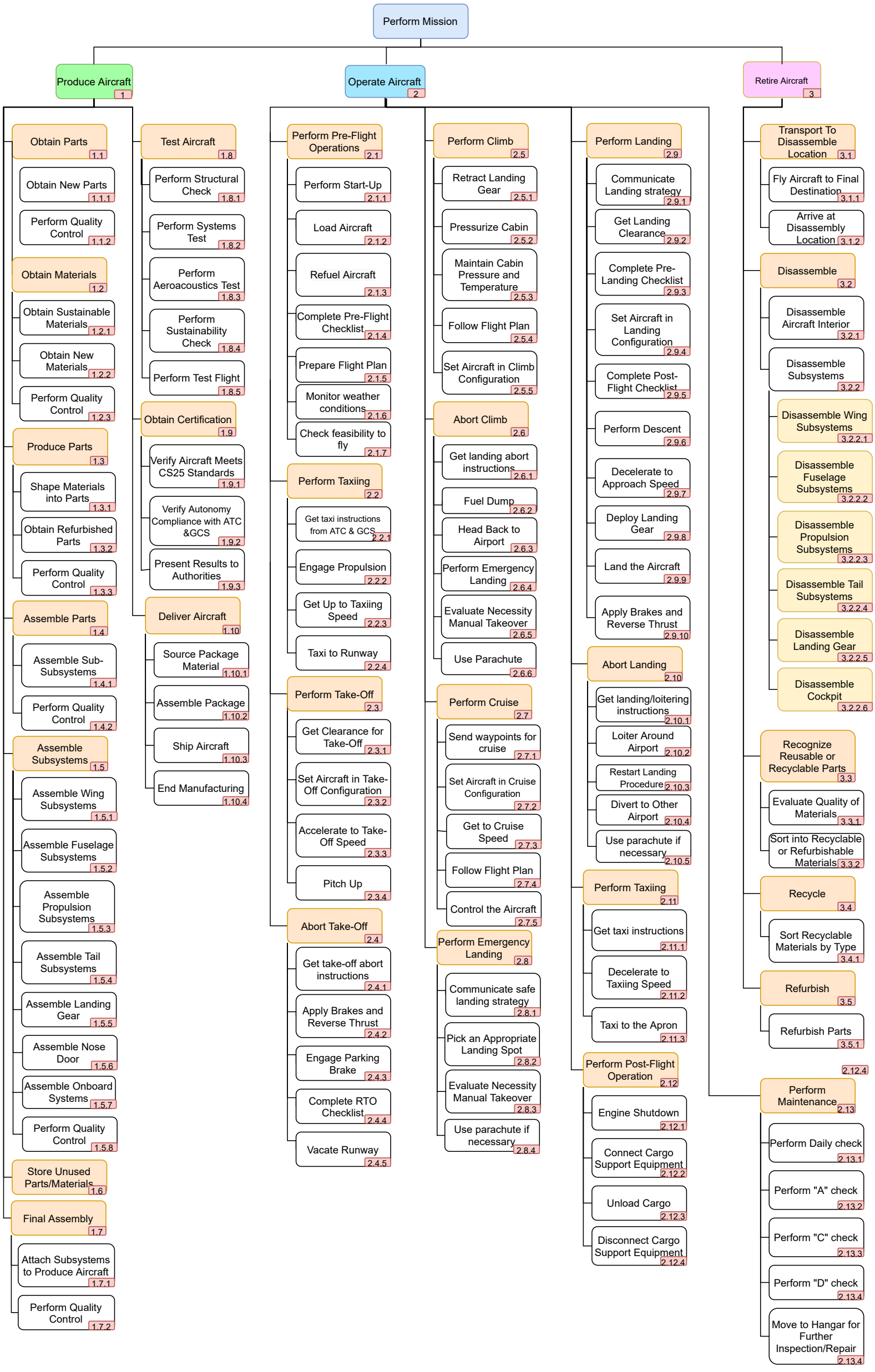

Figure 1.2: Functional breakdown diagram

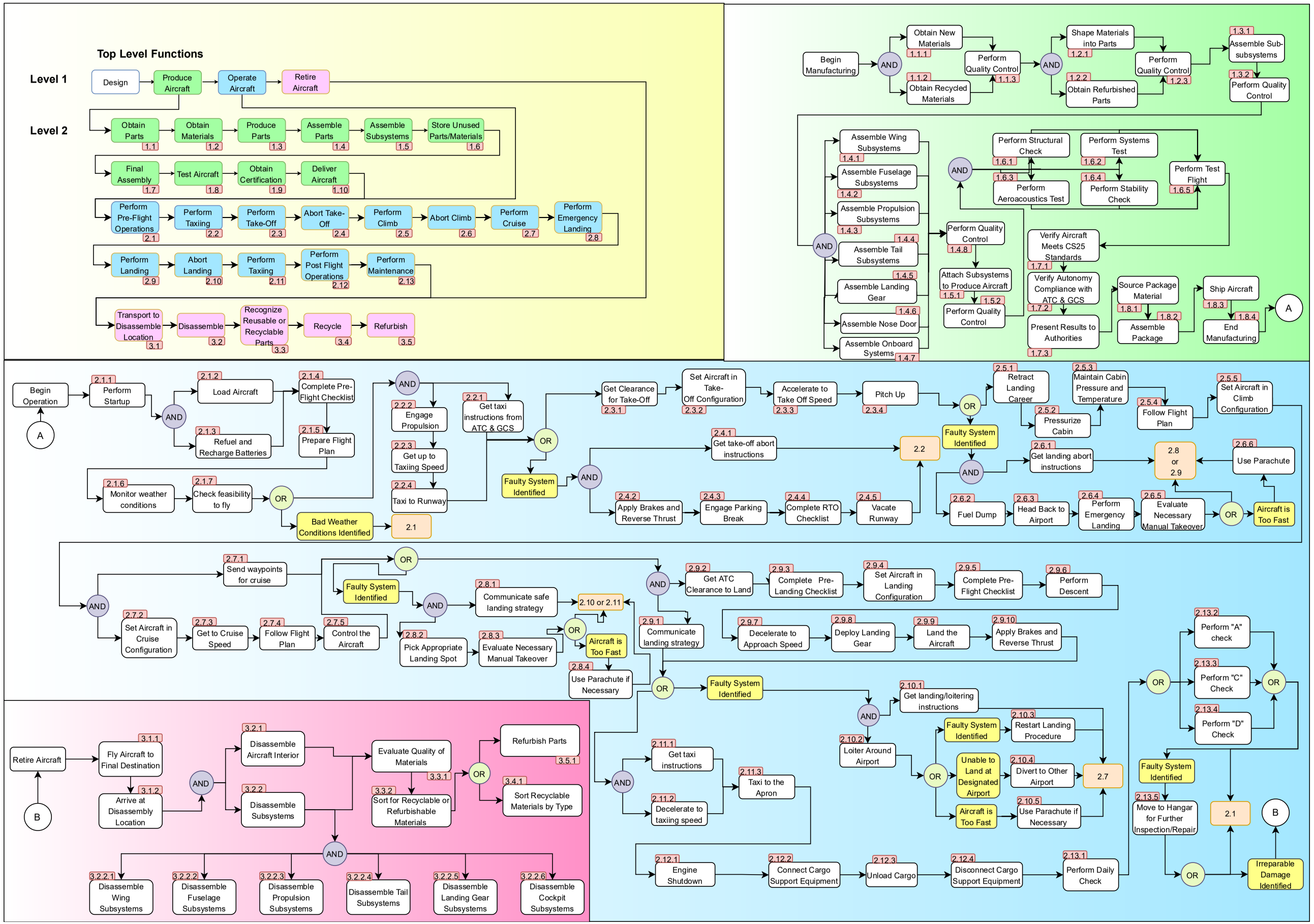

Figure 1.3: Functional flow diagram

2
Market Analysis and Business plan

This chapter discusses the market analysis performed on the UCA. The aim of the market analysis is to look for a certain market gap and to place the UCA in that specific market. First some research on the current air cargo market is done and the market gap is determined, which is discussed in Section 2.1. The future market and potential routes are evaluated in Section 2.2. Section 2.3 calculates the expected market share and touches upon the opportunity in the market. The business model will be discussed in Section 2.4. The chapter finishes with an SWOT analysis performed in Section 2.5.

2.1. Air Cargo Market

Due to the CoViD-19 travel restrictions the airline industry faced one of its deepest recessions. However, full-freighter aircraft have become more important than ever. In the current market there are several option to transport cargo via the airline industry. It is possible to transport cargo in full-freighter aircraft, combi-aircraft and in the belly of passenger aircraft. During the pandemic, the availability of belly capacity was heavily decreased since passenger aircraft normally accounts for 54% of the world air cargo capacity [1]. This created a shortage on the air cargo capacity. Due to this shortage, full-freighter aircraft were used at their maximum capacity. The pandemic has been going on for more than a year right now and the air cargo industry is recovering from the consequences it has endured during these times. This can also be seen in Figure 2.1[1]. After a big decrease in Cargo-Tonne-Kilometer (CTK) at the start of the pandemic, the CTK has reached it highest position in 2021 since March 2018.

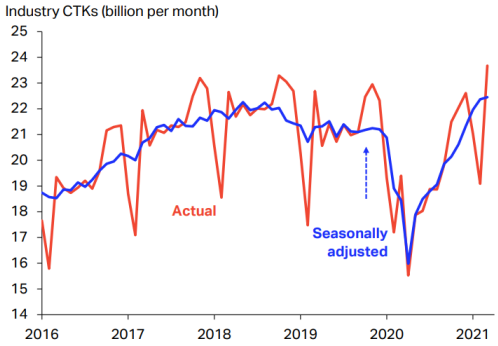

Figure 2.1: Cargo Tonne Kilometres from 2016 until 2021

In the Baseline Report [2] an extensive analysis had been done on several reference aircraft. The aircraft were compared to each other with respect of their payload capacity and range. From this it was concluded that there is yet to be an aircraft that can fly a medium range with a small payload. This is exactly the market gap the UCA will satisfy.

2.1.1. Air Cargo Networks

An important factor in the current cargo market are the air cargo routes flown the most. This will also be important when during the final design as the range is a limiting factor. A small table has been generated with the top 5 of the most used air traffic routes in 2019. The results of this can be seen in Table 2.1. The market share percentages are based on the worldwide Freight Tonne-Kilometres (FTK).

From the table it becomes clear that the North America-Asia and Europe-Asia are the most used routes by far. These two routes together take care of almost 45% of the total market share. With the range requirement of 3000 $[nm]$ the UCA will be able to fly all the routes mentioned in the table. The potential routes will be further explained in Subsection 2.2.2.

[1] `https://www.iata.org/en/iata-repository/publications/economic-reports/air-freight-monthly-analysis---march-2021/` [Accessed on: 21-05-2021]

2.1.2. Transported Goods

Besides the most used transportation networks in the air cargo industry it is also interesting to know what kind of goods are shipped via air transportation. The kind of goods will play a role in determining whether the cabin should be pressurized, the temperature of the cabin and the general lay-out of the cabin itself.

The general lay-out of the cabin is determined by the volume of the cargo. In order to obtain the volume of the cargo, the specific densities of different goods are calculated. The results can be seen in Table 2.2 [2]. From this the volume can be calculated to obtain a payload of 2 metric tons. This volume is then incorporated into the lay-out design of the cabin.

The overall demand for the air cargo industry is limited by cost. As transportation by sea or train is cheaper, most bulk and low value goods will be transported in that way. Air cargo is typically priced four to five times that of road transport and 12 to 16 times the price of sea transport [3]. This means that mainly high value or time-sensitive goods are transported by air. This can also be seen in the table.

Table 2.1: Top 5 most used air cargo network routes

Route	Market Share
North America - Asia	22.4
Europe - Asia	20.8
North America - Europe	13
Within Asia	8.8
Asia - Middle East	6.6

Table 2.2: Weighted Mean Density of high value cargo commodities, accordingly to Tzimourtos [4, p.76]

Cargo Description	Weighted Mean Density $[kg/m^3]$
Aerospace Cargo	142.23
Art	175.86
Audio/Video Media	271.86
Automotive Goods	194.34
Chemicals	312.9
Computers	165.41
Jewellery	207.95
Express Freight	161.69
Electrical Goods	179.57
Machine Parts	263.29
Pharmaceuticals	163.81
Precision instruments	161.47
Telecom equipment	170.91
Average	**197.79**

2.1.3. Competition between Container Ships and Air Cargo Carriers

The main competitors that will compete in the cargo industry are container ships. Those ships can transport cargo volumes in the order of 20.000 containers [3]. Furthermore, those container ships have a range that can easily cross the oceans. The downside is however, that it takes much longer to transport cargo by ship than transporting it by air. Furthermore, cargo transportation by ship relies on routes that can get easily congested because there are is a lack of alternative routes. For example the blockage in the Suez Canal in March 2021 caused more than 6 days of delays for more than 200 container ships. The UCA will therefore be a better option to transport high value and time-critical goods. However, as mentioned before, the price of transporting good using ships is 12 to 16 times lower than transporting good using aircraft. This makes the container ships more attractive to use when transporting cargo. Note that container ships focus on transporting large amount of goods. Although the UCA will focus on transporting a limited amount of high value goods. This means that the costs for transporting the goods is relatively low compared to the cost of the actual product that is being transported.

2.2. Future Market and Potential Routes

In Subsection 2.2.1 a small market prediction will be made. After that, Subsection 2.2.2 will discuss several types of routes that are attractive for the UCA that will be designed.

2.2.1. Future Market

The air cargo traffic industry is projected to grow 4.1% for over the next 20 years[1]. The revenue per ton kilometer, RTK, will double over the next 20 years from 264 billion RTK in 2019 to 578 billion RTK in 2039. As a consequence of this growth, a larger cargo fleet is needed. According to the Boeing report used earlier, the fleet will grow by 20% over the next 20 years. This means that 2430 new freighters are required to fulfill this need. 1180 of those 2430 freighters

[2] https://www.statista.com/statistics/1114034/air-freight-traffic-international-freight-tone-kilometers-route/ [Accessed on: 25-05-2021]

[3] https://www.costamare.com/industry_containerisation [Accessed on: 07-05-2021]

will be replacing retired aircraft and 1250 freighters will be needed due to the growth of the market. This can also be seen in Figure 2.2. The American Federal Aviation Administrations predicts that in forty years, around 40% of the total air cargo will be transported by unmanned aircraft[4]. This is a positive future outlook for the UCA.

Figure 2.2: The predicted growth of the freighter fleet [1]

As discussed in Section 2.1 there are two options for air cargo transport, namely in the belly of a passenger aircraft and main-deck freighters. As the COVID-19 pandemic highlighted the importance of the main-deck freighters, dedicated freighters will continue to transport at least 50% of the world air cargo. There are several reasons for this:

- Most passenger aircraft do not serve key cargo trade routes.
- Normal passenger routes have to stick to a certain schedule. In this way time-sensitive goods will not arrive on time
- Some hazardous materials such as lithium batteries are not allowed on passenger aircraft
- As the cargo payload on passenger aircraft is depended on the range most of the times not all cargo capacity is utilised. This results into late arrivals of some cargo.

All the items stated above will not be an issue for the UCA. Especially the fact that there is also no crew on board. This means that the costs of operating the UCA will also be lower as there are no stop-over crew costs. No crew also means that there is no crew scheduling needed, which means that the UCA can fly all over the world without taking the crew back home. Thus there are no limitations on the amount of routes and where to fly to.

2.2.2. Potential Routes

As the aim is to design an UCA that can carry two metric tons of payload, this means it will eventually unlock the economic potential of regions which were not able to operate air cargo transportation in a large scale. This includes many regions in Africa, South America, and parts of inner Asia. These regions lack the infrastructure to transport goods from and to large transport aircraft. Besides some potential economic areas there are also regions which are located far away from habited areas. So called "remote communities". Below are listed some of those potential regions for which the UCA will be an option.

1. Regions which are located at a large distance from a hub airport. This means that time-sensitive goods have to travel too far to arrive at the international transport hub. In this case the UCA can land at small regional airport and transport the relevant goods.
2. Regions which produce high value goods, but in too small volume to make a full freighter flight profitable. Besides, these regions are too small to schedule regular passenger flights with belly cargo.
3. Regions which suffer from an underdeveloped infrastructure. This can be due to lack of development or environmental aspects.

The regions described by points 1 and 3 are also known as remote communities. Remote communities, such as islands in the Pacific and Atlantic Oceans or areas with extreme weather conditions, like deserts and the polar regions, are highly dependent cargo aircraft and container ships when it comes to cargo supplies for those areas. The remote communities are difficult to reach by car or truck. During the CoViD-19 pandemic it became clear that supplying these areas became more difficult. This has to do with the aforementioned fact that passenger aircraft account for 54% of the total air transportation of cargo. During the pandemic the total number of passenger flights dropped significantly.

[4] `https://www.platformuca.org/factsheet-1-civil-unmanned-cargo-aircraft` [Accessed on: 26-04-2021]

2.3. Target Market

The target market is an important parameter to estimate the expected market share. The higher the market share will be the lower the production cost can be. As mentioned earlier the air cargo industry is expected to grow even more. A consequence of this growing market will be that more cargo aircraft are needed. As indicated in Section 2.2 2430 new full-freighter are needed in the next 20 years. The year of introduction of the UCA will be 2035. So these numbers will probably have the same order of magnitude in the year of introduction. However, one thing should be noted. The amount of new freighters also include medium wide body and large freighters with a respective payload above 40 metric tonnes. So when these are not taken into account 1270 new freighters are needed in the standard body segment[1]. This segment accounts for aircraft carrying around 40 metric tons of payload. So the assumption can be made that for one standard body freighter 20 UCA aircraft are needed. With a full potential market this means that a potential of 25400 aircraft could be sold. This is of course not a realistic number for a new aircraft entering the market. Therefore the assumption was made that the a potential market of share of 20% could be obtained. This will lead to a potential market volume of 5080 aircraft. This number is purely based on the market share assumption on the current market and not on the performance of the aircraft itself. The fact that it is an autonomous aircraft will bring several advantages, from which the exclusion of crew cost is the major one, which will create a market on its own. As there is no unmanned aircraft market at this stage the estimations made are on the regular air cargo market. However, as mentioned in Section 2.2 in forty years around 40% of the total air cargo market will be unmanned.

So to conclude, there is a market opportunity of 5080 aircraft, which can fill the market gap as discussed in Section 2.1 and partly in Section 2.2.

2.4. Business Model

In order to actually turn the aircraft into potential profit a market strategy has been developed. First, potential clients will be analysed. Afterwards potential cargo hubs fitting these clients and lastly three potential routes will be shown.

2.4.1. Potential Customers

Nowadays, air cargo carriers make use of large aircraft that can transport a massive amount of payload. However, the downside is that those air freighters mostly fly to large airports. Meaning that the extra distance that the cargo needs to travel will be covered using trucks. This is less time-efficient as moving the cargo from plane to truck takes extra time. Furthermore, the aircraft is way faster than a standard cargo truck. The aircraft that is being designed by the project team will be able to transport a lower amount of cargo, although its range is 3000 [nm]. This means that the aircraft will be able to cross parts of the Pacific and Atlantic Oceans. Furthermore it can operate to much smaller airports, which means it can fly in a point-to-point network. Time that is normally being used for loading can now be used to complete other steps in the shipping process. The demand on routes in a point-to-point network is usually lower than routes in a hub-and-spokes network. This sometimes results in aircraft not being fully loaded, which is not efficient. This problem will not be an issue for the aircraft that is being designed by the project team since the maximum payload is around 2000 [kg], which is only a small fraction of the payload a Boeing 747-400 freighter can carry [5]. Taking the advantages together makes the aircraft that is being designed interesting to delivery companies such as FedEx, UPS and DHL.

Remote areas such as regions in Canada, Australia and islands in the Pacific and Atlantic Oceans are not highly populated. Meaning that the demand on routes to those areas is relatively low compared to routes to cities that are more populated. The performance and characteristics of the aircraft that is being designed fit perfectly for the demand on those routes. The business model can be set up in a way that the aircraft can be sold to delivery companies that use air transportation to transport their goods.

In September 2020 FedEx announced that the company was looking for autonomous aircraft that can be used on routes to remote areas [6]. It shows that FedEx is interested in market of relatively small autonomous cargo aircraft. This is a perfect opportunity for a collaboration with FedEx. Moreover, FedEx is a global leader in cargo delivery and the market share of FedEx is relatively high. This means that the concept of small autonomous cargo aircraft may also be interesting for other (large) cargo delivery companies such as DHL and UPS.

Moreover, there are specific airlines that fly mainly on routes to islands in the Pacific or Atlantic Ocean. Asia Pacific Airlines is a cargo operator that operates in the Asia-Pacific region. The airline currently uses the Boeing 757-200 freighter aircraft [7]. This type of aircraft can transport 17 times the payload weight of the UCA. However, the UCA has a much smaller turn-around time and flies autonomously which reduces the operational costs. Furthermore, the aircraft can be used to transport much lower amounts of cargo which makes the aircraft more attractive to use on routes to small remote islands. Asia Pacific Airlines is therefore a potential customer.

[5] `https://www.cargolux.com/Our-Expertise/cargo-equipment/aircraft/747-400f-specifications` [Accessed on: 11-06-2021]

[6] `https://www.bloomberg.com/news/articles/2020-09-21/fedex-seeks-to-add-small-self-flying-planes-for-remote-areas` [Accessed on: 11-06-2021]

[7] `https://www.asiapacificairlines.com/757-200f/` [Accessed on: 14-06-2021]

2.4.2. Potential Cargo Hubs

After determining the potential routes and customers, it is important to have a better look at the main airports the aircraft could operate from. These hubs will be needed for heavy maintenance and ground control stations (GCS). All hub airports are selected on being in a completely different region to increase the accessibility. Next, most airports are cargo hubs and are the basis of many cargo carriers, such as FedEx Express, DHL Aviation or Lufthansa SkyCargo. A trade-off has been made between the companies operating at a certain airport and the number of annual passengers (2019). It is preferred to have airports with many cargo companies and few passenger flights. This is due to the fact that larger airports have only a limited amount of slots available. A list of all hub airports is given in Table 2.3[8]. The most promising cargo clients, the total cargo transported, and the ground handling companies are given in this table as well. The total coverage operating from these hubs is shown in Figure 2.3[9]. Next to these main hubs, secondary hubs will be used for small maintenance and fast refueling. These are Honolulu Airport (HNL), Anchorage Airport (ANC), Tenerife South Airport (TFS), and Jakarta Airport (CGK).

Therefore, this aircraft can be sold to companies already operating at the main hubs. For the hub in Durban, Emirates and Qatar Airways are already operating passenger flights to this airport. Meaning this could also become an interesting airport to operate cargo flights from. After selling the aircraft, ground handling will be outsourced using companies already operating at these airports. On all airports except Bahrain Airport, Swissport is operating. This means that Swissport will be able to train personnel if it would be handling the aircraft on multiple hubs. Local ground handling companies will be used on non-hub airports. Swissport will also be able to deliver maintenance on all hubs. If the aircraft would need maintenance at another airport and is not be able to fly back, a maintenance crew can be send towards this airport. For Bahrain, BAS could be used for ground operations. It would also be possible to use Swissport if they would decide to extend their business to this airport as well. [10]

Table 2.3: Main Hubs for the UCA, * indicating passenger carriers

Airport	**Region**	**Cargo Carriers**	**Cargo** $[megatonne]$	**Ground Handling**
Frankfurt (FRA)	Europe	FedEX Express Lufthansa Cargo Emirates SkyCargo	2.1	WFS, Swissport
Memphis (MEM)	North-America	FedEX Express DHL Aviation UPS Airlines	4.9	WFS, Swissport
Santiago (SCL)	South-America	Lufthansa Cargo UPS Airlines Cargolux	0.4	Swissport
Durban (DUR)	Africa	Emirates* Qatar Aiways*	Unknown	Swissport
Bahrain (BAH)	Middle-East	DHL aviation Emirates SkyCargo Lufthansa Cargo	0.3	BAS
Narita (NRT)	Asia	FedEX Express DHL aviation UPS Airlines	2.0	Swissport
Christchurch (CHC)	Oceania	DHL Aviation Qantas Air	0.02	Swissport

[8] `https://www.statista.com/` [Accessed on: 14-06-2021]
[9] `http://www.gcmap.com/`[Accessed on: 14-02-2021]
[10] `https://www.swissport.com/` [Accessed on: 14-06-2021]

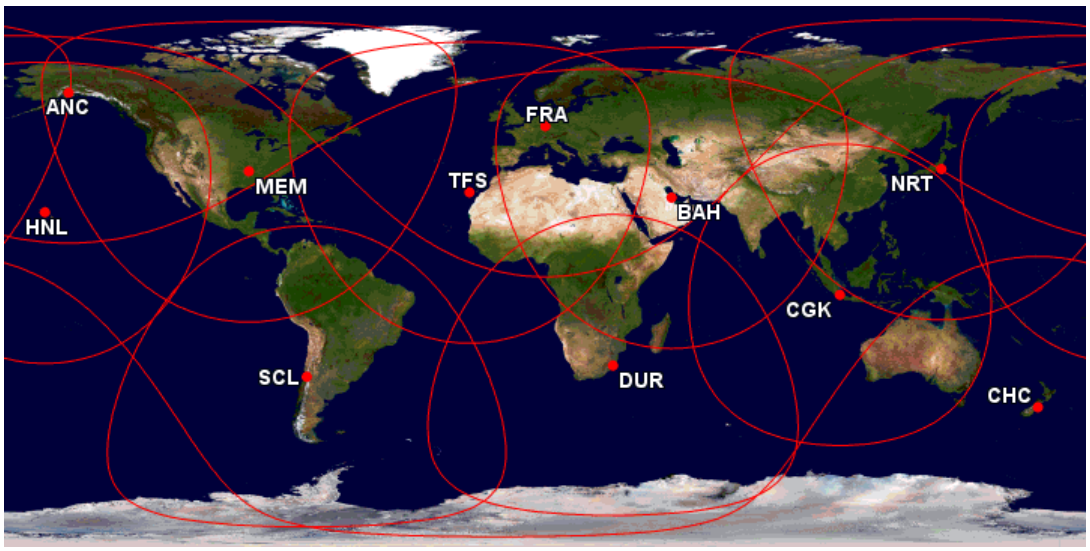

Figure 2.3: Main hubs and secondary hubs for the UCA, including the range from every hub

2.4.3. Business Examples

In this subsection 3 specific business examples will be explained. Each of the three examples can be related to the routes explained in Subsection 2.2.2. The three examples will help in better understanding the place of the UCA in the market. The first example is about the transportation of seafood from Newfoundland and Labrador. The second example will elaborate on flights inbound and outbound from Saint Helena. The last example is about the distribution of the CoViD-19 vaccines.

Newfoundland and Labrador, Canada

The seafood market in Newfoundland and Labrador (Canada) has a market value of 1.4 billion dollars[11] which is expected to increase more in the coming years. The seafood industry in this region of Canada is relatively large. The Provincial government of Newfoundland and Labrador looked into the possibility whether air cargo is a practical way to get seafood from Newfoundland to the world. Especially, lobsters are an important part of the seafood industry in Newfoundland. The UCA could help in the market of seafood to transport seafood to the rest of the world and especially Asia[12]. Seafood Processors of Newfoundland and Labrador (SPONL) said that they were willing to help to attract the cargo carrier, for example to make sure that the cargo holds are filled, and "not necessarily limited to seafood" products[13]. Their main goal is to realise a fast, continuous service that can transport their seafood as well as other products. The advantage of using air transportation is the decreasing transportation time. It makes it possible to get the seafood within three or four days from time of catch to the place of destination, which improves the quality of the seafood. The UCA is an aircraft that can perfectly be used to transport seafood from the Newfoundland and Labrador province to other parts of the world. Figure 2.4 shows that the UCA can transport the seafood to Japan (Asia) via Anchorage (Alaska) given its 3000 $[nm]$ range.

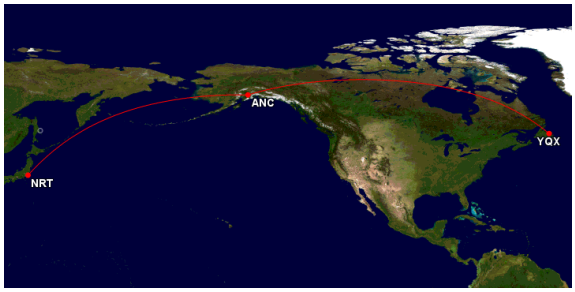

Figure 2.4: Seafood Transportation Route from Newfoundland and Labrador to Asia

Figure 2.5: Air Transportation Route from South Africa to Saint Helena

Saint Helena

Saint Helena is an island located in the Atlantic Ocean west of Africa. The island is heavily dependent on cargo that is delivered by ship or air transportation. Transporting cargo is usually done by sea using cargo ships or air using passenger aircraft. It takes a couple of days to transport cargo by sea from Johannesburg to Saint Helena and a few

[11] `https://www.findnewfoundlandlabrador.com/buy/seafood/` [Accessed on: 14-06-2021]
[12] `https://bit.ly/3wmTxTX` [Accessed on: 14-06-2021]
[13] `https://bit.ly/3wmTxTX` [Accessed on: 14-06-2021]

hours to transport the cargo by air. This is much faster, and therefore air transportation is preferred over sea transportation when time critical goods are being shipped. Passenger aircraft are used to transport the cargo by air. In the event passenger aircraft are not able to fly to Saint Helena, the air transportation is disturbed. This shows that the cargo transportation is dependent on the frequency of passenger flights, which is noticeable during the CoViD-19 crisis. Saint Helena imposed travel restrictions to prevent CoViD-19 from spreading [14]. Those restrictions resulted in a little amount of cargo transport possible by passenger aircraft. The use of the UCA is therefore a useful alternative, especially during events such as the CoViD-19 pandemic. The UCA ensures that the cargo transportation to Saint Helena is less dependent on passenger flight only. The UCA does not require specialised equipment at the airport, which means that the UCA is a suitable option to use to transport cargo to Saint Helena. Figure 2.5 shows the route from the potential hub in Durban to Saint Helena. The distance is less than 3000 $[nm]$ which means that the UCA is able reach Saint Helena from Durban. In the case one cannot land on Saint Helena, the UCA could divert to Ascension Island. This will exceed the range. Therefore, making a stop at Walvis Bay Airport in Namibia would be a good option. In this case the aircraft could divert to Ascension Island or could fly back to Namibia.

Vaccine distribution
The CoViD-19 pandemic and the distribution of the vaccines that are developed to fight the virus are viral topics at this moment. Different types of vaccines have been developed and are being produced as fast as possible to provide them to the world. One of the vaccines that is being produced is the BioNtech-Pfizer vaccine, which is developed by BioNtech (Germany) and Pfizer (United States). One of the BioNtech-Pfizer production locations is located in Marburg, Germany. This facility is able to produce the vaccines at a rate of 8 million doses within three to seven days[15]. To transport the vaccines to the airport, the highway between Frankfurt and Marburg will be used. The distance is about 100 $[km]$ and it takes about 75 minutes to reach Frankfurt. The vaccines can be shipped from Frankfurt to other countries in Europe, West-Asia and North and Central-Africa given the range of the aircraft. Figure 2.6 shows the radius of the aircraft when it takes off in Frankfurt. The vaccine needs to be stored at extremely low temperatures. However, it is allowed to transport the vaccines using a portable freezer between -25 and -15 degrees Celsius, under the condition that it is used within 2 weeks of transportation. [16]

Currently, the World Health Organization has big concerns regarding the Covid-19 infections in Africa. The Indian and South African variants are increasing the infections in a rapid manner. Also a new variant emerged in Nigeria. In order to decrease the chance of creating new variants, the use of this aircraft could lead to a rapid distribution of vaccines within Africa.[17]

Figure 2.6: BioNtech-Pfizer vaccine distribution from Frankfurt to Europe, Northern-Africa and West-Asia

2.5. SWOT Analysis

In Figure 2.7 the SWOT analysis performed on the UCA can be seen. This shows the Strength, Weaknesses, Opportunities and Threats of the UCA in the potential market. Both internal and external factors are taken into account. These internal and external factors can either be helpful or harmful for the design.

From Figure 2.7 it can be concluded that most of the helpful factors are the reduced costs, reduced emissions and the

[14] https://www.sainthelena.gov.sh/coronavirus-covid-19/travel-tourism/ [Accessed on: 07-05-2021]
[15] https://time.com/5955247/inside-biontech-vaccine-facility/ [Accessed on: 15-06-2021]
[16] https://www.cdc.gov/vaccines/covid-19/info-by-product/pfizer/downloads/pfizer-transporting-vaccine.pdf [Accessed on: 15-06-2021]
[17] https://www.bbc.com/news/world-africa-53181555 [Accessed on: 15-06-2021]

expected growth of the air cargo market. However, the harmful elements mostly have to deal with the little experience with the design of an autonomous aircraft and the regulations associated with that. These elements are harmful and could therefore turn out very negative for the design team. To avoid this, extra attention should be given to these specific elements. In that way the risk of a potential failure on the aircraft market can be avoided.

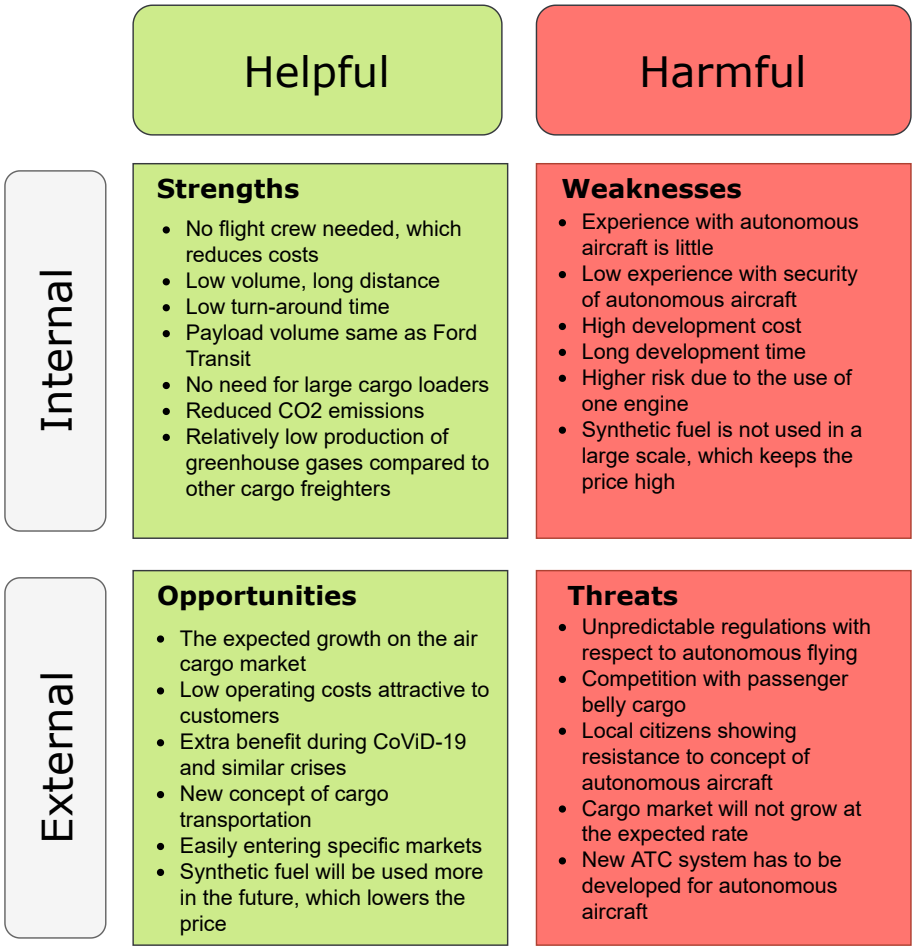

Figure 2.7: SWOT analysis

3
Design Philosophy

This chapter will discuss the overall design philosophy for all technical section. First the technical layout will be discussed in Section 3.1. Afterwards the verification, validation and sensitivity analysis will be discussed in Section 3.2-Section 3.4. Section 3.5 will discuss the methodology for system budgeting, including weight, power, cost, sustainability budgets. Lastly the iteration methodology will be discussed in Section 3.6.

3.1. Technical Design Layout

In order to have a consistent technical design for all departments, the following structure will be used during the design:

- **Requirement Analysis:** All relevant stakeholder, system, and subsystem requirements will be included for each technical department. These requirement must be met during the technical design. This could also include the assumptions made.
- **Technical Design:** All relevant results and designs will be presented including the methodology.
- **Verification and Validation:** Verification and validation procedures including results will be displayed.
- **Sensitivity analysis:** Sensitivity Analysis will be included for the assumptions made during the design and/or for a technical trade-off. This will be part of the verification and validation.
- **Conclusion and Recommendations:** Summary of all relevant results obtained from the technical design including further recommendations.

3.2. Verification Methodology

Verification is needed in order to determine if the simulation model accurately represents the numerical model. This implies checking if errors are made within the calculations, checking if errors are made in the code, and checking the effect of discretization. In general this can be performed by means of code verification and calculation verification. This section will describe both code verification, which will include unit tests and system tests

3.2.1. Unit Tests

Code verification will be used for checking of potential programming errors. Unit tests will be performed on small units of code in order to test single functions and verifying the desired output result. This will occur simultaneous with the development of the code. There are four methods that can be used in order to check the code, which are Proportional Comparison (Changing sign/magnitude of input values), Visual Verification (Correct data input), Point Check (Check values at important nodes within the model, for instance using Kirchoff's rule), Manual Calculation (Comparing model value with manual calculations).

System Tests

System tests are needed to verify if the model behaves in a correct manner. Checking can be done by changing the magnitude or sign of input values and verifying the desired output values. In general the desired expected behaviour could be: linearly increasing/decreasing, quadratic increasing/decreasing, stable/unstable, dependent/independent. In order to check the entire system, one would perform first small scale tests and will increase the size to include the entire system in the end.

3.3. Validation Methodology

Validation is needed in order to validate the assumptions made as well as to ensure that models used represent reality. Two methods will be used to validate the models, which are Comparison and Reference Inputs.

Comparison

A database is generated in order to check the design output with reference aircraft. If subsystems are closely resembled with reference aircraft subsystems a comparison of data can be used to validate the results. When the range of parameters is less concentrated, linear regression can be used to validate the calculations. The accuracy of the linear regression model can be obtained when compared to the real aircraft using the coefficient of determination, also known as R-squared, R^2.

Reference Inputs

Another method to validate models is using reference inputs from the database. The outputs should lie in a predetermined range that can differ per parameter. If the output values are not in the predetermined range, the assumptions made are not valid and models and assumptions must be re-evaluated in order to improve the accuracy.

3.4. Sensitivity Analysis Methodology

A sensitivity analysis can be applied to both a trade-off and assumptions made for specific models. For a trade-off, the sensitivity analysis will be used to validate the trade-off itself. A single variable will be altered to see its effect on the entire multivariate system. If it is found to vary greatly to small changes, it means that the system is too sensitive and that the potential is high that the trade-off result is not trust worthy. While if it is found to not vary that much, the analysis is rather stable, and more confidence can be derived from that result. The method will involve changing each criterias weighting independently, to the maximum and minimum (1 - 5). To assess the system sensitivity, the different systems maximum ranking position and minimum ranking position will be plotted, this will yield a plot of each concept showing how their position has changed based on the variation of each criteria individually.

Sensitivity analysis can also be performed on the made assumptions. This will be merely done for the assumptions with the highest uncertainties involved. It will discover if certain uncertain assumptions could make the design unfeasible. Recommendation for further design will be included if this is the case.

3.5. System Budgeting Methodology

Every design of considerable scale can be characterized by the occurrence of contingencies. Due to the complexity of a project this size, unforeseen circumstances are almost guaranteed to occur and shall thus be taken care of in advance. Namely, it is extremely hard to predict outcomes beforehand due to the involvement of large teams as well as the level of complexity of the issues at hand. As a result of this, technical resources like man hours, but also cost, always have the tendency to increase throughout the design phase. The two major consequences of these contingencies are the possibility of exceeding the cost budget and significant time delays. This will dissatisfy all stakeholders involved, and shall thus be avoided at all times.

In order for the final design of the UCA to not exceed limitations, budgets have been determined beforehand. The aim of these budgets is to be used as a target value for resources which are likely to be altered during the design. By closely monitoring these budgets, deviations can be identified in time and appropriate action can be taken. Throughout the design, more information is acquired such that an increasing level of accuracy of these budgets can be achieved. It is desired for the initial estimation to have an offset smaller than 30%, and reducing the next phases. The involved budgets include weight, power, cost, CO_2 emission and noise emission. The convergence of these budgets is presented in in the respective .

3.5.1. Weight

For the weight of the UCA, the initial target values acquired during the conceptual design originated from regression [2]. By means of a Class I weight estimation which could be performed next, new values for the weight of the aircraft as a whole were found for the preliminary design. Afterwards, these values again serve as an input for more elaborate calculations in later design phases. Namely, once this preliminary value is known a more detailed weight could be achieved through the use of a Class II weight estimation, entering the detailed design. In Table 3.1, the convergence of the weight budget throughout the different design phases is presented.

Table 3.1: Weight contingency budget

	MTOW [kg]	**Contingency [%]**
Conceptual Design	10724	≈ 30
Preliminary Design	<TBD>	≈ 15
Detailed Design	<TBD>	<5

3.5.2. Power

The propulsion system of the UCA is mainly responsible for the performance of the aircraft, and shall thus be extensively analyzed. In the conceptual design stage, by means of linear regression of reference aircraft an initial value for the required thrust was obtained. Notwithstanding this, by means of the T/W - W/S diagram computed in the preliminary design of the aircraft an updated value of this thrust level was acquired, following from the calculated weight mentioned above. After this, elaborate iteration during the detailed design finalised the thrust level. This value is based on both iterated results from the T/W - W/S diagram of performance as well as computed drag magnitudes in aerodynamics. These iterated values are summarized in Table 3.2.

Table 3.2: Power contingency budget

	Thrust [kN]	**Contingency** [%]
Conceptual Design	19.6*	≈ 30
Preliminary Design	<TBD>	≈ 10
Detailed Design	<TBD>	<1

*The reference aircraft mostly were propelled by two engines, while the final design will only have 1 engine which should provide the total thrust.

3.5.3. Cost

Cost is always one of the main constraining resources in a project, since often the objective is to become as profitable as possible. In order to achieve this, it is important to have a clear picture of what unit cost of the final product can be expected. Similarly to the other budgets, the level of accuracy of this budget will improve as the design progresses until it is finalised. In the early stage, the cost could only be based on data available of certain reference aircraft as well as requirements set by the stakeholder. However, throughout the design a higher accuracy of details was achieved since all the required components, systems, materials, supporting resources and development costs were identified. Based on this, a more accurate estimation on the cost could be made which can be visualised in Table 3.3

Table 3.3: Cost contingency budget

	Unit cost [M€]	**Contingency [%]**
Conceptual Design	7.8	≈ 30
Preliminary Design	<TBD>	≈ 15
Detailed Design	<TBD>	<5

3.5.4. Sustainability

Sustainability has been gaining importance over the past decades, and is allocated a substantial role in current design processes. Consequently, one can not ignore the incorporation of sustainable practices within the manufacturing and operation of the final product. The two most relevant forms of sustainability to the UCA are CO_2, as well as noise emission, which will be elaborated upon below. All sustainability budgets mainly follow from a close collaboration between the sustainability and propulsion department.

CO_2 Emission

There exist multiple methods to qualitatively express and compare the CO_2 emission of different aircraft. The most convenient unit for the UCA was been found to be kg of emitted CO_2 per kg of fuel burned. During the conceptual design, this CO_2 emission was based on the fuel types of reference aircraft, which is the main contributor towards this type of emission. Moreover, in the preliminary design the CO_2 emission was iterated by means of an elaborate analysis of the selected fuel type for the UCA. Eventually, the conclusive CO_2 emission was obtained based on an iteration of the burned fuel following from the weight estimations and performance computations. For this conclusive emission the requirement posed by the stakeholder was also taken into account. All these values are presented in Table 3.4.

Table 3.4: CO_2 Emission contingency budget

	CO_2 Emission [kg CO_2/kg fuel]	**Contingency [%]**
Conceptual Design	1.5	≈ 15
Preliminary Design	<TBD>	≈ 10
Detailed Design	<TBD>	<1

Noise Emission

Besides CO_2 emission, noise pollution is another negative contributor towards sustainability. In order to appropriately express the noise emission, the unit Decibels [dB] measured at a distance of 300 meters is selected. During the conceptual design stage, only reference aircraft could be consulted to obtain a first order estimate. This was mainly based on the certifications which the reference aircraft adhered to according to regulations. Subsequently, again by means of a collaboration between the propulsion and sustainability departments more accurate noise levels were obtained throughout the design. This could only initiate once selected noise-lowering configurations like more aerodynamic nacelles embodying the engine or a V-tail were introduced and the definite engine was selected. The outcomes are presented in Table 3.5.

Table 3.5: Noise Emission contingency budget

	Noise Emission [dB]	**Contingency [%]**
Conceptual Design	95	≈ 30
Preliminary Design	<TBD>	≈ 15
Detailed Design	<TBD>	<1

3.6. Iteration Methodology

Designing an aircraft can be described as an iterative process. This entails that all computed values constantly need to be updated until a certain convergence is achieved. On top of this, most of the computations which have to be performed are dependent on inputs which requires its respective outputs first, thus assumptions will have to be made initially. In order to manage this complicated process, appropriate measures will have to be taken. Namely, it is important that each department clarifies which calculations they are dependent on, and who is then dependent on their outputs as well. On top of this, each department needs to be able to easily iterate the calculations once updated inputs are available.

In order to correctly navigate this process, an N2-chart was created so each department can refer back to this and find the origin and destination of all inputs and outputs respectively. This chart can be visualised in Figure 3.1, where the horizontal blocks represent outputs of certain departments while the vertical blocks describe inputs for each department. Besides this, each diagonal block characterises one of the departments involved in the design process. Next to the N2-chart, each department shall also make sure that updated input values can be easily processed. In order to achieve this, programs like Excel or Python are consulted where the altered values are incorporated as variables so variations can be simply updated.

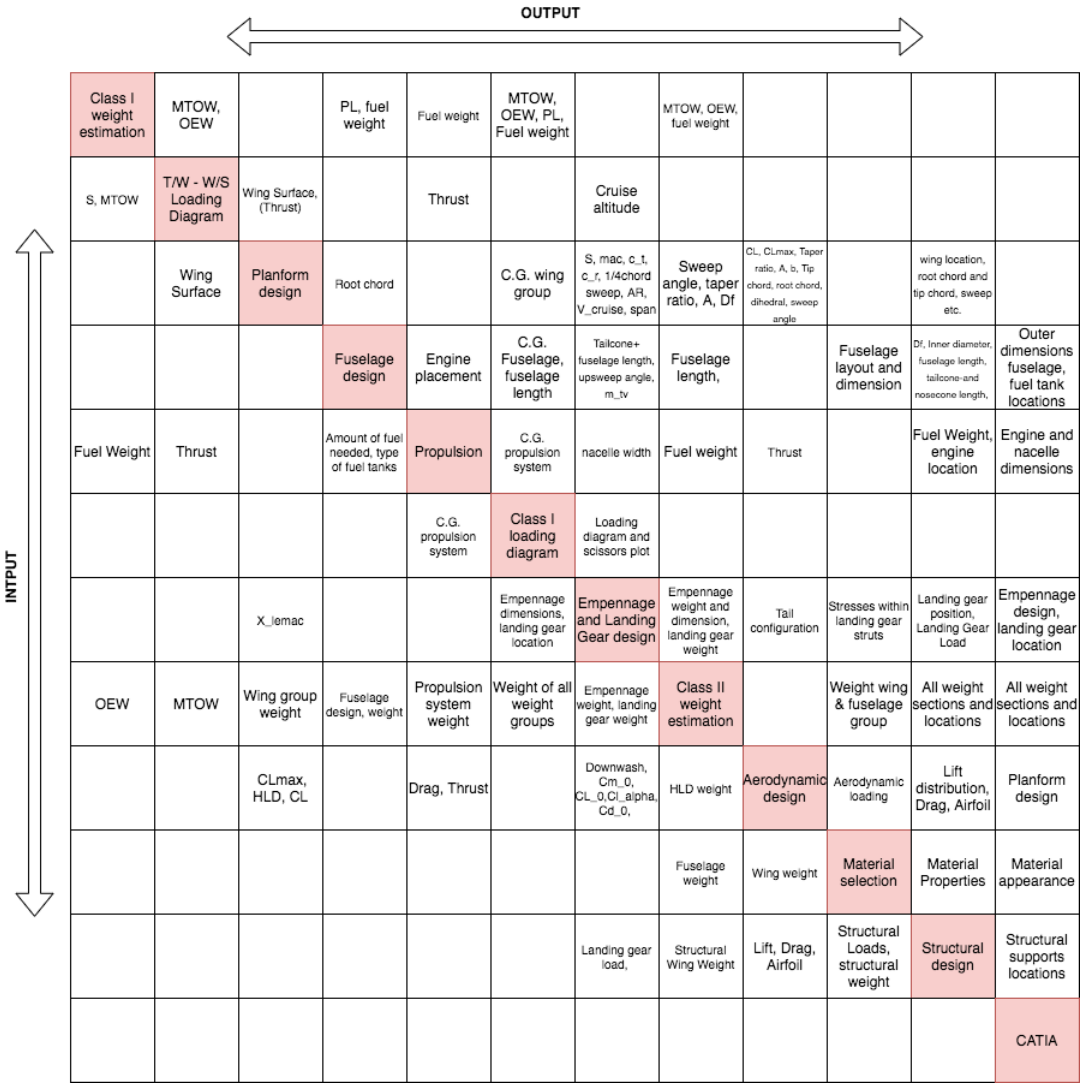

Figure 3.1: N2 chart applied for the iteration process

4
Preliminary Design

This chapter addresses the early design choices regarding the Unmanned Cargo Aircraft. These results form the basis for all technical departments which will eventually be implemented to form the finalised design. The early design choices are mainly based on the requirements which will be presented in Section 4.1. In Section 4.2, the technical design methodology is explained. Next up, the class I weight estimation is introduced in Section 4.3. After, the T/W-W/S diagram and the subsequent planform design are presented in Section 4.4 and Section 4.5 respectively. Next, the fuselage layout and design is discussed in Section 4.6. Ultimately, in Section 4.8 both verification and validation procedures are described as well as the budgets. Conclusively, the findings of the preliminary design will be concluded in Section 4.9.

4.1. Requirement Analysis

The aircraft should adhere to a number of requirements, originating from communication with the stakeholder. These requirements drive the entire design and are listed below, so they should be adhered to at all times:

- **REQ-STK-03:** The UCA shall transport a quantity of goods similar to what fits in a road capable delivery van.
- **REQ-SYS-FLT-2.3.03:** The UCA shall have a wing span smaller than 24 $[m]$.
- **REQ-SYS-MIS-3.1.00:** The UCA shall have a range of at least 3000 nautical miles for maximum payload.
- **REQ-SYS-MIS-3.1.01:** The UCA shall carry at least 2 metric tonnes of payload.
- **REQ-SYS-MIS-3.1.02:** The UCA shall have a payload volume capacity of at least 5 $[m^3]$.
- **REQ-SYS-MIS-3.1.03:** The UCA shall be able to carry 4967 $[kg]$ of fuel to reach the desired range safely.
- **REQ-SYS-MIS-3.1.04:** The UCA shall have 500 $[kg]$ of reserve fuel to loiter for 45 minutes. ***CS 25.343 Design fuel and oil loads*** [5]

4.2. Technical Design Methodology

Once the configuration and mission objective for the aircraft have been determined, the weight estimation can initialise. This design step uses a tool where based on different empirical relations, first order and more elaborated estimations on for example the MTOW, OEW and fuel weight can be formed. After the class I weight estimation has been performed, the class II weight estimation can be executed based on inputs following from the prior estimation. Only when the OEW results of class II are within 1% of the OEW flowing from class I, no further iteration is required and the design process can continue. At the same time, these weight estimations also form an input for other branches of the preliminary design such as planform design, fuselage design and fuselage layout.

4.3. Class I Weight Estimation

In order to determine different weights of the aircraft, dozens of methodologies exist which can be applied. Based on the preliminary weight estimations as described in [6], a Class I weight estimation could be performed next adhering to the analytical theory of Roskam.

From linear regression of reference aircraft which are ought to have resembling characteristics, preliminary estimates on the relation between OEW and MTOW could be determined. Next up, through use of the fuel fractions method based on statistics a preliminary estimate on the fuel weight could be derived. In order to achieve this, multiple first order estimations on lift and drag coefficients had to be made, as well as for the specific fuel consumption, aspect ratio and cruise speed. Based on empirical data provided by the theory of Roskam, values for these parameters were derived from a combination of both transport and business jets, due to comparable performance requirements. For this, additional fuel to loiter was also taken into account as proposed by **REQ-SYS-MIS-3.1.04**. Additionally, variables like the range and payload weight were obtained from the requirements posed by the stakeholder.

Eventually, the computed OEW, together with the found fuel weight and required payload amount to the new MTOW that can all be used in the next stage of the design. The values are presented in Table 4.1, and will later form the input for the class II weight estimation.

Table 4.1: Weight results from class I weight estimation

Component	Weight [kg]
OEW	6231
Payload	2000
Wfuel	4967
MTOW	13198

4.4. T/W-W/S Diagram

After the class I weight estimation has been completed, the next step is to generate a T/W-W/S diagram. In order to accomplish this, many parameters will have to be estimated flowing from empirical data again. Based on this diagram, the aircraft can be sized for different flight phases hence increasing the development of the design already at this stage.

Firstly, suitable values for the maximum lift and drag coefficients will have to be estimated. From this, the first vertical relations in the diagram can be plotted which sizes the aircraft for stall speed by means of the lift equation. Subsequently, based on the requirement regarding maximum take-off distance following from CS25, a Take-Off Parameter (TOP) was selected from an empirical relation derived by Roskam. From this quantification, the aircraft could also be sized in terms of take-off through Equation 4.1 and Equation 4.2.

$$TOP_{jet} = \left(\frac{W}{S}\right)_{TO} \cdot \left(\frac{W}{T}\right)_{TO} \cdot \frac{1}{C_{Lto}} \cdot \frac{1}{\sigma} = k \qquad (4.1)$$

$$C_{L_{TO}} = \frac{C_{L_{\max,TO}}}{1.1^2} \qquad (4.2)$$

In Equation 4.1, σ represents the density ratio which can be set equal to 1 since take-off is performed at sea level. By replacing $(\frac{W}{S})$ with 'x' and $(\frac{W}{T})$ with 'y' and linearly varying 'x', the relation can be graphed and the limitations on the sizing with respect to take-off can be visualised. Similarly, from another statistical relation by Raymer a plot can be generated describing the sizing limitations in terms of landing and cruise speed. For both these design parameters, appropriate values have to be identified with respect to velocity and weight for that flight phase.

Moreover, the aircraft also needs to be sized for climb performance. This subject can be divided into climb rate performance as well as climb gradient performance. The former only requires a desired climb rate c together with an optimum lift over drag ratio for this type of maneuvering before its curve can be included in the graph. In the mean time, the latter implements a relation between the rate of climb over the velocity to form this horizontal plot. Lastly, the T/W-W/S can be concluded by a relation describing the sizing in the aspect of maneuvering performance. This relation is mainly based on the maximum load factor, following from CS25 requirements. Ultimately, combining all plots together in a diagram is equivalent to the T/W-W/S which is showed in Figure 4.1.

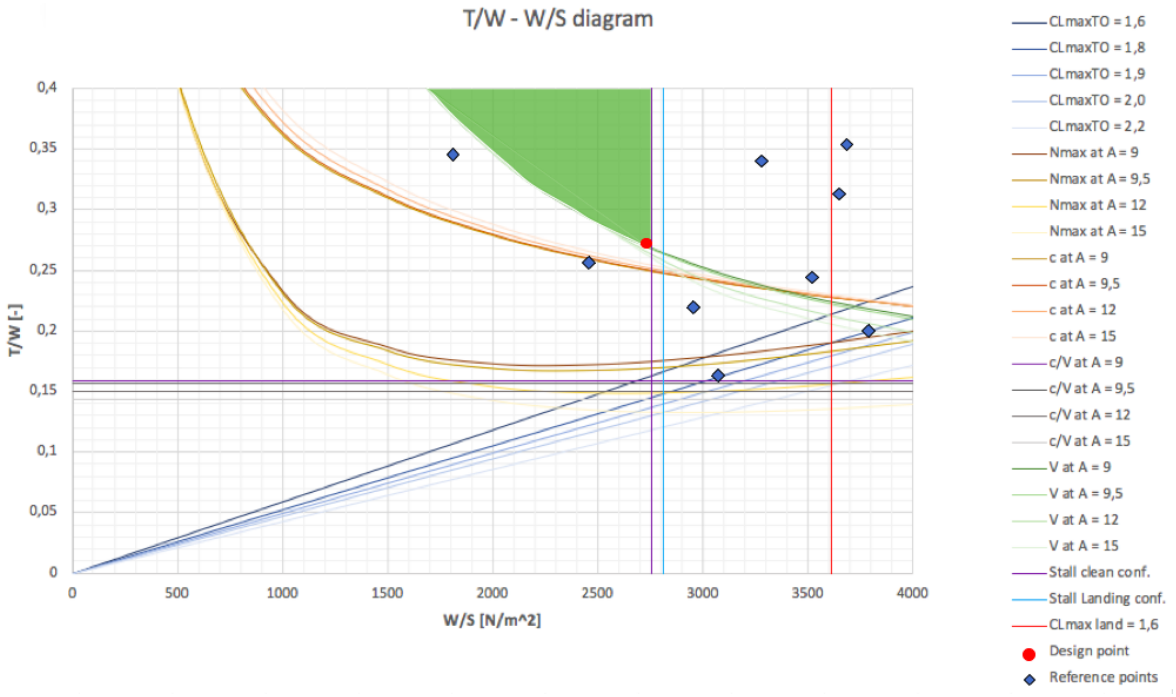

Figure 4.1: T/W-W/S diagram for the UCA

In Figure 4.1, all the different relations of T/W and W/S can be visualised for each different flight phase. As can be concluded from the legend on the right, each of these relations is plotted for different values of either the lift coefficient or the aspect ratio. In this way, it can be easily found which parameter poses a limitation on the design and must thus be adhered to. With respect to the y-axis, the T/W of the UCA may not be lower than the highest flight phase curve. Besides this, with respect to the x-axis the wing loading of the aircraft shall be smaller than the lowest vertical wing loading plot. This leaves the UCA with a design space that is indicated by the green coloured area in the diagram.

The objective is to place the design point such that the aircraft will have the highest possible wing loading, while having the lowest possible thrust-to-weight ratio. This yields that the placement of this design point shall be as much to the right and as much down as possible. As can be seen above, the design is constrained by stall in clean configuration, as well as cruise speed performance. In other words, the aircraft shall have an aspect ratio of at least 9.5 while having a maximum clean lift coefficient of at least 1.7. It should be noted that the blue diamonds in the graph represent reference aircraft to validate the decision for the design point. The final design point is indicated by the red dot, having a T/W of 0.27 and a W/S of 2755 $[N/m^2]$.

4.5. Planform Design

The wing planform of the aircraft can be designed after the T/W-W/S diagram has been constructed. Using the wing loading and the maximum take-off weight from the class I weight estimation the wing surface can be calculated. With a wing loading of 2755 $[N/m^2]$ and a MTOW of 12.9 $[kN]$, the wing surface has been determined to be 46.97 $[m^2]$. Other values that are needed, is the $C_{L_{max}}$, assumed to be 1.7 and the aspect ratio which is 9.5, selected from the T/W-W/S diagram.

4.5.1. Wing Sweep

The first step is to determine the sweep angle, this is done using the method from Torenbeek [7]. For this the drag divergence mach number, M_{dd} is needed, which is 0.03 higher than the mach cruise number, M_{cruise}. The mach number at cruise can be calculated using Equation 4.3, where V_{cruise} and a are the cruise speed and speed of sound respectively in $[m/s]$.

$$M_{cruise} = \frac{V_{cruise}}{a} \tag{4.3}$$

With a service ceiling of 41000 feet as in Section 4.4 the speed of sound can be calculated using Equation 4.4, where γ is the adiabatic gas constant, (1.4 [−]), R is the specific gas constant, (287 $[J/kg \cdot K]$), and T is the absolute temperature in $[K]$.

$$a = \sqrt{\gamma RT} \tag{4.4}$$

Using the same maximum design cruise speed of 222 $[m/s]$ and a speed of sound of 295 $[m/s]$, the M_{cruise} and M_{dd} have been determined to be 0.753 and 0.783 respectively.

The relation of the quarter chord sweep angle with the drag divergence mach number can be found in Torenbeek [7]. A M_{dd} of 0.783 results in a quarter chord sweep angle, $\Lambda_{0.25c}$ of 25 degrees.

4.5.2. Taper Ratio

The next main design parameter of the wing is the taper ratio which is the ratio between the tip and root chord. This controls the span-wise lift distribution, changing this parameter will have consequences for the structural weight of the wing, the lift induced drag and wing stall characteristics. High aspect ratio's and low taper ratio values may be beneficial for the structural weight, but then the maximum lift coefficients close to the tip will be lower due to a reduction in the local Reynolds number when compared to the root [8].

In order to determine the taper ratio, Equation 4.5 [7] can be used, which is only dependant on the quarter chord sweep angle in degrees. The taper ratio is determined to be 0.3127.

$$\lambda = 0.2\left(2 - \Lambda_{0.25c}\frac{\pi}{180}\right) \tag{4.5}$$

Several wing dimensions can now be calculated with the taper ratio. The wing span and root chord are calculated with Equation 4.6 and Equation 4.7 respectively and the tip chord is calculated using the taper ratio.

$$b = \sqrt{SA} \tag{4.6}$$

$$c_r = \frac{2S}{(1+\lambda)b} \tag{4.7}$$

In both equations, b is the wing span in $[m]$, S is the wing surface in $[m^2]$, A is the aspect ratio and c_r is the root chord in $[m]$. Based on the values above the wing span was found to be 21.1 [m], therefore satisfying **REQ-SYS-FLT-2.3.03**. With the acquired dimensions the mean aerodynamic chord can be obtained graphically which is 2.35 $[m]$.

For the preliminary design the thickness-to-chord ratio is limited to 18% thickness, in later stages the thickness can be changed to reduce for example the drag or to improve stall characteristics. The thickness is limited by the mach drag-divergence and the half chord sweep angle, $\Lambda_{0.5c}$ as can be seen in Equation 4.8.

$$(t/c) = \min\left[\begin{array}{c} \frac{(\cos\Lambda_{0.5c})^3\left(M^\dagger - M_{dd}\cos\Lambda_{0.5c}\right) - 0.115\hat{C}_L^{1.5}}{(\cos\Lambda_{0.5c})^2} \\ 0.18 \end{array}\right] \tag{4.8}$$

Using Equation 4.8 the upper limit due to drag divergence is 0.169. For this calculation the cruise lift coefficient has to be calculated which is done at cruise altitude. And a first order estimation of the spars are positioned at 20% and 75% of the local chord length.

The default dihedral angle for unswept wings at mid-wing location is 3 degrees, but since the aircraft has a low-wing configuration 2 degrees have to be added. And for every 10 degrees of quarter-chord sweep angle, the dihedral angle should be reduced by 1 degree resulting in a dihedral angle of 2.5 degrees [9]. The final preliminary dimensions of the wing planform can be found in Table 4.2.

Table 4.2: Summary Wing Dimensions

	Dimensions
Wing Span $[m]$	21.1
Wing Surface $[m^2]$	47.0
Root Chord $[m]$	3.39
Tip Chord $[m]$	1.06
MAC $[m]$	2.35
Sweep Angle 0.25c [deg]	25.0
$(t/c)_{max}$ $[-]$	0.169
Dihedral angle [deg]	2.5

4.6. Fuselage Design and Layout

After the wing planform has been designed, it is time to determine the dimensions of the fuselage. This includes sizing the fuselage length, diameter. On top of this, also the inner layout of the fuselage shall be identified while also taking into account the cargo and fuel. Eventually, the cargo and fuel placement over the fuselage shall be accounted for as well.

4.6.1. Inner Fuselage

The first step in the fuselage design is to create the cross section of the fuselage for the UCA. This was done by identifying a floor location and height, together with selecting the cargo pallet dimensions. Regarding the floor, it was opted for a 0.04 [m] high floor located at 0.3 [m] from the bottom. The reasoning behind this is to reserve sufficient space for fuel tanks and other electrical systems under the floor, while also optimizing the use of space fitting the rectangular pallet inside a circular fuselage. Furthermore, in terms of the cargo pallet a PYB pallet was selected, due to the combination of its dimensions and cargo weight capacities. A PYB pallet has a standard width of 1.4 [m], length of 2.4 [m] and height of 0.03 [m] [1]. Moreover, in terms of height it has been decided to load the pallets up to a maximum height of 2.16 [m], based on the fact that the stakeholder desires to transport the cargo to and from the aircraft in a typical-sized van [2] as stated in **REQ-STK-03**.

By means of a technical sketch, the floor and cross section of the pallet were surrounded by a circular inner fuselage with the smallest radius to minimize the experienced drag and weight. However, small clearances have been taken into account to allow that due to offsets during loading procedures neither the cargo or the aircraft will be damaged. This sketch can be visualised in Figure 4.2.

[1] `https://www.satco-inc.com/air-cargo-pallets/` [Accessed on: 26-05-2021]
[2] `https://www.caranddriver.com/ford/transit/specs` [Accessed on: 2-06-2021]

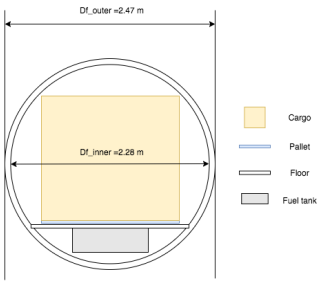

Figure 4.2: Cross section of the fuselage

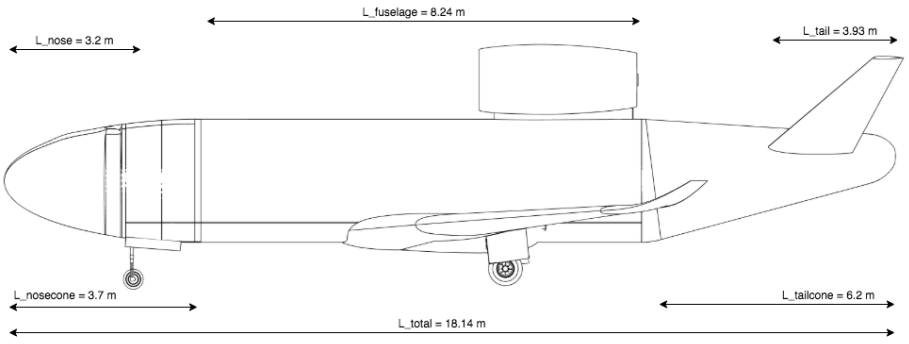

Figure 4.3: Side view of fuselage with its dimensions

As can be seen in Figure 4.2, the fuselage cross-sectional layout was sketched in scale leading to an inner fuselage diameter of 2.28 [m]. As is noticeable, the cargo, together with the pallet, floor and fuel tank are implemented in the sketch. In terms of the fuel tank, Subsection 4.6.4 will elaborate on the locations and dimensions of all different fuel tanks.

4.6.2. Outer Fuselage

Once the inner fuselage diameter has been determined, the outer fuselage diameter can be found accordingly. This procedure is executed by application of the following equation:

$$D_{f,outer} = 1.045 \cdot D_{f,inner} + 0.084 \tag{4.9}$$

In Equation 4.9[8], $D_{f,outer}$ represents the outer fuselage diameter and $D_{f,inner}$ the inner fuselage diameter respectively. This then results in an outer fuselage diameter of 2.47 [m] which can also be noted in Figure 4.2. Based on this outer diameter, the next step will then be to find the fuselage length of the UCA. This can be done through selecting a representative fineness ratio in the graph by Corke, leading to a total aircraft length of 18.14 [m]. Similarly, by means of two fineness ratios from Torenbeek and Roskam, the tail cone and nosecone length could also be identified. The fineness ratios were 2.5 and 1.5 respectively, leading to a nosecone length of 3.7 [m] and tail cone length of 6.2 [m]. Next up, exactly the same method is applied to obtain the lengths of the nose and tail as well. With a fineness ratio for the tail and nose of 1.6 and 1.3 respectively [8], a tail length of 3.93 [m] and nose length of 3.2 [m] were obtained. All these individual cone and component lengths as well as their location is structurally represented in Figure 4.3. By also implementing a scrape angle of 15 [degrees] [8] on the tail cone, the outer sizing of the fuselage is finalised.

4.6.3. Cargo

Next up, once the inner and outer fuselage are completed the fuselage itself can be equipped. As was already mentioned in Subsection 4.6.1, specifically selected air cargo pallets will be utilised to transport the goods amounting to a total weight of 2000 [kg]. A single pallet is capable of carrying up to 850 [kg] of cargo respectively [3]. Consequently, it has been decided that the fuselage shall accommodate for 3 of such PYB pallets lined up in sequential order to make the payload requirements **REQ-SYS-MIS-3.1.01** and **REQ-SYS-MIS-3.1.02**. Hence, in total the aircraft can allow for 3 pallets weighing a combined amount of 2550 [kg]. Notwithstanding this, this increased payload capacity is at the cost of a smaller range since less fuel can be carried as the MTOW is reached earlier in this scenario.

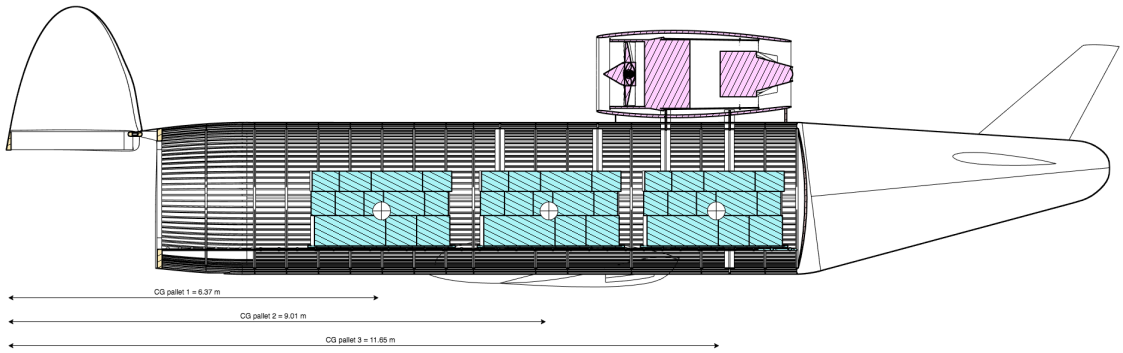

Figure 4.4: Centre of gravity locations of the cargo pallets

[3] https://www.satco-inc.com/air-cargo-pallets/ [Accessed on: 26-05-2021]

As can be concluded from the figure above, the configuration of the placed pallets is described. The first pallet starts at an longitudinal location of 5.16 [m] starting from the nose and is 2.44 [m] long. In between each pallet, there will be a clearance of 0.2 [m] to account for offsets and anchoring of the cargo. The last pallet will end at a location of 12.97 [m] starting from the nose. As can be concluded from this, the payload is placed more or less in the very middle of the aircraft. This is due to the fact that the cargo pallets are rather large, and thus require the full diameter of the fuselage. Since both the nose-and tail cone have a smaller diameter and make up for a substantial part of the total fuselage, these areas are unsuitable for placement of the cargo. By taking into account this, together with the centre of gravity range and scissor plot these locations were agreed upon. The final placement of the pallets can be seen in Figure 4.4. Since the nose-and tail cone remain unloaded until this stage, these available volumes are assigned to the placement of fuel tanks as well as other subsystems as will be described in Subsection 4.6.4 and Chapter 13.

4.6.4. Fuel

In order to cover the range requirement of 5556 [km] following from **REQ-SYS-MIS-3.1.00**, a significant amount of fuel will have to be carried by the UCA. To be exact, a total amount of 4967 [kg] fuel will be needed to fly this range as was determined during the class I weight estimation in Section 4.3 hence satisfying **REQ-SYS-MIS-3.1.03**. However, in order to provide the opportunity to the operator to also fly longer ranges but hence with a lower payload, the fuel tanks will be able to carry an additional 25% of this design fuel weight. By means of the density of 840 $[kg/m^3]$ [4], this mass yields a required total fuel tank volume of 7.4 $[m^3]$. During the design, several suitable locations have been selected to place the fuel tanks. During this placement, multiple pros and cons were kept in mind to accomplish to most optimal configuration. These pros and cons regard weight distribution, availability of space, controllability and connection to the propulsion system. In the end, it was opted for to install 5 individual fuel tanks distributed over the centre and aft part of the aircraft which can be seen in Figure 4.5 and Figure 4.6.

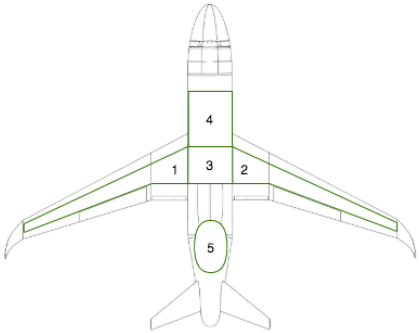

Figure 4.5: Top view of the aircraft with fuel tank locations

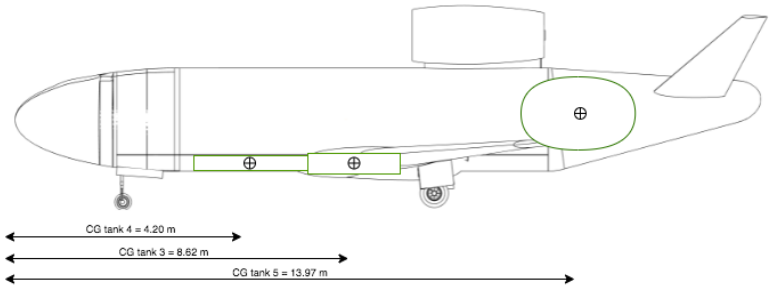

Figure 4.6: Side view of the aircraft with fuel tank locations

First of all, in both the wings fuel tank 1 and 2 will be located inside the wing box in between the front and aft spar placed at 15% and 65% respectively. These 2 fuel tanks will cover the full wing span, and have a trapezoidal shape adhering to the planform layout as can be visualised above. Taking into account the varying height of the fuel tanks, as well as implementing the assumption that only 95% of the space could be used for fuel storage, the total volume could be computed. This results in a total fuel volume of 2.79 $[m^3]$ to be carried by the two wing fuel tanks. The ideology behind the placement of these two fuel tanks was both the availability of space inside the wing, together with posing a bending stress relief on the wing structure during flight.

Moreover, inside the fuselage in between the two wings a third fuel tank is located under the floor. In this way, it does not constrain the loading of the fuselage with cargo pallets. Due to the required reinforcing structure here to join the fuselage and the wing together, a large volume is created here which is ideal to place a fuel tank. Moreover, as a result of its central location this fuel tank does not pose any issues regarding centre of gravity limits. Fuel tank 3 has a total length of 3 [m], width of 1.57[m] and height of 0.3 [m] leading to a total volume capacity of 1.4 $[m^3]$.

Next up, fuel tank 4 will be located right in front of fuel tank 3 as depicted in Figure 4.5. The reasoning behind this front fuel tank was mainly due to stability and controllability purposes which will be further clarified in Chapter 10. In short, due to this fuel tank the centre of gravity range could be shifted forward. Due to the reduced available volume here since there is no wing box intersection, this fuel tank has a significantly smaller cross section than fuel tank 3. Namely, the rectangular fuel tank 4 will have to adhere to the circular shape of the fuselage while still fitting under the floor. It has a height of just 0.25 [m], width of 0.9 [m] and is 5.44 [m] long with a total volume of 1.23 $[m^3]$.

Lastly, a total amount of 1.98 $[m^3]$ of fuel still needs to be accommodated for. Regarding the limited available space that is left, it has been opted to utilise a cylindrical fuel tank with hemispherical ends and locate it inside the tail cone.

[4] `https://www.engineeringtoolbox.com/fuels-densities-specific-volumes-d_166.html` [Accessed on: 26-05-2021]

In this way, highly efficient use is being made of the space since the configuration of this fuel tank even fits inside the oddly shaped tail. Fuel tank 5 will have a radius of 0.75 [m] and total length of 1.6 [m] as outer dimensions. In total, the entire propulsion system will thus be able to carry up to 7.4 [m^3] of fuel.

4.7. Class II Weight Estimation

After having sized the aircraft, a class II weight estimation can be performed. The new operational empty weight that will be computed by the class II estimation has to be within 1% of the OEM of the class I estimation. If the two weights differ too much from each other, iterations have to be made starting with the class I again but now implementing the result of the class II estimation on the OEW. It has been decided to select the class II weight estimation method from Raymer [9], this method consists of 18 component which are applicable to the UCA in the 'Cargo/Transporter Category'. For simplicity only the statistical relations of the wing, fuselage and empennage are discussed.

The wing structure is estimated using Equation 4.10 which is dependant several things such as the design gross weight, wing surface, sweep angle and control surface area, which is assumed to be 13% of the total wing surface. This results in a weight of 2557.4 [lbs] which is comparable to the weight from the cg excursion.

$$W_{\text{wing}} = 0.0051\left(W_{dg}N_z\right)^{0.557} S_w^{0.649} A^{0.5} (t/c)_{\text{root}}^{-0.4} (1+\lambda)^{0.1} (\cos\Lambda_{0.25c})^{-1.0} S_{csw}^{0.1} \tag{4.10}$$

The weight of the fuselage can be found using Equation 4.11, important parameters here are the type of cargo doors used,K_{door}, and how the landing gears, K_{Lg} are mounted to the fuselage. Furthermore, things such as the fuselage length and wetted surface area are needed as well as the lift-to-drag ratio. Using Equation 4.11 resulted in a weight of 3896.7 [lbs] which is higher than expected, but this can be explained by the fact that different weight estimation methods group components differently, resulting in a difference.

$$W_{\text{fuselage}} = 0.3280 K_{\text{door}} K_{Lg} \left(W_{dg}N_z\right)^{0.5} L^{0.25} S_f^{0.302} (1+K_{ws})^{0.04} (L/D)^{0.10} \tag{4.11}$$

For the empennage weight estimation, Raymer's method estimates the horizontal and vertical tail apart as expected, but the UCA has a V-tail configuration which does not comply to the equations. However, the surfaces of a conventional tail still happens to be the same despite having a 'wing' less [5]. Thus it has been decided to estimate what the empennage weight would be if a conventional tail had been used and using this as the weight for the V-tail.

All other weight components which are also taken into account for the class II weight estimation are for example the landing gears, flight control and avionics. However, since the aircraft is unmanned the furnishing and furnishing weights were discarded. One particular component which has been added to the UCA is the weight of the parachutes. Since the UCA only has one engine it was deemed necessary to have parachutes to slow down the aircraft in case of engine failure, this topic will be further elaborated upon in Section 13.2. The final values for the weight of different components can be seen in Table 4.3.

Table 4.3: Weight of separate subsystem components from Raymer class II weight estimation method.

Component	**Weight [lbs]**	**Component**	**Weight [lbs]**	**Component**	**Weight [lbs]**
Wing Structure	2557.3	Engine Controls	30.9	Avionics	1235.3
Fuselage Structure	3896.7	System Starter	64.3	Anti-ice	58.2
Horizontal Tail	416.1	Fuel Systems	580.4	Handling Gear	8.7
Vertical Tail	212.1	Flight Controls	312.8	Cargo Handling system	372.1
Main Landing Gear	671.5	Battery	75.6	Parachute	430.0
Nose Landing Gear	110.1	Hydraulics	96.6		
Nacelle Group	467.0	Electrical Weight	1944.9	**Total OEM**	30170

4.8. Verification and Validation

Throughout the preliminary design, several calculations had to be executed. As most of these were still highly conceptual and probable to change, they were mainly executed using Microsoft Excel or Python to have a clear overview of the most actual values for all departments. In this way, the process was kept as iterable as possible such that changes in the design could be easily taken care off in a later stadium. In order to ensure the correctness of all computations, numerous verification and validation practices had to be performed.

[5] `https://www.fzt.haw-hamburg.de/pers/Scholz/HOOU/AircraftDesign_9_EmpennageGeneralDesign.pdf` [Accessed on: 04-06-2021]

4.8.1. Verification

As mentioned above, all calculations have been executed using either Microsoft Excel and Python. The verification procedure consists of both manual hand calculation, as well as calculations in the contrary computer program than the one which was originally applied. The results of this verification process are presented in Table 4.4.

Table 4.4: Performed unit tests for preliminary design.

Tested Unit	**Method & Description**
Class I weight estimation	The fuel fractions method computed by means of Python was verified by hand calculations and no difference was found.
T/W-W/S Diagram	The plots for each flight phase included in the diagram were derived in Microsoft Excel and verified through hand calculations and a short Python script, leading to no observed differences.
Planform design	The relatively simple calculations were originally performed in Excel and verified by hand calculations which turned out exactly the same.
Fuselage layout	The outer dimensions of the aircraft were calculated in Excel and again verified through hand calculations, finding no difference.
Class II weight estimation	The weight of all weight groups calculated through Microsoft Excel were verified by both hand calculations and Python.

Once the unit tests are executed, system tests shall be performed to verify the entire system as a whole. Nevertheless, most of the calculations of the preliminary design were extremely simple and thus real system tests appeared to be redundant here. However, for the two weight estimations a system test was appropriate since these computations were slightly more complicated. This was done by adjusting the input of one of the weight component calculations, and monitoring the impact on the new OEW. The behaviour of both class I and class II weight estimations was linearly related to the variation in input, and thus the whole systems were verified.

4.8.2. Validation

In terms of validation, the acquired results from computation were compared to reference aircraft in general. Firstly, the findings of the class I weight estimation in Section 4.2 were validated by means of regression of the MTOW of the UCA together with the data of similar aircraft. Next up, the generated T/W-W/S diagram was validated by means of indicating the design points of reference aircraft which can be seen in Figure 4.1. As can be noticed here, the design points lie sufficiently close to the actual design point and thus validate the result.

Subsequently, the planform and fuselage design could again be validated by means of a comparison to reference aircraft. The acquired results could be regressed linearly with respect to MTOW leading to validated results in Microsoft Excel. Lastly, the class II weight estimation was validated in a similar fashion as the class I. Namely, the new results on different weights could be plotted in combination with existing aircraft which lead to the conclusion that this is also validated. On top of this, the class I and class II weight estimations were also validated by a comparison with each other, leading to a final difference of only 0.83% which is ought to be sufficiently close.

4.8.3. Sensitivity Analysis & Engineering Budget

As was forecasted in Section 3.5, contingencies did take place throughout the preliminary design which had some significant consequences. One of the budgets was especially relevant during the preliminary design, which turned out to be the weight. As a result of this, constant iteration was required in order to eventually have the class I and class II weight estimation differing less than 1% from each other.

The target MTOW value acquired during the conceptual design was 10724 [kg], by means of linear regression of reference aircraft. This value served as an preliminary input but still involved a significant level of uncertainty. Afterwards, during the class I weight estimation an updated MTOW of 13198 [kg] was found which already was determined with higher certainty. Eventually, from this class I weight estimation result a class II weight estimation could be performed. This value was established at 13250 [kg] for the final design, having a level of uncertainty of just 0.83 %.

4.9. Conclusion and Recommendations

In conclusion, the preliminary design forms the basis for more detailed design steps executed by the different technical departments. The MTOW was established at 13250 [kg], while the wing surface area and aspect ratio are 46.97 $[m^2]$ and 9.5 respectively. On top of this, the outer fuselage dimensions were all determined and the airplane will be equipped with 5 fuel tanks, in order to transport 3 loaded air cargo pallets. It is however recommended to perform another iteration on the T/W-W/S diagram once the aerodynamic department established a finite wing surface area S, if more time is available.

5
Aerodynamic Wing Design

In this chapter, the aerodynamic wing design is presented. This starts by selecting the driving requirements and stating assumptions, which is done in Section 5.1. Next up is selecting the most optimal airfoil, which is done in Section 5.2. Aerodynamic analysis of the finite wing is then done in Section 5.3, including the lift curve and drag estimation. In Section 5.4, selection and sizing of high lift devices is presented. Furthermore, the complete wing design, including final remarks, is presented in Section 5.5. Finally, verification and validation of the applied methods is discussed in Section 5.6 and a conclusion is given in Section 5.7.

5.1. Requirement Analysis

The aircraft should be as aerodynamically efficient as possible. Therefore, aerodynamic wing design should be optimized. Furthermore, the requirements that drive the aerodynamic design of the wings, should be attained at all times:

- **REQ-SUBSYS-WNG-2.3.00:** The lifting devices shall produce $9.19 \cdot 10^4$ $[N]$ of lift at a cruise speed of 222 $[m/s]$ with clean configuration at an altitude of 12497 $[m]$.
- **REQ-SUBSYS-WNG-2.2.00:** The lifting devices shall produce $1.72 \cdot 10^5$ $[N]$ of lift at take-off speed (52 $[m/s]$) in take-off configuration.
- **REQ-SUBSYS-WNG-2.2.01:** The lifting device shall produce $1.58 \cdot 10^5$ $[N]$ of lift at approach speed (48 $[m/s]$) in landing configuration.

5.1.1. Assumptions

During the aerodynamic design, various methods from literature are used to calculate aerodynamic parameters. Furthermore, software is used to simulate aerodynamic behaviour of airfoils and wings. While these methods and software are useful, limitations are present in the application. The assumptions made while applying theory and simulations should be documented:

- **Use of Prandtl-Glauert correction:** Since, $M_{cruise} = 0.75$, aerodynamic calculations have to account for compressible flow. The Prandtl-Glauert rule is accurate for Mach numbers under 0.7 [7]. Therefore, the aerodynamic calculations done with the Prandtl-Glauert correction are underestimating drag and overestimating lift. In future design, this should be further investigated.
- **Steady flow assumption:** All calculations assume steady flight and thus steady flow.
- **Incompressible flow for M < 0.2:** For landing and take-off calculations, incompressible flow was assumed. Since the corresponding flight speeds are under Mach 0.2.
- **Use of XFLR5:** Aerodynamic analysis of airfoils and the wing is mainly done with XFLR5. This program uses algorithms based on potential flow theory. This means that computations for high angles of attack are not very accurate.[1] In future design, this should be further investigated.

It should be noted that more assumptions are made for specific calculations. These are stated when used in this chapter.

5.2. Airfoil Selection

The airfoil will have an impact on several parameters during landing, take-off and cruise. Therefore an extensive analysis on the final airfoil selection is important. The first step in the airfoil selection process is to determine the design lift coefficient of the airfoil. This is done for the flight condition at which the aircraft will fly most of the time, which is cruise flight. The desired lift coefficient is derived from the required aircraft performance during cruise. The design lift coefficient for the wing is calculated using Equation 5.1. This equation considers that the weight changes during the cruise due to fuel consumption. To compensate for fuel consumption, the average weight between the start and end of cruise is taken.

$$C_{L_{deswing}} = 1.1 \frac{1}{q} \left\{ \frac{1}{2} \left[\left(\frac{W}{S} \right)_{start\_cruise} + \left(\frac{W}{S}_{end\_cruise} \right) \right] \right\} \tag{5.1}$$

[1] `http://www.xflr5.tech/docs/Part%20IV:%20Limitations.pdf` [Accessed on: 11-06-2021]

The total lift coefficient was overestimated by 10% due to the negative lift contribution from the tail. However, the design lift coefficient obtained from Equation 5.1 is for the finite (three dimensional) wing. In order to convert the design lift coefficient from the wing to the airfoil lift coefficient, Equation 5.2 is used. This equation takes the sweep angle of the wing into account. Since the sweep angle is dependent on the selected airfoil, the sweep angle used in Equation 5.2 is based on an initial estimate of 25°. The final sweep angle will be calculated with the help of the Mach drag divergence number.

$$C_{l_{des}} = \frac{C_{L_{deswing}}}{cos(\Lambda)^2} \tag{5.2}$$

The cruise Mach number (M_{cruise}) for the aircraft is 0.75. The comparison of different airfoils will be done for $M_{cruise} = 0$ (due to the limitations of Xfoil). The actual airfoil design coefficient has to be adjusted for this. This can be done with the Prandtl-Glauert compressibility correction given by Equation 5.3, where $C_{l_{des0}}$ is the design airfoil lift coefficient for $M_{cruise} = 0$. To comply with the cruise lift requirement **REQ-SUBSYS-WNG-2.3.00** (see Section 5.1), all further aerodynamic design is based on the calculated value of $C_{l_{des0}}$ from Equation 5.3.

$$C_{l_{des0}} = C_{l_{des}} \cdot \sqrt{1 - M_{\infty}^2} \tag{5.3}$$

With $C_{l_{des0}}$ known, the airfoil selection process can be started. The airfoil selection will be based on this parameter, since different airfoils can have a different optimum $C_{l_{des0}}$. A total of five supercritical airfoils were considered for an airfoil trade-off. Initially, the plan was to also include NACA 6-series airfoils in the trade-off, due to their ability to encourage laminar flow [10]. However, it was soon established that, for $M_{cruise} = 0.75$, the NACA 6-series airfoils suffer from strong shock waves due to sonic flow conditions on the airfoil [10]. The calculated wing sweep to then prevent sonic flow conditions on the 6-series airfoils exceeded the maximum sweep angle given by the structures department. Therefore, the 6-series airfoils were not considered in the trade-off.

Supercritical airfoils are designed to increase the Mach drag divergence number, delay the formations of supersonic shock waves on the upper wing surface and decrease the strength of said shockwaves [10]. A supercritical airfoil is flatter on the top, rounded on the bottom, and the trailing edge is accented with a downward curve to restore lift lost by flattening the upper surface[2]. At the current high subsonic cruise speed, the use of a supercritical arfoil means less drag. This allows the aircraft to get to destinations faster with less fuel, while also resulting in a longer range.

For the airfoil trade-off, multiple supercritical airfoils were considered, with each having different thicknesses and characteristics. Multiple criteria influence the selection of best possible airfoil. Some important airfoil trade-off criteria are [10]:

- **Thickness to chord ratio:** The thickness to chord ratio influences the stall characteristics, zero-lift drag coefficient and the drag-divergence Mach number of an airfoil. Furthermore, a high thickness to chord ratio allows for a lighter wing structure, more fuel storage space in the wing and more space to store the landing gear.
- **Airfoil design lift coefficient:** Each airfoil has an optimum lift coefficient. It is important that this optimum airfoil lift coefficient is close to the earlier calculated value for $C_{l_{des0}}$. Essentially, this means the airfoil is used in it's optimum condition, with the least drag as a result.
- **Drag divergence Mach number (M_{dd}):** A high M_{dd} means that M_{cruise} can be higher without the aircraft having to suffer a heavy drag penalty due to the formation of shockwaves on the wing.
- **Maximum airfoil lift coefficient (C_{lmax}):** A high C_{lmax} means less high lift devices are needed to meet take-off and landing requirements.
- **Minimum airfoil drag coefficient (C_{dmin}):** Ideally, C_{dmin} should be as low as possible.
- **Width of the drag bucket:** All airfoils compared in the trade-off have a drag bucket in the C_l/C_d curve. It is preferred that this drag bucket is wider, as the value of $C_{l_{des0}}$ might change in future design stages.
- **Stall behaviour:** A smooth stall behaviour is preferred for an airfoil. This can be deducted from the C_{l_α} curve of an airfoil. A steep drop in C_l after stall should be avoided.
- **Airfoil moment coefficient (C_m):** The value for C_m should be as low as possible, since a wing with high aerodynamic moment needs a larger tail surface for static stability. Furthermore, less C_m also means less torsional loads on the wing, leading to a lighter wing structure.

Furthermore, a complete overview of all trade-off criteria can be found in Table 5.1.

All the airfoils have been analyzed with XFLR5. XFLR5 is an analysis tool for airfoils, wings and planes. Due to the limitations of XFLR5 the results for the high angles of attack may be overestimated. However, as all the airfoils are compared with the same program and at the same conditions the trade-off is still valid and useful. The input of the Reynolds number for all the airfoils will be the same and the Reynolds number is calculated with Equation 5.4.

[2] `https://www.nasa.gov/pdf/89232main_TF-2004-13-DFRC.pdf`[Accessed on: 02-06-2021]

$$Re = \frac{\rho V \overline{c}}{\mu} \tag{5.4}$$

With the use of the aforementioned methods and using Xfoil (incorporated in XFLR5), five supercritical airfoils could be compared in a trade-off. The results of the airfoil trade-off are presented in Table 5.1. Note that a green cell means that the corresponding airfoil is the best choice for the corresponding criterion. Multiple airfoils can be the best choice for a single criterion. Furthermore, if all airfoils have an equal score in a criterion, the cells are marked in orange and no points are given. This is the case for the criterion: is CL cruise inside the drag bucket?

Table 5.1: Airfoil Trade-off Table

Airfoil:	**SC(2)-0406**	**SC(2)-0410**	**SC(2)-0412**	**SC(2)-0414**	**LG10SC**
Thickness ratio (Highest is best)	0.06	0.1	0.12	0.14	0.1
Cl for AOA = 0 (Close to Cl-des is best)	0.17	0.24	0.276	0.317	0.11
AOA for Cl = 0	-1.4	-2	-2.2	-2.5	-1
Cl_max (Highest is best)	1.81	2.13	2.18	2.23	1.86
AOA for Cl_max (Highest is best)	17	20	21	22	19
Behaviour after Stall	Smooth	Less Smooth	Less Smooth	Less Smooth	Smooth
Cd_min (Lowest is best)	0.0053	0.0057	0.0059	0.006	0.0048
Cl of Cdmin (Close to cruise is best)	0.20	0.30	0.33	0.32	0.36
(Cl/Cd)_max (Highest is best)	105	116	130	130	144.5
Cl of (Cl/Cd)max (Low Cl is best)	1.17	1.05	1.26	1.47	1
Cm_cruise	-0.044	-0.074	-0.083	-0.092	-0.0092
Drag buckets starts at Cl	-1	-0.6	-0.3	-0.2	0.1
Drag buckets ends at Cl	0.8	0.6	0.4	0.4	0.5
Is CL cruise inside drag bucket	Yes	Yes	Yes	Yes	Yes
M_crit @ AOA of Cldes	0.558	0.623	0.635	0.641	0.612
M_dd	0.928	0.877	0.852	0.827	0.877
Total Score:	**3**	**1**	**1**	**5**	**5**

From Table 5.1 it can be seen that the SC(2)-0414 airfoil and the LG10SC airfoil are the winners of the trade-off. The SC(2)-0414 airfoil performs better on the maximum C_l at the highest AOA and has a value of C_l at a zero AOA closer to $C_{l_{des0}}$. On the other hand, the LG10SC airfoil has a lower $C_{d_{min}}$ and a higher C_l/C_d at a lower C_l. The LG10SC airfoil also has a lower C_m.

In the end, the SC(2)-0414 airfoil was selected as the preferred airfoil to use. This is due to the fact that the SC(2)-0414 airfoil has a higher thickness to chord ratio than the LG10SC airfoil, resulting in a lighter wing and more space for fuel storage. The geometry of the SC(2)-0414 airfoil is shown in Figure 5.1[3].

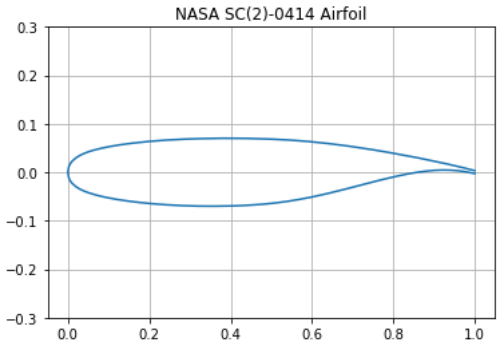

Figure 5.1: NASA SC(2)-0414 geometry

5.3. Finite Wing Analysis

With the final airfoil selected, the actual full wing design can be started. This section will describe how the wing lift curve is established with all the relevant parameters, a drag analysis will be performed, which includes the zero lift drag coefficient and the lift induced drag.

[3] `http://airfoiltools.com/airfoil/details?airfoil=sc20414-il` [Accessed on: 08-06-2021]

5.3.1. Wing lift curve

The wing lift curve was evaluated with the DATCOM method. The method is based on both numerical and experimental data [9]. Therefore the method is also valid for the subsonic speeds the UCA is operating at. First the wing lift curve was evaluated using Equation 5.5 [11].

$$\frac{dC_L}{d\alpha} = C_{L_\alpha} = \frac{2\pi AR}{2 + \sqrt{4 + \left(\frac{AR\beta}{\eta}\right)^2 \cdot \left(1 + \frac{tan^2 \Lambda_{0.5c}}{\beta^2}\right)}} \tag{5.5}$$

In Equation 5.5 β is the Prandtl-Glauert compressibility correction factor. This factor is calculated with Equation 5.6 where M_∞ is the freestream Mach number. The other parameters used in the equation are $\Lambda_{0.5c}$ which is the sweep angle with respect to the half chord line and η is the airfoil efficiency factor. As there is no experimental data on the supercritical airfoil a value of 0.95 was used, which is a good approximation [11].

$$\beta = \sqrt{1 - M_\infty^2} \tag{5.6}$$

With the slope of the lift curve evaluated, the trim angle of attack during cruise can be calculated using Equation 5.7. In this equation α_{trim} is the required angle of attack and α_{0L} is the zero lift angle of attack which is obtained from the airfoil analysis in XFLR5. To reduce the trimming of the aircraft the incidence angle of the wing is equal to the trim angle of attack. The wing incidence angle (i_w) is the angle of the wing with respect to the fuselage.

$$\alpha_{trim} = \frac{C_{L_{des}}}{C_{L_\alpha}} + \alpha_{0L} \tag{5.7}$$

Next up is the maximum lift coefficient $C_{L_{max}}$ of the wing, at landing and take-off conditions. This coefficient is determined using Equation 5.8. The $C_{l_{max}}$ is maximum lift coefficient of the airfoil itself obtained by the airfoil analysis. $\frac{C_{L_{max}}}{C_{l_{max}}}$ and $\Delta C_{L_{max}}$ are obtained from literature [9]. It should be noted that for low speeds the last term in Equation 5.8 is not relevant. This is due to the fact that this factor accounts for the effect of the Mach number higher than 0.2. Thus, for the landing and take-off evaluation this factor is not used [11].

$$C_{L_{max}} = C_{l_{max}} \left(\frac{C_{L_{max}}}{C_{l_{max}}}\right) + \Delta C_{L_{max}} \tag{5.8}$$

With the $C_{L_{max}}$ of the wing is obtained, the stall characteristics of the wing can be analysed. The stall angle of attack of the wing is computed using Equation 5.9. Where α_{0L} is the airfoil zero lift angle of attack and $\Delta\alpha_{C_{L_{max}}}$ accounts for the non linear effects of the leading edge (LE) vortices [11].

$$\alpha_{stall} = \frac{C_{L_{max}}}{C_{L_\alpha}} + \alpha_{0L} + \Delta\alpha_{C_{L_{max}}} \tag{5.9}$$

The stall angle obtained from this equation will still be an estimation due to complex flow behaviour during stall. More research should be done in this field with the help of for example CFD simulations.

Now the most important parameters for the finite wing design related to the lift are analysed. This has been done for both cruise conditions as well as for landing conditions at sea-level in clean wing configuration. The method described in this section was used for several iterations to come up with the most efficient wing design. Furthermore, with the parameters obtained in this section, the the high lift devices (HLDs) can be sized. This will be discussed in Section 5.4, together with the wing lift curve plots.

5.3.2. Drag Analysis

The drag of the aircraft can be divided into two different components. Namely, the zero lift drag coefficient (C_{D_0}) and the drag due to the lift of the aircraft. First the zero lift drag of the aircraft will be analysed and after that the lift induced drag component. After the computation of those two components the drag polar curve can be established. This is done by merging the two different components into Equation 5.10.

$$C_D = C_{D_0} + \frac{C_L^2}{\pi ARe} \tag{5.10}$$

Zero Lift Drag Analysis

The zero lift drag coefficient is estimated for every aircraft separately and summed up to get the total. All the values are calculated at the cruise conditions of the aircraft. Two methods can be used to calculate the zero lift drag coefficient. Namely, the equivalent skin-friction method and the component build-up method [11]. As the first one is simpler but less precise, the component build-up method is used. The zero-lift drag of each component can be calculated with Equation 5.11. The equation takes account of the individual drag of each component adds them all up and divides the total drag delivered by the surface area. However, the zero-lift drag of some of the components are difficult to calculate exactly. Therefore $C_{D_{misc}}$ is added which also includes the drag from special features such as flaps and the landing gear.

$$C_{D_0} = \frac{1}{S_{ref}} \sum_{c}^{n} C_{f_c} \cdot FF_c \cdot IF_c \cdot S_{wet_c} + C_{D_{misc}} \tag{5.11}$$

The main drag components are the wing, fuselage, nacelle and V-tail. The equation consist out of 4 parameters. C_{f_c} is the skin friction coefficient. This coefficient describes the drag of a longitudinal flow along a flat plate. The skin friction coefficient is dependent on the Reynolds number and on the type of boundary layer. The component can experience both laminar and turbulent flow. The higher the laminar flow percentage the lower the friction as the turbulent boundary layer is thicker and therefore has a higher friction. As there is no exact procedure to calculate the percentage of laminar flow, reference data is used. Based on this reference data the percentage of laminar flow on the wing and tails is 35% and on the fuselage this is 10% [11]. The skin friction coefficient for laminar flow can be calculated via Equation 5.12 and for turbulent flow via Equation 5.13. The total friction coefficient is the weighted average of the laminar and turbulent C_f [11].

$$C_f = \frac{1.328}{\sqrt{Re}} \tag{5.12}$$

$$C_f = \frac{0.455}{(log_{10}Re)^{2.58}(1+0.144M^2)^{0.65}} \tag{5.13}$$

The next parameter in Equation 5.11 is the component form factor. The component form factor (FF_c) estimates the pressure drag due to viscous separation. The wing and V-tail both have the same equation to calculate this factor and for the fuselage and nacelle there are specific equations. The form factor equations are retrieved from literature [9][12]. The last factor is the interference factor (IF_c), this factor estimates the effect of each component on the drag of the other components. The interference factor of the different components is retrieved from literature. There is no interference factor for the fuselage, because the interference of the components exist with the fuselage. The interference drag appears due to the fact that at the connection of two components there is a boundary layer interaction. This will result in a thicker boundary layer. The final parameter is the wetted surface area of all the components. For each component a different equation was obtained from literature [7].

With the all the components described above the total zero lift drag coefficient was calculated of each component and 5% of the total drag was added to compensate for excrescence and leakage which is represented by $C_{D_{0,misc}}$. The final values and the total C_{D_0} can be seen in Table 5.2.

Table 5.2: The C_{D_0} values for the main components

Coefficient	Value
$C_{D_{0,wing}}$	0.00498
$C_{D_{0,fuselage}}$	0.00734
$C_{D_{0,vtail}}$	0.00176
$C_{D_{0,nacelle}}$	0.000817
$C_{D_{0,misc}}$	0.000744
$C_{D_{0,total}}$	0.0156

Lift Induced Drag

The lift induced drag is the second part of Equation 5.10. The lift induced drag is dependent on the Oswald efficiency factor e and the effective aspect ratio of the wing. The effective aspect ratio of the wing is different compared to the normal aspect ratio as the effect of the wing tip shape should be taken into account. It is chosen to equip the aircraft with a raked wing tip. This wing tip will increase the aspect ratio by 0.5 - 1.5 [11]. This means that the tip is positioned further back than the rest of the wing. The raked wing tips improves fuel efficiency due to the higher aspect ratio and diminish wingtip vortices [13].

As there is no specific equation to calculate the exact increase in aspect ratio it is assumed that the increase will be 0.75 to compensate for the yehudi placed to store the landing gear. The second parameter in the equation is the Oswald efficiency factor. The initial estimation for the Oswald factor was 0.85. However, as this is this is an initial estimation and does not take into account sweep a new Oswald efficiency factor had to be calculated. This was done using Equation 5.14 [14]. Where most of the parameters are already discussed expect for N_e which is the number of engines on the wing, which is zero for the aircraft, and $f(\lambda)$. This parameter can be calculated with Equation 5.15 where λ is the wing taper ratio.

$$e = \frac{1}{(1+0.12M^2)\left(1+\frac{0.142+f(\lambda)\cdot A\cdot(10\cdot\frac{t}{c})^{0.33}}{(cos\Lambda_{25})^2}+\frac{0.1\cdot(3N_e+1)}{(4+A)^{0.8}}\right)} \tag{5.14}$$

$$f(\lambda) = 0.005\left(1+1.5(\lambda-0.06)^2\right) \tag{5.15}$$

Combining the increased effective aspect ratio and the new Oswald efficiency factor the lift induced drag component was calculated. Together with the zero lift coefficient, which was obtained earlier, Equation 5.10 was filled in for various lift coefficients. The resulting drag polar is plotted in Figure 5.2

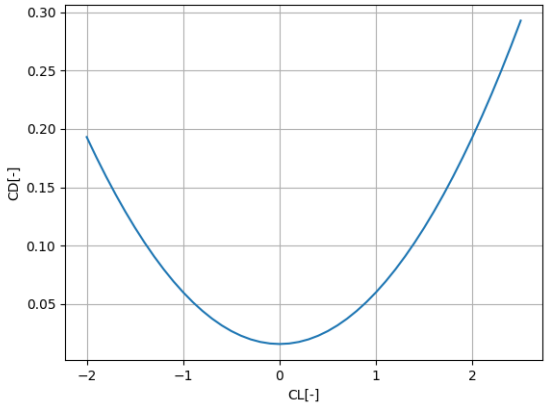

Figure 5.2: Drag polar of the aircraft during cruise

5.4. High Lift Devices

Now the finite wing analysis is finished and the wing is optimised for cruise conditions performance. As a consequence of this the $C_{L_{max}}$ obtained in clean configuration at low speed will not meet the requirements defined by the performance department for landing and take-off conditions. In order to meet those requirements, high lift devices (HLDs) are needed. HLDs allow for an increase in lift during take-off and landing while also keeping the most optimal performance during cruise flight. There are two types of HLDs, namely HLDs placed at the leading edge of the wing and HLDs placed at the trailing edge of the wing. For the UCA, only trailing edge HLDs are used.

The design process of the HLDs was started by evaluating the $\Delta C_{L_{max}}$. This value was computed by taking the difference between the maximum C_L of the wing in clean configuration at landing conditions and the $C_{L_{maxlanding}}$ required for take-off and landing due to requirements. As landing flight needed the highest value of C_L this value was used for the sizing of the HLDs. The maximum lift coefficient needed during landing was multiplied by a value of 10% due to the negative lift created by the empennage to trim the aircraft.

The increase in the maximum lift coefficient can be calculated using Equation 5.16 [7] for both leading edge and trailing edge devices. For the trailing edge hinge line sweep angle, the hinge line was selected to be at 7.5% chord after the rear spar. This 7.5% chord buffer comes from the fact that this space should be available for control system elements.

$$\Delta C_{L_{max}} = 0.9\Delta C_{l_{max}}\frac{S_{wf}}{S}cos\Lambda_{hingeline} \tag{5.16}$$

Initially, the plan was to also use a leading edge HLD. However, during the preliminary sizing it became clear that a leading edge HLD was not needed. The maximum lift coefficient could be decreased slightly and therefore no leading edge HLDs where needed anymore. This saves weight and decreases the complexity of the wing.

Thus in the end, only trailing edge HLDs where used. Therefore, all the required difference in maximum lift coefficient

($\Delta C_{L_{max}}$) had to come from the trailing edge HLDs. The chosen type of trailing edge HLDs are flaps. There are different kinds of flaps, where the most commonly used ones are: plain, slotted and Fowler flaps [11]. For the current design, single slotted flaps were chosen due to their simplicity and low weight. Furthermore, single slotted flaps take up less space inside the wing compared to Fowler flaps.

With the help of Equation 5.16 $\frac{S_{wf}}{S}$ was calculated. After some iterations with updated values given by the performance department it was confirmed that the chosen single slotted flaps provide enough $\Delta C_{L_{max}}$ to reach the desired $C_{L_{max}}$ values of 2.2 and 2.42 (for take-off and landing respectively).

A margin of 10 cm between the fuselage and the trailing edge flaps was chosen. This was done to ensure the flaps can extend to the maximum deflection angle and taking into account some margin for installation and maintenance. The final values of the sizing, placement and deflection angle for both take-off and landing can be seen in Table 5.3.

Table 5.3: Final design HLDs with all the parameters

Parameter	**TE HLD**
Flap type	**Single slotted flap**
S_{wf}/S	0.626
Starting position [bi/(b/2)]	0.13
Ending position [bo/(b/2)]	0.70
$\delta_{ftake-off}$	10 °
$\delta_{flanding}$	40 °

After the final sizing of the HLDs the lift curve of the wing in landing and take-off configuration could be computed. The new lift curves have a higher $C_{L_{max}}$ and are shifted to the left due to the application of the HLDs. The shift of the zero lift angle of attack was calculated using Equation 5.17. For $\Delta\alpha_{0l_{airfoil}}$ -15° is used for landing and -10° for take-off. After that the increase of the slope due to the flapped wing was evaluated using Equation 5.18. Here, S' is the increased wing surface area by the extended flaps. As the slotted flaps do not increase the wing surface area the lift curve slope does not change and the slope obtained for clean, landing conditions was used.

$$\Delta\alpha_{0_L} = (\Delta\alpha_{0_l})_{airfoil}\frac{S_{wf}}{S}cos\Lambda_{hingeline} \tag{5.17}$$

$$C_{L_{\alpha flapped}} = \frac{S'}{S}C_{L_{aclean}} \tag{5.18}$$

Using both equations the new lift curve for the flapped wing in both configurations can be computed. The lift curve for take-off configuration can be seen in Figure 5.3 and for landing in Figure 5.4. Note that $C_{L_{max}}$ for take-off and landing have values of 2.2 and 2.42 respectively, as was required by the flight performance department. With the HLD's sized for these values of $C_{L_{max}}$, the design complies with **REQ-SUBSYS-WNG-2.2.00** and **REQ-SUBSYS-WNG-2.2.01**: the lift requirements for take-off and landing (see Section 5.1).

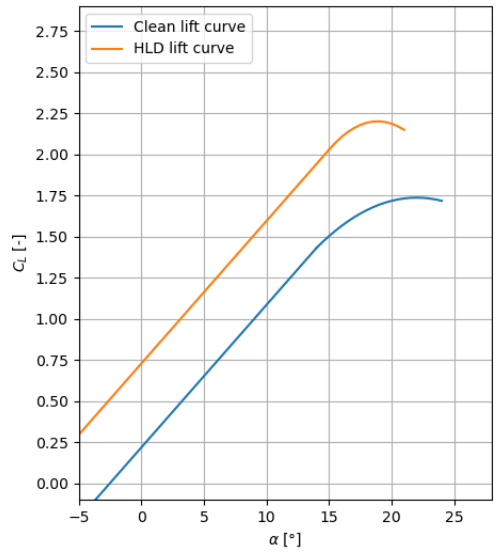

Figure 5.3: $C_{L\alpha}$ curve for the aircraft in take-off configuration

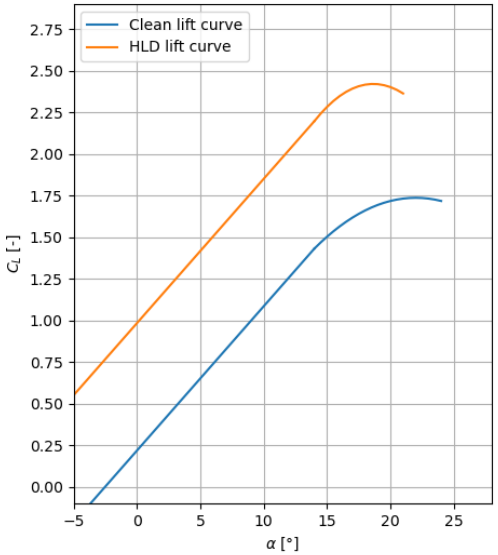

Figure 5.4: $C_{L\alpha}$ curve for the aircraft in landing configuration

5.5. Final Remarks on Wing Design

As was stated in Subsection 5.3.2, the wings will have raked wing tips to increase the aspect ratio and aerodynamic performance. Furthermore, a wing twist of -3 degree is included in the final wing design, to reduce the chances of tip-stall and increase the spanwise lift distribution [11].

With these final additions and the calculated wing dimensions from the performance department (see Chapter 4), the wing design can be presented. Figure 5.5 shows a 3D isometric view of the current wing design. Figure 5.6 show the top view of the wing planform design.

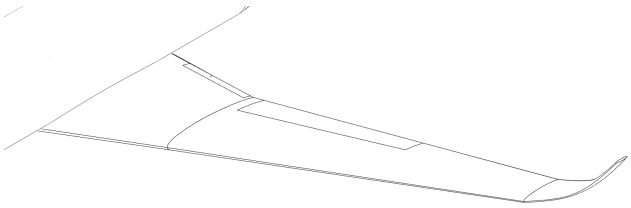

Figure 5.5: Isometric view of the wing design

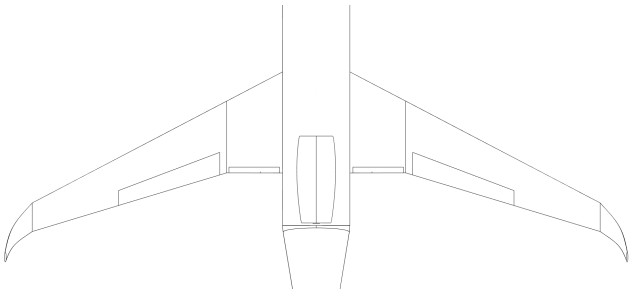

Figure 5.6: Top-view of the wing planform design

5.6. Verification and Validation

For all computations done in this chapter, Python and Excel tools were built for an effective iteration process. These tools had to be verified and validated to ensure correct, accurate calculations.

5.6.1. Verification of Tools

For all units of code, verification by inspection was done first. This allowed for the discovery of multiple code errors, as well as some equations not being up to date. Furthermore, it was discovered that the calculations for the Reynolds numbers did not take into account the wing sweep, resulting in a too high Reynolds number calculation. The Reynolds numbers for cruise, landing and take-off were adjusted, and the XFLR5 analysis was done again.

Next, all units of Python and Excel code were tested with manual calculations. For the Excel tools, some small errors (< 1%) were encountered due to the trigonometric definitions that Excel uses. For the Python tools, computer accuracy was achieved.

System tests were also done, to check if the calculations behave as expected. The most important system tests for the DATCOM calculations are:

- **Calculation of $C_{L_{max}}$:** Increasing $C_{l_{max}}$ of the airfoil should lead to an increase of the calculated $C_{L_{max}}$, according to Equation 5.8. This is verified to be the case.
- **Calculation of C_{L_α}:** Decreasing the Mach number leads to a decrease in C_{L_α} in the system. Graphs in Raymer [9], show that this is indeed the case.
- **Calculation of α_{trim}:** An increase in $C_{L_{des}}$ should lead to an increase in α_{trim} and vice versa, according to Equation 5.7. It is verified that this is indeed the case.
- **Calculation of α_{stall}:** According to ADSEE-II lectures [11], lowering the aspect ratio AR increases α_{stall} of a wing. This is also verified to be true in the code outputs.

This playing around with variables was also done for all other system code from both Excel and Python tools (including plots). Verification was done for all but one case: the case where the Mach number M = 1. The Prandtl-Glauert correction introduces a singularity, since it diverges to infinity for M = 1. However, with the current cruise speed of the aircraft of M = 0.75, this does not pose a problem for correct functioning of the calculation tools.

5.6.2. Sensitivity Analysis

A sensitivity analysis was done for the airfoil trade-off. Since most direct influence on the trade-off comes from the airfoil design lift coefficient ($C_{l_{des}}$), this parameter is used to measure sensitivity. $C_{l_{des}}$ was increased in small steps, until the outcome of the trade-off showed a different winner. The same was done with decreasing $C_{l_{des}}$. The results of the sensitivity analysis are shown in Table 5.4. Note that $C_{l_{des}}$ = 0.294 is the original situation, where the currently selected SC(2)-0414 airfoil is the winner.

Table 5.4: Results of the airfoil trade-off sensitivity analysis

Situation	**Δ %**	**Winner**
$C_{l_{des}} = 0.294$	-	SC(2)-0414
$C_{l_{des}} > 0.4$	+36.25	LG10SC
$C_{l_{des}} < 0.205$	-30.17	LG10SC

5.6.3. Validation

The outcomes of the aerodynamic design should also be validated. For validation of $C_{L_{cruise}}$ and $C_{D_{cruise}}$, data[4] from reference aircraft is used. With data from the reference aircraft shown in Table 5.5, $C_{L_{cruise}}$ can be calculated with the lift equation. According to ADSEE-I lectures [8], typical values for $(L/D)_{cruise}$ for business jets range between 10 and 12. A range for $C_{D_{cruise}}$ is then calculated by dividing $C_{L_{cruise}}$ by the values of $(L/D)_{cruise}$.

Table 5.5: Validation table with reference Aircraft

Aircraft	$\mathbf{C}_{L_{cruise}}$	$\mathbf{C}_{D_{cruise}}$	$\mathbf{(L/D)}_{cruise}$	$\Delta\%\ C_L$	$\Delta\%\ C_D$
UCA	0.351	0.0212	16.6	-	-
Cessna Citation III	0.220	0.0183-0.0220	10-12 *	37	4-14
Gulfstream G200	0.246	0.0205-0.0246	10-12 *	30	3-16
Fokker 100A	0.293	0.0244-0.0293	10-12 *	17	15-38

As can be seen in Table 5.5, the values for $C_{L_{cruise}}$ and $C_{D_{cruise}}$ are within an acceptable difference, for this stage of the design.

Furthermore, the values of $C_{L_{max}}$ that are calculated in Section 5.4 can be validated using figure Figure 5.7. In Figure 5.7, typical $C_{L_{max}}$ values for different HLD configurations are displayed. The wing section with a single slotted flap shows a $C_{L_{max}}$ of up to 2.9. It should be noted that this value is for a wing section and that for a 3D wing, the value will probably be lower. Nevertheless, the calculated value of $C_{L_{max}}$ for the UCA's finite wing is about 2.4 for landing and 2.2 for take-off. This allows for some validation, because it shows that the calculated values for $C_{L_{max}}$ are in the right ballpark.

5.7. Conclusion and Recommendations

The finalized aerodynamic wing design resulted in the selection of the NASA SC(2)-0414 airfoil. Furthermore, the finite, three dimensional wing was analyzed for lift and drag, and single slotted flaps were selected and sized to act as HLDs for the wing. The resulting drag polar and C_{L_α} curves were plotted, demonstrating that $C_{L_{max}}$ (2.42 and 2.2 for take-off and landing respectively) could be achieved with flaps deployed.

It should be noted that the chosen airfoil, due to it's thickness to chord ratio of 0.14, could suffer from steep, abrupt stall behaviour [10]. Therefore, it is recommended that further wing analysis is done for angles of attack close to the stall angle of attack. This could be done with a CFD analysis. In the future, it could also be decided to incorporate an anti stall response in the UCA's control system, to prevent the aircraft from getting too close to the stall angle of attack.

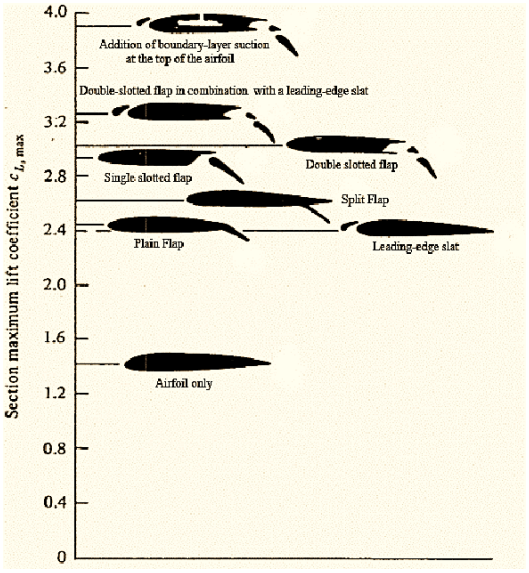

Figure 5.7: Typical $C_{L_{max}}$ values for different HLD configurations [15].

[4] `https://customer-janes-com.tudelft.idm.oclc.org/janes` [Accessed on: 14-06-2021]

6
Flight Performance

This chapter discusses the flight performance of the Unmanned Cargo Aircraft. The performance characteristics is dependant on many factors, ranging from the aerodynamic properties such as C_L and C_D, to propulsion for thrust settings and the mission objectives for which the aircraft should be designed for. The mission profile is first discussed in Section 6.2 followed by the manoeuvre and gust diagrams Section 6.3 from the design load factors can be obtained. The climb and descent performance during take-off, cruise and landing as well as gliding flight is discussed in Section 6.4. Moreover, the airfield and cruise performance are elaborated upon in Section 6.5 and Section 6.6 respectively. Finally, the turning flight performance is analysed in Section 6.7 and the chapter will end with verification and validation in Section 6.8.

6.1. Requirement Analysis

The requirements for the flight performance analysis are listed below in this section.

- **REQ-SYS-FLT-2.2.03:** The UCA shall have a required take-off runway less than 2000 [m] at maximum take-off weight and 0 [m] ISA.
- **REQ-SYS-FLT-2.2.04:** The UCA shall have a required landing runway less than 1500 [m] at maximum landing weight and 0 [m] ISA.
- **REQ-SYS-FLT-2.2.05:** The UCA shall be able to take-off and land safely on dry runways with a 90°cross component of wind velocity of at least 37 [km/h] (20 knots) or 0.2 V_{SR0}, whichever is greater.
- **REQ-SYS-FLT-2.2.06** The UCA shall be able to safely abort take-off up to the decision speed of 46 [m/s].
- **REQ-SYS-FLT-2.3.00:** The UCA shall have a cruise speed of 650 [km/hr].
- **REQ-SYS-FLT-2.3.01:** The UCA shall have a cruise altitude of 11000 [m].
- **REQ-SYS-FLT-2.4.04:** The UCA shall have a reference stall speed V_{SR} of 51.4 [m/s], which may not be less than a 1-g stall speed.
- **REQ-SYS-FLT-2.4.05:** The UCA shall have a steady gradient of climb which may not be less than 3.2%, with a climb speed of at least 1.13 V_{SR} in landing configuration with all engines operating.
- **REQ-SUBSYS-CON-2.4.00:** The UCA shall have manoeuvring capabilities able to perform a bank angle of 40° en-route in a constant speed coordinated turn at forward centre of gravity.
- **REQ-SYS-MIS-3.1.00:** The UCA shall have a range larger than 3000 nautical miles for the design payload.

6.2. Mission Profile

The mission profile of the UCA is shown in Figure 6.1 where the first step is to start up the engine in order to taxi to the runway. After take-off the UCA will climb from 1500 [ft] to the initial cruise altitude. As the aircraft is flying to the destination, fuel is being burned which leads to losing weight in flight. Therefore, the most optimal cruise level at cruise speed will increase, thus the UCA will climb in steps until it has reached the service ceiling of 41000 [ft]. Once the cruise phase comes to an end, the aircraft will descent and prepare for approach to land at the destination. However, in case of a missed approach or busy airports the UCA may have to loiter. The UCA will then climb to the designated loiter altitude where it will descent once again, when given permission to, in order to land.

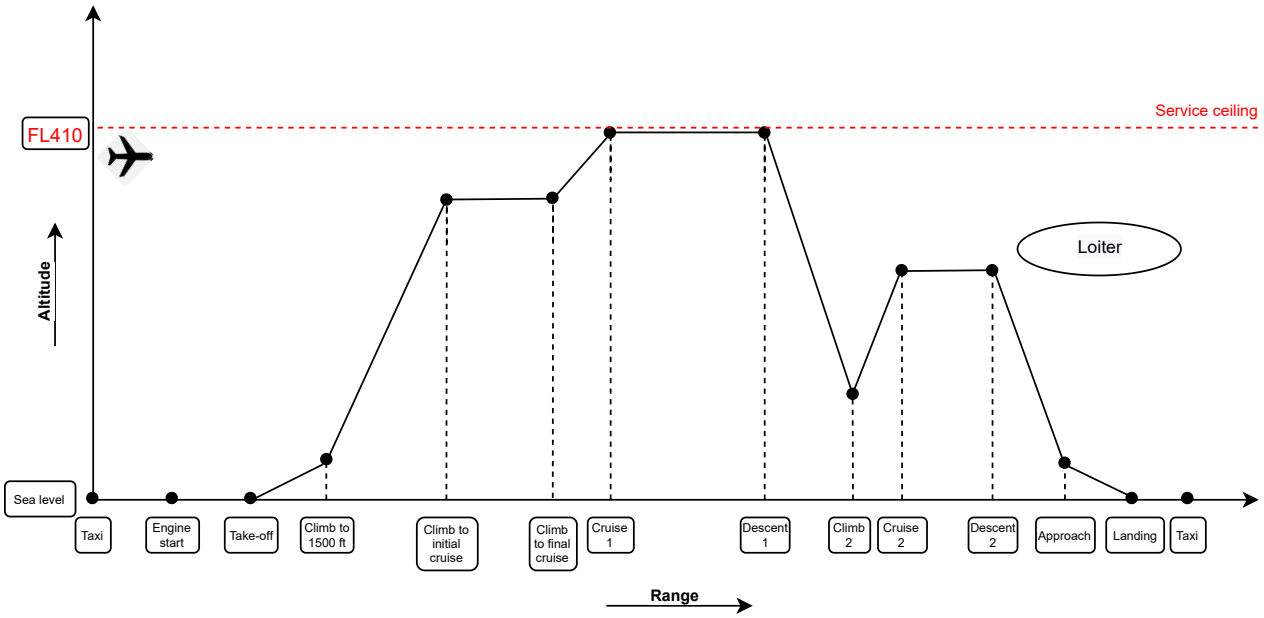

Figure 6.1: The mission profile of the UCA

6.3. Manoeuvre and Gust Diagram

The manoeuvre and gust diagram are important for determining the maximum load factors for which the UCA should be designed for. It shows the load factors that can be reached at various airspeeds which are limiting to the overall aircraft performance. First, the manoeuvre diagram is constructed followed by the gust diagram.

The first step in constructing a manoeuvre diagram is to determine the maximum and minimum load factors. For aircraft with a MTOW between 4100 and 50000 [lbs] the following relation in Equation 6.1 is given [16] and the minimum load factor is -1.

$$n_{max} = 2.1 + \frac{24000}{10000 + W} \tag{6.1}$$

Using a maximum take-off weight of 29102 [lbs] the maximum load factor which should be able to be achieved during manoeuvres is 2.713. Hereafter, the different speeds have to be determined. V_S is the calibrated stall speed when the load factor is 1. Since the stall speed depends on the aircraft configuration and altitude, the manoeuvre diagram will be constructed in clean configuration at sea level conditions. V_A is the minimum speed at which n_{max} is reached, this can be determined using Equation 6.2.

$$V_A = \sqrt{\frac{2n_{\max} mg}{C_{L_{\max}} S}} \tag{6.2}$$

V_C is the design cruise speed at sea level conditions, which is 687 [km/h] had been determined in Section 4.4 when constructing the T/W-W/S diagram, and the dive speed or maximum allowable speed V_D is 1.5 times higher than the cruise speed [16]. The manoeuvre diagram is outlined in blue in Figure 6.2 and shows how the airspeeds and load factors are related to each other.

The gust diagram is based on the possible loads which can be experienced due to gusts. V_B is located where the maximum gust speed and stall curve intersect, if a pilot flies slower than V_B the aircraft may stall in bad weather and therefore V_B is then considered as the lower limit. This speed can be calculated using Equation 6.3

$$V_B = V_{s1}\sqrt{1 + \frac{K_g(\mu_g) U V_C a}{498 w}} \tag{6.3}$$

where V_{s1} is the stall speed in clean configuration, U is the gust load and V_C is the cruise speed in [ft/s]. a is the lift curve slope and w is the wing loading in [lbs/ft^2], K_g is defined by Equation 6.4 and μ_g is given by Equation 6.5.

$$K_g = \frac{.88\mu_g}{5.3+\mu_g} \tag{6.4}$$

$$\mu_g = \frac{2w}{\rho cag} \tag{6.5}$$

In Equation 6.5 ρ is the density in $[slug/ft]$, c is the mean aerodynamic chord in $[ft]$ and g is the gravitational acceleration in $[ft/s^2]$. Furthermore, there are three limits for gust speeds at sea level, these are shown in Table 6.1.

Table 6.1: Maximum gust limits for various speeds and altitude [16]

Altitude	V_B	V_C	V_D
0-20000 ft	66 fps	50 fps	25 fps
20000-50000 ft	66 → 38 fps	50 → 25 fps	25 → 12.5 fps

The additional load factor, Δn caused by the gust can be calculated using Equation 6.6.

$$\Delta n = \frac{\rho V C_{L_\alpha} U}{2(W/S)} \tag{6.6}$$

The Δn is added to the load factor of 1 and then plotted in the gust loading diagram at the corresponding velocities, the result of the gust envelope is outlined in orange and can be seen in Figure 6.2. Figure 6.2 shows that the highest load factor achievable at sea-level is 3.4, the 1-g stall speed is 45.2 $[m/s]$ and the gusts the aircraft can withstand at different airspeeds.

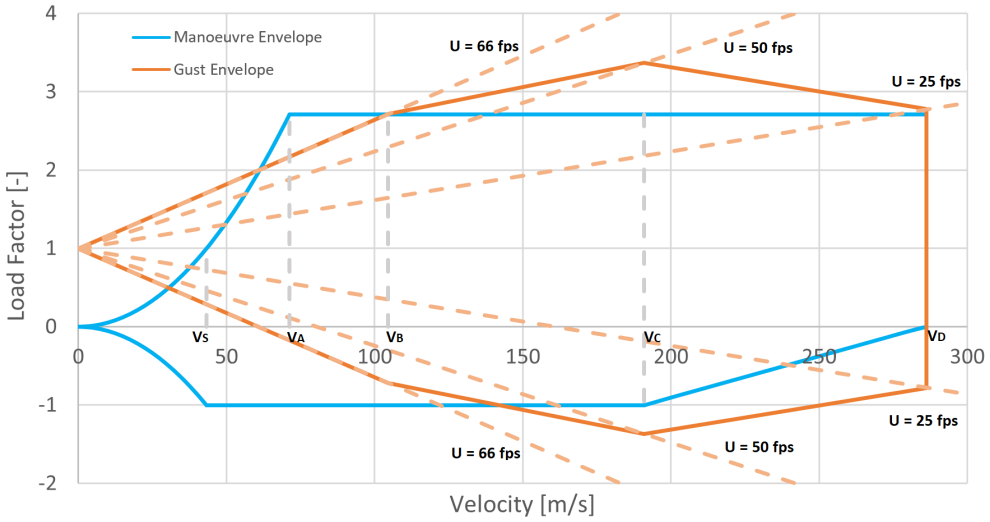

Figure 6.2: Manoeuvre and gust diagram of the Unmanned Cargo Aircraft at sea-level.

6.4. Climb and Descent

Having a good climb and descent performance is important for the aircraft during take-off and landing. Depending on the environment, aircraft may have to avoid obstacles during take-off or due to noise abatement regulations aircraft may have to follow at steeper descent angles during landing. A large part of the analysis will be performed in steady symmetric flight in which the general equations of motion shown in Equation 6.7 and Equation 6.8 are used.

$$T\cos\alpha_T - D - W\sin\gamma = 0 \tag{6.7}$$

$$L - W\cos\gamma + T\sin\alpha_T = 0 \tag{6.8}$$

Using the small angle approximation the equations of motion reduce to Equation 6.9 and Equation 6.10 respectively.

$$T - D - W\sin\gamma = 0 \tag{6.9}$$

$$L - W = 0 \tag{6.10}$$

6.4.1. Take-Off

For take-off, the climb angle and rate of climb are calculated since these will be the most important performance characteristics during this phase.

The climb angle, γ, can be calculated using Equation 6.11 for which the thrust, drag and weight are needed during take-off in $[N]$.

$$\sin\gamma = \frac{T - D}{W} \tag{6.11}$$

The take-off thrust is the maximum engine thrust available which is 37969.3 $[N]$ as determined in Section 7.4 and the maximum take-off weight is 129428 $[N]$ as mentioned in Section 4.7. The drag force can be calculated using Equation 6.12, which is dependant on the drag and lift coefficient as well as the weight.

$$D = \frac{C_D}{C_L} W \tag{6.12}$$

Using the relation in Equation 6.10, the lift coefficient can be calculated using Equation 6.13, where ρ is the sea level density (1.225 $[kg/m^3]$), V is the take-off speed (52.17 $[m/s]$), which is 1.1 times higher than the stall speed during take-off [17] and the wing surface in $[m^2]$. The drag coefficient is found using Equation 5.10.

$$L = W = C_L \frac{1}{2} \rho V^2 S \tag{6.13}$$

Combining the results, the climb angle during take-off is 11.63 $[deg]$. The rate of climb (ROC) at take-off can be found using Equation 6.14, which is simply the difference between the power available and power required divided by the weight. The same values used for the climb angle calculation can be used for determining the rate of climb which results in a ROC of 10.66 $[m/s]$.

$$RC = \frac{TV - DV}{W} = \frac{P_a - P_r}{W} \tag{6.14}$$

6.4.2. Cruise

The altitude will have a certain effect on the climb performance of an aircraft. An increase in altitude will results in a lower power available due to lower thrust levels caused by a lower air density and the power required increases. The maximum rate of climb will thus decrease and the velocity at which this is achieved, increases with altitude.

From climb to cruise altitude the climb angle will vary, the climb path will have a curvature with becomes less steep when closer to the cruise altitude. In order to do so the velocity will change over time, thus unsteady climb, $\frac{dV}{dt} \neq 0$ and it may be assumed that the climb path is quasi-rectilinear, $\frac{d\gamma}{dt} \approx 0$. With these assumptions in mind the actual rate of climb may be calculated using Equation 6.15.

$$\frac{RC}{RC_{\text{steady}}} = \frac{1}{\left[1 + \frac{V}{g}\frac{dV}{dH}\right]} \tag{6.15}$$

In Equation 6.15 V is the true airspeed in $[m/s]$, g is the gravitational acceleration in $[m/s^2]$ and dV/dH is given by Equation 6.16.

$$\frac{dV}{dH} = V_{EAS} \frac{d}{dH}\left(\sqrt{\frac{\rho_0}{\rho}}\right) \tag{6.16}$$

For compressible flows, the equivalent airspeed which has been accounted for compressibility effects should be adjusted to for the air density as can be seen in Equation 6.17. The adjusted speed is the true airspeed at which the aircraft is really flying at in the air.

$$V_{TAS} = \sqrt{\frac{\rho_0}{\rho}} V_{EAS} \tag{6.17}$$

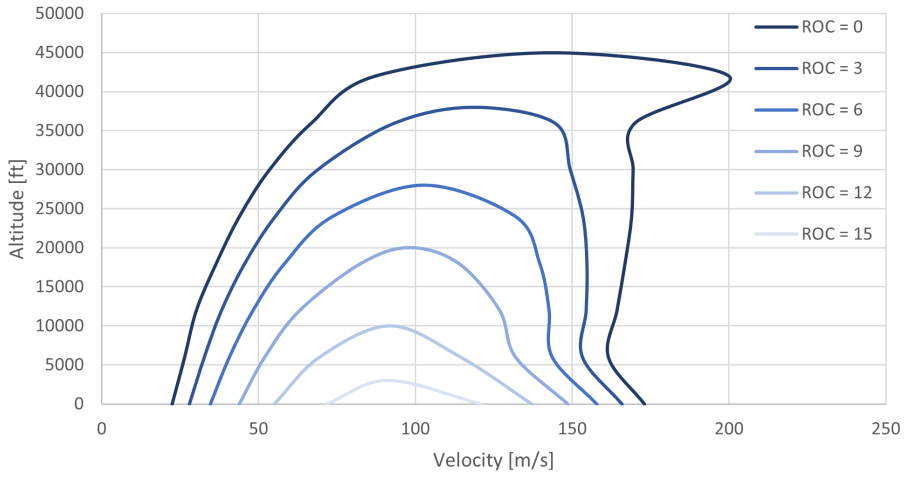

Figure 6.3: Constant rate of climb with varying altitude and speed

In Figure 6.3 the constant rate of climb lines are graphed in an altitude versus velocity plot. This plot shows the effect the altitude has on the rate of climb and the theoretical ceiling at which an aircraft could fly. The UCA has a theoretical ceiling of approximately 45000 $[ft]$ since this is the highest altitude at which the rate-of-climb is 0, and given that the definition for the service ceiling is defined by a maximum rate of climb of 2.5 $[m/s]$, the service ceiling is located at approximately 41000 $[ft]$.

6.4.3. Landing

During the approach phase to the runway, the aircraft normally follows a 3 degree glide slope with the help of a glide slope transmitter. After passing a certain point the aircraft will use other visual indicators to reach the touchdown point. The landing speed is 56.84 $[m/s]$, which is 1.3 times higher than the landing stall speed [17] and using the glide slope angle and calculating the drag during landing resulted in a thrust of 21.2 $[kN]$ using Equation 6.11.

6.4.4. Gliding Flight

The glide performance of the UCA is important to investigate since the aircraft has only one engine. If engine failure happens during cruise the only option would be to glide to a safe location to land and emergency parachutes will be used to minimize the damage. In clean configuration at a cruise altitude of 38000 ft. the average glide angle is 4.42 degrees for optimum CL during cruise calculated using Equation 6.18

$$\bar{\gamma} = \sin^{-1}\left(\frac{C_D}{C_L}\right) \tag{6.18}$$

The optimal glide speed can be calculated using Equation 6.19 in which $C_{L_{opt}}$ for gliding flight is defined by $\sqrt{\frac{C_D}{k}}$. The glide speed is also calculated using the values during cruise, this resulted in an airspeed of 122 $[m/s]$

$$V = \sqrt{\frac{W}{S}\frac{2}{\rho}\frac{1}{C_{L_{opt}}}} \tag{6.19}$$

The glide ratio of the UCA is 13 in clean configuration, and in case of engine failure at FL380 the UCA is able to glide a distance of 150 $[km]$ to a safe location for touch down.

6.5. Airfield Performance

The airfield performance depends once again on several factors, such as the air density, weight and flap settings. During take-off it is for example beneficial to have a high lift coefficient and low aircraft weight and during landing thrust reversers and spoilers help slowing the aircraft down. The performance analysis will be done at sea level conditions and the following assumptions are made in order to calculate the take-off and landing distances:

- Ground effect will not be taken into account.
- The wind has zero velocity, meaning there will be no headwinds or tailwinds influencing the aircraft .
- The runway has no slope.

6.5.1. Take-Off

The take-off length consists of the parts, the ground run and an airborne phase as can be seen in Figure 6.4. First, the ground run will be elaborated upon, followed by the airborne phase and what happens in case of engine failure.

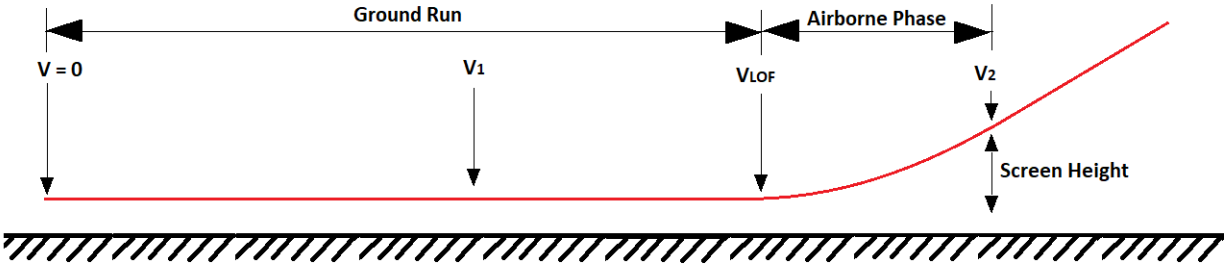

Figure 6.4: Caption

The ground run distance can be calculated with Equation 6.20 where V_{LOF} is the lift off speed which is 1.05 times higher than the minimum airspeed in $[m/s]$, and $\bar{a}$ is the average acceleration from stand still till lift off in $[m/s]$.

$$s = \frac{V_{LOF}^2}{2\bar{a}} \tag{6.20}$$

The average thrust and drag forces in Equation 6.21 are calculated at a speed which is $V_{LOF}/\sqrt{2}$. With respect to V_{LOF}, a value of 49.8 $[m^2]$ was obtained which is equal to 1,05 times the stall speed. It is assumed that the aircraft takes-off with an engine setting at 95% N1 and the friction coefficient which is needed to calculate the ground friction drag in Equation 6.22 has been determined to be 0.05. The ground run distance which is needed is 1047 $[m]$ and taking into account a 15% buffer [17] the required field length without engine failure for take-off is 1204 $[m]$

$$\bar{a} = \frac{g}{W}(\bar{T} - \bar{D} - \bar{D_g}) \tag{6.21}$$

$$\bar{D_g} = \mu(W - \bar{L}) \tag{6.22}$$

The airborne phase can be further divided into a transition and climb phase which are given by Equation 6.23 and Equation 6.24 respectively.

$$x_{trans} = \frac{V_{lof}^2}{0.15g}\sin\gamma_{climb} \tag{6.23}$$

$$x_{climb} = \frac{h_{scr} - (1-\cos\gamma)\frac{V_{lof}^2}{0.15g}}{\tan\gamma} \tag{6.24}$$

The screen height, h_{scr} is set to 35 ft. [1] and the climb angle during take-off which has been determined from [2] is 3 degrees. The transition distance and climb distance following from the equations are 88.2 $[m]$ and 160 $[m]$ respectively which results in a total airborne distance of 248 $[m]$. Finally, adding up the distance on the ground and when airborne the total take-off length is 1295 $[m]$.

Apart from the calculated total take-off length, there are also distances in case the take-off is aborted or if there is an engine failure. By plotting the accelerate-stop distance and accelerate-climb distance the balanced field length and the decision speed V_1 can be found. The balanced field length is the point where the distance to accelerate and stop or climb is the same for a certain runway condition, weight and thrust setting.

In Figure 6.5 the balanced field length plot is given for take-off configuration at maximum take-off weight with a thrust setting at 95% N1. The runway which has been chosen is runway 02/20 at Saint Helena Airport which has a length of 1950 $[m]$ [3].

[1] https://www.faa.gov/documentLibrary/media/Advisory_Circular/AC% [Accessed On: 02-06-2021]

[2] https://foxnomad.com/2018/08/15/how-much-does-the-average-passenger-plane-angle-up-during-take-off/ [Accessed On: 28-06-2021]

[3] https://web.archive.org/web/20160616084743/http://www.atns.com/downloads/FHSH%20AD%202-11.pdf [Accessed on: 10-06-2021]

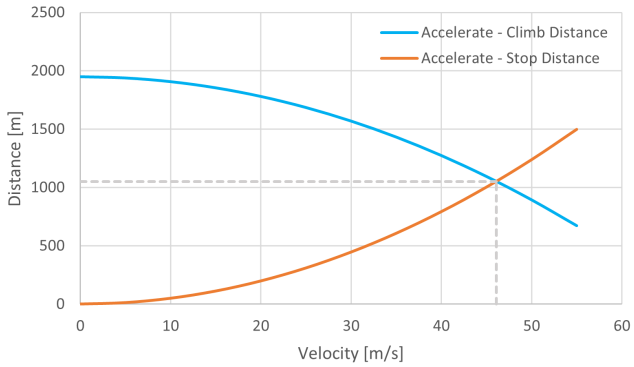

Figure 6.5: Balanced field length of the Unmanned Cargo Aircraft.

From Figure 6.5 the balanced field length is determined to be 1050 $[m]$ and the decision speed, V_1, is 46.1 $[m/s]$. The UCA operator should thus make the decision to abort or continue take-off before V_1, after the decision speed the only option is to continue the take-off. However, in case of engine failure the UCA will not be able to perform take-off after V_1 since it only has 1 engine. Therefore, drag parachutes will be used to slow the aircraft down as much as possible.

6.5.2. Landing

The landing distance consists of an airborne and ground phase as well. The aircraft approaches the runway with a glide angle of 3 degrees at approach speed, 47.8 $[m/s]$, which is 1.3 times higher than the minimum airspeed [17] and will require a total airborne distance which can be calculated using Equation 6.25.

$$x_{total} = R\sin\gamma_a + \frac{h_{scr} - (1-\cos\gamma_a)R}{\tan\gamma_a} \tag{6.25}$$

The radius, R, in the transition phase is given by Equation 6.26 where Δn is determined by empirical data, for subsonic jet aircraft this variable is 0.10g.

$$R = 1.3^2 \frac{\frac{W}{S}\frac{2}{\rho}\frac{1}{C_{L_{max}}}}{\Delta n \cdot g} \tag{6.26}$$

The weight used in Equation 6.26 is the landing weight which is the operational empty weight, a payload weight of 2000 $[kg]$ and assuming 10% of the total fuel weight is left in the fuel tanks. Furthermore, using the $C_{L_{max}}$ of 2.2 in landing configuration a radius of 238 $[m]$ has been found which resulted in a total airborne distance of 210 $[m]$

The ground run distance consists of the rotation and braking distance. The rotation distance is simply the time needed to rotate, assumed to be 2 seconds, multiplied by the approach speed. And the braking distance can be calculated using Equation 6.27.

$$x_{brake} = \frac{W^2}{2gS}\frac{2}{\rho}\frac{1.3^2}{C_{L_{\max}}}\frac{1}{\bar{T}_{rev} + \bar{D} + \mu(W - \bar{L})} \tag{6.27}$$

The transition distance and braking distance using thrust reversers at 70% engine settings (24 $[kN]$), are 95.6 $[m]$ and 269 $[m]$ respectively, adding up to a total ground run length of 364 $[m]$. The total landing distance is therefore 574 $[m]$, which consists of both the airborne and ground phase. If thrust reversers are not used for decelerating, the total ground run distance is 852 $[m]$, resulting in a total take-off length of 1060 $[m]$.

6.6. Cruise Performance

The cruise performance of an aircraft is important for determining the maximum range. This depends on several things such as the altitude, specific aerodynamic coefficients and optimum airspeed. The best flying strategy during cruise is to keep a constant throttle, airspeed and angle of attack with a gradual climb. But in realty this is not possible, one of the reasons is that air traffic control should have clear view of incoming and outgoing aircraft and keeping the airspace organized. Therefore, aircraft will climb in steps during cruise to optimize performance. The range can be calculated with the Equation 6.28 where V is the optimum cruise speed in $[m/s]$, C_T is the specific fuel consumption in $[kg/Ns]$, and W_{start} and W_{final} are the aircraft weight at the start and end of the cruise phase in $[N]$.

$$R = \frac{V}{C_T}\frac{C_L}{C_D}\ln\left(\frac{W_{\text{start}}}{W_{\text{final}}}\right) \tag{6.28}$$

The optimal cruise speed for jet aircraft can be calculated with Equation 6.19 where $C_{L_{opt}}$ is given by Equation 6.29. $C_{L_{opt}}$ has been calculated at cruise condition and happens to be 0.475 and taking the density at service ceiling height resulted in an optimal airspeed of 185 $[m/s]$.

$$C_{L_{opt}} = \sqrt{\frac{1}{3}C_{D_0}\pi Ae} \tag{6.29}$$

6.6.1. Payload-Range Diagram

From the aircraft layout design in Section 4.6 the maximum payload and maximum fuel on board have been determined. Furthermore, the specific fuel consumption is $17.71 \cdot 10^{-6}$ $[kg/Ns]$ and the optimal lift coefficient during cruise has been used to calculate the drag coefficient. Using Equation 6.28 the payload-range diagram of the UCA is constructed and can be seen in Figure 6.6

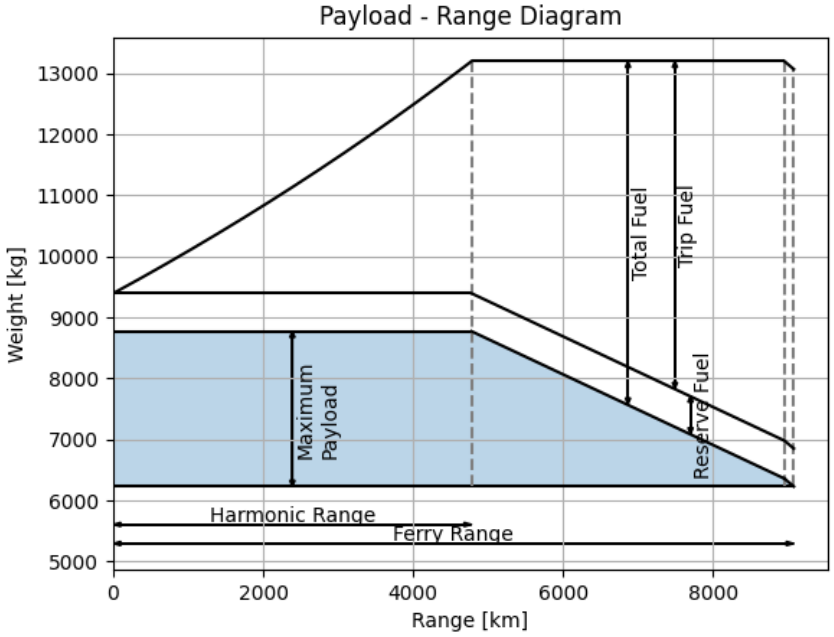

Figure 6.6: Payload-Range diagram of the unmanned cargo aircraft.

From Figure 6.6 it can be seen that the harmonic range is 4781 $[km]$ and the ferry range is 9080 $[km]$. The most important range is from **REQ-SYS-MIS-3.1.00** which states that the UCA shall have a range larger than 3000 $[nm]$ at 2 metric tonnes payload as specified by **REQ-SYS-MIS-3.1.01**. These corresponding payload-range values are summarized in Table 6.2

Table 6.2: Important values from the payload-range diagram

	Range $[km]$	**Payload** $[kg]$
Harmonic Range	4781	2543
Required Payload Range	5723	2000
Ferry Range	9080	0

6.7. Turning Flight

The turning performance of an aircraft depends on the aerodynamic and propulsion characteristics but as well on the altitude and aircraft weight. The UCA should be able to fly fully autonomously without external control, thus the aircraft should be able to manoeuvre safely and avoid possible collisions in a timely manner. Since most of the manoeuvres in flight occur during approach, the performance analysis on turning flight will be done at FL100 [4] with

[4] `https://www.platinumairways.org/files/DOTW_Charts/EHAMCharts.pdf` [Accessed On: 07-06-2021]

an approach speed of 150 $[m/s]$.

6.7.1. Standard Turns

There are 3 standard turns mainly used by air traffic control to guide aircraft, these are called rate 1/2, rate 1 and rate 2 turns each with an angular rotation speed of 1.5, 3, and 6 $[deg/s]$ respectively. For every standard turn there is a corresponding turn radius and bank angle which is dependant on the airspeed of the aircraft. The higher the speed the larger the turn radius and bank angle are. Using Equation 6.30 and Equation 6.31 the turn radius in $[m]$ and bank angle in $[deg]$ can be found respectively.

$$R = \frac{V}{\Omega} \tag{6.30}$$

$$\tan\Phi = \frac{V^2}{gR} \tag{6.31}$$

The results from these standard turn calculations can be found in Table 6.3.

Table 6.3: Turn radius and bank angle for standard turn at approach speed (150 m/s).

Standard Turns (150 [m/s])	**Angular Rotation [deg/s]**	**Turn Radius [m]**	**Bank Angle [deg]**
Rate 1/2	1.5	5730	21.8
Rate 1	3	2865	38.7
Rate 2	6	1432	58.0

6.7.2. Maximum Turning Performance

In order to find the maximum turning performance the maximum load factor has to be first determined which can be found by plotting the performance diagram. For this diagram the drag force has to be known at all available speeds for a certain load factor. The first step is to calculate the lift coefficient to the corresponding velocity using Equation 6.33. Afterwards, the drag coefficient can be calculated using Equation 5.10 from which the drag is found using Equation 6.32

$$D = n\frac{C_D}{C_L}W \tag{6.32}$$

$$V = \sqrt{\frac{nW}{S}\frac{2}{\rho}\frac{1}{C_L}} \tag{6.33}$$

By doing these steps for several load factors, the performance diagram can be plotted as can be seen in Figure 6.7. The thrust which is used has been calculated by the propulsion department at FL100 and since the analysis is done for the approach phase it is assumed that approximately 15% is left over in the fuel tanks, the weight is therefore 88022 $[N]$. The stall limits are calculated using Equation 6.33, by considering the maximum lift coefficient during cruise and a range of load factors from 0 to 3.5. The maximum load factor which can be reached is limited by the thrust, this value is 3.41.

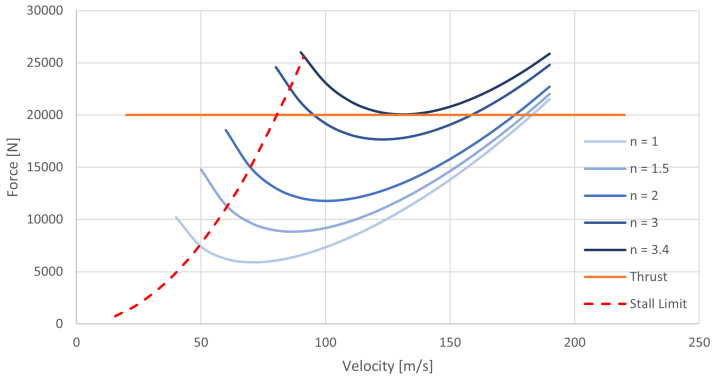

Figure 6.7: Performance diagram for different load factors at FL100.

The other limiting load factors at different speeds are either bound by the thrust or stall speed. For the load factor curves of 1, 1.5 and 2, at low speed is limited by the stall speed whereas for the rest the thrust is the limiting factor. The maximum load factor curves with varying speed which can be reached in turn at FL100 is presented in Figure 6.8.

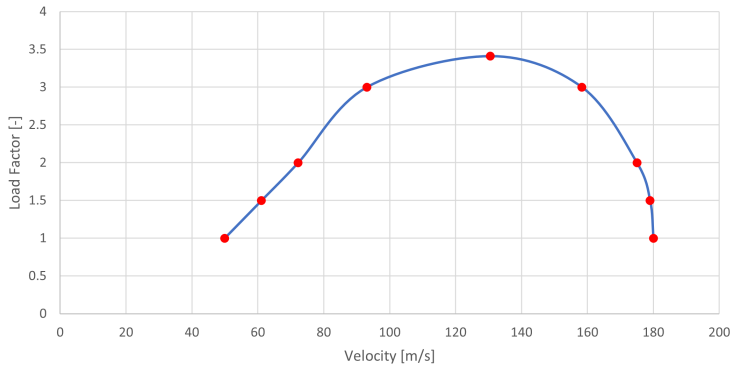

Figure 6.8: Maximum load factor diagram at FL100.

Using the load factors in Figure 6.8 the minimum turn radius can be found using Equation 6.34. The results can be seen in Figure 6.9 and the minimum turn radius happens to be 307 $[m]$ with a load factor of 2 and velocity of 72.22 $[m/s]$.

Furthermore, the minimum time to turn can be found using Equation 6.35 and the load factors in Figure 6.8. The results can be seen in Figure 6.10 and the minimum time to turn happens to be 21.1 $[s]$ with a load factor of 3 and velocity of 93.06 $[m/s]$.

$$R = \frac{V^2}{g\sqrt{n^2-1}} \tag{6.34}$$

$$T_{2\pi} = \frac{2\pi R}{V} \tag{6.35}$$

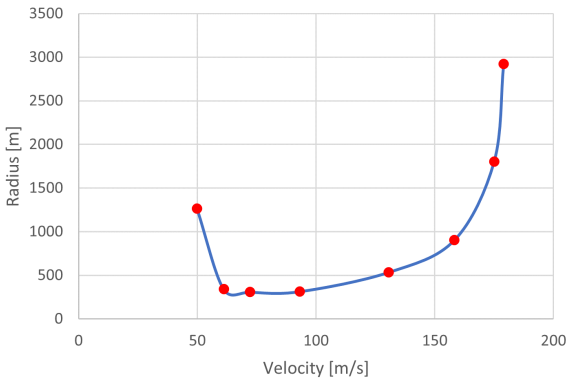

Figure 6.9: Minimum turn radius at FL100.

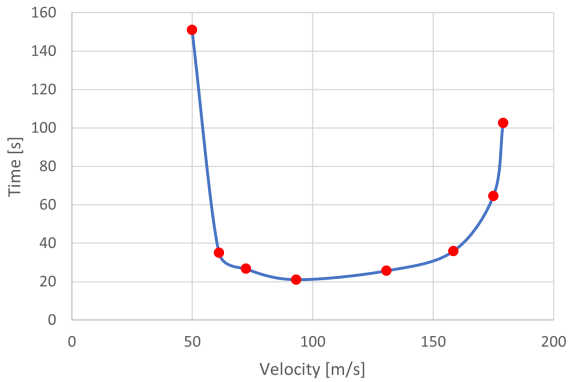

Figure 6.10: Minimum time to turn at FL100.

The results are summarized in Table 6.4. The minimum turn radius can be normally achieved just below the maximum bank angle, whereas the minimum time to turn is reached above the minimum turn radius. The speed at which the maximum turning performances are reached can be concluded as following: $V_{Rmin} \leq V_{Tmin} \leq V_{nmax}$

Table 6.4: Maximum turning performance for maximum load factor, minimum turn radius and minimum time to turn at FL100

Load Factor $[-]$	**Velocity** $[m/s]$	**Turn Radius** $[m]$	**Time to Turn** $[s]$
1	49.9	1263	151
1.5	61.1	340.5	35.0
2	72.2	**307.1**	26.7
3	93.1	312.2	**21.1**
3.4	130	533.2	25.7
3	158	903.4	35.9
2	175	1803	64.7
1.5	179	2922	103
1	180	-	-

6.8. Verification and Validation

This section will explain the verification and validation procedures for flight performance. First, the verification will be discussed in Subsection 6.8.1 including unit tests and system tests, the validation procedures are discussed in Subsection 6.8.2

6.8.1. Verification

The calculations which have been done for flight performance were executed using Microsoft Excel since this allowed for organizing the results and parameters in a clear and easy way to find which were needed by other departments. The unit tests are therefore performed by manual hand calculations, a table of the unit tests done is shown in Table 6.5. All results showed little to no difference.

Table 6.5: Performed unit tests for flight performance.

Tested Unit	**Method & Description**
Climb angle	The climb angle during take-off had been verified with hand calculations, a small difference 0.35% had been found due to trigonometric definitions used in Excel.
Steady rate of climb	The steady rate of climb had been verified with hand calculations, no difference was found.
Actual rate of climb	The Actual rate of climb had been verified with hand calculations, no difference was found.
Glide angle	The glide angle had been verified with hand calculations, no difference was found.
Glide distance	The glide distance had been verified with hand calculations, no difference was found.
Total take-off distance	The total take-off distance had been verified with hand calculations, initially a small error was present due to trigonometric definitions used in Excel, after resolving the issue no difference was found.
Total landing distance	The total landing distance had been verified with hand calculations, Initially a small error was present due to trigonometric definitions used in Excel, after resolving the issue no difference was found.
Optimal cruise speed	The optimal cruise speed had been verified with hand calculations, no difference was found.
Range	The range had been verified with hand calculations, no difference was found.
Load factor	The load factors had been verified with hand calculations, no difference was found.
Turn radius	The turn radius had been verified with hand calculations, initially a error was present due to mistyping the formula, after resolving the issue no difference was found.
Time to turn	The time to turn had been verified with hand calculations, no difference was found.

For the systems test the calculations are tested to see if they behave as expected, for example doubling the airspeed should double the turn radius. The performance analysis consisted for a large part of simple calculations which could easily unit tested without needing extensive system testing. However, the actual rate of climb and turning flight performance consisted of more calculations and will therefore be system tested.

For the actual rate of climb several variables are changed to examine the effect on the results. Increasing the thrust level, increased the steady rate of climb as expected since the difference between power required and power available is larger. With changing altitudes the thrust changed accordingly with density following the relation in Equation 6.36.

$$\frac{T}{T_0} = \frac{\rho}{\rho_0} \tag{6.36}$$

The maximum load factor achievable during turning flight is assessed next, increasing the weight resulted in a lower maximum load factor which is logical since $n = \frac{L}{W}$. At higher altitudes the air density is lower, which also affects the

thrust negatively, limiting the manoeuvrability of the aircraft, thus resulting in lower load factors. This was also seen in the test results.

6.8.2. Validation

For validation the results from the calculations are compared to data from reference aircraft or analysed on whether the results behave as it should in reality. First, the manoeuvre and gust diagram, which can be found in Section 6.3, will be validated based on comparison and visual inspection. The stall speed is located at where the manoeuvre diagram has a load factor of 1. Furthermore, a large margin should be present between V_A and V_C for manoeuvres, which is approximately 120 $[m/s]$ and V_D should be larger than V_C which is also the case. The gust diagram starts at $V = 0$ with a load factor of 1 as expected, and comparing the diagrams of reference aircraft the shapes are comparable to each other [16].

The constant rate of climb plot in Section 6.4 consists of curves of constant ROC which vary with altitude and speed. The curve of lowest rate of climb should be the one able to reach the highest altitude and should enclose the curves with a higher rate of climb completely. Due to altitude effects the maximum points of the curves should shift the right with increasing altitude, thus the top of the lowest ROC curve should be located at a higher speed compared to higher ROC curves. Figure 6.3 meets the requirements and is therefore deemed valid.

The glide distance of the UCA of had been determined to be 150 $[km]$ from a cruise altitude of 38000 $[ft]$. Comparing this distance to other reference aircraft [18] resulted in a R-squared value of 0.9248 showing a clear correlation, thus validating the glide distance.

The turning performance diagram in Section 6.7 shows the curves representing load factors which vary with speed and drag. When in creasing the load factor the curve moves to the top right direction of the plot as expected. The results from this plot are the maximum load factors experienced at different speed. Using these load factors the minimum turn radius and time to turn can be found. The results should show that $V_{Rmin} \leq V_{Tmin} \leq V_{nmax}$ [17] which is also the case here, therefore the turning flight performance is deemed valid.

6.9. Conclusion and Recommendations

The purpose of this chapter is to analyse the flight performance characteristics using the parameters which have been determined from the preliminary design and aerodynamic research. The flight performance results are able to meet the requirements and the EASA certification specifications for large aerosplanes (CS25).

From the manoeuvre diagram a 1-g stall speed of 45.2 $[m/s]$ has been found and at take-off the climb is 11.6 degrees or the aircraft can have a rate of climb of 10.7 $[m/s]$. In gliding flight the average glide angle is 4.4 degrees, with which a glide distance of 150 $[km]$ can be reached in clean configuration having a glide ratio of 13. The take-off and landing distances are 1884 and 1499 $[m]$ respectively, taking runway 02/20 (length of 1950 $[m]$) at Saint Helena Airport, the balanced field length is 1050 $[m]$ with V_1 being 46.1 $[m/s]$. A parachute will be used in case of engine failure at speeds higher than the decision speed. For cruise characteristics, the optimal cruise speed is 667 $[m/s]$ and the service ceiling has been determined to be FL410. The harmonic and ferry ranges are 4781 and 9080 $[km]$ respectively. In turning flight, the minimum turn radius is 307 $[m]$ and the minimum time to turn a circle is 21.2 $[s]$

Recommendations for further research is find the optimal climb path to minimize time using the constant rate of climb lines and to optimize flight conditions by finding ideal thrust setting to reduce fuel consumption. Optimization may lead to reduced costs and CO_2 emission which helps in improving sustainability

7
Propulsion System Design

This chapter focuses primarily on the propulsion system of the UCA. This includes the fuel type, fuel system, and the engine. All aspects regarding fuel are first discussed in Section 7.2. Within the section, the fuel type is first decided upon, then the green house gas emissions of the UCA with the selected fuel type is calculated and compared to those of a Boeing 747-400F, and lastly, the properties of the fuel system is discussed. The subsequent section, Section 7.3, a small trade off was performed in order to obtain the most compatible engine for the UCA and once chosen, all its relevant characteristics are presented. Section 7.4 presents the model made of the engine which yields the thrust and SFC produced by the engine at different velocities and at different altitudes. Accordingly, Section 7.5 presents the method at which the propulsion model is verified and validated. Lastly, the chapter is closed off with the conclusion found in Section 7.6.

In the midterm report, after an extensive trade off, it was determined that a single turbofan engine would be most suitable for the purpose of the UCA. However, several improvements can be made to this propulsion system to improve its overall performance in the trade off criteria. An example of this is by looking at sustainability. Though this propulsion system performs fairly well regarding sustainability when performing the trade off, this does not mean changes cannot be made to further improve this aspect of the system.

The single turbofan engine propulsion system was based upon the RQ-4 Global Hawk design. As evident from the name, instead of the conventional two engine layout widely used in the aviation industry worldwide, it uses a singular engine. This is due to the layout's simplicity, low operational cost, and low maintenance cost [6]. Additionally, representative propulsion data was already obtained and estimated in the midterm report through use of relevant and similar aircraft's data. It is important to note that the data obtained was an estimation and not by any means a definite estimation as it was simply used to perform a trade off. With this, it is in this chapter that a definitive estimation will be conducted of the systems performance characteristics.[6]

7.1. Requirement Analysis

In order to choose the most suitable fuel type, fuel system, and engine, the following requirements needed to be met:

- **REQ-STK-04:** The UCA shall emit less CO_2 relative to other cargo aircraft.
- **REQ-STK-08:** The UCA shall reduce local emissions as much as possible.
- **REQ-SYS-SUS-4.1.00:** The CO_2 emission of the UCA shall be less than 50% per metric tonne when compared to a 747-400F.
- **REQ-SYS-FLT-2.6.00:** The UCA shall have a propulsion system to generate thrust.
- **REQ-SUBSYS-PRP-2.2.00:** The propulsion system of the UCA shall be able to accelerate the UCA from stationary to take-off speed (52.17 [m/s]) in 2000 [m] at maximum take-off weight.
- **REQ-SUBSYS-PRP-2.5.00:** Each fuel tank must be able to withstand the vibration, inertia, fluid and structural loads that it will be subjected to in operation.
- **REQ-SUBSYS-PRP-2.6.00:** The UCA shall have a number of 1 engines.
- **REQ-SUBSYS-PRP-2.6.01:** Each engine of the UCA shall generate 35,000 [N] of thrust.
- **REQ-SUBSYS-PRP-2.6.02:** The generated thrust of the engines shall be able to be throttled independently.
- **REQ-SUBSYS-PRP-4.1.00:** The propulsion system of the UCA shall emit less CO_2 than 50% per metric tonne when compared to a 747-400 freighter.

7.1.1. Assumptions

In order to be able to obtain the thrust and SFC produced by whichever engine chosen at different altitudes and at different speeds, a model of the chosen engine had to be produced. In order to simplify the process of modelling, several assumptions were made. There assumptions are as follows:

1. **Constant Specific Heats**: For air and gas, the specific heats is assumed to stay constant at 1000 $[J/kg \cdot K]$ and 1150 $[J/kg \cdot K]$ [19]. This is for the fact that even though specific heat does change with heat, it does not have a significant impact on the analysis.
2. **Constant Specific Heat Ratios**: For air and gas, the specific heat ratios are assumed to be 1.4 and 1.33 respectively [19]. These numbers are sufficient to perform the analysis with.

3. **Efficiencies**: Each component found within a turbofan brings with it its own efficiencies. To determine these efficiencies, trends of existing engines were used [19].
4. **Turbine Inlet Temperature**: The turbine inlet temperature is the temperature of the combustion chamber exhaust gases. By looking at trends of modern turbofans, it was determined that the TIT, turbine inlet temperature, will be 1750 [K] [19].
5. **Fuel Properties**: The LHV, lower heating value, for synthetic kerosene will be assumed to be 43 [MJ/kg] due to it having similar chemical properties to regular kerosene[1].
6. **Constant Potential Energy**: No change in potential energy is assumed as air flows through the engine. This is valid because on average, the air flows along the central axis of the engine with no change in height during level flight.
7. **Air Velocity**: For the air velocity entering the engine during flight, it was assumed to be equal to the airspeed at which the UCA is flying at. This assumption does not have a insurmountable impact on the analysis and the results that comes with it.

7.2. Fuel

Fuel is an important aspect regarding the propulsion system as it is the substance which powers the engine. This section presents the type of fuel chosen to power the aircraft, the green house gas emissions associated with the chosen fuel type, and the configuration of the fuel system.

7.2.1. Fuel Type

To meet the emissions requirements, regular kerosene is out of the question as it produces too much emissions in order to meet the requirements. Therefore, sustainable alternative fuels have to be used. An evaluation of these fuels will be performed in order to determine which would be best suited for the aircraft.

Electricity

Electricity is one of the most well known sustainable alternative fuel and is most popular in the auto-motives industry as more automotive brands are entering the electric motor vehicle market[2]. However, this is the opposite in the aviation industry as there has been no commercially available electrical planes. This is not without reason.

In cars, batteries are used as electrical power sources in order to power the vehicle. This however cannot be done for the UCA as the range required to be flown by the aircraft would require a battery which would have an insurmountable weight. This is for the reason that batteries do not have as high specific energy as regular kerosene do. With current technology, lithium-ion batteries have a specific energy of 260 [Wh/kg] [3] whereas fossil fuel has an specific energy of around 12,000 [Wh/kg] [4]. Consequently, in order to produce as much energy as 1 [kg] of kerosene, a battery with a weight of around 46.15 [kg] have to be incorporated. With an estimated required fuel weight of 4,424.53 [kg] for the UCA, this would mean that a battery with a weight of 204,209.2946 [kg] or 204 metric tonnes would be required. The shear weight of the battery makes electrical flight powered by batteries unfeasible. However, when it comes to accessibility in airports, it is safe to assume that electricity will already be located at the airports, both primary and secondary, and no need of fuel transportation is required. The only extra step needed is the installation of a charging point. Nevertheless, as stated before, the shear weight of battery renders the fuel type unusable and an alternative is needed. Fortunately, there is an alternative in hydrogen, specifically the use of hydrogen directly to create propulsion by means of combustion or the use of hydrogen fuel cells to produce electricity.

Liquefied Natural Gas

Before discussing hydrogen, a quick discussion will be given for the use of liquefied natural gas as a fuel type. Though liquefied natural gas proves to be environmentally and economically beneficial, they only result in a reduction of 16% to CO_2 emissions compared to the use of regular kerosene. As will be seen and demonstrated in Subsection 7.2.2, if the UCA were to use regular kerosene, it would produce 15,707.117 [kg] of CO_2. By using, liquefied natural gas, this number would decrease to 13,193.978 [kg] of CO_2, a 53.4% increase in CO_2 emitted per tonne of cargo. This therefore does not meet the requirement regarding the reduction of CO_2 emissions [20].

Hydrogen

Hydrogen is the most viable zero CO_2 emissions alternative fuel as shown by ZEROe, Airbus's venture into producing zero emission aircraft. To do so, Airbus is using hydrogen to power the engines by reacting it with oxygen[5]. An alternative method to use hydrogen is to have it undergo redox reactions with oxygen to produce electricity. This is essentially how a hydrogen fuel cell works and is a more energy dense alternative to producing electricity compared to batteries.

[1] https://royalsociety.org/-/media/policy/projects/synthetic-fuels/synthetic-fuels-briefing.pdf [Accessed on: 11-06-21]
[2] https://edition.cnn.com/interactive/2019/08/business/electric-cars-audi-volkswagen-tesla/ [Accessed on: 02-06-21]
[3] https://c2e2.unepdtu.org/wp-content/uploads/sites/3/2019/09/analysis-of-hydrogen-fuel-cell-and-battery.pdf [Accessed on: 02-06-21]
[4] https://www.vennershipley.co.uk/wp-content/uploads/2020/07/Europes_new_aviation_vision_is_electric_the_future1.pdf [Accessed on: 02-06-21]
[5] https://www.airbus.com/innovation/zero-emission/hydrogen/zeroe.html [Accessed on: 02-06-21]

These two uses of hydrogen are due to its desirable attributes. When hydrogen reacts with oxygen, the only byproduct of the combustion process is water vapour. No carbon dioxide is produced in the slightest. Additionally, it has a high specific energy, more than three times of regular jet fuel, 40,000 $[Wh/kg]$ compared to 12,000 $[Wh/kg]$ respectively[6]. This means that 1 $[kg]$ of hydrogen contains 120 $[MJ]$ of energy whereas kerosene has 43 $[MJ/kg]$ and batteries have 1 $[MJ/kg]$. However, hydrogen does have its downsides.

Hydrogen has the downside of being inefficient from its production to its end use. Hydrogen may be the most abundant element in the universe but it does not exist solely by itself. It exists in molecules such as H_20 and CH_4. Therefore, hydrogen, H_2, needs to be produced. The most widespread method of producing hydrogen is through steam reforming which uses oxygen and methane, obtained through fossil fuel. This means that carbon emissions are produced in this hydrogen production method and due to this, hydrogen produced through steam reforming is dubbed grey hydrogen. Therefore, although hydrogen may be sustainable, it is only as sustainable as its production methods and steam reforming would not solve the problem hydrogen was meant to. In addition, the method is extremely inefficient and the grey hydrogen produced contains less energy than the natural gas used. An alternative is to produce hydrogen through electrolysis. However, this process is expensive, energy intensive, and inefficient, 14% to 18% loss in efficiency by time of launch using future technology[7], though it does allow the use of renewable energy sources as energy input and therefore being carbon emissions free. When it comes to storing hydrogen, hydrogen has to be compressed and stored in pressurised tanks or turn into liquid by cooling it down to extremely low temperatures, 20.15 $[K]$ to be exact[8], in cryogenic tanks due to its low energy density in volume. Pressurised hydrogen storage comes in two different pressures, 300 bars and 700 bars, where hydrogen stored at 300 bars is the simplest of all storage methods and the most commercially available. Both, however, are inefficient as the compressors result in a energy loss of between 5% to 20% with hydrogen stored in 700 bars needing more energy than hydrogen stored at 300 bars [21]. When using cryogenic tanks, the storage containers required are complex as it has to be heavily insulated in order to prevent the hydrogen from boiling and they need to be handled with caution. Due to this, as keeping the hydrogen cool is energy intensive, the energy loss of using cryogenic tanks ranges from 30% to 40% which is much higher than the alternative [21]. When it comes to using hydrogen, various power train components have to be used in order to make the hydrogen usable. Though most of the components, the ones responsible for power delivery and conversion, have high energy efficiencies at 95%, the fuel cell itself has a much lower energy efficiency of 50% [21]. Therefore, from production to use, best case in scenario using improved technology by launch, hydrogen has an end to end energy efficiency of around 27%.

The next biggest issue regarding the use of hydrogen is its low energy density in volume compared to kerosene. To mitigate this and as stated before, hydrogen has to be compressed and stored in pressurised tanks or turn into liquid by cooling it down to extremely low temperatures in cryogenic tanks. When it comes to the two different storage pressures, though 300 bars is the simplest of all storage methods and the most commercially available, by the time on launch using improved technology, hydrogen stored at 700 bars brings with it an increase of storage efficiency, 20% compared to the 10% of hydrogen stored in 300 bars, along with an increase in hydrogen density, 40 $\left[kg/m^3\right]$ compared to 20 $\left[kg/m^3\right]$ of hydrogen stored in 300 bars [21]. Note that storage efficiency is different than the energy efficient elaborated upon in the previous paragraph; storage efficiency is the ratio of fuel mass to the filled tank mass and energy efficiency is the ratio of the output energy to the input energy. Cryogenic tanks however prove to be more beneficial than storing pressurised hydrogen as tanks holding liquefied hydrogen are much lighter than the alternative which as the hydrogen density surpasses the alternatives a density of 70 $\left[kg/m^3\right]$ along with a storage efficiency of up to 50%[21]. Therefore, even though cryogenic tanks are extremely large, complex, and heavy, the use of pressurised tanks, which are more commonplace and simpler, would result into a heavier and larger tank. For these reasons, cryogenic tanks would be most ideal for the UCA. However, even though turning hydrogen into liquid would result into a more energy dense fuel, it is still less energy dense in volume than kerosene as seen in Table 7.1. To calculate the volume of hydrogen required depending upon the storage method and its respective fuel tank, the aforementioned Table 7.1 is used. Note that the numbers represented are numbers of future technology by time of launch.

Given that the mass of kerosene required for the UAC is estimated to be 6,216.61 $[kg]$, Table 7.2 presents the respective mass and volume of the different forms of hydrogen fuel tanks.

As seen in Table 7.2, even the storage method which yields the smallest fuel tank volume wise, liquid hydrogen, gives a required volume of 45.30 $[m^3]$. In comparison, using regular kerosene, the aircraft would simply required a fuel tank with a volume of 7.41 $[m^3]$, almost 6 times less than the one required by liquid hydrogen. To accommodate the shear size of the liquid hydrogen fuel tank, the fuselage of the aircraft would either need to be redesigned into an unconventional shape in order to hold the same amount of cargo or reduce the amount of cargo able to be hold by the aircraft in order to not change the shape of the aircraft's body. Both will result into an increase cost in flying as the

[6] https://c2e2.unepdtu.org/wp-content/uploads/sites/3/2019/09/analysis-of-hydrogen-fuel-cell-and-battery.pdf [Accessed on: 02-06-21]

[7] https://www.fch.europa.eu/sites/default/files/Nov22_Session3_Panel%205_Slot%202_NOVEL-MEGASTACK_Thomassen%20%28ID%202891376%29.pdf [Accessed on: 11-06-21]

[8] https://www.sag.at/en/development/hydrogen/ [Accessed on: 02-06-21]

Table 7.1: Future Hydrogen storage properties [21]

	Kerosene	**300 bar** H_2	**700 bar** H_2	**Liquid** H_2
$\rho_{fuel}[kg/m^3]$	800	20	40	70
$LHV_{fuel}[MJ/kg]$	43	120	120	120
Energy Density $[MJ/m^3]$	34,400	2,400	4,800	8,400
$\nu_{storage}[-]$	0.95	0.10	0.20	0.50
$\nu_{vol}[-]$	0.95	0.50	0.50	0.50

Table 7.2: Mass and volume of full fuel tanks for each storage method

	300 Bar H_2	**700 Bar** H_2	**Liquid** H_2
Mass $[kg]$	15,854.59	7,927.30	3,170.92
Volume $[m^3]$	158.55	79.27	45.30

former will lead to more drag which in turn will require more fuel and the latter will lead to less cargo being held and therefore fewer sources of income.

Regarding accessibility in airports, both primary and secondary, there are two options regarding the transporting of hydrogen from its production site to the airport. The first option is a large centrally located hydrogen production site. These sites are able to produce hydrogen at a lower cost due the simple fact that its producing more. However, this hydrogen needs to be transported to different primary and secondary airports. This is an issue as it will cost more to transport the hydrogen as the airports are further away from the production site. Additionally, as stated before, hydrogen tanks are extremely large and heavy. Therefore, when transported, vast amounts of hydrogen cannot be transported at once and multiple trips are required. This in turn will simply add to the costs of using hydrogen and emissions produced by transporting the hydrogen. The alternative is to have a distributed hydrogen production site at the airports. This will in turn vastly reduce the transportation costs of hydrogen but it will increase the costs to produce the hydrogen due to less production volumes. Though the alternative may seem better, there are only a few distributed hydrogen production sites around the world and are all located at car refueling stations. This form of hydrogen production therefore is not widespread and does not seem to greatly change by time of launch. Thus, it is safe to assume that the hydrogen used to fuel the fuel system would be transported from a centrally located hydrogen site which would result into a large spike in costs and emissions.

With these issues arising from hydrogen, regardless of its method of use, an alternative has to be introduced. This alternative discussed will be synthetic kerosene.

Synthetic Kerosene
The use of batteries and hydrogen as means of producing power in an aircraft are still unfeasible for a majority air travel as they suffer from poor energy density in weight and in volume respectively when compared to kerosene. However, there is an already existing alternative which does not suffer the same problems, synthetic kerosene. Additionally, synthetic kerosene has the benefit of having the almost exact same physical and chemical properties as regular kerosene [9].

It is important to note that there is alternative to synthetic kerosene and that is bio fuel. Biofuel comes in three forms, first, second, and third generation. First generation of bio fuel is made using edible biomass whereas the second generation is made using inedible bio mass. The third generation of biofuel is made through the use of algal biomass. The most cost effective method would be to use first and second generation biofuel, however, there simply is not enough of these resources to produce the amount of fuel needed by the aviation industry. The production of bio fuel through the use of biomass is unfeasible as the amount of land needed to grow the amount of biomass required to meet demand is too large, and would severely affect the already scarce global land, water, and food resources [22]. The alternative is third generation biofuel. However, they are simply not economically feasible at time of launch [23]. Due to these limitations, bio fuel cannot be scaled sustainably and is not a viable fuel alternative.

Synthetic kerosene, unlike bio fuel, can be scaled sustainably and this is due to its production methods. Synthetic kerosene, which is essentially liquid hydro carbon, is produced by synthesizing hydrogen with carbon. As previously mentioned, hydrogen can be produced in two different ways, steam reforming and electrolysis. However, to ensure that fuel is truly sustainable, electrolysis has to be the production method used when producing the hydrogen required for synthetic kerosene. Carbon on the other hand can be produced through a method called direct air capture. To elaborate upon direct air capture, it works by utilising large fans to draw in air from the atmosphere. Then, the air goes through a filter containing chemicals, typical sodium hydroxide, in order to filter out the CO_2 from the air. The

[9] `https://royalsociety.org/-/media/policy/projects/synthetic-fuels/synthetic-fuels-briefing.pdf` [Accessed on: 11-06-21]

filter material is then heated to release the filtered CO_2 and to be stored. The filtered air is then subsequently released back into the atmosphere as clean air[10]. Both electrolysis and direct air capture can be powered by renewable energy sources such as wind and solar energy. However, these methods are extremely energy intensive, inefficient, and due to their infancy, are expensive as well. This is shown as it was calculated that to produce enough synthetic fuel to supply the aviation industry in the UK in 2018, 75% of the UK's total grid generation running all year would have been needed[11]. This is equivalent to twice the electricity produced by renewable energy sources if run all year.

Regarding accessibility in airports, synthetic kerosene would need to be transported in the same manner as regular kerosene from a centralised production site. However, due to its similarity to regular kerosene, the logistics needed to transport synthetic kerosene is already present and some slight modifications would be required. Additionally, unlike hydrogen, a vast amount of synthetic kerosene can be transported at once due to its higher energy density.

7.2.2. GHG Emissions

As synthetic kerosene does not have the same issues as either batteries or hydrogen regarding specific energy and energy density respectively, it is then necessary to see whether or not the emissions produced by using synthetic kerosene indeed is less than 50% per metric tonne of cargo of those emitted by a Boeing 747-400F. It was determined that a Boeing 747-400F produces a total of 426,745.5 $[kg]$ of CO_2 per flight with maximum payload as it has a fuel weight of 120,210 $[kg]$ with 3.55 $[kg]$ of CO_2 produced per $[kg]$ of fuel used. It was estimated that the UCA would require 4,424.54 $[kg]$ of fuel. Therefore, to determine the amount of CO_2 produced, it is necessary to determine the amount of CO_2 produced per kg of synthetic kerosene used. From the midterm report, it was determined that by the time of launch, synthetic kerosene will produce 1.33 $[kg]$ of CO_2 per $[kg]$ of fuel used [6]. Therefore, in total, the UCA will produce a total of 5,884.638 $[kg]$ of CO_2 per flight with maximum payload. As the requirement is to determine whether the UCA producs 50% less CO_2 per metric tonne of cargo, the tonne of cargo each can hold needs to be obtained. For the Boeing 747-400F, it is 124 tonnes and for the UCA, it is 2.5 tonnes. Therefore, per metric tonne, the Boeing 747-400F produces 3,441.496 $[kg]$ of CO_2 per tonne of cargo and the UCA produces 2,353.855 $[kg]$ of CO_2 per tonne of cargo. This means that there is only a reduction of 31.6% in CO_2 emission per metric tonne when the UCA is compared to the Boeing 747-400F, nowhere near the required 50%. Had UCA used regular kerosene instead of synthetic kerosene, the UCA would be emitting 15,707.117 $[kg]$ of of CO_2 per flight with maximum payload with 6,282.847 $[kg]$ of CO_2 per tonne of cargo, 62.6% more than the CO_2 emissions produced by the Boeing 747-400F. As can be seen, the use of synthetic kerosene is very much needed to ensure that the amount of CO_2 produced per tonne of cargo is kept to a minimum. This can be summarised by the table below.

Table 7.3: CO_2 Emitted per Aircraft during Flight at Max Payload

Aircraft	CO_2 **Emitted [kg]**	CO_2 **Emitted per Tonne of Cargo [kg]**	**Percentage Difference to Boeing 747-400F per Tonne of Cargo [%]**
Boeing 747-400F	426,745.5	3,441.496	-
UCA (Synthetic Kerosene)	5,884.638	2,353.855	31.6% Less
UCA (Regular Kerosene)	15,707.117	6,282.847	82.6% More

However, it is important to state that a fuel is only as sustainable as the means of producing it. Therefore, it is necessary to determine the amount of CO_2 emitted by producing synthetic kerosene and compared to the amount of CO_2 emitted by producing regular kerosene.

In order to ensure sustainability, electrolysis will be used to obtain the hydrogen required for synthetic kerosene production. CO_2 will be obtained through the use of direct air capture. Both will be able to be powered through the use of renewable sources of energy such as wind and solar. It was estimated that both will have a CO_2 emission of 34.11 $[g]$ and 49.91 $[g]$ of $[CO_2/kWh]$ over their lifetime respectively[12]. With synthetic kerosene having the same energy density as regular kerosene, 12,000 $[kW/h]$, the total energy required to be supplied to the aircraft can be computed. Due to synthetic kerosene being relatively new and its production methods being in its infancy stage, its power to fuel efficiency can be assumed to be quite low. By the time of launch, electrolysis technology loss in efficiency will decrease to between 14 - 18% thanks to the addition of a proton exchange membrane in the electrolysis process, meaning a 82 -

[10] `https://www.iea.org/reports/direct-air-capture` [Accessed on: 11-06-21]

[11] `https://assets.publishing.service.gov.uk/government/uploads/system/uploads/attachment_data/file/791297/Press_Notice_March_2019.pdf` [Accessed on: 11-06-21]

[12] `https://journalistsresource.org/environment/lifecycle-greenhouse-gas-emissions-solar-wind-energy/` [Accessed on: 15-06-21]

86% efficiency. Due to direct air captures infancy as well, it can be assumed that it will likely have a similar efficiency to electrolysis, albeit a bit lower, at 80%. Therefore, the overall efficiency in order to capture the materials needed to produce synthetic kerosene would be the average of the two at 83%. To use the resources to produce synthetic kerosene, they have to go through three main processes, a reverse water gas shift, a Fischer-Tropsch process, and refining the fuel [24]. Again, due to the infancy in the process of creating synthetic fuel, it can be assumed that each chemical process, which tend to be fairly efficient, will have an efficiency of around 90% [25]. Overall, taking into account all the steps needed to produce synthetic kerosene and its efficiencies, the overall process will have a power to fuel efficiency of around 60.5%.

Additionally, it was also necessary to calculated the amount of CO_2 taken by the direct air capture to produce the required amount of fuel. By using the reaction equation used to produce synthetic kerosene from Hydrogen and CO_2 and the use of atomic weights, it was determined that 13,774 $[kg]$ of CO_2 is required to produced the required amount of fuel. Therefore, regardless of the value obtained when calculating the amount of CO_2 emitted from producing synthetic kerosene, 13,774 $[kg]$ has to be reduced from from value to take into account the CO_2 needed to produce the required amount of synthetic kerosene.

With synthetic kerosene having an energy density of around 12,000 $[Wh/kg]$, and by taking into account the fuel mass of the aircraft during max payload, 4,424.54 $[kg]$, the total energy required will be 53,094,480.0 $[Wh]$. Taking into account the power to fuel efficiency, the amount of energy needed to be produced by solar or wind energy would be 87,749,318.261 $[Wh]$. As wind energy is the more clean and efficient power source, the total emissions will be calculated using the numbers regarding wind energy. Therefore, the amount of CO_2 produced in producing synthetic kerosene would be 2,993.129 $[kg]$ or around 2.993 metric tonnes of CO_2. Taking into account the amount of CO_2 needed to produce the synthetic kerosene, this number goes into the negative, -10,781.382 $[kg]$ or around -10.781 metric tonnes of CO_2. This means that producing the required amount of kerosene is actually beneficial for environment. However, this is unrealistic as this is assuming the use of 100% renewable energy. In reality, this is not the case. In 2019, it was determined that in Europe, only 34% of the electricity consumed was produced from clean energy. Assuming the same percentage, it can be determined that only 29,834,768.209 $[Wh]$ will be produced using clean energy. Therefore, the remaining 57,914,550.052 $[Wh]$ have to be producing using fossil fuels. In 2019, it was determined that in Europe, 255 $[g]$ of $[CO_2/kWh]$ was emitted when producing electricity. Bearing this in mind, it was determined that realistically, synthetic fuel would produce 15,785.874 $[kg]$ or around 15.785 metric tonnes of CO_2. Taking into account the amount of CO_2 needed to produce the synthetic kerosene, it was determined that synthetic fuel would produce 2,011.363 $[kg]$ or around 2.011 metric tonnes of CO_2.

Regular kerosene has a CO_2 emission of 260 $[g]$ of $[CO_2/kWh]$ when produced[13]. In order to power the Boeing 747-400F, 1,442,520 $[kWh]$ of power is needed and to produce that much kerosene, 375,055.2 $[kg]$ or around 375 metric tonnes of CO_2 would be released. Additionally, in order to power the UCA, if it were fueled by regular kerosene, 22,814.822 $[kg]$ or around 22.814 metric tonnes of CO_2 would be released.

This is all summarised in the following table. Note that Clean UCA is in reference to the assumption that the synthetic kerosene required is produced by 100% clean energy.

Table 7.4: CO_2 Emitted per Aircraft from Production of Fuel

Aircraft	CO_2 **Emitted [kg]**	CO_2 **Emitted per Tonne of Cargo [kg]**	**Percentage Difference to Boeing 747-400F per Tonne of Cargo [%]**
Boeing 747-400F	375,055.2	3,024.639	-
Clean UCA (Synthetic Kerosene)	-10,781.382	-4,312.553	242.6% Less
Realistic UCA (Synthetic Kerosene)	2,011.363	804.545	73.4% Less
UCA (Regular Kerosene)	22,814.822	9,125.929	201.7% More

Thus, the total CO_2 emissions produced in the production of kerosene and during use on flight for the 747-400F is 801,800.7 $[kg]$, for the UCA assuming full clean energy source, it is -4,896.744 $[kg]$, for the UCA assuming realistic energy mixture, it is 7,896.001 $[kg]$, and for the UCA fueled entirely by regular kerosene, it is 38,521.940 $[kg]$. Using the payload weight of the aircraft in tonnes stated before, the amount of CO_2 per metric tonne when taking into account the production of the fuel is 6,466.135 $[kg]$ for kerosene, -1,958.698 $[kg]$ for Airgo with synthetic kerosene with fully

[13] `https://www.volker-quaschning.de/datserv/CO2-spez/index_e.php` [Accessed on: 03-06-21]

clean energy, 3,158.4 [kg] for Airgo with synthetic kerosene with a realistic energy mixture, and 15,408.776 [kg] for Airgo fueled with regular kerosene. By comparing the values obtain for the 747-400F and the UCA fueled by synthetic kerosene with a realistic energy mixture, this yields a CO_2 emission reduction of 51.2%. This reduction in emissions does indeed prove that the use of synthetic kerosene is more sustainable.

Table 7.5: Total CO_2 Emitted per Aircraft

Aircraft	CO_2 **Emitted [kg]**	CO_2 **Emitted per Tonne of Cargo [kg]**	**Percentage Difference to Boeing 747-400F per Tonne of Cargo [%]**
Boeing 747-400F	801,800.7	6,466.135	-
Clean UCA (Synthetic Kerosene)	-4,896.743	-1,958.698	130.3% Less
Realistic UCA (Synthetic Kerosene)	7,896.001	3,158.45	51.2% Less
UCA (Regular Kerosene)	38,521.940	15,408.776	138.3% More

7.2.3. Fuel System

To deliver the selected fuel to the engine and charge the battery, an appropriate fuel system is desirable. When designing a fuel system, redundancy has to be taken into account in order to reduce the risk of negative outcomes. In this case, a negative outcome would be a fuel tank leaking and a fuel pump failing amongst other outcomes.

As seen in Figure 7.1, there are five fuel tanks found in the aircraft. There is a fuel tank in each wing, LFT for the left fuel tank and RFT for the right fuel tank. The remaining three are found in the fuselage, FFT for the forward fuel tank, CFT for the central fuel tank, and RFT for the rear fuel tank.

The fuel system will work by having the central fuel tank be the main tank to transfer fuel to the engine and have the remaining four tanks move their fuel to the central fuel tank in the following order, FFT, RFT, and lastly, LFT and RFT simultaneously. To circumvent the case that a fuel tank leaks, all the tanks are connected to each other which will allow the transfer of fuel in case a tank leaks. Additionally, in the case that the central fuel tank leaks, instead of the central fuel tank pumping the fuel to the engine, the FFT will be tank responsible for the transfer, followed by the RFT in the case the FFT also leaks, and the LFT and RFT simultaneously in the case that they are the last remaining functionaing tanks. Additionally, for redundancy, two pumps are used for each fuel tank in the case that one fails and for every line seen in Figure 7.1, it represent a pair of fuel lines in case one fails. Regarding valves, they allow the movement of fuel to their desired locations. It is important to note that the figure is not drawn to scale nor are the placement of the components absolutely accurate. The figure is simply meant to provide an understanding as to how the fuel system operates.

Additionally, the use of synthetic kerosene brings with a needed change in the fuel system, specifically the o-rings used. This is due to synthetic kerosene's lack of aromatic content compared to regular kerosene's 15% to 16% aromatic hydrocarbon content. When the two most commonly used o-rings in aviation fuel systems were used, o-rings made from AMS-P-5315 and MIL-STD-25988, with a 50 to 50 blend of synthetic and regular kerosene, the reduction of aromatic contact caused a significant increase in compression set, the difference between the original thickness of the o-ring and the thickness after compression expressed in percentage, which leads to a reduction in service life. If pure synthetic kerosene was used, a hypothetical o-ring that experiences 60% compression set while maintaining functionally would spike up to 80% compression set which would cause an immediate leak. Therefore, instead of the two most common o-rings, the fuel system in the aircraft will use an o-ring made from AMS 7379 fluorocarbon seal materials as it has been proven to not experience any consequences when used with synthetic kerosene and will also allow possibility of holding regular kerosene or mixture of both[14].

[14] `https://www.sae.org/works/committeeResources.do?resourceID=236915` [Accessed on: 15-06-21]

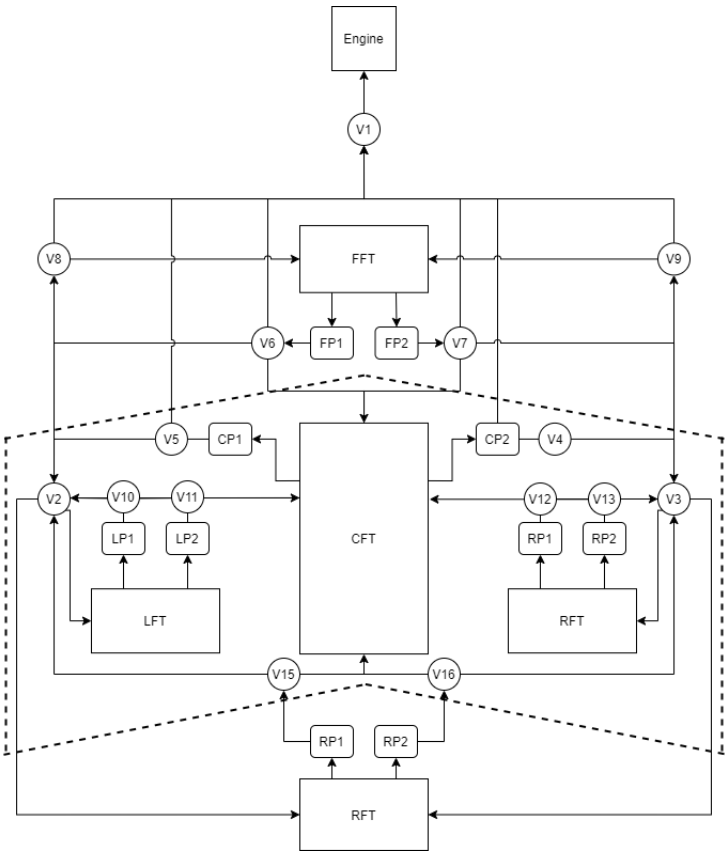

Figure 7.1: Fuel System

7.3. Engine

In order to find a suitable engine for the concept, it was first necessary to determine the amount of thrust required at take off as this when the thrust required to be supplied by the engine peaks. This was determined to be 35 [kN].

With this in mind, it was possible to determine a turbofan engine which provides roughly the same amount of thrust. To do so, it was decided that a viable engine would be chosen for each of four major manufacturers of turbofan engines, General Electric, Rollys-Royce, Pratt & Whitney, and Honeywell. Therefore, the four viable turbofan engines are, the General Electric CF34, the Rolls-Royce AE 3007, the Pratt & Whitney Canada PW300, and the Honeywell HTF7000. A table representing the specifications of each engine can be found below.

Table 7.6: Engine Specifications Comparison [26]

Model	**Takeoff Thrust Range** [kN]	**Cruise SFC** [$mg/N \cdot s$]	**Dry Weight** [kg]
GE CF34	38.48 - 82.26	18.39 - 20.13	717 - 1,724
R-R AE 3007	28.66 - 42.3	17.71	717.1 - 719.4
P&WC PW300	20.81 - 32.9	19.23 - 19.29	450 - 473
Honeywell HTF7000	33.36 - 39.14	19.34	618.7

From Table 7.6, a trade-off can be performed to determine which engine would be most suitable for the UAC. First, it can be determined that the Pratt & Whitney Canada PW300 is ill-suited for the UAC due to its thrust range capping out at a thrust of 32.9 [kN] whereas the UAC requires a minimum thrust of 35 [kN]. Second, due to its SFC and weight being higher than two alternative engines, the General Electric CF34 is also ill suited for the UAC. Therefore, this leaves two remaining engines, the Rolls-Royce AE 3007 and the Honeywell HTF7000. Each of these two engines brings with it its own benefit; the Rolls-Royce AE 3007 has a lower SFC and the Honeywell HTF7000 has a lower weight. Due to the lower SFC allowing a reduced weight as less fuel is consumed and therefore less fuel is required to be brought upon the UAC which adds the benefit of less emissions being produced, the Rolls-Royce AE 3007 was chosen to be the engine of choice for the UAC.

The next step in engine determination is the determining of the specific variant of the engine which would be best suited for the UAC. There are two main variants of the Rolls-Royce AE 3007, the AE 3007A and the AE 3007C. As seen

in Table 7.7, The AE 3007C simply does not produce enough thrust to meet the required minimum amount of thrust. Therefore, the Rolls-Royce AE 3007A is the specific engine most suitable for the aircraft.

Table 7.7: Variant Specifications Comparison[15]

Variant	**Takeoff Thrust Range** $[kN]$	**Cruise SFC** $[mg/N \cdot s]$	**Dry Weight** $[kg]$
AE 3007A	33.7–42.3	17.71	719.4
AE 3007C	28.66–31.32	17.71	717.1

The complete relevant specifications of the Rolls-Royce AE 3007A engine is shown in Table 7.8. Note that the cruise SFC in Table 7.8 is different than the one in Table 7.7 and Table 7.6 as the former is the one calculated using the propulsion model, which will be discusses in the subsequent section, for the cruise of the UCA whereas the latter is determined by looking into the cruise SFC trend of the aircraft incorporating the specfic engine.

Table 7.8: The Rolls-Royce AE 3007A Specifications [26] [27]

Specification	**Value**
Takeoff Thrust at Sea Level $[kN]$	33.7–42.3
Stationary Thrust at Sea Level$[kN]$	33.717
Cruise SFC $[mg/N \cdot s]$	17.71
Dry Weight $[kg]$	719.4

Specification	**Value**
Fan Mass Flow $[kg/s]$	109 - 127
Stationary SFC at Sea Level$[mg/N \cdot s]$	10.2
Bypass Ratio $[-]$	5.3:1
Overall Pressure Ratio $[-]$	24:1

Specification	**Value**
Length $[m]$	2.923
Fan Diameter $[m]$	0.978
Width $[m]$	1.172
Height $[m]$	1.415

7.4. Propulsion Model

As stated before, in order to be able to obtain the thrust and the SFC produced by the engine at different altitudes and at different speeds, a model of the engine had to be produced. This was done by using ideal cycle analysis whilst taking into account the inefficiencies of each stage and the assumptions stated in Subsection 7.1.1. This allowed the obtaining of the temperature and pressure at each subsequent stages and allowed the obtaining for the thrust available produced by the engine.

The Rolls-Royce AE 3007A has a design found typical in most turbofans, it has a twin spool design with the following components: one intake fan, two compressors, an LPC, low pressure compressor, and a HPC, high pressure compressor, a combustion chamber, and two turbines, an LPT, low pressure turbine, and a HPT, high pressure turbine. Each components can be dubbed as station and at each station, the pressure and temperature will change. These stations are numbered as shown in Figure 7.2 for the purpose of clarity in reporting and equations. The model is produced by following the movement of air going thorough these stations starting at station 1 and ending simultaneously at station 8 and 18.

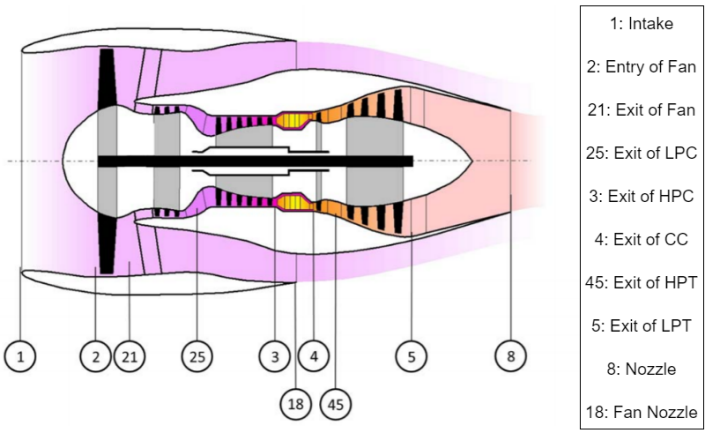

Figure 7.2: Turbofan Schematic and Stations [19]

Various fixed parameters are needed to be able to estimate the performance of the engine. These parameters are shown below in Table 7.9 BPR is the bypass ratio, Π is pressure ratio, $\dot{m}$ is mass flow, η is efficiency, LHV is lower heating value, R is the specific gas constant, κ is the constant specific heat ratio, C_p is the constant specific heat, TIT is the turbine inlet temperature, d_{FAN} is the diameter of the fan.

[15] `https://rgl.faa.gov/Regulatory_and_Guidance_Library/rgMakeModel.nsf/0/ec513c57c0969be5862580980053a0aa/\protect\T1\textdollarFILE/TE6CH_Rev29.pdf` [Accessed on: 15-06-21]

Table 7.9: Fixed Parameters [26] [27] [19]

Parameter	Value
BPR [–]	5
$\dot{m}_0$ $[kg/s]$	109
η_{NOZZLE} [–]	0.98
R $[J/kg \cdot K]$	287
TIT $[K]$	1,750

Parameter	Value
Π_{FAN} [–]	1.4
η_{FAN} [–]	0.9
η_{MECH} [–]	0.99
κ_{air} [–]	1.4
d_{FAN} $[m]$	0.978

Parameter	Value
Π_{LPC} [–]	2.15
η_{LPC} [–]	0.94
η_{LPT} [–]	0.94
κ_{gas} [–]	1.33

Parameter	Value
Π_{HPC} [–]	8.05
η_{HPC} [–]	0.94
η_{HPT} [–]	0.94
$C_{p,air}$ $[J/kg \cdot K]$	1000

Parameter	Value
Π_{CC} [–]	0.99
η_{CC} [–]	0.99
LHV $[MJ/kg]$	43
$C_{p,gas}$ $[J/kg \cdot K]$	1150

It is important to take note of values Π_{LPC}, Π_{HPC}, and Π_{FAN}. These values were not available directlty and instead the overall pressure ratio was given. This means that only the pressure ratio of the air after the HPC to the air before the before the intake fan was given. Therefore, a range of values was possible for the Π_{LPC}, Π_{HPC}, and Π_{FAN} to have in order to meet the given overall pressure ratio. To ensure the values are logical, the pressure ratio of the fan was limited to range of 1.4 and 1.6, LPC was limited to a range between 1 to 2.5 and the the HPC was limited to a range between 8 and 15. From this, the ratios which gave the thrust closest to the maximum required thrust for take off at sea level was chosen.

Lastly, to perform the analysis, certain inputs are required. These inputs are shown in Table 7.10. V_0 is velocity, p_0 is ambient pressure, and T_0 is ambient temperature.

Table 7.10: Inputs

Input	Unit
V_0	m/s
p_0	Pa
T_0	K
ρ_0	kg/m3

With all the parameters and inputs determined, it is now possible to describe the model. Essentially, the model calculates the pressure and temperature at each station shown in Figure 7.2 except at station 1. First, the total pressure and temperature is calculated from the mach number, the ambient pressure and the ambient temperature. Mach number was calculated using Equation 7.1, total pressure was calculated using Equation 7.2, and total temperature was calculated using Equation 7.3.

$$M_0 = \left(\frac{V_0}{\kappa_{air} \cdot R \cdot T0} \right)^{\frac{1}{2}} \quad (7.1) \qquad p_O = p_0 \cdot \left(\frac{T_O}{T} \right)^{\left(\frac{\kappa}{\kappa - 1} \right)} \quad (7.2) \qquad T_O = T_0 \cdot \left(1 + \frac{\kappa - 1}{2} M^2 \right) \quad (7.3)$$

From station 21 up to station station 4, the methods are the exact same. Pressure was calculated using Equation 7.4 and temperature was calculated using Equation 7.5. It is important to note that the 01 and 02 subscripts do not indicate stations 1 and 2 but instead indicate relative subsequent stations. However, Equation 7.5 was not used to calculate the temperature at station 4, exit of the combustion chamber, as that is given by TIT.

$$\frac{p_{02}}{p_{01}} = \Pi_{is} \quad (7.4) \qquad \frac{T_{02}}{T_{01}} = 1 + \frac{1}{\eta_{is}} \left[\left(\frac{p_2}{p_1} \right)^{\left(\frac{\kappa - 1}{\kappa} \right)} - 1 \right] \quad (7.5)$$

Alongside this, the mass flow that goes into the core, $\dot{m}_{hot}$, and the mass flow of the bypass stream, $\dot{m}_{cold}$, was calculated using the BPR and Equation 7.7 and Equation 7.8 respectively. Beforehand, the mass flow sucked in by the fan needs to be calculated using Equation 7.6. Furthermore, using the calculated core mass flow, the mass flow of the fuel, $\dot{m}_f$ was obtained using Equation 7.9

$$\dot{m} = \dot{m}_0 + \rho_0 \cdot V_0 \cdot \pi \cdot \left(\frac{d_{FAN}}{2} \right)^2 \quad (7.6) \qquad \dot{m}_{hot} = \frac{\dot{m}}{BPR + 1} \quad (7.7)$$

$$\dot{m}_{cold} = \dot{m} - \dot{m}_{hot} \quad (7.8) \qquad \dot{m}_{fuel} = \frac{\dot{m} \cdot c_{p,gas} \cdot (TIT - T_3)}{LHV \cdot \eta_{cc}} \quad (7.9)$$

Before analyzing the turbine, the work required by the fan and the compressors needed to be obtained. They are obtained using Equation 7.10, Equation 7.11, and Equation 7.12 respectively.

$$W_{fan} = \dot{m} \cdot c_{p,air} \cdot (T_{21} - T_O) \tag{7.10}$$

$$W_{LPC} = \dot{m}_{hot} \cdot c_{p,air} \cdot (T_{25} - T_{21}) \tag{7.11}$$

$$W_{HPC} = \dot{m}_{hot} \cdot c_{p,air} \cdot (T_3 - T_{25}) \tag{7.12}$$

Then, the power required to be generated by the turbines can be computed using Equation 7.13 and Equation 7.14.

$$W_{LPT} = \frac{W_{LPC} + W_{FAN}}{\eta_{mech}} \tag{7.13}$$

$$W_{HPT} = \frac{W_{HPC}}{\eta_{mech}} \tag{7.14}$$

Then, both the pressure and temperature can be calculated for the stations after the LPT and HPT, stations 45 and 5 respectively, using Equation 7.15 and Equation 7.16. As stated previously, it is important to note that the 01 and 02 subscripts do not indicate stations 1 and 2 but instead indicate relative subsequent stations.

$$\frac{p_{02}}{p_{01}} = \left[1 - \frac{1}{\eta_{is}}\left(1 - \frac{T_2}{T_1}\right)\right]^{\frac{\kappa_{gas}}{\kappa_{gas}-1}} \tag{7.15}$$

$$T_{02} = T_{01} - \frac{W}{\dot{m}_{hot+fuel} \cdot C_{p,gas}} \tag{7.16}$$

Afterwards, it is to be determined whether or not the nozzle and the fan nozzle of the engine are chocked. Therefore, the critical pressure ratio and actual pressure ratio of the nozzle and the fan nozzle needs to be calculated. This is done using Equation 7.17, Equation 7.18, and Equation 7.19 respectively.

$$\Pi_{crit} = \left[\frac{1}{\left(1 - \left(\frac{1}{\eta_j}\right) \cdot \left(\frac{\kappa_{gas}-1}{\kappa_{gas}+1}\right)\right)^{\frac{\kappa_{gas}}{\kappa_{gas}-1}}}\right] \tag{7.17}$$

$$\Pi_{real,nozzle} = \frac{p_5}{p_0} \tag{7.18}$$

$$\Pi_{real,fannozzle} = \frac{p_{21}}{p_0} \tag{7.19}$$

However, the engine, regardless of atmospheric conditions, is always choked. Therefore, to calculate the thrust produced by both core and the fan, first the pressure and temperature needs to be calculated using Equation 7.20 and Equation 7.21. Then, the density, jet velocity of the exhaust, and effective exhaust area is to be calculated using Equation 7.22, Equation 7.23, and Equation 7.24 respectively. With all these calculated, the final net thrust produced by the engine is given by Equation 7.25 and the SFC is given by Equation 7.26. As stated before and for the final time, it is important to note that the 01 and 02 subscripts do not indicate stations 1 and 2 but instead indicate relative subsequent stations. Additionally, $\dot{m}_n$ represent either $\dot{m}_{hot+fuel}$ or $\dot{m}_{cold}$ depending upon whether it is the thrust of core or the fan that is being calculated respectively.

$$p_{02} = p_{01}\left(\frac{1}{\Pi_{crit}}\right) \tag{7.20}$$

$$T_{02} = T_{01}\left(\frac{2}{\kappa_{gas}+1}\right) \tag{7.21}$$

$$\rho = \frac{p}{R \cdot T} \tag{7.22}$$

$$V = \sqrt{\kappa_{gas} \cdot R \cdot T} \tag{7.23}$$

$$A = \frac{\dot{m}_n}{\rho \cdot V} \tag{7.24}$$

$$F_N = \dot{m}_n(V - V_0) + A(p_{02} - p_0) \tag{7.25}$$

$$SFC = \frac{\dot{m}_{fuel}}{F_N} \tag{7.26}$$

7.5. Verification and Validation

The verification of the propulsion model was done using hand calculations. This is a valid method for verification as the production of the propulsion system required the re-utilisation of the same limited amount of formulas. After finishing the verification procedure, no errors were found. Validation was performed by comparing the model to the thrust produced and SFC needed by the chosen engine, the Rolls-Royce AE3007A, at different conditions such static at sea level, take-off at sea level, and cruise [27]. The results showed a discrepancy of around 16%. Additionally, the

model was further validated by comparing it to exercises which utilised the same exact process found in the program [19]. When compared, the results were the exact same. Therefore this model is deemed valid.

7.5.1. Sensitivity Analysis

A sensitivity analysis was conducted for the engine trade-off. Regarding the engine, in order to allow a change in the choice of engine variant, a 10% decrease in the takeoff thrust requirements would have changed the winner of the engine variant trade-off. Alternatively, a 10% increase in the takeoff thrust requirement would have instead resulted into a change in the winner of the engine trade-off rather than engine variant trade-off. Lastly, if more weight was put on the dry weight criterion rather than the SFC criterion, then another engine would have also been chosen in the engine trade-off.

7.6. Conclusion

The aim of this section was to get definite characteristics of the fuel type of the engine, the corresponding fuel system, and determining an appropriate engine for the UCA. This was all achieved. Though there are different fuel options available in order to reduce CO_2 emissions, the most promising and feasible one appeared to be synthetic kerosene and therefore will be used for the UCA. This was proven true when it was determined using synthetic kerosene could result into up to a 51.2% reduction in CO_2 emissions. However, fuel systems which are used for regular kerosene cannot be used with synthetic kerosene and therefore, o-rings made of a different material have to be used, MS 7379 fluorocarbon seal materials to be exact. Additionally, in order to produce enough thrust to fly, the Rolls-Royce AE 3007A was determined to be the most suitable engine for the UCA. Lastly, a model was produced in order to simulate the thrust produced by the engine at different altitudes and at different altitudes which was verified and validated.

8
Structural Wing and Fuselage Design

This chapter will investigate the feasibility and interaction of multiple key structures, these being the wing structure, the fuselage, and the interaction between the wing spars, the fuselage and the engine mounting. Before conducting the analysis, boundary conditions are required which were derived from the requirements identified in the baseline report [2]. Section 8.2 will discuss in detail the tool that was developed to iterate the wing design, and the methods that the wing was designed with, finally presenting a wing capable of performing in the given conditions. Section 8.3 will investigate whether the conventional semi-monocoque structure for the fuselages is still the best approach, as well as size stringer and skin for fuselage. The chapter is concluded by discussing the verification and validation procedures used, followed by a chapter conclusion.

8.1. Requirement Analysis

This section discusses all requirements related to the fuselage and wing structure. The requirements have been divided into three sections.

General requirements:

- **REQ-SYS-FLT-2.5.01:** The UCA shall have a factor of safety of 1.5 applied to the prescribed limit load which are considered external loads on the structure. ***CS 25.303 Factor of Safety*** [5]
- **REQ-SYS-FLT-2.5.02:** The UCA shall withstand the ultimate flight loads for 3 seconds without failing. ***CS 25.305 Strength and Deformation*** [5]
- **REQ-SYS-FLT-2.5.03:** Support limit loads without detrimental, permanent deformation. ***CS 25.305 Strength and Deformation*** [5]
- **REQ-SYS-FLT-2.5.04:** Deformation may not interfere with safe operation ***CS 25.305 Strength and Deformation*** [5]
- **REQ-SUBSYS-LDG-2.7.01:** Operate within the entire flight envelope CS 25.33

Wing:

- **REQ-SUBSYS-LDG-2.7.00:** Sustain loads up-to a load factor of 3.57 CS 25.321
- **REQ-SUBSYS-LDG-2.7.01:** Operate within the entire flight envelope CS 25.33

Fuselage:

- **REQ-SUBSYS-CAR-2.5.00:** The UCA shall be able to maintain a cabin pressure altitude of no more than 4572 [m] (15000 [ft]) in the event of any reasonably probable failure or malfunction in the pressurisation system. ***CS 25.841 Pressurised Cabins*** [5]
- **REQ-SUBSYS-FUS-2.6.00:** The structure supporting any power unit must be designed for the loads, including gyroscopic loads. CS 25.365 [5]
- **REQ-SUBSYS-FUS-2.6.01:** Structure must be strong enough to withstand flight loads combined with the pressure differential. CS 25.364 [5]

8.2. Wing Design

The wing of an aircraft experiences the highest loads and is the most critical in terms of structurally being able to withstand the loads encountered during the whole flight envelope. In this section, the design of the wing box is carried out with two main design goals in mind; the first is sustaining the aerodynamic loading along with safety margins and the second is being able to do so while being as light as possible.

8.2.1. Assumptions

A wingbox is a complex structural model which can be idealized as a simpler model that behaves almost identically under the same loading conditions. The number and type of assumptions is the main factor dictating the accuracy and the level of complexity of the model. The following assumptions are made:

- Stiffeners and spar flanges carry axial stresses only
- Web, skin and spars carry both axial and shear stresses
- Shear stress is constant in between nodes (booms)

- The wingbox is assumed to be a thin-walled structure
- No distortion between the cells (regions separated by spars) in the wingbox, thus the whole cross section rotates with the same angle
- The weight of wing and high lift devices is neglected since it is much smaller than the aerodynamic loading acting on the wing. It is also acting in an opposite direction to the internal loads, thus this is a conservative assumption

8.2.2. Finite Element Model

A design process requires constant iteration until requirements are satisfied , to be able to do so, a modular tool had to be developed enabling the design team to quickly alter design values and see the effect of of these modifications on the structural performance and integrity of the design.

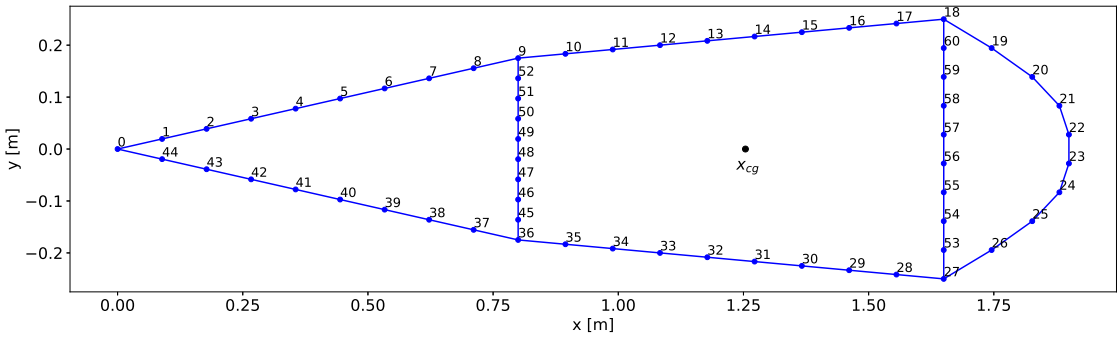

Figure 8.1: Example cross-sectional mesh grid

A mesh grid of booms is setup to idealize and discretize the cross-section of the wing. A boom is an idealized structural element represented as a fictious circle that has its own area, this area is obtained from the elements it is idealizing. Longitudinal stiffeners are simply idealized by adding their geometrical cross-sectional areas to the nearest boom. This follows from the assumption that stiffeners and spar flanges carry direct stresses only. Web, skin, and spars on the other hand are more complex to determine since they are assumed to carry both axial and shear stresses. The contribution of these elements to the boom area can be calculated as follows:

$$B_1 = \frac{t_{skin} b_{skin}}{6}\left(2 + \frac{\sigma_2}{\sigma_1}\right) \tag{8.1}$$

$$B_2 = \frac{t_{skin} b_{skin}}{6}\left(2 + \frac{\sigma_1}{\sigma_2}\right) \tag{8.2}$$

With B_i being the area, t_{skin} the skin thickness, b_{skin} the length of the skin, and σ_i the stress that is carried by the ith boom. For this reason, each boom has to be aware of its neighboring booms and the dimensions of the skin connecting them together.

Boom areas are initially set to zero and once skin dimensions and stiffening elements are added to the cross section, their contribution is added to the respective booms. Stringers can only be added to locations where a boom exists on the mesh, thus making the mesh finer is beneficial for two reasons. The first is that stringers can be positioned more accurately and the second is that the stress distribution becomes smoother and a more accurate representation of the physical model, thus diminishing the effects of the third assumption made earlier.

The centre of gravity location is obtained after the structural elements are constructed using Equation 8.3 and Equation 8.4:

$$x_{cg} = \frac{\sum B_i x_i}{\sum B_i} \tag{8.3}$$

$$y_{cg} = \frac{\sum B_i y_i}{\sum B_i} \tag{8.4}$$

With x_i and y_i referring to the coordinates of each boom with respect to the coordinate system seen in Figure 8.1. Afterwards the moment of inertia around each axis can be determined as follows:

$$I_{xx} = \sum_{i=1}^{n}(y_i - y_{cg})^2 B_i \quad I_{yy} = \sum_{i=1}^{n}(x_i - x_{cg})^2 B_i \quad I_{xy} = \sum_{i=1}^{n}(x_i - x_{cg})(y_i - y_{cg}) B_i \tag{8.5}$$

The model is constructed to allow for the following free (design) variables:

- Number of booms, determining the mesh smoothness
- General dimensions such as chord length and angles
- Spar locations and dimensions
- Stringers locations and dimensions
- Skin thickness
- Sweep and taper ratio

8.2.3. Aerodynamic Loading

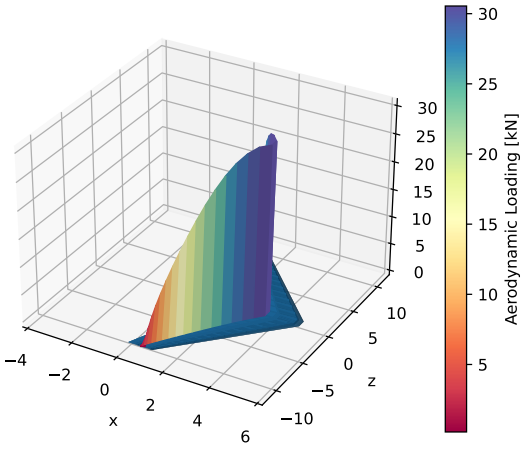

Figure 8.2: Aerodynamic loading acting on the wing

The aerodynamic loading acting on the wing has been obtained using a simulation in XFLR5. The loading can be seen illustrated in Figure 8.2

8.2.4. Internal Loading

The internal loading considered are the shear forces V_x and V_y, bending moments M_x and M_y, and the torsion T_z. They are calculated as follows:

$$V_y = \int_{z=b}^{\tilde{z}} F_y(b-z)dz \tag{8.6}$$

$$V_x = \int_{z=b}^{\tilde{z}} F_x(b-z)dz \tag{8.7}$$

$$M_x = V_y(b-z) \tag{8.8}$$

$$M_y = V_x(b-z) \tag{8.9}$$

With F_y and F_x being the distributed loading in the y and x direction respectively. The results are plotted in the diagrams below.

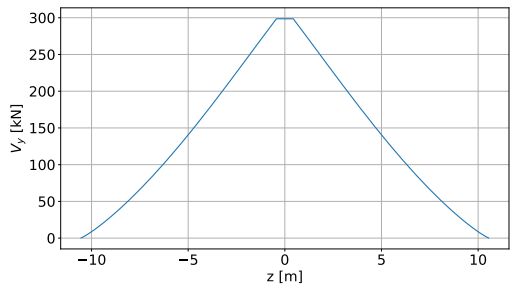

Figure 8.3: Internal loading diagram

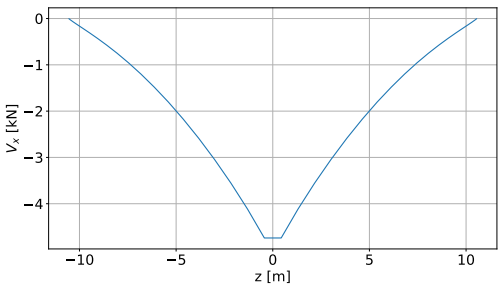

Figure 8.4: Internal loading diagram

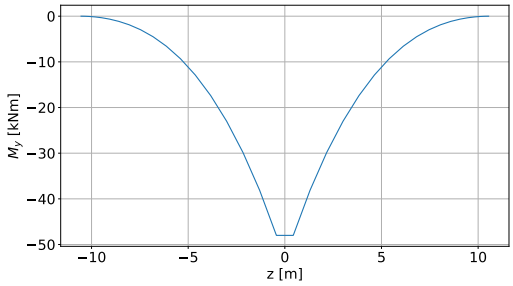

Figure 8.5: Internal loading diagram

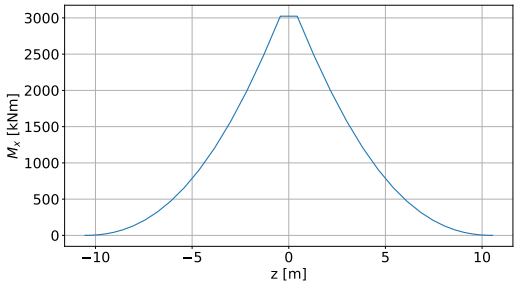

Figure 8.6: Internal loading diagram

8.2.5. Stress Calculation

The internal forces and moments are then added to the model to evaluate the resultant direct and shear stresses in each cross section. The normal stress, σ_z, for an unsymmetric section is evaluated using:

$$\sigma_z = \frac{\left(M_x I_{yy} - M_y I_{xy}\right) y + \left(M_y I_{xx} - M_x I_{xy}\right) x}{I_{xx} I_{yy} - I_{xy}^2} \tag{8.10}$$

The cross section can be seen as a multicell beam, each closed cell or section within is statically indeterminate. To make the cross section statically determinant, each of the cells has to be virtually cut to determine the basic shear flow, q_b, which is the shear flow in an open section. At the skin element where the cut is made, the shear flow has to be 0 since it is a free edge. Afterwards the cut shear flow, q_{s_0} can be determined for each cell. The cuts in this model are made in the locations represented by the red lines in Figure 8.1.

The basic shear flow carried by a skin element can then be found by adding the boom's shear contribution, Δq_k, to the basic shear flow of the previous skin element; or:

$$q_{b_j} = q_{b_{j-1}} + \Delta q_k \tag{8.11}$$

$$\Delta q_k = -\frac{I_{xx} V_x - I_{xy} V_y}{I_{xx} I_{yy} - I_{xy}^2} B_k x_k - \frac{I_{yy} V_y - I_{xy} V_x}{I_{xx} I_{yy} - I_{xy}^2} B_k y_k \tag{8.12}$$

At junctions, where the booms and spars meet, it is more complex. The shear flow through the junctions has to be in equilibrium, meaning that the sum of the shear flows flowing into the boom in addition to Δq_k of the respective boom has to be equal to the shear flow going out of the boom. To maintain the equilibrium condition, as well as the boundary conditions determined by the cuts; a linear system of equations has to be created and solved. Giving as a result the basic shear flow carried by each skin element.

The angle of twist for each of the cells is found using:

$$\left(\frac{d\theta}{dz}\right)_i = \frac{1}{2A_i} \oint \frac{\left(q_{b_i} + q_{s_{0_i}}\right) ds}{t_i G_i} \tag{8.13}$$

By assuming no distortion and a constant angle of twist throughout the entire cross-section, the following compatibility equations are found to be valid:

$$\left(\frac{d\theta}{dz}\right)_I = \left(\frac{d\theta}{dz}\right)_{II} = \left(\frac{d\theta}{dz}\right)_{III} = \frac{d\theta}{dz} \tag{8.14}$$

Bringing 4 unknowns to the system of equations; $q_{s_{0_1}}$, $q_{s_{0_2}}$, $q_{s_{0_3}}$ and $\frac{d\theta}{dz}$ and the 3 equations. Adding the moment equivalency equation, stating that the moment caused by shear forces V_x and V_y must be the same as the moment caused by the shear flows (q_b and q_{s_0}) about the same point gives the last equation needed to solve for the unknowns. Once q_{s_0} is known for each cell, it is added to the basic shear to get the total shear acting on the element.

$$q_s = q_b + q_{s0} \tag{8.15}$$

Now that the normal and shear stresses are evaluated, the Von Mises yield criterion is calculated at each stress element. The von Mises stress can be calculates using:

$$\sigma_v = \left[\frac{(\sigma_1 - \sigma_2)^2 + (\sigma_2 - \sigma_3)^2 + \left(\sqrt{3} - \sigma_1\right)^2}{2}\right]^{1/2} \tag{8.16}$$

The expression can be further simplified since the shaft is subjected to shear, axial stress and a normal stress caused by the bending.

$$\sigma_v = \sqrt{\sigma_z^2 + 3\tau^2} \tag{8.17}$$

8.2.6. Design Process and Optimization

The sizing of the stringers, spars and skin thickness needs to be done such that the structure is able to withstand the aerodynamic loading at the maximum load factor and including the safety margin, while being as light as possible. Thus, an optimization algorithm is set up to achieve that.

At first thought, one might think of obtaining the optimal stringer dimensions by maximising the moment of inertia to area ratio of the stringers. Thinking that as this ratio increases, the weight of the stringers is reduced while its load carrying performance is increased. However, it is important to realize that the moment of inertia of the entire cross section is mainly dependent on the Steiner term of the stinger and not the moment of inertia across its own axis. This term, from the parallel axis theorem, is the area multiplied by the square of the vertical distance from the x-axis. Thus it is considered to be a naive approach because the optimization algorithm would be trying to minimize the stringer area which is the dominant contributor.

An alternative optimization algorithm is thus considered; the area of the stringers, spar dimensions and skin thicknesses are permuted. More specifically, the Cartesian product, which is the set of all possible ordered triplets is obtained. With each triplet being a set containing of a stringer area, specific spar dimensions and a skin thickness. A stress analysis is then carried out for each triplet in the Cartesian product set to obtain the maximum stress value that is encountered by the structure. Once each triplet is considered and the corresponding stress value is evaluated, all triplets that have a stress value higher than the yield strength are discarded. The remaining triplets represent combinations of design choices for a structure that is at least able to carry the required loads. The triplet that has the least total area of stringers, spars and skin is chosen.

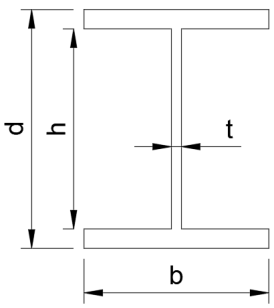

Figure 8.7: I-beam stringer design variables

The area of each of the stringers is now obtained, however, the specific dimensions are still unknown. An optimization process is carried out again to maximize the moment of inertia of the stringer around its own axis, while subject to an equality constraint that guarantees the area remains the same as found in the previous optimization process.

Inequality constraints are also used ensuring that the dimensions of the stringer are sane, feasible to manufacture and within airfoil dimension limits. All values are in [mm].

$$
\begin{array}{lccccc}
\max & I_{xx} & & & & \\
\text{s.t.} & b\cdot d - h\cdot(b-t) & = & area & & \\
 & b & \geq & t+2.0 & & \\
 & d & \geq & h+2.0 & & \\
 & 10.0 & \geq & b & \geq & 80.0 \\
 & 20.0 & \geq & d & \geq & 110.0 \\
 & 25.0 & \geq & h & \geq & 135.0 \\
 & 2.0 & \geq & t & \geq & 15.0
\end{array}
\tag{8.18}
$$

There is an important difference between the two methods. The first method would have first determined the stringer dimensions by maximizing its moment of inertia to area ratio. Once this is done, the stringer areas are no longer free variables but a constraint. The free variables remaining would thus be the spar and skin dimensions. However, with the used method, the stringer area, spars and skin are all free variables initially. The stringer area is obtained such that it yields sufficient structural performance, and then the dimensions are found using objective function and constraints set in Equation 8.18.

8.2.7. Results

Through iterations, it was possible to optimize the required number of stringers to be eight stringers on top, and eight stringers below. This is capable of handling the given loads at the maximum load factor while achieving a maximum stress at the yield strength corrected by the safety factor at the root of the wing.

The dimensions of the stringers in [mm] are shown in Figure 8.8 below. The skin thickness is 1.8 [mm] and the spar web thickness is 5.3 [mm].The spar caps have the same dimensions as the stringer flanges.

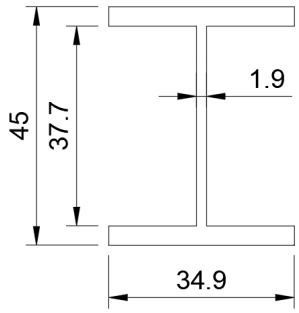

Figure 8.8: I-beam stringer dimensions

Figure 8.9 represents the wing with only the spars and skin. The stress distribution is large, and it can be seen that the maximum Von Mises stresses at the root will lead to yield and failure. To compensate for this, stringers were distributed on the top and lower portion of the skin between the two spars.

Figure 8.10 is the resulting Von Mises stresses throughout the wing with stringers applied. A noticeable result is that the stress is considerably less at the tips, this is a combination of assuming the stringers run the entire span at this stage of iteration, and the fact that the bending stress is considerably less at the tips. Reducing the numbers of stringers intermittently along the span between ribs would allow for a reduction of weight, while still achieving safe and manageable stresses.

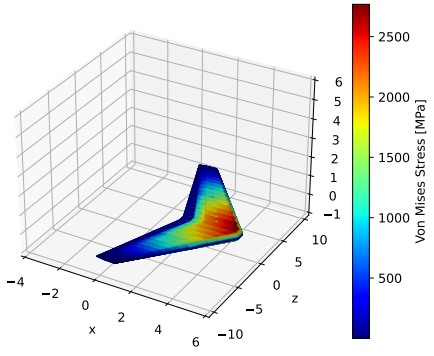

Figure 8.9: Von Mises stress with skin and spars

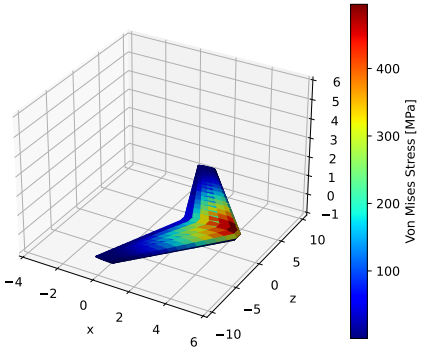

Figure 8.10: Von Mises stress after adding the stringers

The primary focus for the feasibility of the wing structure was whether the root could support all of the loads, as this is the highest loaded region. An additional objective was to already develop a tool which would allow for the further improvement and ease of iteration. Both have been considered achieved, as the structure has been designed and shown to support the required loads, with the benefit of a tool having been made which can be used as a more detailed tool to iterate with before a true FEM is conducted.

8.3. Fuselage Design

The fuselage is the primary structure of the aircraft, it protects the cargo from external effects, while also being capable of safely carrying the loads of all the lift and propulsion devices on-board. A well designed fuselage, is light-weight, while remaining stiff enough allowing for the continued operation of the aircraft without detrimental effects to performance.

8.3.1. Loading and Assumptions

In order to properly assess the feasibility of the fuselage in the given time frame, idealisations will have to be made. This will be in the form of how the aircraft is being loaded, with the addition of how the structure is represented.

For the loading of the aircraft, a beam system was assumed. Multiple uniform distributions were used to represent weights. Starting with the overall fuselage weight, which spanned the fuselage. The cargo was also taken into account as a distributed load. The wings generate lift which result in one of the only upward forces; this lift and any moments within the wing are transferred to the spars that interface with the fuselage. The engine location of the aircraft is a novel feature of the aircraft, its weight was taken to be a distributed load along its length, while a moment about the centre axis of the fuselage was placed to accommodate the induced moment from the displaced thrust on the structure The effect of the empenage is assumed to be negligible for this feasibility analysis, however its structure will still be discussed. The main landing gear will be connected to the main-wing spars, which will result in the main gear stress acting on the spars. The nose landing gear will be assumed to be a point load on the structure.

This distributed loading does not include the pressurization, as this characteristic is considered later in the stress analysis.

Structure idealization

The fuselage cross section of the aircraft is idealized to simplify the calculation of the moment of inertia. Boom areas are used to represent the stringers, while the skin is assumed to be a thin-walled structure.

Frames are assumed to be spaced evenly at a 50 $[cm]$ pitch, and the stringer area is assumed to be 100 $[mm^2]$.

8.3.2. Load Transfer

Fuselage design is a rather well understood concept, particularly for conventional semi-monocoque wing mounted engine aircraft, and dual rear mounted engines. However, the mounting of a single engine on the top of the fuselage is a relatively novel concept, with only a handful of commercial aircraft having adopted it in the past.

To investigate the feasibility of the fuselage, the decision was made to focus on the load path between the wing spars, the fuselage, and the engine. As the wing, landing gear, and engine produce significant loads that must be capable of supporting one another. During the creation of the beam loading, the moment induced by the off set engine was significant, requiring proper support for the engines thrust and weight. The thrust most notably must be transferred to the entire fuselage to distribute the stress as much as possible, in addition to accelerating the entire structure forward.

The solution that fuselage mounted engines have made use of are by creating local reinforcements by using the bulkheads or specialised frames to distribute the loads as best as possible to the stringers and skin. An example of this can be seen in Figure 8.11. The use of frames to attach the engine mounting points and pylons, allows for the thrust and weight to be transferred to the local circumference of the fuselage. This however does not ensure a proper transfer of the loads along the fuselage. The frames will only carry the shear, and not distribute the load longitudinally. The solution these aircraft employ is to use longerons and stringers throughout the fuselage, these will be connected to all of the frames with added reinforcement on the the spar and engine frames. In combination with the frames, this structure allows for shear, torsion, bending and direct stresses to be distributed throughout the structure and appropriately supported. This is best represented in Figure 8.12, where the numbered frames are the frames that are directly connected to the engine or spars, accompanied by smaller frames and stringers.

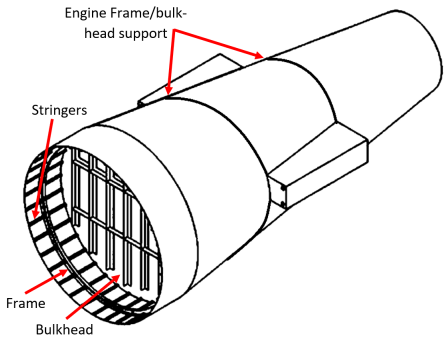

Figure 8.11: an example of current rear engine mounted fuselages [28]

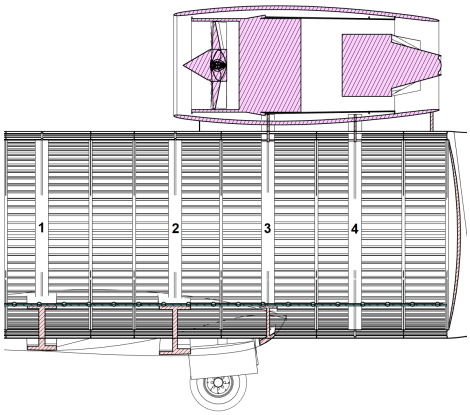

Figure 8.12: Engine and wing mounting points, making use of conventional frame, stringer and longeron structure.

The use of longerons, stringers, and frames to transfer the loads is an effective solution, but it might not be the only one. Another consideration was whether a more direct load path and support could be made. Since the wings and engine are located within the pressurized cargo area, any novel idea had to adhere to the skin of the fuselage. The concept was to use angled frames to directly connect the engine mounting points to the spars of the wing/landing gear, creating a truss structure of sorts.

The solution could introduce considerable weight savings if applied properly since both structures will be making use of the same frame. Many considerations had to still be made, by considering the manufacturability, practicality, and structural aspect of such a concept. The truss structure will require the creation of angled frames, where the stringer and frame cutouts will be at an angle with respect to the circumferential plane of the angled frames. This poses great difficulties in manufacturing the angled frames, and loses the benefits that scaled mass produced vertical frames will have on the cost of the section. The advantages from using the angled frames will also be negated by having to still compensate for buckling, and the general eccentricity and stiffness of the aircraft. The angle will make the optimising and predictability of the buckling in the structure more difficult.

The conclusion was drawn that for the feasibility and ease of manufacturing of the first version of this design, continuing to use the longerons, stringers and frames to transfer the loads is still the best solution under the time constraints. This design choice will still work in transferring the shear, buckling and direct stresses while maintaining the shape of the fuselage. It will still be advised for future development to do an in-depth analysis on the novel truss concept, as this might be a potential weight saving design change in later models of the aircraft. Without the novel concept, it will still be possible to share frames. Figure 8.12 shows how frame number 3 is connected to both the rear spar and leading engine mount.

8.3.3. Maximum Fuselage Loads

In order to determine magnitude and location of the maximum loads, multiple loadcases had to be analysed. By examining the gust loads, maneuver loads, and ground loads, the following maximum loadcases were considered. It should be noted that an additional consideration was the effect of the engines thrust to the structure in the form of the induced moment. This meant that for every loadcase, there were two possibilities, when with the maximum thrust, and another with zero thrust.

- Stable flight 1g, thrust
- Maximum flight loading 3.57g, thrust
- Stable flight 1g, zero thrust
- Maximum flight loading 3.57g, zero thrust

- Ground condition, thrust
- Ground condition, zero thrust

Generating distributed loadings of each case, allowed for the maximum shear and moment forces to be identified. Figure 8.14 is the resulting shear and moment diagram of the maximum case which was identified to be the Maximum maneuver load of 3.57 with engine thrust. The maximum moment and shear were identified to be acting at X-pos: 8.51 $[m]$ and 8.48 $[m]$ with loads of -360 kN and -645 kNm respectively.

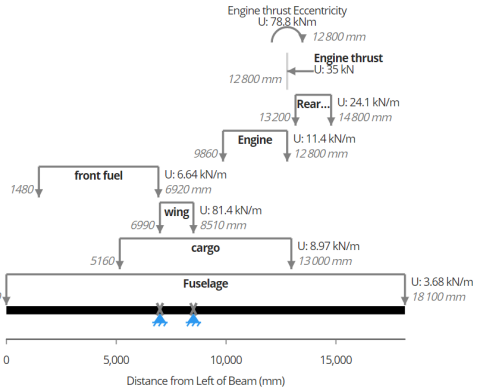

Figure 8.13: Load distribution for the Flight maneuver load of N=3.57

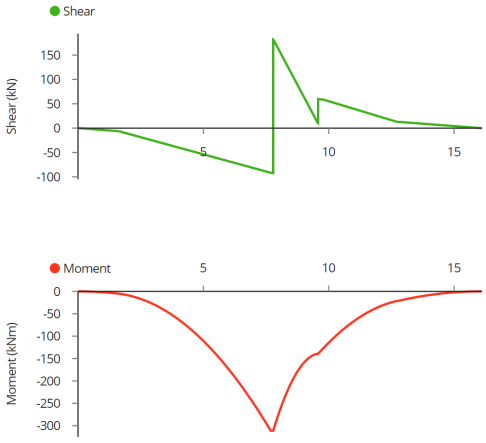

Figure 8.14: Shear and moment diagrams for the Flight maneuver load of N=3.57

This maximum load is occurring between the leading edge spar, and the rear engine mount. Referring to Figure 8.12, the location of this load is more specifically between frames 1 and 2. In this area a considerable amount of direct stress will exist due to the wing drag and engine thrust, and will have to be additionally considered to the shear and bending loads.

8.3.4. Stringer spacing and fuselage design

With the maximum loads identified, the critical resulting stress must be identified, whether it will be shear or bending. Quickly estimating the required skin thickness of the shear and the bending stress relative to AL-2024's respective tensile yield strength and respective shear strength was done by using Equation 8.19 & Equation 8.20. Using the selected material properties, and fuselage dimensions, the stress in bending case required a larger thickness, resulting in it being the dominant case to design for. This led to the conclusion that bending compliant fuselage will be shear compliant (at this level of design).

Once bending was determined to be the critical case, a more thorough equation had to be derived for the fuselage design, this resulted in Equation 8.21 which took into account the idealised booms within the fuselage, as well as the pressurization on the fuselage, and the direct stress.

$$t = \frac{Mz + Pr_{\text{fus}}^4 \pi}{\pi r_{\text{fus}}^3 \sigma_{\text{y}}} \tag{8.19}$$

$$t = \frac{VQ}{\pi r_{\text{fus}}^3 \tau_{\text{Shear}}} \tag{8.20}$$

$$\sigma_y = \frac{2P\pi r_{\text{fus}}^2 + F_{\text{Direct}}}{n_{\text{boom}} B_{\text{str}} + 2\pi r_{\text{fus}} t} + \frac{Mz}{I_{yy}} \tag{8.21}$$

Difficulty exists in optimising the skin thickness to the stringer boom area under bending, as the minimization of the skin thickness will converge to zero as the number of booms increases, or their area increases. Another design parameter had to be accounted for which depended on skin thickness, buckling was used as this design parameter, as failure under buckling dictates how the stringers, frames and skin should be sized to prevent failure under those loads. Equation 8.22 is the buckling equation for flat sheets, where the value K_c denotes the buckling coefficient, a value dependent on the ratio of length to the width of the sheet. This value is dependent on how the sheets are constrained, and for the case of the fuselage, they are considered to have a K_c of 4, under the assumption of the sheet being clamped to the frame, and under a hinged support from the stringer. The value of K_c changes with the ratio, so the value is adjusted as the value of the stringer spacing changes. For most aircraft the frame spacing is around 0.5 $[m]$ [1]. In Equation 8.22 the b variable, represents the width between the stringers. Finally a critical stress must be determined as a basis of determining the required skin thickness.

[1] `http://bluetunadocs.com/downloads/acsguide.pdf` [Accessed on: 03-06-2021]

$$\sigma_{cr} = K_c \frac{\pi^2 E}{12(1-\nu)} \left(\frac{t}{b}\right)^2 \tag{8.22}$$

A critical stress for buckling in aircraft is often a third of the ultimate stress [29]. Iterating upon this calculation in combination with the specific mass of the fuselage, calculated by the density multiplied by the area of the cross section. This iterative process yields a result of 80 stringers, with a pitch of 10 $[cm]$ (4.5 degrees), along the circumference. The resulting weight, with stringers of area 100 $[mm^2]$, results in a specific weight of 59.9 kg/m, at a skin thickness of 1.72 $[mm]$. This result is for the maximum case, and between frames 1 and 4 in Figure 8.12 will be this high stringer count, where the size of the stringers and frames can taper off at the front and rear of the fuselage.

The specific weight estimate is only for stringers and skin, this excludes the weight of the floor, the frames and other reinforcing structures that will be placed on the fuselage.

8.4. Verification and Validation

Wing

The verification of the model has been carried out mainly by creating a simple cross-section with a coarse mesh (small number of booms) and analysing the stresses acting on the model analytically. The model proved to be very consistent to the analytical solutions. The numerical solution found by the model always tended to a unique value as the mesh density increased, proving mesh convergence.

In addition, unit tests have been carried out throughout the whole process. For example, the shear flows calculated were integrated and resolved in the x and y direction and compared to the the vertical and horizontal shear forces applied. The moment due to the shear flow was also evaluated and compared to the moment of V_x and V_y.

Furthermore, a sensitivity analysis has been carried out to see if the results are as expected. Stringers were added only to the top skin to see whether the stresses in the top section would decrease in comparison to the bottom section or not. The same was conducted for varying stinger dimensions, spar dimensions and locations.

Fuselage

For the loading diagram, clearcalc's loading diagram tool was used. This company creates tools to calculate these exact problems. As a method of verifying whether their tool was producing accurate results, a small excel spread sheet was created that made simple load diagrams, this excel program was similarly verified using hand calculations. The result was that Clearcalc's software works accurately to create the loading diagrams required.

For the fuselage design, a python script was created. This script makes use of the formula's mentioned in the section. using a simple case with 4 booms, the problem could be solved by hand. The results were found to correspond with those of the software.

Finally, to ensure the software was performing as intended, a sensitivity analysis was conducted to see whether the result would change as expected. By changing the number of booms, it was expected that the required skin thickness would increase in order to still meet the buckling requirement. The conclusion of this test was considered a success as the software reacted exactly as expected. The same tests were conducted for fuselage radius, and the materials properties. All reacting as predicted.

To validate this result is difficult as it would require a real world example to compare to. Aircraft companies do not make the numbers of stringers inside their fuselage easy to access by the public. As a result, it would be advised that this information be acquired in future to make the program more trust worthy.

8.5. Conclusion and Recommendations

The aim of this section was to ensure the primary structures would be capable of performing their requirements under and exceeding the normal loads.

Internal loads had to be calculated given the aerodynamic loading distribution acting on the wing. The aerodynamic loading that the wing is designed to sustain is multiplied by a load factor of 3.57 as well as a safety load factor of 1.5. A design tool was then developed to analyse the Von Mises stresses under the given loads. The most critical stresses were found to be acting near the root, as expected. The tool was then used to optimize the number and dimensions of the stringers such that the maximum Von Mises stress on the wing is less than the yield strength of Al 7075-T6 (503 $[MPa]$).

Further weight reduction is possible to achieve by having some of the stringers running only midway through the wing, and the others continuing all the way until the tips. A more detailed analysis would have to be carried out to take into account the local stress concentration at the area the stringers are cut. It is also recommended to consider using tapered stringers, this however complicates the manufacturing process and thus increases the cost.

As for the fuselage, various loading diagrams were created of the fuselage, this resulted in the identification of the highest loading on the fuselage. The fuselage had to be capable of withstanding a load factor of 3.57. After considering shear and bending, it was found that bending was the critical design case. To effectively size the skin thickness and stringer pitch buckling was considered. The result was a stringer pitch of 10 $[cm]$ around the fuselage, at a skin thickness of 1.72 $[mm]$ and stringer area of 100 $[mm^2]$

The fuselage feasibility study only investigates the critical region, further weight reduction is possible by optimising the stringer count and skin thickness between the frames along the length of the fuselage. Sizing the frames is also suggested, as the spar and engine mounting frames will require appropriate sizing and reinforcing.

9
Material Selection

This chapter will discuss the material characteristics needed for several subsystems. Firstly, a requirement analysis will be included and is discussed in Section 9.1. The suitable materials for these different subsystems will be introduced in Section 9.2. After, the performance of all these materials is investigated in Section 9.3. Furthermore, a material trade-off is performed in Section 9.4. Subsequently, in Section 9.6 the sensitivity analysis is presented. Ultimately, the conclusion and recommendations are given in Section 9.7.

9.1. Requirement Analysis

The following requirements set in the Baseline Report [2] are of importance towards obtaining the different materials used in the design as well as determining the end-of-life strategy:

- **REQ-STK-12:** The UCA shall be profitable to manufacture and sell.
- **REQ-SYS-SUS-4.3.00:** The UCA shall be able to have 90 % of the structure recycled at the end of the useful life cycle.
- **REQ-SYS-FLT-2.5.01:** The UCA shall have a factor of safety of 1.5 applied to the prescribed limit loads which are considered external loads on the structure.

9.1.1. Assumptions

For the material selection, only 4 different structural systems will be analysed. This will be the wing box, fuselage, empennage and landing gear. In order to decrease the complexity of the design, only 1 material will be selected for every subsystem instead of a combination of different materials. The following assumption regarding the materials can be made:

- **ASU-MAT-01:** All metal alloys are homogeneous and isotropic.
- **ASU-MAT-02:** All material cost prices are estimations. This price will only be used for the trade-off.

9.2. Suitable Materials

In order to design all structures a suitable material selection will be made. An appropriate material must be selected for the wing box, fuselage, empennage and landing gear. For every structure only 1 material will be selected in order to reduce the complexity of the structural design itself. For structural components mainly two kind of materials are used, which are metal alloys and carbon fibres. Regarding the metal alloys, 2 different aluminium alloys, 1 titanium alloy, and 1 high strength steel alloy will be analysed. The first 2 metals together with carbon fibre will be considered for the wing box, fuselage and empennage. The latter two metal alloys of titanium and steel will be considered for the landing gear. The selection of these materials is based on the most used materials in aerospace industry [30].

9.2.1. Metal alloys

First the general characteristics of all alloys will be discussed, as well as the overall benefits and drawbacks of metal alloys compared to carbon fibre. The general characteristics will be given below:

- **Aluminium 7075-T6:** This alloy has very high strength and is used for structural parts experiencing high stresses. It is also one of the most used alloys within the aircraft industry. In general, most aluminium alloys have the following properties: low cost, light-weight, easy fabrication, resistant to corrosive atmospheres, and are non-toxic. [1]
- **Aluminium 2024-T6:** This alloy has good machinability and is used often in the aerospace industry. The same general properties as described for AL7075-T6 apply to this alloy. [2]
- **Titanium 6Al4V:** This alloy is the most commonly used titanium alloy within aerospace due to its high strength and high resistance against corrosion. It also has a low density, but involves higher cost compared to aluminium or steel alloys. [3]
- **AISI 4340 Steel:** This alloy is known for its high strength as well as its toughness. Using heat treatment, higher corrosion resistance as well as wear resistance and fatigue strength levels can be reached. The downside of this

[1] `https://www.aerospacemetals.com/aluminum-distributor.html` [Accessed on: 26-05-2021]
[2] `http://www.matweb.com/search/DataSheet.aspx?MatGUID=ecf8530875cb4ded9675b827f77bfac5` [Accessed on: 26-05-2021]
[3] `https://www.azom.com/article.aspx?ArticleID=9299` [Accessed on: 26-05-2021]

material is the high density. Therefore, it will only be considered for the landing gear to minimise the impact on the weight. [4]

9.2.2. Carbon Fibre

Carbon fibre has been receiving increasing popularity within the aviation industry over the last decades. Taking into account for example the Boeing 787, having a structure consisting of advanced composites for 50% and only 20% of aluminium. Carbon fibre offers a weight reduction of 20 percent compared to conventional designs, according to Boeing [5]. However, carbon fibre also has its downsides. Composites are only capable of handling tension loads, but are not able to deal with compressive stresses. This is because carbon fiber materials are anisotropic material. In structures subjected to highly compressive stresses this could thus form an issue. More structural weight is needed and therefore it could be not beneficial to use composites over metal alloys. Furthermore, due to the fact that the material is more novel, higher safety factors will be needed to account for uncertainty. This will also increase the overall weight, not resulting in the desired weight reduction in the end. Regarding the manufacturing and the sustainability of carbon fibre, there are several issues compared to metals. These will be discussed in the next two subsections. Overall the cost of carbon fibres are higher compared to most metal alloys. Currently the cost per metric tonne is between €70000 and €181000 for aerospace graded carbon fibre [6]. This is a rough estimate, but anyhow using this material will definitely increase the unit cost.

9.2.3. Manufacturability

This section will briefly discuss the differences between forming processes of metal alloys compared to composites. The manufacturing and production plan will be extensively discussed in Subsection 18.1.2. For metal alloys, the main advantage is that for large batch sizes, metal alloys are more cost-effective to produce compared to composites. The main disadvantage is the limitation in creating complex shapes. However, for the aircraft structure this will be less of a problem due to its conventional shape [7]. For composites, creating complex shapes is one of its benefits, but for highly stress parts, the free edges must be treated carefully. Also, manufacturing is in general more time consuming.

9.2.4. Sustainability

Looking at aluminium alloys, large parts of aluminium structures and parts can be reused at the end-of-life. According to Airbus, the recovered scrap material is reasonably pure, indicating that aluminium alloys can be reused within the aerospace industry. Implicating that if the structure would be made of an aluminium alloy, it would be 100% reusable. Recycling has its economical and environmental benefits. Aluminium manufacturing is an energy intensive process, however 90% reduction in energy consumption can be achieved when recovering and reusing the material compared to raw material processing [30]. Further detail regarding the end of life strategy and the recyclability will be discussed Section 9.5. [31]

Regarding titanium alloys, at this stage recycling has not been applied on industrial scale. This is mainly due to its limited volume within the aerospace industry. However, titanium can be recycled and the current recycling rate is very high. The only downside at the moment are the impurities of oxygen and iron concentrations within the material, reducing its quality after end-of-life. Therefore, new methods have to be developed in order to increase the overall quality of the recycled titanium. Thus using titanium will be less sustainable compared to aluminium. [32]

Steel is not the most common material used in aircraft structures, due to its high density. It can however be used for the landing gear due to its high toughness. Steel is currently the most recycled metal and it is profitable for all parties involved. Namely, up to 40 % of the steel production comes from recycled material. In the next few years, the consumption of steel will decrease, meaning large amounts of material will be available for recycling. The only concern at the moment is that the accumulation of tramp elements after numerous recycling cycles could reduce the overall quality of the material. However this issue will arise for all metal alloys [33].

Lastly, the sustainability of carbon fibre will be addressed. Currently, 30% of carbon fibre ends up as waste and cannot be recycled. Also valuable material ends up at landfills at the moment. Even though the production process already exists for several years, the composite recycling industry is still developing and therefore not capable to secure a constant supply chain [8]. Currently, recycling involves shredding, cutting and grinding of fibres in order to re-use them. This will wear down the fibres, reducing its properties and making it unusable for the aerospace industry [9]. Therefore, carbon fibre can be regarded less sustainable as more waste is generated at the end.

In conclusion, metal alloys can be recycled better compared to carbon fibre, due to the fact that recycled carbon fibre

[4] https://steelforge.com/alloy-steel-4340/ [Accessed on: 26-05-2021]
[5] https://www.boeing.com/commercial/aeromagazine/articles/qtr_4_06/article_04_2.html [Accessed on: 27-05-2021]
[6] https://www.compositesworld.com/articles/the-vexing-economics-of-carbon-fiber-manufacturing [Accessed on: 27-05-2021]
[7] https://axenics.com/blog/custom-metal-fabrication-advantages-and-disadvantages [Accessed on: 28-05-2021]
[8] https://www.compositesworld.com/articles/the-state-of-recycled-carbon-fiber [Accessed on: 27-05-2021]
[9] https://www.aviationtoday.com/2021/03/15/new-research-improve-recycling-remanufacturing-commercial-airplane-carbon-fiber/ [Accessed on: 27-05-2021]

has reduced properties compared to its original material. The weight reduction of carbon fibre with respect to metal alloys also needs to be treated with some skepticism, as higher safety factors are needed.

9.2.5. Material Characteristics

For all discussed materials, the properties can be found in Table 9.1 [34].[10][11][12][13][14] The cost price is an indication in order to compare different materials with each other. This include raw material cost and estimation of manufacturing cost according to [35]. However this paper is from 1991, so the overall cost is not a good indication of the current cost price.

Table 9.1: Material Properties of different alloys and carbon fibre

Material	ρ $[kg/m^3]$	σ_{ult} $[MPa]$	σ_{yield} $[MPa]$	E $[GPa]$	K_{1C} $[MPa \cdot m^{1/2}]$	τ_{ult} $[MPa]$	G $[GPa]$	$Cost/Kg$ $[\$/kg]$
Al 2024-T3	2780	440	290	73.1	25	283	28	10
Al 7075-T6	2810	572	503	71.7	29	331	26.9	10
Titanium 6Al4V	4430	1170	1100	114	84	760	44	33
ST CFRP	1600	600	600	70	50	90	5	59
AISI 4340 Steel	7850	1282	862	200	50	1150	78	8

9.3. Material Performance

In order to select the best suitable material for all structural components considered, the performance of each material has to be determined. It will be mainly focused on the strength and stiffness of a material compared to its density. For all structural components the main loading cases will be given in the following list:

- Wing box: The wing will experience bending and torsional loads from aerodynamic forces. Therefore the wing structure will consist of a thin skin with stringers and spars. Stringers and spar will mainly carry bending stresses, while the skin will carry shear stresses. [36, p.47-48]
- Fuselage: The fuselage is merely a semimonocoque construction. The fuselage will exist of a thin shell structure with longerons and stringers in longitudinal direction and transverse rings in radial direction. Due to lift forces generated at the wing and the tail the fuselage will bend. Also cabin pressurisation will result in shear and tensile stresses. The skin must be able to carry the shear loads, the longerons and stringers must be able to carry both tensile and compressive loads, and the transverse rings must be able to carry tensile hoop stresses. [36, p.43-47]
- Empennage: Same as the wing, the empennage will mainly carry bending and torsional loads from aerodynamic forces. Therefore the structure will carry shear, and bending stresses. [36, p.48-49]
- Landing Gear: The landing gear will be mainly loaded in compression for both landing and take-off. The structure must be able to carry the high impact load during landing. Therefore the structure must have high strength, fracture toughness and fatigue strength. Most commonly used materials are high-strength steel or titanium alloys, and therefore differ from other structures. [36, p.49-50]

After analysing the main loads, the performance equations, also known as material indices, will be given. For all indices the function, constraints, and free variable will be mentioned. The objective is to minimise the mass. The first equation is for stiffness-limited design, the latter for strength-limited design. Indices 7 and 8 are for damage tolerant design. [37, p.407-412]

1. $E/\rho, \sigma_{ult}/\rho$: Tie; length specified; section area free.
2. $E/\rho, \sigma_{ult}/\rho$: Cylinder with internal pressure; pressure and radius specified; wall thickness free.
3. $G/\rho, \sigma_{ult}/\rho$: Shaft; length and outer radius specified; wall thickness free.
4. $E^{1/2}/\rho, \sigma_{ult}^{1/2}/\rho$: Beam; length and shape specified; section area free.
5. $E^{1/2}/\rho, \sigma_{ult}/\rho$: Column; length and shape specified; section area free.
6. $E^{1/3}/\rho, \sigma_{ult}^{1/2}/\rho$: Panel; length and width specified; thickness free.
7. K_{1C}: Maximise strength for load-controlled design, for ties, schafts and beams.
8. σ_{ult}: Maximise strength for load-controlled design, for ties, schafts and beams.

The following indices will be important the wing box and empennage design: stringer and spars (1,4,5,7,8), skin (3,6,7,8). For the fuselage the following indices will be important: Longerons and stringers (1,4,5,7,8), skin (2,3,6,7,8). For the landing gear the following will be considered: 4,5,7,8.

[10] `http://www.matweb.com/search/DataSheet.aspx?MatGUID=57483b4d782940faaf12964a1821fb61&ckck=1` [Accessed on: 28-05-2021]
[11] `http://www.matweb.com/search/DataSheet.aspx?MatGUID=4f19a42be94546b686bbf43f79c51b7d&ckck=1` [Accessed on: 28-05-2021]
[12] `http://www.matweb.com/search/DataSheet.aspx?MatGUID=fd2df45bffa54018b54989bc14092d9f` [Accessed on: 28-05-2021]
[13] `http://www.matweb.com/search/DataSheet.aspx?MatGUID=10d463eb3d3d4ff48fc57e0ad1037434` [Accessed on: 28-05-2021]
[14] `http://www.performance-composites.com/carbonfibre/mechanicalproperties_2.asp` [Accessed on: 28-05-2021]

9.4. Material Trade-off

After determining the material indices, a trade-off for all structural components will be performed. The trade-off performed will both be quantitative for all material indices and cost. It will be qualitative for the trade-off criteria, sustainability and manufacturability. The same trade-off methodology has been used as explained in Chapter 3 of the Midterm Report. For every trade-off the material indices combined are deemed twice as important compared to sustainability or manufacturability. These two are deemed twice as important as opposed to cost. Thus material indices is assigned a score of 4, sustainability and manufacturability a score of 2 and cost a score of 1. For briefness, the trade-off table is not included but for the wing box, fuselage and empennage Aluminium 7075-T6 will be used. For the landing gear Titanium 6Al4V will be used.

9.5. End of Life Strategy

The end-of-life (EOL) strategy of aircraft has been neglected for over several decades. Currently, most aircraft are stored on landfill sites. Landfilling is not a suitable long-term solution and therefore an EOL strategy will be proposed for this aircraft in order to reduce the overall environmental footprint of this aircraft. Boeing started the PAMELA (Process for Advanced Management of End-of-Life Aircraft) Project in the beginning 2000s and a similar strategy will be proposed for the UCA. The main goal of the end-of-life strategy will be to recycle or reuse most parts in order to produce as least waste as possible. There are three phases that will be considered [31]:

- **Decommissioning:** During this phase the aircraft is taken out of service. The aircraft will first be inspected. A list of aircraft parts will be compiled to determine what can either be disassembled, reused or recycled. Afterwards operational liquids will be removed and will be either, reused, sold or environmentally disposed.
- **Disassembly:** Disassembly will take place after it is decided that the aircraft will not be reused or resold in total. The first step will be to disassemble the aircraft to reusable parts. The parts that can be re-used are the following: engine, landing gear, avionics and automation system. Structural parts can be ordered within different families in order to determine what can be re-used.
- **Dismantling:** After disassembly, all unsellable parts will be dismantled in order to obtain different groups of metal alloys. These groups of materials can be sold to metal recycling companies. Recycled materials can be returned to their appropriate markets. The end goal is to obtain a cradle-to-cradle design, where the recycled materials are of the same quality compared to the original material. As discussed in Section 9.2 aluminium alloys as well as titanium alloys will have the same properties after recycling. More research must be done to examine the long-term effects of impurities after multiple cycles.

After proposing the end-of-life strategy, the aircraft will be at least 90 % recyclable. During disassembly most parts will be resold, including materials which could otherwise not be fully recycled. During dismantling all recyclable materials will be separated and recycled. Making an 100 % recyclable aircraft will not be possible due to fact that during decommissioning not all fluids can be reused or during dismantling not all sub component materials can be recycled. However the aim is to increase the recyclability towards 100 %. In 2007, it was demonstrated that 85 % of a Airbus A300 can be recycled. Implementing the strategy as mentioned above would increase this value for the UCA. Choosing sustainable materials as well as not having a cabin will increase the overall recyclability. Therefore the aircraft will be at least 90% recyclable at the end of life. [31]

9.6. Verification and Validation

A sensitivity analysis has been performed in order to check the validity of the overall trade-off. This is a form of verification. For the wing box and empennage an increase of 600% for the cost criteria is needed in order to change the winner. For material properties this increase is 225%. For the landing gear, titanium will win in all scenarios. For the fuselage an increase of 700% for the cost criteria is needed to change the winner and 125% for material properties. Therefore, this trade-off is verified.

9.7. Conclusion and Recommendations

Multiple materials have been considered during the selection procedure. These are Al7075-T6, Al2024-T6, Ti 6Al4V, AISI 4340 Steel, and Carbon fibre. For four different subsystems a material selection has been made. These are the wing box, fuselage, empennage and landing gear. Taking into account the material performance, cost and sustainability Al7075-T6 has been chosen for the wing box, fuselage and empennage. For the landing gear Ti6Al4V has been chosen as the most suitable material. In order to improve sustainability an end-of-life strategy has been drafted. The first step will be decommissioning, where the aircraft is taken-out of service, list of inventory is compiled, and cleaned. The next step is to disassemble the aircraft and selling the reusable parts. Lastly the unsellable pats will be dismantled and recycled. In 2007, it was demonstrated that 85 % of a Airbus A300 can be recycled. Implementing the strategy as mentioned above would increase the value for the UCA. Choosing sustainable materials as well as not having a cabin will increase the overall recyclability. Therefore the aircraft will be at least 90% recyclable at the end of life.

10
Empennage and Control Surface Design

This chapter will elaborate on the design of the empennage and the aileron control surface. Section 10.1 will briefly describe the corresponding requirements. Section 10.2 will explain the chosen tail configuration. After that, Section 10.3 determines the most forward and aft centre of gravity position. Using the centre of gravity range the tail can be designed using a scissor plot, which will be explained in Section 10.4. After that, the sizing of the aileron control surfaces is done, as described in Section 10.5. Finally, verification, validation will be described in Section 10.6 and the conclusion and recommendations are discussed in Section 10.7.

10.1. Requirement Analysis

In order to design an aircraft that is stable and controllable it is important to fulfill the corresponding requirements. During the design of the empennage the following control and stability requirements have to be fulfilled:

- **REQ-SUBSYS-CON-1.3.00:** The UCA shall be controllable on the ground with a 90° cross component of wind velocity of at least 37 $[km/h]$ (20 knots) or 0.2 V_{SR0}, whichever is greater.
- **REQ-SUBSYS-CON-2.3.00:** Any short period oscillation, not including combined lateral-directional oscillations, occurring between 1.13 V_{SR} and maximum allowable speed appropriate to the configuration of the aeroplane must be heavily damped with the primary controls.
- **REQ-SUBSYS-CON-2.3.01:** Any combined lateral-directional oscillations ('Dutch roll') occurring between 1.13 V_{SR} and maximum allowable speed appropriate to the configuration of the aeroplane must be positively damped with controls free, and must be controllable with normal use of the primary controls.
- **REQ-SYS-FLT-2.2.05:** The UCA shall be able to take-off and land safely on dry runways with a 90° cross component of wind velocity of at least 37 $[km/h]$ (20 knots) or 0.2 V_{SR0}, whichever is greater.
- **REQ-SYS-FLT-2.4.00:** The UCA shall be able be controllable in yaw, pitch and roll direction.
- **REQ-SYS-FLT-2.4.01:** The UCA shall be statically stable during all phases of flight.
- **REQ-SYS-FLT-2.4.02:** The UCA shall be dynamically stable during all phases of flight.
- **REQ-SYS-FLT-2.4.03:** The UCA shall be controllable during take-off, climb, cruise, descent, approach and landing.

10.2. Tail Configuration

The choice of the tail configuration is the outcome of a selection process, not the result of mathematical calculations. Thus, the evaluation of the different design options will be purely qualitative. Since the possibilities for tail configurations seem to be endless, there is a general rule to simplify the process. In most cases the conventional tail configuration suffices for the design. Therefore, it is recommended to start with a conventional aft tail and then evaluate its features against the rest of the aircraft design [38]. If the tail choice conflicts with the rest of the design and it is implied a different configuration would be a better fit, it should change.

Having this in mind the thought of using a conventional tail was quickly discarded. The vertical stabiliser would be located directly in the exhaust stream of the engine, which results in a disruption of the engine flow and a reduction in thrust. Furthermore, it leads to additional wear on the stabiliser due to the extreme exhaust heat. The issue could be resolved by integrating the engine within the vertical tail section, however, this solution comes with more structural complexity. Additionally, integrating the engine and the vertical stabiliser would move the centre of gravity even more aft, meaning the aircraft becomes less stable. A T-tail configuration would encounter the same problem as the conventional aircraft, and was therefore also disregarded.

Mainly due to the placement of the engine, tail configurations with off-centre vertical stabilisers were considered next. These are: (inverted) V-tail, (inverted) Y-tail, and H-tail. Although these were all viable options they have their advantages and disadvantages. For example, since the inverted V-tail and Y-tail are pointed downwards, longer landing gear would be needed to achieve enough ground clearance. Furthermore the V-tail is rather complex due to the lateral and longitudinal control surfaces being combined in the so called ruddervator, and has to deal with the effect of adverse yaw coupling. H-tails, on the other hand are straightforward but are heavier since to the horizontal tail must be strong enough to support both vertical tails. Ultimately it was decided the V-tail was the best fit for the UCA's design. Due to the reduced amount of parts and components the V-tail's design will be the lightest. Additionally, it will experience less drag for there is less interference between empennage and fuselage [39].

10.3. Loading Diagram and Centre of Gravity Range

When designing an aircraft it is important to know the centre of gravity (cg) range. This will be used to determine the horizontal tail surface area, and for positioning and sizing the landing gear. The cg range will be determined using two loading diagrams.

$$\Delta cg = \frac{\sum x_i \cdot W_i}{\sum^i W_i} \tag{10.1}$$

Two loading diagrams are shown in Figure 10.1 and Figure 10.2. Figure 10.1 shows the loading diagram in case 2000 $[kg]$ of payload is being transported. Figure 10.2 shows the case that no payload is being transported. In order to produce a loading diagram the weight and cg of several components are needed. The operational empty weight (OEW) is the sum of all components excluding the fuel and payload. The OEW is used as a starting point for the loading diagram. From there the aircraft will be loaded with payload and fuel which causes the centre of gravity to shift. The cg shift is determined using Equation 10.1. Where W is the weight of the component and x the position of the component. When loading the fuel and each pallet a Δcg is added to the diagram. First the payload is loaded using the cargo door at the nose. Three pallets are loaded from the back to the front of the aircraft since this is the most convenient way to load the aircraft. When comparing Figure 10.1 and Figure 10.2 it can be concluded that the cg range of the case where no cargo is loaded does not influence the cg range of the aircraft, because the cg range of Figure 10.2 is within the cg range of Figure 10.1. The most forward cg position is determined when loading the last pallet at the most forward position in the aircraft. This can be seen in Figure 10.1. Afterwards the fuel is loaded which causes the centre of gravity to shift backwards. The most aft cg position is determined when loading the first cargo pallet closest to the rear of the aircraft, which can be seen in Figure 10.1. When determining the cg range a margin of 2 percent is used to account for cg variations caused by landing gear retracting, and ground staff moving around etc. From the loading diagrams it is concluded that the cg range is from 0.181 X_{cg}/MAC to 0.359 X_{cg}/MAC.

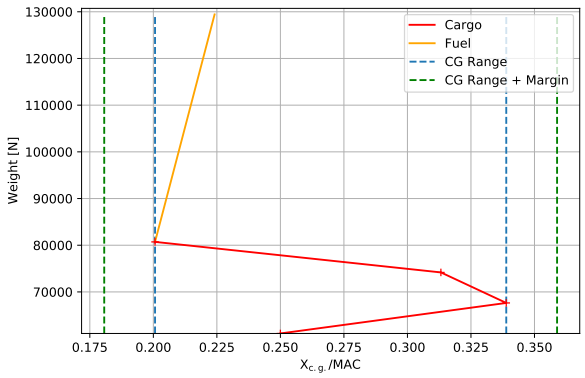

Figure 10.1: Loading diagram, 2000 $[kg]$ payload

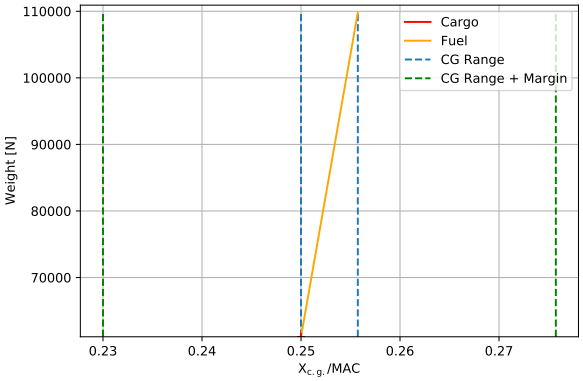

Figure 10.2: Loading diagram, 0 $[kg]$ payload

10.4. Tail Design

When designing the V-tail, first the tail will be designed as if a conventional tail configuration is used. Meaning that both the horizontal and vertical tail area will be determined. The horizontal area will be determined using a scissor plot. The vertical tail area will be determined using statistical data. Using the values for the horizontal tail area and the vertical tail area the V-tail can be sized.

10.4.1. Horizontal and Vertical Tail Sizing

To determine the horizontal tail area a scissor plot will be constructed. The scissor plot consist of a stability and controllability line. The lines for stability and controllability are computed using the stability equation Equation 10.2 and the controllability equation Equation 10.3. The term 0.05 in Equation 10.2 is the stick-fixed static margin (S.M.). When leaving out the S.M. term, the result is the neutral stability line.

$$\bar{x}_{cg} = \bar{x}_{ac} + \frac{C_{L_{a_h}}}{C_{L_\alpha}}\left(1 - \frac{d\epsilon}{d\alpha}\right)\frac{S_h l_h}{S\bar{c}}\left(\frac{V_h}{V}\right)^2 - 0.05 \tag{10.2}$$

$$\bar{x}_{cg} = \bar{x}_{ac} - \frac{C_{m_{ac}}}{C_{L_{A-h}}} + \frac{C_{L_h}}{C_{L_{A-h}}}\frac{S_h l_h}{S\bar{c}}\left(\frac{V_h}{V}\right)^2 \tag{10.3}$$

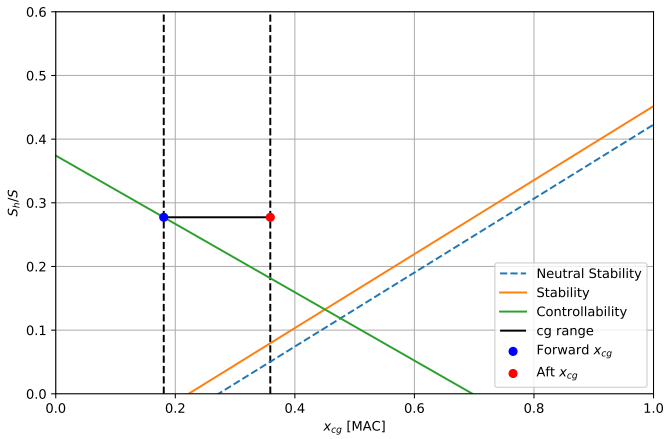

Figure 10.3: Scissor plot

Figure 10.3 shows the scissor plot with the stability and controllability line. Using Figure 10.3 the optimum horizontal tail area and position of the wing is determined. The aircraft is deemed both stable and controllable if the cg range is within the area on the left side from the stability line and right side of the controllability line. It is found that the aircraft is stable and controllable with an optimum S_h/S of 0.2773, horizontal tail area S_h of 13.02 $[m^2]$ and position of the wing, X_{lemac}, of 8.90 $[m]$. Note that the S_h/S ratio does not seem optimal as the cg range could be moved more to the bottom right if the loading diagram is changed. In theory it is possible to shift the entire cg range towards the right in Figure 10.1 by moving the position of the wing. However, when the most aft cg position is too far aft it would not be possible to position the landing gear such that ground stability is ensured. Chapter 11 will explain the design of the landing gear and how ground stability is ensured.

The vertical tail area is determined using statistical data from Roskam II [40]. For the statistical data of tails, business jets (Table 8.5b in Roskam II) are used as a reference since they are closest to the type of aircraft that is being designed. From this data an average vertical tail volume coefficient is obtained. Using the vertical tail volume coefficient and Equation 10.4 the vertical tail area S_v is calculated, which is 8.97 $[m^2]$.

$$S_v = \frac{\bar{V_V} bS}{L_v} \tag{10.4}$$

10.4.2. V-Tail Sizing

The tail can be sized using the variables determined in Subsection 10.4.1. The area of the left and right tail can be determined using Equation 10.5, which is the relation between a conventional tail and V-tail. Furthermore, the dihedral angle $[deg]$ of the tail can be computed using Equation 10.6 [41] and is found to be 34.54 $[deg]$. This yields enough clearance with the jet exhaust stream as will be explained in Subsection 15.1.6. After that, the aspect ratio and sweep angle could be determined. When determining those values it is important to consider some effects of those parameters. Increasing the aspect ratio results in a increased weight and effectiveness of the tail and decreased stall angle of attack of the aircraft. Furthermore, when increasing the sweep angle, the stall angle of attack and the moment arm to the cg will increase but the effectiveness of the tail decreases [39]. Keeping this in mind and using statistical data from Roskam II [40], the aspect ratio is determined. It was found that the aspect ratio of the tail AR_{vt} is 6. The sweep angle of the tail is assumed to be five degrees larger than the sweep angle of the main wing[1]. Finally, the root chord, tip chord and the span of the tail are calculated in the same way as has been done for the main wing.

$$S_{vt} = 0.5(S_v + S_h) \tag{10.5}$$

$$\Gamma_{vt} = atan\left(\frac{S_v}{S_h}\right) \tag{10.6}$$

10.5. Aileron Sizing

Ailerons are control surfaces located in the main wing. They work by being extended in opposite direction. On one side the aileron is deflected upwards so less lift is generated while on the other side it is deflected downwards to create more lift such as shown in Figure 10.4. This results in a rolling moment allowing the aircraft to make a turn. Depending on the size, weight and maneuverability of the aircraft different roll rates are required. The UCA can be considered a

[1] https://www.fzt.haw-hamburg.de/pers/Scholz/HOOU/AircraftDesign_9_EmpennageGeneralDesign.pdf [Accessed on: 31-05-2021]

light to medium weight cargo aircraft. Therefore it should, in the most critical case, be able to achieve a bank angle of 45° in 1.4 seconds [38].

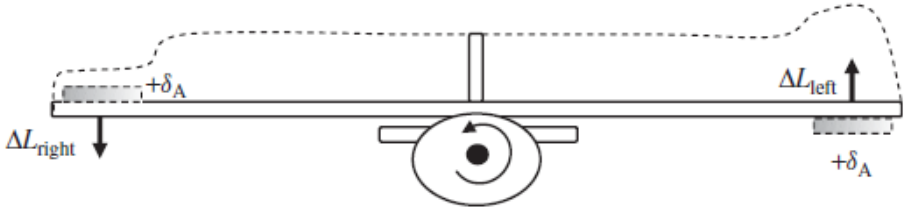

Figure 10.4: Front view of change in lift and rolling moment due to aileron deflection [38]

The sizing method as described in [38] and [42] is used. Designing the aileron control surface is an iterative process. First of all, based on reference aircraft, the preliminary aileron geometry should already be determined, i.e. the spanwise location of the aileron, the ratio of aileron chord to wing chord, and the maximum aileron deflection. Having decided upon values for these parameters it would be nice to know what happens to the roll characteristics of the aircraft as a result of the aileron. Equation 10.7 gives the formula for the rolling moment. Note that C_l in this formula stands for the rolling moment coefficient and not for lift. Furthermore $C_{l_{\delta_a}}$ is the aileron roll control derivative, δ_a is the aileron deflection in $[rad]$, C_{l_p} is the roll damping coefficient, P is the roll rate in $[rad/s]$, and finally V is velocity in $[m/s]$. The equation amounts to zero since the roll rate is considered to be steady. The formula for the roll moment can be rewritten to Equation 10.8.

$$L = qSbC_l = qSb\left(C_{l_{\delta_a}}\delta_a + C_{l_p}\frac{Pb}{2V}\right) = 0 \tag{10.7}$$

$$P = -\frac{C_{l_{\delta_a}}}{C_{l_p}}\delta_a\frac{2V}{b} \tag{10.8}$$

Remaining unknowns are the aileron roll control derivative $C_{l_{\delta_a}}$ and the roll damping coefficient C_{l_p}. Fortunately equations for these coefficients can be derived They are given in Equation 10.9 and Equation 10.10 respectively.

$$C_{l_{\delta_a}} = \frac{dC_l}{d\delta_a} = \frac{2C_{l_\alpha}\tau_a}{Sb}\int_{b1}^{b2} C(y)ydy \tag{10.9}$$

$$C_{l_p} = \frac{4(C_{l_\alpha} + C_{d_0})}{Sb^2}\int_0^{b/2} y^2C(y)dy \tag{10.10}$$

This time C_{l_α} does stand for a lift coefficient, the airfoil lift curve slope to be exact. Furthermore, τ_a is the aileron effectiveness, which is directly related to the ratio of the aileron chord to the wing chord C_a/C such as seen in Equation 10.11. C_{d_0} is the airfoil zero lift drag coefficient. The term $C(y)$ gives the chord length as function of the location along the span of the wing as shown in Equation 10.12, and integration boundaries $b1$ and $b2$ indicate the spanwise start and end position of the aileron.

$$\tau_a = \frac{0.8}{\sqrt{0.7}}\sqrt{\frac{C_a}{C}} \tag{10.11}$$

$$C(y) = C_r\left[1 + 2\left(\frac{\lambda - 1}{b}\right)y\right] \tag{10.12}$$

As aforementioned the design of the aileron control surfaces will be an iterative process. After obtaining the initial estimates for the aileron geometry the roll rate can be calculated with the use of Equation 10.8 to Equation 10.12. This roll rate should be evaluated against the required roll rate, which in case of the UCA is 0.561 $[rad/s]$. This process can continue until the requirement is met. Eventually it was decided to place the aileron from 71% to 90% of the half span to have some clearance with the high lift devices and enough space for the wing tips. Furthermore the ratio aileron chord to wing chord is restricted by the rear spar located at 65% of the chord length. To leave room for some control system elements the aileron chord spans over the final 25% of the wing chord. In combination with a maximum deflection of 20° this set of control surfaces is readily able to meet the roll requirement.

10.6. Verification and Validation

During the empennage design and aileron sizing three python programs have been used. The programs were used to construct the scissor plot and loading diagram and to size the ailerons. To ensure that all three programs were built right, verification procedures were conducted. The verification procedures consisted of performing several unit and system tests. First verification by inspection of the scissor plot and loading diagram was done. For the loading diagram it was checked whether the order of loading the cargo pallets and fuel tanks was correctly presented in the diagram. Furthermore, as the cg is plotted as a functions of the MAC, a shift of the wing of the aircraft should result in the diagram moving forward and vice versa. From inspection it was found that this was correct. For the scissor plot

inspection was performed as well. During this inspection it was found that there was an error in the code. Both the stability and controllability line were relatively steep and intersecting a relatively high value for S_h/S. Subsequently, unit test were used to find the error as well as to find other possible errors. Hand calculations were used as the calculations involved were not complex. The hand calculations showed two errors in the code. The tail arm was expressed in millimeters instead of meters. The second error had to do with the tail/wing speed ratio V_h/V. This variable was squared two times which is wrong if you look at Equation 10.2 and Equation 10.3. Both errors were solved and no other errors were found after completing the hand calculations. This concludes the verification procedures of the empennage design.

The python code that was used to size the aileron was verified with some simple unit and system test. The code was simple enough that hand calculations could be used to verify each step taken. Additionally, the system was tested in its entirety by changing input parameters to see if the resulting roll rate changes accordingly.

Validation of the python code used to create the loading diagram and scissor plot was carried out by running it with aircraft data of the AVRO RJ85. These values were obtained from data bases, calculated, or determined via a technical drawing. The resulting scissor plot in Figure 10.5 shows that the cg range nicely fits between the stability and controllability line for the known horizontal tail surface area. The difference between the real tail dimension and the most optimal tail dimension according to the plot at the given cg range is only 3.7%. Considering that not all aircraft dimensions were known and some had to estimated, this accuracy is rather good.

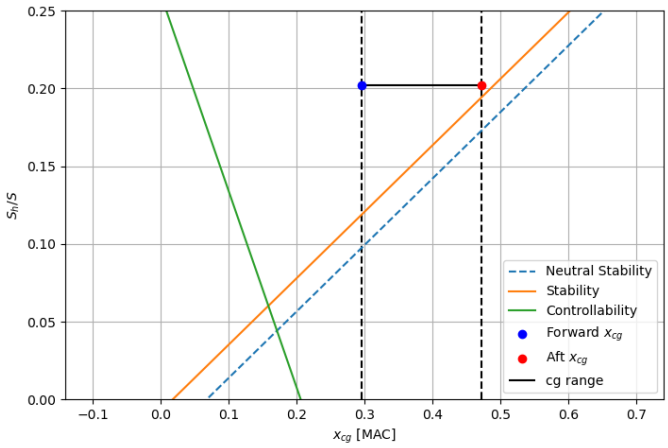

Figure 10.5: Scissor plot for the AVRO RJ85

An additional validation procedure for the horizontal tail sizing is comparison to reference aircraft as displayed in Table 10.1. Since such specific aircraft characteristics as horizontal tail characteristics are hard to find, the selection of reference aircraft is not optimal. However, some useful conclusions can still be drawn. Although the tail surface area to wing surface area ratio which is on the larger side it is still within the range of the reference aircraft. The same can be said about the horizontal tail volume coefficient $\bar{V}_H$ which is related to S_h/S, the tail arm, and the mean aerodynamic chord in an equation similar to the vertical tail volume coefficient. Finally, the tail aspect ratio is rather large which will make the tail heavier and its structural design slightly more difficult. However, its feasibility is confirmed by the Fokker F-27.

Table 10.1: Horizontal tail characteristics comparison with reference aircraft [38]

Aircraft	$W_{MTOW}[kg]$	**Tail type**	S_h/S	$\bar{V}_H$	AR_h
Cessna Citation III	9979	Fixed	0.26	0.75	5.2
Fokker F-27	19733	Fixed	0.23	0.96	6
Boeing 737-100	50300	Adjustable	0.32	1.14	4.16
UCA	13250	Adjustable	0.28	0.95	6

Furthermore, a sensitivity analysis was performed for the scissor plot. Table 10.2 shows a table with four variables, the aspect ratio of the wing and tail, wing surface area and the tail arm. The values in the table are showing the change in percentage of S_h/S due to +/- 10 % change of the four variables. From the table it is evident the tail arm has a relative large effect on S_h/S. Changing the aspect ratio of the tail however has no effect on S_h/S. Changing the aspect ratio of the tail only moves the stability line up and down and this does not result in a new S_h/S value. The last thing that

can be noticed is that when changing the wing surface area there is a smaller change if S is decreased with -10%. The stability line is the limiting line when S is decreased with 10% and the controllability line is the limiting line when S is increased with 10%.

Table 10.2: Sensitivity analysis for horizontal tail area, change in S_h/S [%]

Changing variable	AR	AR_h	S	l_h
-10%	-0.60%	0%	-3.9%	11%
+10%	+0.48%	0%	3.3%	-9.1%

For validation of the aileron sizing its geometry is compared to reference aircraft in Table 10.3. The span of the ailerons is quite short in comparison. This can be explained however, by the aircraft's large wingspan and high maximum deflection. This maximises the rolling moment created in the relatively short aileron span ratio. Furthermore, the aircraft dimensions of a Cessna Citation III were used as input to see if, according to the model, its roll rate matches the requirement. This was easily achieved, thereby confirming the validity of the model.

Table 10.3: Aileron geometry comparison with reference aircraft [38]

Aircraft	$m_{to}[kg]$	$b[m]$	C_a/C	$b_i/(b/2)$	$b_o/(b/2)$	$\delta_{a_{max}}$
Cessna Citation III	9979	16.31	0.3	0.56	0.89	12.5
Gulfstream 200	16080	17.7	0.22	0.6	0.86	15
Fokker 100A	44450	28.08	0.24	0.6	0.94	20
UCA	13250	21.125	0.25	0.71	0.9	20

10.7. Conclusion and Recommendations

Following a qualitative selection process the V-tail configuration was chosen to be the most optimal fit for the UCA's design. This configuration provides stabilising surfaces in both horizontal and vertical direction, while being able to avoid the exhaust stream of the engine. With the aircraft layout concerning the cg of the OEW and the position of the payload and fuel tanks a loading diagram could be constructed. Using the resulting cg range the required horizontal surface area was thereafter sized with help of a scissor plot. The vertical surface area was based on statistical values. Using a relation between conventional tail and V-tail the total surface area was determined to be 10.995 $[m^2]$, while the tail dihedral is 34.54 $[deg]$. This tail dihedral provides enough clearance so the V-tail can avoid the engine exhaust stream. Figure 10.6 and Figure 10.7 show the rear and side view of the empennage. Furthermore aileron control surfaces were designed which allow the aircraft to achieve its required roll rate. The programs used for the sizing were extensively verified and validated. This confirmed the empennage and control surfaces were sized correctly.

Nevertheless, there are some complications that must be taken into account during the future design phases of the UCA. These include the sizing of the complex ruddervator control system. Also the effect of adverse yaw coupling must be considered.

All in all, this chapter proves that it is possible to have a realistic tail design that results in a stable and controllable aircraft, is applicable for all possible cg positions, and can avoid the engine exhaust stream.

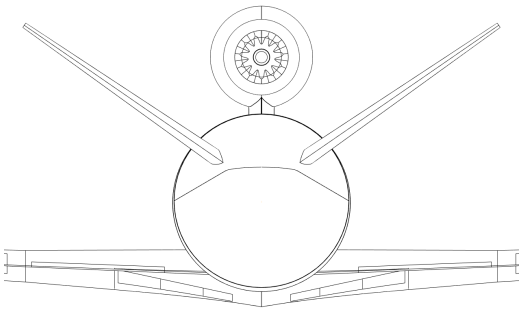

Figure 10.6: Empennage rear view

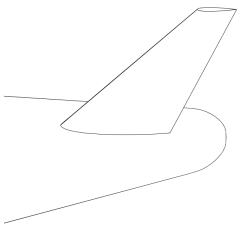

Figure 10.7: Empennage side view

11
Landing Gear Design

The design of the landing gear subsystem is important as it determines the ground stability of the aircraft during taxiing, landing and take-off. This chapter will elaborate on the design of this subsystem. The Section 11.1 will briefly describe the requirements that are linked to this subsystem. Section 11.3 and Section 11.4 will explain the actuator design and integration of the landing gear. Finally, Section 11.5 explains the positioning of the landing gear.

11.1. Requirement Analysis

In order to design an aircraft that is stable on the ground it is important to fulfill the corresponding requirements. During the design of the landing gear the following requirements have to be fulfilled:

- **REQ-SYS-GRD-1.1.03:** The UCA shall have a ground clearance of 5 [deg] measured from the most outer landing gear .
- **REQ-SYS-GRD-1.3.01:** The UCA shall be able to maintain stability during all ground operations.
- **REQ-SUBSYS-LDG-2.2.00:** The landing gear shall support the aircraft at MRW.
- There shall be brakes present in the landing gear wheels that can decelerate the UCA from landing speed (56.84 [m/s]) to stationary in 1500 [m] at maximum landing weight.
- **REQ-SUBSYS-LDG-2.2.02:** The loading of the nose wheel shall be between 8% and 15% of the total UCA weight for all CG positions.
- **REQ-SUSBYS-LDG-2.2.03:** The main landing gear shall be positioned at a location that ground stability is ensured.
- **REQ-SUBSYS-LDG-2.2.04:** The main landing gear shall be positioned at a location that a safe take-off is ensured.
- **REQ-SUBSYS-LDG-2.3.00:** The landing gear shall be retracted during flight.

11.2. Tire Sizing

The first component to size for in the landing gear are the tires. The tires are the first point of contact for aircraft to the ground, and as such a lot of consideration must go into sizing the tires.

The first value that had to be identified was the Load Classification Number (LCN). This value represents the classification of a runways quality and ultimately relates to the required pressure. Equation 11.1 calculates the required pressure for the tires, this value is within an approximate 10% error [43].

$$p = 430ln(LCN) - 680; 10 < LCN < 100 \tag{11.1}$$

Next the static loads for the main landing gear and nose gear were determined using Equation 11.2 and Equation 11.3. This assumes that at maximum take off weight 8% of the weight will be on the nose wheel for steering, and likewise 92% for the main gear [43].

$$P_{mw} = 0.92W_{TO}/N_{mw} \tag{11.2}$$

$$P_{nw} = 0.08W_{TO}/N_{nw} \tag{11.3}$$

Finally by making use of the pressure and static loads it is possible to determine the required size of the tires. By making use of Figure 11.1, it is possible to use the pressure and static loading to determine the required size of each tire.

Through use of this method, the LCN was determined to be 32 [1], this value was determined based on the reference airport that were found through our market analysis. Capetown's airport had the lowest LCN and was chosen to be used as such. Following the steps and equations, the final tire dimensions for the main gear and the nose gear were found to be 66.04x16.75cm and 40.64x11.18 respectively.

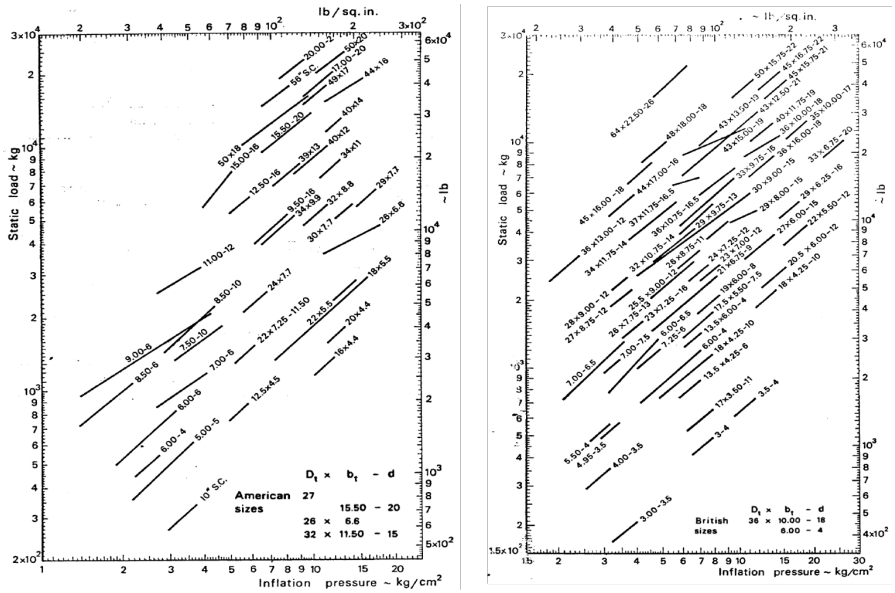

Figure 11.1: Plots allowing for the determination of tire size (sizes are in inches)[7]

11.3. Actuator Design

The landing gear will have to absorb a large amount of the aircraft's energy upon landing. An actuator is essential to absorb the vertical component of the aircraft's energy.

In the worst case scenario, one of the main-landing gears must absorb all of the aircraft's energy upon landing due to the others not contacting the ground. This can be a result of uneven terrain, crosswinds or other factors.

In-order to ensure a feasible landing gear, the shock absorber must be sized. For the best performance, Oleo pneumatic absorbers were chosen [7]. This is an industry standard solution, and a proven technology in landing gears.

The energy that must be absorbed by the single landing gear is defined with Equation 11.4 [7]. This energy is the kinetic energy of the aircraft, with w being the vertical velocity of the aircraft, and W being the maximum landing weight.

Adjacent to that equation, is Equation 11.5 [7]. This equation looks at the deformation of the landing gear to absorb this energy. N_s represents the number of shocks per landing gear; P_s is the maximum load the gear must endure (in this case 92% of the tot aircraft mass); λ is the ratio of maximum load to static load; η represents the efficiency that the tires and shock respectively have; S represents the respective deflection of the tires and shock absorber respectively. With the deflection of the tires being estimated with Equation 11.6 [7].

$$E = \frac{W}{2\,g} w^2 \qquad (11.4) \qquad E = N_s P_s \lambda \left(n_t s_t + n_s S \right) \qquad (11.5) \qquad s_t = 0.5 \frac{\lambda_w}{p\sqrt{D_t b_t}} \qquad (11.6)$$

To determine the deflection of the shock absorber, Equation 11.4 and Equation 11.5 are equated with one another, and S is solved for. This results in Equation 11.7[7]. In order to size the diameter of the landing gear, a first order empirical approximation is used, this being Equation 11.8.

$$S = \frac{1}{n_s} \left(\frac{w^2}{1.84 g \lambda} - n_t s_t \right) \qquad (11.7) \qquad D = 1.3 + .11\sqrt{P_s};\ \text{in cm} \qquad (11.8)$$

With the dimensions of the shock absorber defined, the complete landing gear dimensions can be established. For this the maximum tire dimensions had to be established, a 4% and 10% growth in width and diameter were made respectively [7]. The total length of the absorber can be taken as the stroke length multiplied by a factor of three. and finally the lateral clearance of the wheels to the landing gear were empirically determined to be approximately 1cm on either side [7].

Table 11.1: Landing gear dimensions

Dimension name	Dimension [mm]
Stroke length	251.16
Shock diameter	111.58
Radial tire clearance	15.75
Max. tire width	184.4
Max. tire diameter	686.8
Lateral clearance	10.4

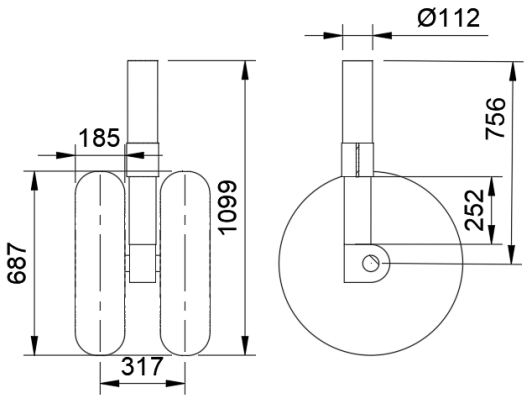

Table 11.2: Landing gear dimensions

Combining all of these values, equations and assumptions, with use of a tool, and CAD software, the followings table and figure were derived to represent what the landing gear may look like. These dimensions define the minimum dimensions that the landing gear must adhere to. Depending on the tail dimensions of the aircraft, and the landing gear location, the overall landing gear might become longer.

11.4. Integration of Landing Gear

The benefit of a low wing configuration, is that the landing gear can also be stowed away in the wing. This will however complicate the wingbox structure slightly as there will effectively be two smaller wing boxes at the root to accommodate the landing gear. The use of a yehudi allows the placement of the landing gear without interrupting the rear spar for the main wing.

In Figure 11.2 it can be seen how the principle of the landing gear will work. With use of a trunnion between two spars, the gear can rotate freely. Making use of struts and hydraulics, it will be possible to retract or extend the landing gear appropriately. Because the bottom skin of the wing where the landing gear is located will have to open, that section of the wing will be considered an open section and will appropriately require reinforcing to ensure the root is properly supported for shear and torsion. Figure 11.3 shows a top view of how the landing gear will be integrated into the wing. The Spar 1 will be continuous throughout the wing, while spars 2 and 3 will start off perpendicular to the fuselage in order to create a small wingbox for the landing gear's trunnion and pin to attach to. All spars will travel along until the end of the yehudi upon which a large rib will distribute the loads of spar 3 to spars 1 and 2, where the rest of the wing will then continue.

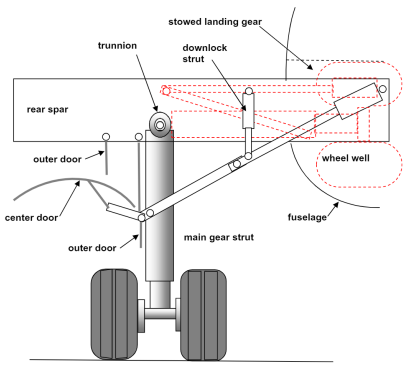

Figure 11.2: Gear retraction mechanism found on wing mounted landing gears [44]

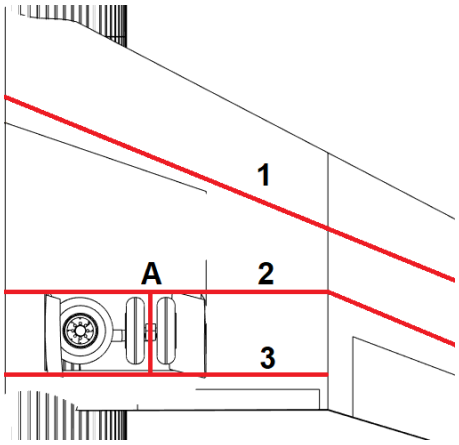

Figure 11.3: Example of spar and landing gear layout

For the nose gear, the implementation is not as complicated. The only consideration is the opening nose of the aircraft, where this was already considered in the placement of the landing gears. Between two frames of the fuselage space can be cleared and compensated with spars, where the same pin and trunnion system can be implemented, and two doors open outwards to allow the gear to extend freely. Figure 11.4 shows how the nose gear will deploy, while Figure 11.5 shows the complete tricycle layout deployed on the aircraft.

[1] https://www.openaip.net/node/160335

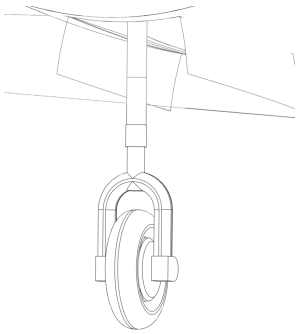

Figure 11.4: Gear retraction mechanism found on wing mounted landing gears [44]

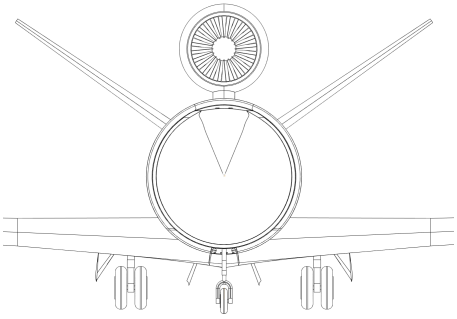

Figure 11.5: Final landing gear configurations, with door mechanism

11.5. Ground Stability and Landing Gear Positioning

The positioning of the landing gear of the aircraft is crucial as the design of this subsystem determines the ground stability of the aircraft. From the requirements shown in Section 11.1 five constraints on the landing gear design can be determined. Those constraints are:

- The loading of the nose wheel is between 8% and 15% of the total aircraft weight.
- The tip-back angle is 15 [deg].
- The pitch angle is larger than the tip-back.
- The turnover angle is smaller than 55 [deg].
- The lateral clearance angle is larger than 5 [deg].

The positioning of the landing gear has been done in combination with iterating the scissor plot and loading diagram of the aircraft. This was needed because the cg range that was initially found made it impossible to position the landing gear and to ensure ground stability. From the start, the nose wheel has been placed 2.55 [m] from the tip of the nose to make sure the cargo door can be used safely. The position of the main landing gear was first placed under the wing of the aircraft. After that, multiple iterations were performed to make sure none of the constraints were exceeded. Those constraints will be further explained in the next subsections. Moreover, it will be shown whether the location of the landing gear does not exceed the constraints. Following from Section 11.3, the height of the landing gear is determined to be 1.1 $[m]$, measured from the ground to the fuselage.

11.5.1. Tip-Back Angle and Pitch Angle

The tip-back angle of the aircraft should be 15 [deg]. This angle is shown by angle theta in Figure 11.7. This angle determines the maximum nose-up attitude without the tail touching the ground during take-off and landing. Furthermore, the pitch angle, shown by angle béta in Figure 11.7, should be larger than tip-back angle theta. When the pitch angle is smaller than the tip-back angle and the tip-back angle goes to its maximum allowable value, the aft cg position would be behind the location of the main landing gear. This means that the moment around the main landing gear would increase, with the result of the tail hitting the ground. To avoid this, the pitch angle should be larger than the tip-back angle. Using the requirements on the tip-back angle and pitch angle, a longitudinal position of the main landing gear has been determined. The optimal longitudinal position was found to be 10.25 $[m]$, measured from the nose of the aircraft. The position of the main landing gear has been determined such that the tip-back angle is 15 $[deg]$ and the pitch angle was set to 15.01 $[deg]$.

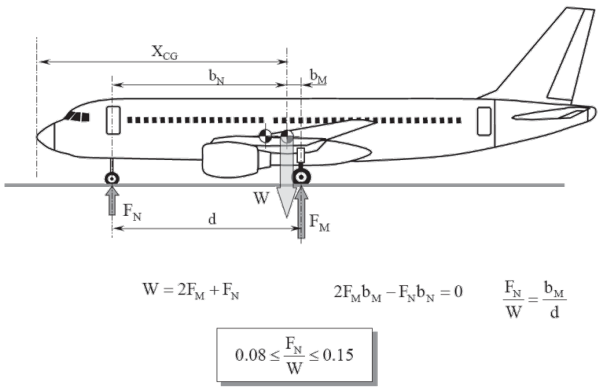

Figure 11.6: Loading Requirement of the Nose Wheel [41]

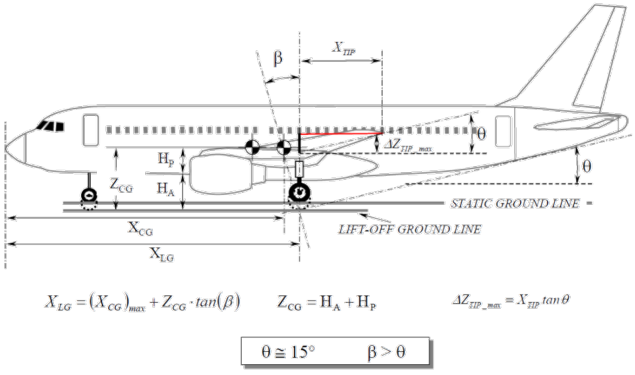

Figure 11.7: Pitch and Tip-Back Angle Requirements [41]

11.5.2. Loading of the Nose Wheel

As mentioned before the nose wheel should be loaded with 8% to 15% of the total aircraft weight. This is required to ensure sufficient manoeuvrability on the ground. If the load on the nose wheel is outside the range of this requirements, it becomes difficult to steer the aircraft on the ground. In order to check whether the position of the landing gear fulfills this requirement Figure 11.6 is being used. As mentioned before, the nose wheel has been placed on the centre line of the fuselage and the longitudinal position was set to 1.45 $[deg]$, measured from the nose of the aircraft. Using the longitudinal positions of the landing gear system and the most forward and aft cg position, the loading of the nose wheel could be determined. The most forward cg position of the aircraft has been obtained from Figure 10.1 and the most aft cg position of the wing has been obtained from Figure 10.2. The most aft cg position of the aircraft from Figure 10.1 has not been used as for that case the aircraft is not loaded with fuel, which means that the aircraft can not move using its own propulsion system. When considering the most forward cg position a load on the nose wheel of 12.04% of the MTOW has been found. The load on the nose wheel, when the most aft cg position has been considered, is found to be 9.14% of the MTOW. Both values are within the allowed range which means that the requirement regarding the nose wheel loading has been met.

11.5.3. Turnover Angle

The turnover angle, indicated by angle psi in Figure 11.8, is required to be smaller than 55 $[deg]$. If this value is exceeded, the aircraft could tip over more easily during a turn while taxiing. To comply to this requirement more easily, the goal is to lower the cg as close to ground as possible and to place the main landing gear closer to the tip of the wing. The lateral position of the main landing gear was determined to be 1.48 $[m]$, measured from the centre of the fuselage for both parts of the main landing gear. Using this position, Figure 11.8 and the equations shown, the turnover angle was found to be 54.40 $[deg]$. This perfectly complies to the requirement as 54.40 $[deg]$ is indeed smaller than 55 $[deg]$.

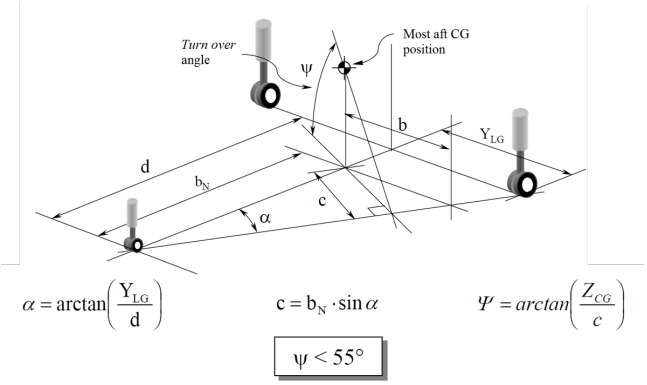

Figure 11.8: Turnover Angle [41]

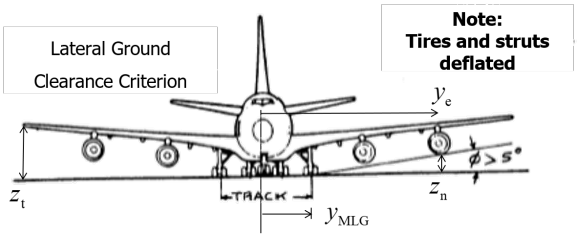

Figure 11.9: Lateral Ground Clearance [39]

11.5.4. Lateral Clearance Angle

Finally, to ensure lateral ground clearance the lateral clearance angle should be larger than 5 $[deg]$. This angle is shown by angle phi in Figure 11.9. Usually, the engines placed under the wing are limiting the lateral clearance angle. However, as the engine for this aircraft design is placed on top of the fuselage, the tip of the wing is the limiting factor. The lateral clearance angle can be calculated using Equation 11.9. Using this equation a lateral clearance angle of 5.84 $[deg]$ has been found. This is sufficient as it fulfills the requirement of the lateral clearance angle, which should be larger than 5 $[deg]$.

$$\phi = atan\left(\frac{z_t}{-Y_{MLG} + \frac{b}{2}}\right) \tag{11.9}$$

11.6. Verification and Validation

The landing gear design has been done using a python program. This program has been used to position the landing gear at the correct place. The program is able to calculate the different angles explained in Section 11.5. Furthermore, the program for the loading diagram (Section 10.3) was used to calculate the loading of the nose wheel. As the positioning of the landing gear required relative simple calculations, the verification of the code has been done using hand calculations. The hand calculations showed one error in the code that calculated the turnover angle. Afterwards this error was solved and the verification procedure of program was finished.

To validate the program CAD software in combination with the final aircraft model was used to compare the final aircraft model to the calculated values to ensure that the values produced a compliant model of the aircraft.

Figure 11.10 Shows what the final tip-back and pitch angles were. Both were found to be 15 degrees, with the tip-back

angle being 99.93% accurate. From this measurement however, the tip-back angle is only barely compliant, and as such great attention must be made to this angle.

Figure 11.11 shows the tip-over angle based on the models placement using given dimensions. The value was found to be 15.1 degrees, which varies only by 0.55% from the calculated 55.4 degrees.

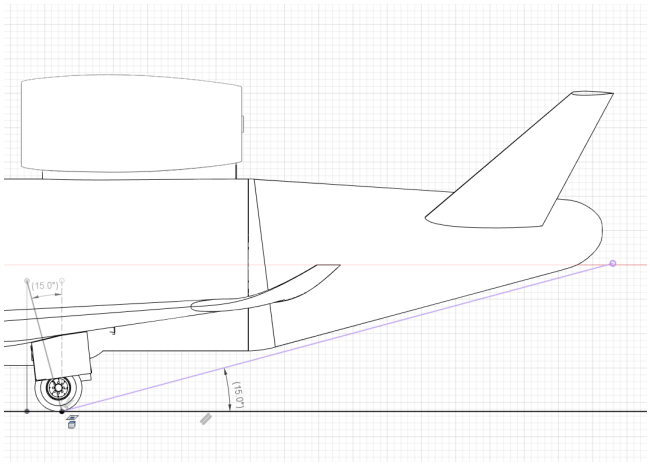

Figure 11.10: Tip-back and Pitch angle validation both having values of 15 degrees

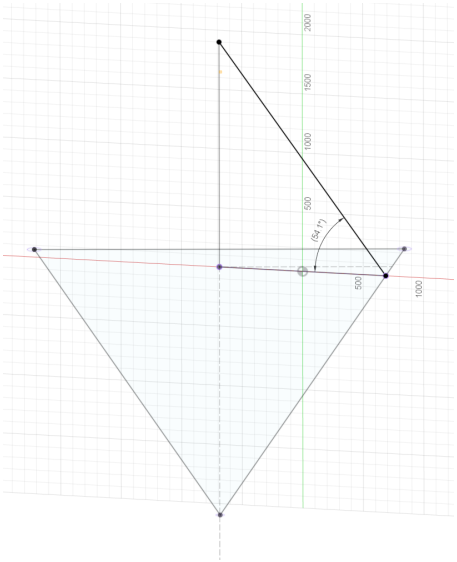

Figure 11.11: Turnover angle measured to be 54.1 degrees

Finally the lateral clearance was validated in Figure 11.12. The value determined was 5.4 degrees, an acceptable value when compared to the boundary conditions. In comparison to the calculated model, where the largest variation was observed. An deviation of 7.53% was found, as this value is below 10% and the angle is greater than 5 degrees it is still acceptable. Although it shows that there might be a an error in the design of the model used to calculate this value, or an error in the 3d model.

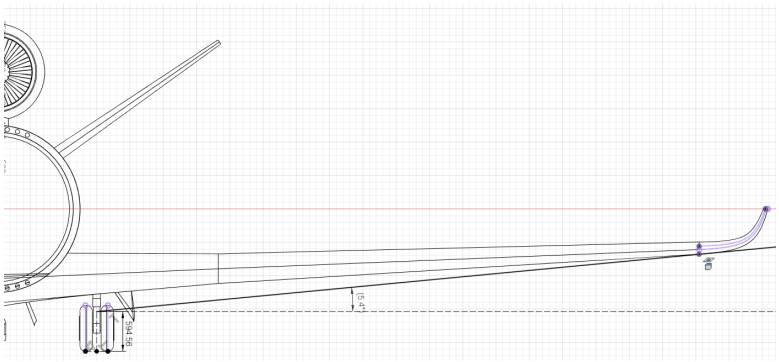

Figure 11.12: Lateral clearance validation with a measured 5.4 degrees

In conclusion the landing gear has been sized correctly, and the validation using CAD shows that the produce coordinates for the landing gear will yield an operational aircraft. The only feature not validated in this section was the centre of gravity, as that can only truly be validated once a complete model of the aircraft is developed, or a scale real-world model.

11.7. Conclusions and Recommendations

This section aimed to size and ensure the aircraft would have a sound and stable manner of interacting with the ground. This section determined the tricycle configuration of the aircraft with a combination of empirical and geometric relations. resulting in a tire pressure, actuator stroke length, and landing gear locations to be determined. The results were all within margin, and ensured a stable layout for the aircraft to serve its purpose.

It is recommended that in future design iterations, that the trunnion and pin system be properly sized, as well as the arms and deployment mechanism. The CAD model made use of preliminary landing gear door layouts, and further detail in optimising this layout could be made. With respect to the spar locations in the yehudi, close work must be done with the structures department if and angled central spar is intended to be used.

12
Unmanned Aircraft Operations

The fact that the UCA is unmanned comes with a number of benefits. First of all, it provides a solution to the high labour costs and logistical challenges involved with a conventional crew. Furthermore it simplifies the aircraft layout and structural design since there is no need for a cockpit or windows. This chapter explains the strategy for the unmanned operations of the UCA. In Section 12.1 the relevant requirements are listed. Furthermore, in Section 12.2, Section 12.3, Section 12.4, and Section 12.5 the unmanned characteristics of the UCA concerning the mission execution, ground control station (GCS), communications and contingencies are explained respectively. Section 12.6 discusses various hardware and software components that are relevant to the unmanned operations. After that, in Section 12.7 the communication flow diagram is shown and in Section 12.8 a link budget is drawn up. Finally this chapter finishes with verification and validation in Section 12.9 and conclusions and recommendations in Section 12.10.

12.1. Requirement Analysis

In order to design the automation system as well as other relevant electrical systems the following requirements must be taken into account:

- **REQ-SYS-FLT-2.1.00:** The UCA shall be able to determine its longitudinal location with a accuracy of at least 4.6 $[m]$.
- **REQ-SYS-FLT-2.1.01:** The UCA shall be able to determine its lateral location with a accuracy of at least 4.6 $[m]$.
- **REQ-SYS-FLT-2.1.02:** The UCA shall be able to determine its altitude with an accuracy of at least 1.5 $[m]$.
- **REQ-SYS-FLT-2.1.03:** The UCA shall have a camera for visual aid.
- **REQ-SYS-FLT-2.7.00:** The UCA shall be able to communicate position and visual information to the operator in 600 $[ms]$.
- **REQ-SYS-MIS-3.2.00:** The UCA shall have a level of autonomy which is able to execute operations safely depending on the phase of flight.
- **REQ-SYS-MIS-3.2.01:** The UCA shall comply with Air Traffic Control while in the air.
- **REQ-SYS-MIS-3.2.02:** The UCA shall fly fully autonomous during cruise without operator intervention.
- **REQ-SYS-MIS-3.2.03:** The UCA shall be able to be controlled directly by an operator on the ground.

12.2. Mission Execution

The UCA's level of autonomy differs depending on the flight phase. Whilst on the ground it should be able to be manually controlled, as this was a customer requirement (**REQ-SYS-MIS-3.2.03**). During take-off, approach, and landing it is opted to let the aircraft fly on its own accoring to a pre-programmed flight plan. Nevertheless, during these flight phases the UCA will be under close watch of a pilot at the GCS who is able to intervene at any point if necessary. A command and control (C2) data link will provide the ground pilot with the ability to control and monitor the aircraft. The uplink of C2 is used for commanding the aircraft while the downlink provides the ground pilot with status updates. The ATC must be able to intervene at this stage according to requirement **REQ-SYS-MIS-3.2.01**. This may occur in case of redirection of the route due to traffic or when weather conditions do not allow for a safe landing. Intervention by the ATC can be done via the pilot in the GCS.

During cruise the aircraft will fly completely autonomous with the only exception that the pre-programmed flight plan can be updated by the ground pilot possibly on orders of the ATC. The flight plan consists of a series of waypoints which are sent to the flight management system (FMS). The autopilot then actually executes the manoeuvres to capture each waypoint. It is essential that the FMS and autopilot interpret the waypoints in the same way. That is to say whether it wants to turn before or after the waypoint, or a mixture of both such as shown in Figure 12.1. For the UCA it is chosen to approach the waypoints by turning before and after the waypoint. Actions such as changing the flight velocity, changing the rate of climb, and lowering the landing gear are also tied to waypoints. Lastly it is worth to mention that the aircraft will not precisely match each waypoint. There will be some errors from position estimation and actual trajectory. The aircraft must fly to a three-dimensional space that is close enough to claim the waypoint as captured.

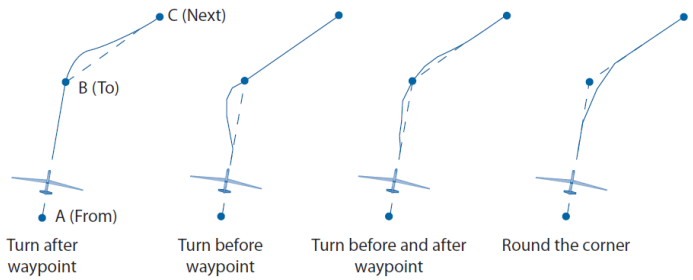

Figure 12.1: Waypoint capture approaches [45]

To comply with **REQ-SYS-FLT-2.1.03** a camera shall be placed on the UCA. The video stream captured by the camera is to be sent to the GCS via the payload link. Payload links generally have a much larger data rate when compared to a C2 link. Digital payload links offer flexibility since they have the ability to compress the video before transmission. Data rates for digital payload links can range anywhere from 1 Mbps for a lower quality highly compressed video stream to 50 Mbps for high quality digital video or multiple video streams [45].

12.3. Ground Control Station

During flight, use will be made of a ground control station (GCS) to monitor and control the aircraft. By looking at existing (military) ground control stations it can be assumed that the GCS of the UCA can be compact enough to be housed within the size of a shipping container. In the GCS there are interfaces to control and communicate with the UCA. The personnel needed to operate an unmanned aircraft is the UA operator, also simply named the pilot. The UA operator directly controls the UCA during taxiing and other ground operations. During take-off and landing the pilot should closely monitor the UCA and be ready to intervene if necessary, since these are critical flight stages. Logically, this means a ground pilot will monitor only one UCA at a time. To deal with the situation that more than one UCA needs close attention, multiple pilots may be present in the GCS. During cruise merely the UCA's status must be monitored. In this phase, the operator can monitor a larger number of aircraft at once. Other tasks for the ground pilot include observing and predicting the weather, and communicating with the ATC and other aircraft. To ensure redundancy, a backup computer will be present for the GCS workstation.

Placing a GCS at every airport serviced by the UCA would be inefficient since it increases investment costs and requires more personnel. It is therefore opted to initially only locate ground control stations at the seven main regional hub airports appointed in Subsection 2.4.2. At the secondary hub airports or other airports that experience large amounts of traffic an unmanned ground control station can be installed to relay the UCA's video stream and command and control link with less latency as will be explained in Section 12.4. When the business expands and more UCA's are employed the number of manned GCS around the world can always increase.

12.4. Communication Strategy

In the communication between the GCS and the UCA a difference can be made based on the so-called 'line of sight'. There are two options in order to transmit data: using direct line-of-sight (LOS) or using indirect beyond-line-of-sight (BLOS). LOS communication is done through 4G cellular communication. BLOS is needed when direct connection is not feasible due to physical blockage caused by terrain or the curvature of the earth. For BLOS communication use is made of one or more relay nodes, for instance a satellite (SATCOM). In general the data rates for LOS communication will be higher when compared to BLOS communication. Furthermore large satellite bandwidth capacity can become really expensive [45]. In Figure 12.2 the communication flow diagram of the UCA is presented.

Line-of-sight operations are only possible if the aircraft is taking off or landing at a hub airport with a GCS. There are important flight phases in which aircraft status updates and a live video stream are to be sent form the UCA to the GCS. The two main reasons for the need of video feed are to check if you are on the correct path to the runway, and to check if no other traffic is on or near the runway. Hence the camera feed is especially important at busy airports. 4G communication supports data rates of 2 Mbps to 100 Mbps at a max system bandwidth of 100 MHz [46]. This means that the hub airports with a GCS can easily receive a high quality video stream via LOS communication. Additionally, 4G links have a latency of only 50 ms and are much cheaper than satellite links [46]. Some serviced airports without a GCS might also experience so much movement that a high quality video stream is desired, for example, the secondary hub airports. In this case an unmanned ground control station can be added to the airport. This is simply a receiver to which the aircraft can directly (LOS) send the video stream. The receiver would then send the video stream to the GCS at the regional hub via internet cables. This allows for a high quality, low latency, and low cost video feed at a large distance.

On less busy airports the UCA will have to take off with BLOS communication. The SATCOM link used for this will by

the Global Xpress network from Inmarsat. This network operates in the Ka-band and covers almost the entire globe. The Global Xpress network facilitates data rates up to 50 Mbps. To save costs, the data rates used by the UCA will be only a fraction of this. During landing and take-off there will still be a video stream from the UCA to the GCS, albeit of a lower quality. Due to the indirect link a latency of roughly 600 ms will be present[1], which is deemed acceptable considering the circumstances. As soon as the aircraft is in cruise the video stream will stop to save satellite costs. During cruise the SATCOM link will only be used for status updates and command and control.

Since a UCA operates in the same airspace as manned aircraft, it is often expected it is able to act as if it is manned. Therefore it is desired that the GCS pilot can converse with the ATC. This voice communication can be relayed from the GCS to the UCA via 4G or SATCOM, depending on the line of sight. The UCA can then transmit the voice communication via the VHF radio to the ATC. In case the GCS and ATC are close enough, voice communication can be performed via the radios present in the GCS. In a similar fashion it will be possible for the pilot in the GCS to communicate with pilots form other aircraft. Finally, anti-collision transponders will be present in the UCA to communicate with other aircraft. This can happen independently from the ATC. The anti-collision systems of the UCA will be discussed more extensively in Section 12.6.

12.5. Contingency Management

During any flight unforeseen events might happen that pose a threat to successfully completing the mission. These are called contingencies. Normally in manned aircraft the pilot would deal with these contingencies. However, since the UCA is unmanned an contingency management algorithm should be drawn up.

The C2 link is the only way the pilot can enforce control over the aircraft. Therefore it is vital to secure it against jamming and unauthorised use. Hence the C2 link will have anti-jamming capabilities and only send encrypted data. Additionally, a backup C2 link will provide redundancy in case the first C2 link fails. Both links will use widely separated frequencies. A triplex system would not be justifiably in this case since there are no calculations or data on which the system can vote. In the event that different GCSs are responsible for take-off and landing, the C2 link will have to be handed over from one GCS to the other at some point. Even though the UCA is flying autonomously at the point of the handoff, it is opted to go for the "make-before-break" approach. Make before break means that the second GCS has already established a C2 link with the UCA before the first one is shut down. After all, it is the safest option and does not seem to have any major downsides.

Although it is unlikely, subsystem failures or malfunctioning, such as engine failure, cannot be ruled out completely. In case of such an event the pilot in the GCS should be able to take back a sufficient level of control via the C2 link. Depending on the situation, this could range anywhere between executing some standard commands to taking full control over the aircraft. To assist the pilot a high quality video stream should be established. If the aircraft is flying beyond line of sight, the SATCOM data rate must be increased to facilitate this. The pilot should then navigate the unmanned aircraft to a selected emergency site and make a safe landing. If this is not possible the pilot could command flight termination and try to perform a controlled crash supported by the parachute system.

Another contingency that can happen is the loss of communication. While momentary loss of communication is not uncommon in unmanned operations, most missions will fail if the link is not reestablished. Hence a planned response to this situation is essential for safe operation. In the event of a lost data link the UCA will autonomously send a unique radar transponder code to alert local ATC and other aircraft in the same airspace. This would be similar to the existing procedure for communication failure on manned aircraft. The UCA should then return to the last waypoint the data link was still active, and circle for 20 minutes waiting for the link to be reestablished. In the mean time the ATC can clear the airspace around the aircraft. If the link is not reestablished within that time the UCA will autonomously terminate flight. If possible this will be done by landing in one of the predetermined remote areas along the flight route. The main goal of this procedure is to rescue the aircraft and its payload at a known location. The transponder (ADS-B) can inform the ATC and surrounding aircraft of the flight plan being executed. If landing at the predetermined remote area is not possible, for instance because the UCA autonomously detects more serious system failures, the aircraft will terminate flight aiming to reduce the kinetic energy at impact. Logically the parachute will be deployed at this point. Letting the UCA fly to an airport, without being able to monitor or control it, would simply be too dangerous. After all, lost communications might be an indication of other system failures [47].

12.6. Hardware & Software

Flight Management System. A flight management system (FMS) is a fundamental part of modern aircraft. It performs critical flight and unmanned aircraft operation functions, including interfacing with the command and control link, the autopilot and other subsystems. Additionally, the pre-programmed flight plan, and the contingency management algorithm as described in Section 12.5 will be implemented into the FMS. Frequently high-level management of the flight plan occurs on the FMS ahead of the autopilot. Even tough contemporary flight computers are generally reliable small errors such as bit flips might occur. Especially at high altitudes were the computers are exposed to stray beams

[1] `https://www.engineeringforchange.org/solutions/product/global-xpress/` [Accessed on: 08-06-2021]

of radiation. To provide redundancy the FMS will be hosted on three computers. This way the system can 'vote' which data or calculations are faulty in the case of deviations.

Autopilot and Flight Control Software. The autopilot is the system that actually controls the aircraft. The UCA will have an advanced autopilot capable of high-level autonomous flight. From the navigation sensors and air data systems the autopilot will get the UCA's status as input. Then using the integrated flight control algorithm it calculates the required control surface actuation, wing configuration, and throttle setting to fly in accordance with the flight plan. The development of the autopilot an the flight control algorithm will be outsourced since it provides access to specialised resources and the know-how of niche technologies. Additionally it saves nonrecurring engineering cost and lets the design team focus its attention on other avionics such as the FMS. Possible contractors include UAVOS Inc., Collins Aerospace, and uAvionix. Similar to the FMS, the autopilot will be hosted on three computers to provide redundancy.

Navigation Sensors. Information on the location heading and velocity is essential for following the waypoints from the flight plan. This data will be provided by a global positioning system (GPS) and an inertial measurement unit (IMU). The IMU measures the UCA's status purely on inertial measurements. Accelerometers measure the accelerations in x, y, and z direction. These can be integrated once with time to find the velocity, and twice to obtain the aircraft's position in all three directions. Gyroscopes measure the pitch, yaw and roll angles. By taking derivatives with respect to time the corresponding angular rates and accelerations can be computed. Although an IMU is a useful device its position estimates are heavily flawed since it estimates drift over time, e.g. any measurement errors, however small, are accumulated over time. This can lead to positional errors of several kilometers for long-endurance missions. GPS can yield much more accurate results since its longitude, latitude, and altitude estimates are based constructed with the help of multiple navigation satellites. Its accuracy for longitudinal an lateral position for aircraft can be as low as 4.6 meter which is sufficient for this design [45]. In conclusion, the IMU provides high-frequency state estimates while the GPS provides absolute position information and bounds the drift. The combination of the IMU and GPS is called an inertial navigation system (INS). For redundancy the UCA will employ a triplex INS architecture, to allow the system to check which data is incorrect in case of deviations.

Air Data Systems. The UCA can obtain information about its status by performing measurements on the surrounding air. A pitot-static system, consisting of a pitot tube and a static port, measures the dynamic pressure by taking the difference between the total pressure and static pressure. From this dynamic pressure the true airspeed can be derived. Furthermore from the static pressure the pressure altitude can be derived. This is altitude is more reliable than the altitude resulting from the GPS, with an average accuracy of 1-2 meter [45]. The mach number and vertical airspeed can also be obtained by the pitot-static system. For redundancy in total four pitot tubes and four static ports will be present on the UCA.

Data Busses. The data busses is the device which distributes data across all aircraft avionics. The data busses send information over an electrical circuit from the data producers to the consumers. Other tasks include data encryption, data decryption, data storage, data retrieval, data fusion, and selecting data feeds for downlink. The data are prioritised in such a manner that the most critical data the highest priority in getting through.

Airspace Integration Systems. The UCA must share the airspace with other manned aircraft. To make other air traffic aware of its presence, transponders will transmit status information. The transponder type that is chosen is mode S since it supports automatic dependent surveillance-broadcast (ADS-B) and traffic collision avoidance system (TCAS). TCAS monitors the airspace round an aircraft for transponders of other aircraft to warn of collision hazards independently of ATC. Along with the warning the system will inform the pilots what maneuvers to make for mutual avoidance. In the case of the UCA the autopilot will respond according to this suggestion, or the ground based pilot could take the necessary action. ADS-B is a transponder which conveys information on the aircraft's GPS location and velocity. The information is primarily meant for ATC but can also be received by other aircraft and the GCS if in direct LOS. Finally, the UCA will be illuminated. Lighting systems that are applied on conventional aircraft can be used for the UCA. These consist of multiple navigation and anti-collision lights. The application of all of these systems is considered to offer sufficient redundancy for airspace integration.

Landing Aids. For visual aid a camera feed will be broadcast to the GCS during landing. Nevertheless, the landing should be largely autonomous. While the GPS provides decent positioning accuracy during flight it falls short for landing procedures. This is similar to the difficulties faced by manned aircraft landing under instrument flight rules (IFR) conditions with zero visibility. Therefore an instrument landing system (ILS) will assist the UCA. ILS is a radio system that provides short-range guidance in horizontal and vertical direction during the approach of a runway.

Weather Avoidance System. It is beneficial for the aircraft to avoid flying through weather. Intense weather conditions like a heavy rainstorm can lead to excessive gust loads, and widespread icing. Additionally, flying through rain has a negative impact on the link budget as will be explained in Section 12.8. The UCA will therefore be equipped with weather radar to avoid these circumstances. Fortunately due to the cruise altitude of the aircraft most weather will already be avoided.

12.7. Communication Flow Diagram

The communication flow diagram in Figure 12.2 shows the flow of information of the UCA with the environment. The internal communication is shown in the data handling diagram in Section 13.8. This diagram puts an emphasis on the communication between the aircraft, ATC and GCS.

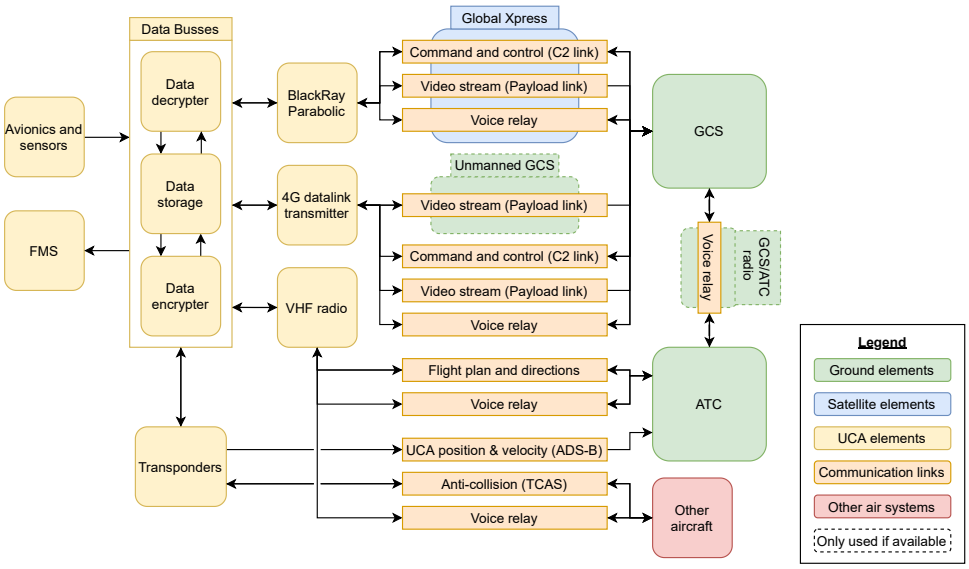

Figure 12.2: Communication flow diagram

12.8. Link Budget

For both BLOS and LOS operations a clear communication link is needed. Using a link budget calculation it can be demonstrated that the communication will be reliable. Methodology from Jay Gundlach [45, p.475-500] will be used to determine if the communication will be reliable on a conceptual design level. The onboard system chosen is the BlackRay Parabolic[2] and its technical specifications are shown in Table 12.1. This system has a high-throughput and is both lightweight and affordable. SATCOM satellites will be used for communication.

In order to determine if the communication is reliable a Signal-to-Noise Ratio (SNR) needs to be calculated. A SNR of 10 dB is required, with a link margin of at least 3 $[dB]$. The SNR can be calculated using Equation 12.1, given in decibel form. EIRP is effective isotropic radiated power, L_P is the absorptive propagation loss, G_R is the receiver antenna gain, L_R is the receiving signal loss of the reicever antenna, λ is the carrier signal wavelength, R is the distance between transmitter and receiver, k is the Boltzmann's constant, T is the ambient pressure, B is the effective noise bandwidth, and NF is the noise factor. $20\log_{10}\left(\frac{\lambda}{4\pi R}\right)$ is also known as the freespace loss and $10\log_{10}(1000k\cdot T)$ is known as the thermal noise density.

$$SNR = EIRP + L_p + G_R + L_R + 20\log_{10}\left(\frac{\lambda}{4\pi R}\right) - 10\log_{10}(1000k\cdot T) - 10\log_{10}(B) - NF \tag{12.1}$$

EIRP is given as a technical specification but entails the transmitter power, antenna gain of the transmitter, and different losses.

L_P can be determined using Equation 12.2, where $L_{P,Atm}$ is the losses of atmospheric absorption of transmitted energy. Detailed atmospheric absorption models are needed to require the total absorption, but for this design phase, it is neglected. This is because for a frequency of 14.5 $[GHz]$ the absorption is almost zero. $L_{P,Precip}$ is the precipitation absorption. This is also neglected as the aircraft will fly at an altitude around 12.5 $[km]$. For LOS, this loss should be taken into account

$$L_P = L_{P,Atm} + L_{P,Precip} \tag{12.2}$$

L_R can be determined using Equation 12.3. The receiver loss is a function of line losses, receiver pointing losses, receiver radome losses, receiver polarization losses and spreading implementation losses. $L_{R,Point}$ can be neglected in azimuth direction as an omnidirectional antenna is used. Also $L_{R,Radome}$ is neglected in this phase of the design. $L_{R,Line}$ can have a value up till -1 $[dB]$ and $L_{R,Spread}$ can have a value up till -2 $[dB]$. The system makes use of circular polarization and $L_{R,Polar}$ is assumed to be -3 $[dB]$. If linear polarisation would be used, it could be calculated by taking the square of the cosine of the misalignment angle, which is equal to the bank angle. For a bank angle of 40

[2] `https://www.gilat.com/wp-content/uploads/2017/02/Gilat-Product-Sheet-BlackRay-Parabolic.pdf` [Accessed on: 02-06-2021]

degrees, the loss would be -2.3 dB.

$$L_R = L_{R,Line} + L_{R,Point} + L_{R,Radome} + L_{R,Polar} + L_{R,Spread} \tag{12.3}$$

After discussing the losses, the gain of the receiving antenna can be determined. This will be a free variable as the diameter of the satellite can be chosen in order to meet the required link margin. The gain can be calculated using Equation 12.4. $\eta_{antenna}$ is the antenna efficiency and is 70% for a good design. D is the diameter of the receiving satellite and can be used as free variable. However, typical values are up till a diameter of 3 meters. λ is the wavelength, which can be calculated by dividing the speed of light by the signal frequency. For this communication link a Ka-band is used.

$$G = \eta_{antenna}\left(\frac{\pi \cdot D}{\lambda}\right)^2 \tag{12.4}$$

Next, the distance of the aircraft to the satellite is determined. As SATCOM satellites are used, the distance between both will be maximum 35758 $[km]$, as these satellites are within a geostationary orbit.

The thermal noise density, $k \cdot T$ can be determined by multiplying the Boltzmann's constant, k, with the Earth standard average temperature, T. The latter has a value of 287.15 $[K]$. Moreover, the receiver noise bandwidth is given in Equation 12.5. R_{Data} is the data rate of the antenna, and this is a technical specification of the transmitter. The ratio between data rate and bandwidth is 0.5 $[dB]$ for BPSK (phase shift keying) modeling. Lastly, NF will be 3 $[dB]$, when using a Ka-band.

$$B(dB) = 10\log_{10}\left(\frac{R_{\text{Data}}}{R_{\text{Data}}/B}\right) \tag{12.5}$$

The overall link budget is shown in Table 12.2. During the design it became evident that the EIRP or the diameter of the satellite antenna was too low in order to meet the required SNR. In order to have a suitable satellite antenna a diameter of 2 $[m]$ is chosen, which can be found on SATCOM satellites. Therefore, the EIRP must be increased, which can be done by increasing the transmitter power. It is assumed that the transmitter gain and losses will not change after increasing the transmitter power. The EIRP of the BlackRay Parabolic is 51.8 $[dBW]$ at transmitter power of 60 $[W]$. In order to have a link margin of at least 3 $[dB]$, the power must be increased to 80.9 $[W]$, as this will result in an EIRP of 82.7 $[dBW]$. Therefore, it can be stated that for BLOS operations a clear communication link is established.

For LOS, the aircraft will communicate with the ground station. It is assumed that a bitrate of 20 $[Mbps]$ will be sufficient in order to transfer video data rates. The aircraft will only be using LOS when it is close to the airport. In order to have a safe take-off and beginning of climb a distance of 40 $[km]$ from the airport to the aircraft is assumed to be sufficient, as this half the distance towards cruise. As the aircraft is flying at low altitudes in this stage, $L_{P,Precip}$ should be taken into account. This loss could be as high as 7 $[dB]$. Using a small antenna with a diameter of only 0.5 $[m]$ and a EIRP of 52.7 $[dBm]$, there will be a link budget of 13.0 $[dB]$, which is sufficient. If the data rate would even be increased to 50 $[Mbps]$, a link budget of 9.1 $[dB]$ is left. This is mainly because of the smaller distance to the aircraft from the receiving antenna compared to the BLOS scenario. Therefore, it can be stated that for LOS operations a clear communication link is established.

Table 12.1: Technical Specifications BlackRay Parabolic

	Value	Unit
Weight	23	kg
Antenna Size	62.7H x 44.3W x 61.8H	cm
Pointing Accuracy	0.2	deg
Data Rates	20+	Mbps
Modulations	BPSK,QPSK,8PSK	-
SNR	-12 to + 13	dB
Frequencies	27.5-30	GHz
Polarization	Linear	-
TX Gain	42.8	dB
EIRP	51.8 (at 60W)	dBW

Table 12.2: Link Budget Table BLOS

	Operation	Value	Unit
EIRP (required)	+	82.7	dBm
Lp	+	0	dB
Lr	+	-6	dB
Gr	+	54.4	dBi
Free Space Loss	+	-213.1	dB
kT	-	-174.0	dBm
B	-	76.0	dB
NF	-	3.0	dB
SNR available		13.1	dB
SNR Required		10.0	dB
Link Margin		3.1	dB

12.9. Verification and Validation

In order to verify the link budget calculation unit tests were performed on all functions in order to check the validity of the code. The following functions were checked: wavelength, gain, loss, bandwidth, signal-noise-ratio. For validation reference inputs were used from Jay Gundlach [45, p.480] in order to validate the code.

12.10. Conclusion and Recommendations

This chapter mainly consisted of drawing up a strategy to ensure the successful and safe execution of unmanned operations. To control and keep track of the aircraft a ground control station (GCS) was considered. In a GCS a pilot can monitor multiple UCA's at once. The GCS are only located at the primary hub airports serviced by the UCA. Smaller airports which still see large amounts of traffic have the option to employ an unmanned GCS which solves latency issues involved with long distance communications.

Furthermore the level of autonomy during mission execution was discussed. The UCA can fly fully autonomous during all flight stages in accordance with a pre-programmed flight plan, altough there always remains the possibility for the pilot to intervene if necessary via a command and control link (C2). Normally the pilot only directly operates the UCA during taxiing and other ground operations. To assist the pilot in these stages there will be a camera stream send via payload link to the GCS.

In manner in which the UCA communicates with the GCS depends on the line-of-sight. Direct line-of-sight communications (LOS), i.e., short range, will go a 4G data link, while the long range beyond-line-of-sight (BLOS) communications will make use of a SATCOM link. Both links are able to support a high quality video stream, however, during most time in BLOS operations no video will be relayed to save costs. Communication with the ATC is done via VHF radio.

Furthermore, for the possibility that unforeseen events happen during flight a contingency management algorithm was constructed. Such events, also called contingencies, include the failure of the C2 link, loss of communications, or any other subsystem failure. If the UCA is unable to continue flight it an emergency landing is attempted at a predetermined remote location. To minimise the kinetic impact of the UCA a parachute system can always be employed in case of emergency.

Thereafter various necessary hardware and software elements were considered. These include a FMS, autopilot, IMU, GPS, pitot-static system, data busses, transponders, landing aids, and a weather avoidance system. A number of elements concerning unmanned aircraft characteristics and their relations were summarised in a communication flow diagram.

Finally a link budget has to be drawn up. In order to have clear communication, a link budget of at least 3 $[dB]$ is needed. Using the BlackRay Parabolic antenna in combination with SATCOM satellites a link budget of 3.1 $[dB]$ is achieved, meaning a clear communication link between the UCA and GCS.

This report only considered the concepts on which the unmanned operations will be based. Future design should go deeper into the actual design of the GCS, communication links, and avionics architecture. In conclusion it can be stated that much though was given to the unmanned operations of the UCA. Considering the careful considerations and high level of redundancy applied in many subsystems, it may be assumed the aircraft is able to execute these unmanned operations in a safe and successful manner.

13
Aircraft Configuration and Electrical Systems

This chapter will describe the environmental control, hydraulic system and electrical system of the aircraft. Furthermore the software, hardware and data handling block diagrams will shown and explained. First the relevant requirements will be given in Section 13.1. Afterwards, the parachute system will be discussed in Section 13.2. Next, the environmental control will be described in Section 13.3. After that the hydraulic system will be presented in Section 13.4. Finally, the software, hardware, electrical and data handling block diagrams will be shown in Section 13.6 up to and including Section 13.8.

13.1. Requirement Analysis

In order to design an aircraft that has the appropriate electrical systems, hardware and software it is important to fulfill the corresponding requirements. During the determining the aircraft configuration and designing the electrical systems the following requirements have to be fulfilled:

- **REQ-SUBSYS-POW-2.6.00:** The UCA's power unit shall provide an average electrical power of 120 $[kW]$.
- **REQ-SUBSYS-POW-2.6.01:** The UCA's power unit shall provide a peak electrical power of 222 $[kW]$.
- **REQ-SUBSYS-POW-2.6.02:** The environmental temperature of the UCA's power unit shall not exceed 45 degree Celsius.
- **REQ-SYS-FLT-2.5.03:** The cargo hold of the UCA shall be pressurised if needed.
- **REQ-SYS-FLT-2.5.04:** The cargo hold of the UCA shall keep the cargo undamaged during all flight phases.
- **REQ-SYS-FLT-2.6.01:** The UCA shall provide electrical power to the aircraft subsystems.
- **REQ-SYS-CAR-2.5.01:** The UCA shall have a cargo compartment which is shielded and insulated from sources of heat within the compartment to prevent igniting the cargo.
- **REQ-SUBSYS-CAR-2.5.00:** The UCA shall be able to maintain a cabin pressure altitude of no more than 4572 [m] (15000 [ft]) in the event of any reasonably probable failure or malfunction in the pressurisation system.
- **REQ-SUBSYS-CAR-2.5.01:** The UCA shall have a cargo compartment which is shielded and insulated from sources of heat within the compartment to prevent igniting the cargo.
- **REQ-SUBSYS-CAR-2.5.02:** The temperature in the cargo compartment of the UCA shall lie between 0 and 25 degree Celsius. [48]

13.2. Parachute System

As mentioned before the UCA only uses one engine. In case of a engine failure the aircraft will only be able to land within a limited radius. This radius could be increased by designing for a higher glide ratio. The higher the glide ratio the larger the distance of forward travel per altitude lost in that distance. This comes with a price however, the higher the glide ratio the more the negative effect is on the cruise performance of the aircraft. Meaning that increasing the glide ratio is not the optimal way to go for this design. Therefore, with help of the customer, the idea of using a parachute has been introduced. A parachute can be used to minimise the impact on the ground when the aircraft is not able to land safely on a runway. This section will elaborate more on the function of a parachute and the preliminary design of it.

13.2.1. Parachute Design

A parachute works on the principle of air resistance. When the parachute is deployed, a surface area of the parachute opens up. This surface area introduces a drag force on the aircraft that is falling down. The drag force of the parachute will counteract the weight force that points downwards. Eventually, the drag force will be equal and opposite to the weight force, which means that the net force equals zero. The equation for force equilibrium can be found in Equation 13.1. [49]

$$F = D - W = C_D 0.5 \rho V^2 S - mg \quad (13.1) \qquad r = \sqrt{\frac{2mg}{\pi C_D \rho v^2}} \quad (13.2) \qquad S_p = 2\pi r^2 \quad (13.3)$$

At the point that the net force equals zero the downward velocity will not change. This velocity is called the terminal velocity. Using the terminal velocity a rough first order estimate of the parachute's surface area can be made. Rear-

ranging the terms in Equation 13.1 will result in Equation 13.2 that can be used to determine the parachute's radius. The density is set equal to sea level conditions, 1.225 $[kg/m^3]$, and the drag coefficient is assumed to be 1.75 [1]. Furthermore, the terminal velocity has chosen to be 42 $[km/h] \approx 11.67\ [m/s]^2$. The mass used for this calculation is set equal to the mass at the beginning of the cruise phase. For this first order estimation of the surface area it is assumed that the parachute has a semi spherical shape. To calculate the total surface area of the parachute Equation 13.3 can be used. Note that in this calculation the drag force of the aircraft has been neglected. Finally, it has been found that the diameter of the frontal area equals 32.32 $[m]$ and the total surface area of the parachute equals 1640.72 $[m^2]$. To determine a first order estimate of the mass of the parachute, it will be compared to a similar parachute that has already been designed. The dimensions of this parachute are in the same order of magnitude as the parachute used for the Europe's ExoMars rover. The total mass of this parachute system is about 195 $[kg]$[3].

The parachute will be deployed in a similar way as the parachute of Cirrus Vision jet[4]. Meaning that the parachute will be deployed using a little rocket. This rocket allows the parachute to deploy quickly as well as it avoids the parachute from being tangled with the engine. It is important to mention that the parachute can only be used if the engine does not run anymore.

13.3. Environmental Control: Pressurisation and Temperature Control System

Following from REQ-SYS-FLT-2.5.04, all cargo should remain undamaged during all flight phases. When the payload gets damaged, the value of the cargo drops significantly. The drop is relatively high since the payload consists of high value goods of which some of the goods are fragile. For the customer it is therefore important that the cargo arrives undamaged. This means, for example, that the cargo should be protected from low temperatures and pressures, especially during cruise. Therefore, it is important to have a system that regulates the temperature and pressure in the cargo hold. Furthermore, the UCA shall be able to maintain a cabin pressure altitude of no more than 4572 $[m]$ if the system fails. Other than passenger aircraft this aircraft does not require oxygen systems as no humans will be on-board during flight. In order to control the pressure in the cargo hold the fuselage will be pressurised. Similar to most existing cargo aircraft it has been decided that the aircraft will be pressurised above 2438 $[m]$ [50]. This means that the cargo hold pressure will be around 75 $[kPa]$, similar to the altitude pressure at 8000 $[ft]$. The temperature required in the cargo hold depends on the type of cargo that is being transported. In order to ensure that the cargo will arrive undamaged, information about the characteristics of the goods is needed. Those characteristics will tell at what temperature the cargo has to be transported. The UCA will be designed such that the cargo can be transported in an environment similar to that of a Boeing 747 freighter. A temperature range from 0 to 25 degree Celsius will be used [48]. In case an extreme temperature is required to transport the cargo, temperature controlled unit load devices will be needed [51]. It is important that the correct temperature is chosen to ensure the quality of the goods.

13.4. Hydraulic System

In order to move control surfaces and systems such as the landing gear and cargo door a hydraulic system is needed. High aerodynamic loads make it difficult to move the control actuators of the aircraft. The hydraulic system of the aircraft is used to transmit power from the engines to several control actuators of the aircraft. The pilot, or in this case the autopilot, uses low power levels to control the aircraft. The hydraulic system is able to convert the low power level to a high power level that is used to move the control actuators. For this design the landing gear, high lift devices (HLDs), control surfaces and cargo door is considered import for the hydraulic system design. The hydraulic system has the advantages of a precise control of the control actuators. During the movement of the control actuators the position, magnitude and load rate can be determined with high precision. The hydraulic system uses hydraulic fluids to transmit the power to the control actuators. Several pumps and valves are used to control the fluid in the hydraulic system. The hydraulic system consists of several pipes with fluids but not all pipes are connected. Therefore, a power transfer unit is used to transfer fluid power between to parts of the system. It is important that the pressure, temperature and flow rate of the fluid does not deviate from the required values. The pressure is usually in a range from 0.69 MPa to 35 MPa depending on the type of aircraft, small or large. Furthermore, fire-resistant hydraulic fluids are available to improve the safety of the hydraulic system [52].

The hydraulic system can be divided in three parts. The left circuit, right circuit and centre circuit. The centre circuit is used in the design to make the system a redundant system. A redundant system is required to ensure that the aircraft can still be controlled if one of the circuits fails. Figure 13.1 shows the layout of the hydraulic system. As you can see the left, right and centre part of the system are present in the figure. They will be used to control the HLDs, control surfaces, and landing gear.

[1] https://www.grc.nasa.gov/www/k-12/VirtualAero/BottleRocket/airplane/rktvrecv.html [Accessed on: 02-06-2021]
[2] https://www.forbes.com/sites/quora/2017/02/03/why-is-it-so-difficult-for-a-returning-spacecraft-to-re-enter-our-atmosphere/ [Accessed on: 02-06-2021]
[3] https://www.space.com/40597-giant-mars-parachute-passes-first-test.html [Accessed on: 02-06-2021]
[4] https://www.youtube.com/watch?v=75m6ZTODxS8 [Accessed on: 02-06-2021]

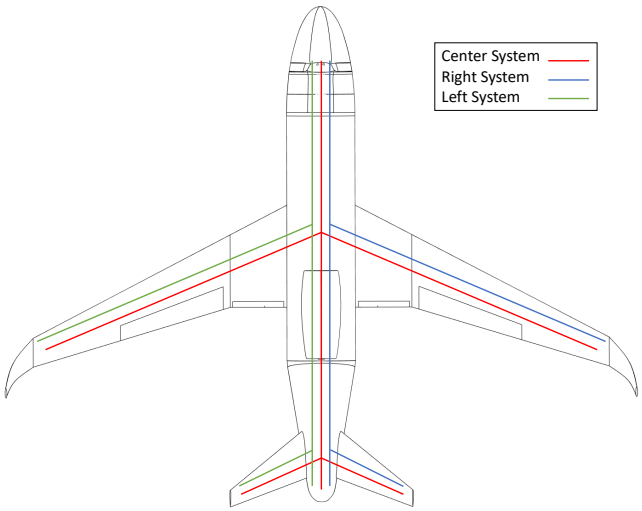

Figure 13.1: Hydraulic system of the UCA

13.5. Electrical Block Diagram

In order to use all on-board systems, electric power needs to be generated. For this aircraft electricity will be of utmost importance, as otherwise the flight management system and autopilot system cannot control the aircraft itself. The main power will come from the lithium-ion battery, which will drive the generator. This will be a high voltage and alternating current, which cannot used immediately by all systems. Therefore, a transformer rectifier unit (TRU) is used in order to both decrease the voltage as well as the change the current from AC to DC. For redundancy a back-up TRU is present, as a failure in the first TRU would otherwise lead to the overall failure of the system. This energy will be transported to the battery and power management system, which will provide a low voltage and DC to all relevant systems.

Regarding the battery, it should be capable of delivering sufficient power to all electric systems. The largest utilizer to account for is the ground power unit, with a total power requirement of 6000 [W]. Apart from this, all other systems have a lower power required and are therefore also accommodated for. It has been estimated that a power supply lasting 1 hour will satisfy, which already includes a safety margin. A lithium-ion battery has a specific energy of approximately 175 $[W \cdot h/kg]$ [5], yielding that the battery will weigh 34.3 [kg]. An APU was not opted for since the weight of such a power supply is substantially higher than batteries. On top of this, a battery is also the safer option since it does not rely on fuel.

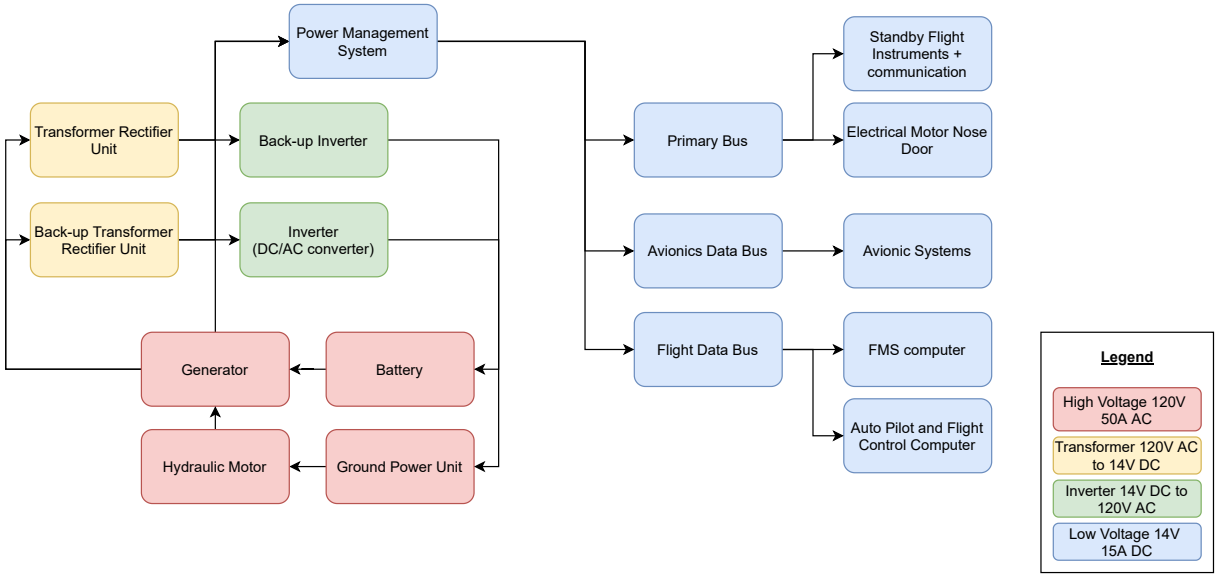

Figure 13.2: Electrical Block Diagram

In order to have also a redundant power supply, the hydraulic motor could be used to power the battery. The ground power unit is a generator, which can be used on the ground when the engine is turned off. This could for instance be

[5] https://www.cei.washington.edu/education/science-of-solar/battery-technology/ [Accessed on: 28-06-2021]

used to generate power in order to open and close the cargo door. Next, the aircraft will have three different data buses, one in order to control the aircraft (Primary Data Bus), one to process and store the data from the avionic systems (avionics data bus), and one in order to process all data from the FMS, auto pilot, and flight control computer. The different data busses can exchange data between one another if necessary. [6] [7] [8]

13.6. Hardware Block Diagram

The hardware block diagram shows all relevant systems and their relationship. The flow of data will be discussed in Section 13.7 and Section 13.8. All relevant systems are shown in Figure 13.3. For avionics, all relevant systems have been included. These systems will interact with the FMS computer, and auto pilot & flight control computer. It should be noted that the power needed to operate the hydraulic systems will come from the engine. The cargo door and the parachute system will not be operated using hydraulic systems, but using an electrical motor.

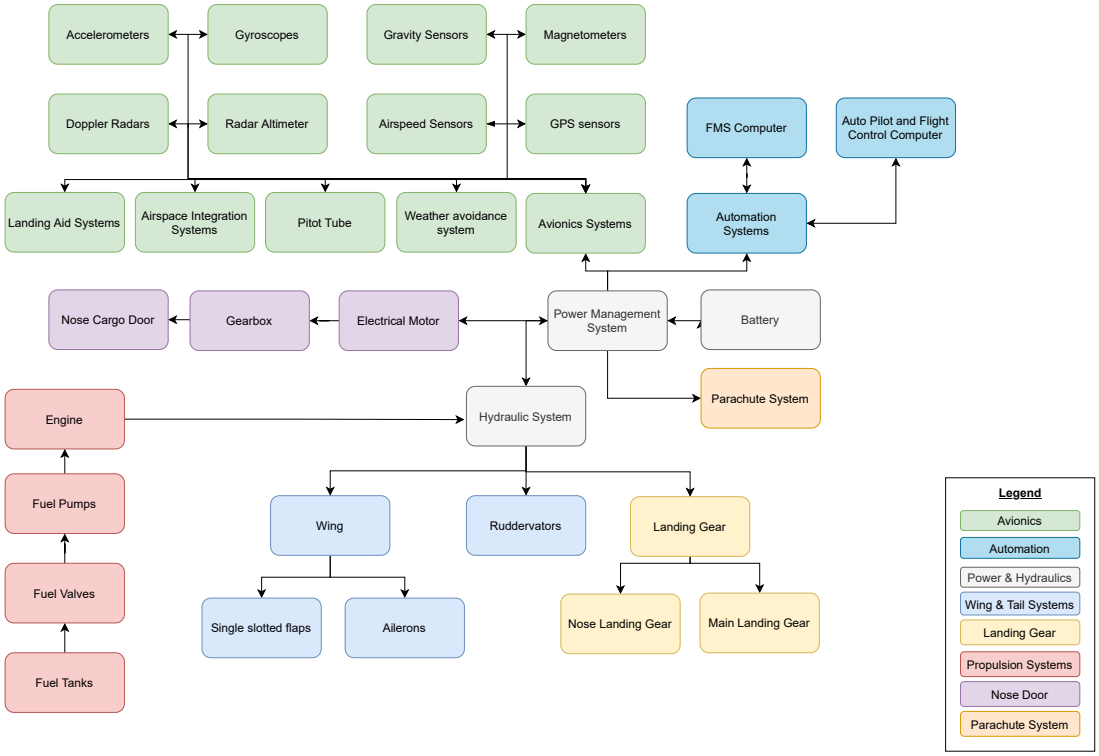

Figure 13.3: Hardware block diagram

13.7. Software Block Diagram

In Figure 13.4, the software diagram and the system interactions are shown. These are more extensively discussed in Section 12.4.3 and 12.4.5. Each software has been color coded to different specific categories for clarity. The main focus of this diagram is to highlight the interaction between all systems. Feedback and Input is given for all systems. The first block following from the data buses are the general systems. Afterwards, the different sensors and the software flowing from it is shown.

13.8. Data Handling Block Diagram

The figure shown in Figure 13.5 presents the data flow in the aircraft. The grey blocks represent the systems of the aircraft with either a green or yellow box immediately connecting it, the boxes being input or output respectively. Each of these subsystem will end in outputting to one of the three busses, the primary, avionics, and flight data bus.

13.9. Verification and Validation

This section will discuss the verification and validation for the parachute. The verification of the parachute surfaces area calculations has been done using hand calculations. Hand calculations is a good option for verification as the design of the parachute surface area required a limited amount of steps. After finishing the verification procedure no errors have been found in the code. Validation has been done by comparing the model to the parachute of the Cirrus Vision jet aircraft. The mass used during validation is the maximum gross weight of the Cirrus Vision jet, which is 6000 $[lbs] \approx 2727\ [kg]$. The diameter of the parachute determined by the model was found to be 15.28 $[m]$. The actual

[6] `https://www.skybrary.aero/index.php/Aircraft_Electrical_Systems` [Accessed on: 10-06-2021]
[7] `https://aerocorner.com/blog/how-airplanes-generate-electricity/` [Accessed on: 10-06-2021]
[8] `flight-mechanic.com/aircraft-batteries-battery-charging/`[Accessed on: 10-06-2021]

diameter of this parachute is 19.8 $[m]$, which means that the difference in diameter is about 4.5 $[m]$. However this model is used for a preliminary estimation of the parachute dimensions and the drag introduced by the aircraft has been neglected. Therefore this model is deemed valid.[9]

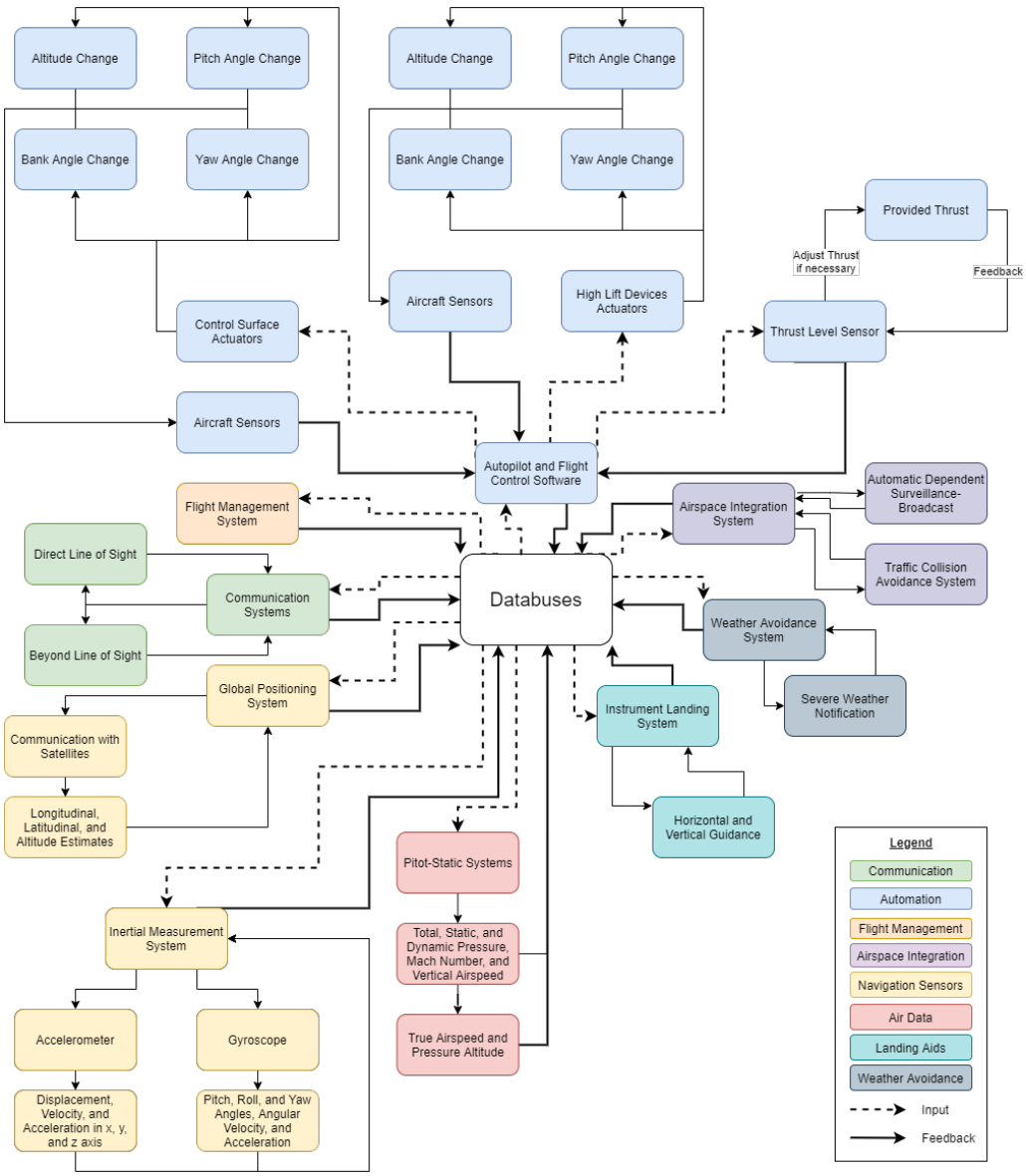

Figure 13.4: Software Block Diagram

13.10. Conclusion and Recommendations

This chapter put an emphasis on several subsystems, which were not discussed before.

In-order to protect the clients payload, near-by residents and the environment, a parachute system has been integrated into the fuselage. A 195 $[kg]$ was designed to deploy upon single engine failure. With a total frontal diameter of 32.32 $[m]$, a terminal velocity of 11.67 $[m/s]$ could be achieved at maximum take off weight. This measure would assist in minimizing the damage that the aircraft could cause on its nearby surroundings and its payload. As this estimate was a first order estimate, the drag force of the aircraft was neglected. It's thus recommended that further optimization on the size of the parachute can be made in further iterations by taking this into account.

Regarding the cargo hold, it will have a pressure of 75 $[kPa]$ and the temperature will range between 0 and 25 degrees. The hydraulic system is divided into three subsystems and will be used for operating the HLDs, control surfaces, and landing gear. Regarding the electrical systems, a lithium-ion battery has been chosen as power source. Multiple generators, TRUs and rectifiers are used for redundancy.

In the post-DSE phase, all electrical and hydraulic systems can be designed in more detail, as this report only entails

[9] `https://cirrusaircraft.com/wp-content/uploads/2014/12/CAPS_Guide.pdf` [Accessed on: 02-06-2021]

a feasibility study.

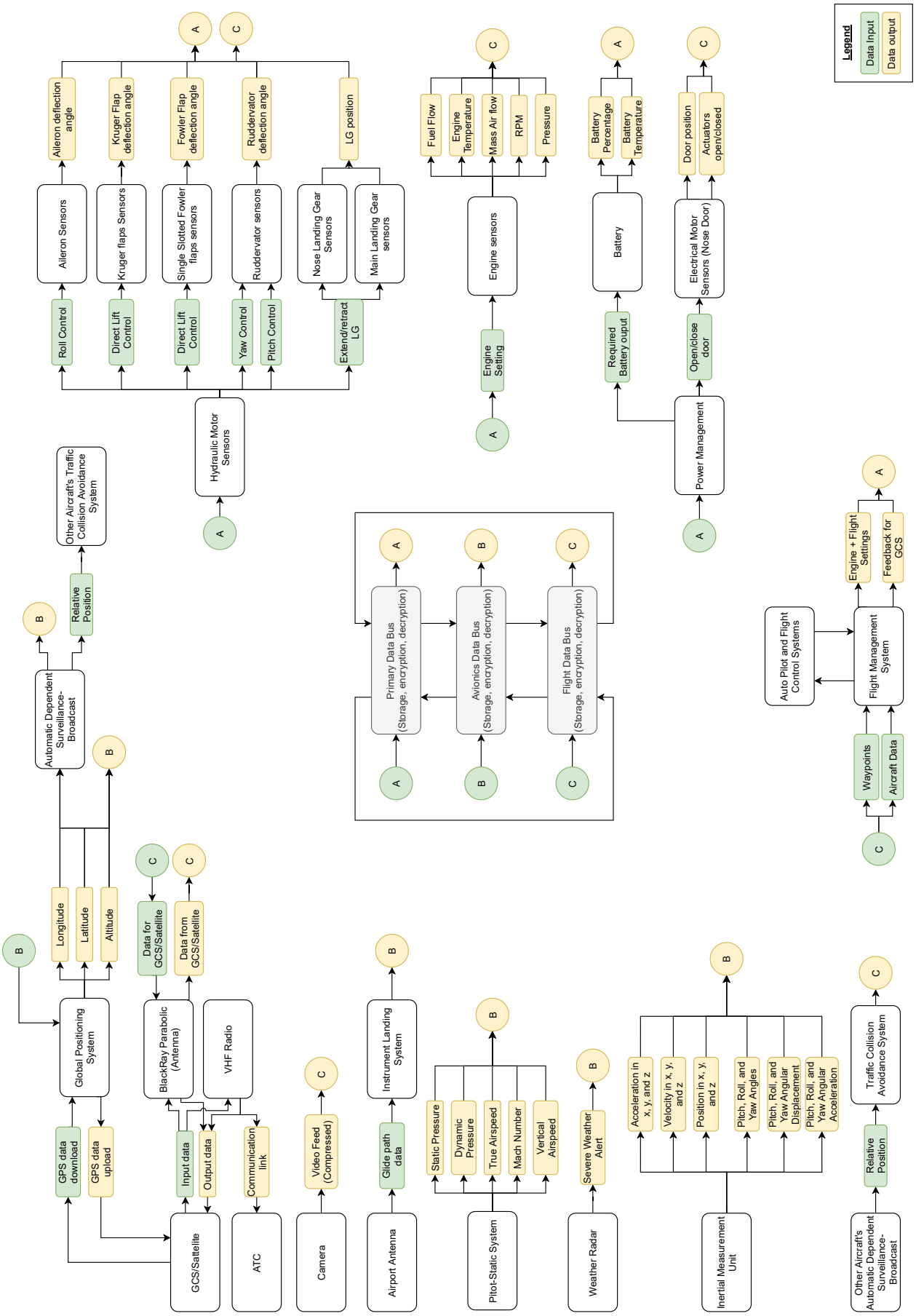

Figure 13.5: Data Handling Block Diagram

14
Noise and Sustainability

The importance of sustainability is increasing by the day in most industries, especially in the aviation industry. New innovation and research lead to improved and optimised designs or operational strategies helping in reducing the environmental impact. The UCA will not only help in reducing CO_2 emission in air cargo operations, but will also contribute to economic sustainability by means of creating new markets and opportunities as well as reducing noise, pleasing residents living near airports.

In Section 14.1 the requirements for sustainability are given, Section 14.2 elaborates on the noise analysis of the UCA. Afterwards, the sustainable development strategy will be discussed in Section 14.3. The chapters end with future sustainable development strategies in Section 14.4.

14.1. Requirement Analysis

In order to contribute to sustainable aviation, requirements have been set to which will help in achieving this goal. The following requirements are listed:

- **REQ-STK-04:** The UCA shall relatively emit less CO_2 than other cargo aircraft
- **REQ-STK-07:** The UCA shall reduce noise disturbance as much as possible.
- **REQ-STK-08:** The UCA shall reduce local emissions as much as possible.
- **REQ-SYS-SUS-4.1.00:** The CO_2 emission of the UCA shall be less than 50% per metric tonne when compared to a 747-400 freighter.
- **REQ-SYS-SUS-4.2.00:** The noise level of the UCA shall be below that of a Cessna Citation 2.
- **REQ-SYS-SUS-4.3.00:** The UCA shall be able to have 80% of the structure recycled at the end of the useful life cycle.

14.2. Noise

Sound can be described as variation in pressure in the air caused by a source, and when it is undesired it is called noise. The magnitude of noise is dependant on many factors such as the aircraft characteristics and flight conditions as well as how the sound waves are propagating through the atmosphere. Communities near airports are most impacted by aircraft noise, this may lead to health issues such as stress, increased blood pressure, sleep disturbance, worsening ability to concentrate on work and even devaluation of property [53]. In order to keep the communities satisfied, noise regulations are enforced limiting the number of flight movements. With regard to increasing flights, noise can be mitigated on three levels, during the planning of a new airport, at an operational level or when designing the aircraft itself. The latter will be discussed in more detail.

Noise produced by aircraft are caused by engines and the airframe, these are the points the UCA will be analyzed on concerning noise. The results will be compared to a Cessna Citation II as required by **REQ-SYS-SUS-4.2.00**. Aircraft noise certification is performed at three positions, for lateral, flyover and approach as can be seen in Figure 14.1. Only the approach phase will be assessed for the noise analysis, since the noise levels during approach are typically the highest [54].

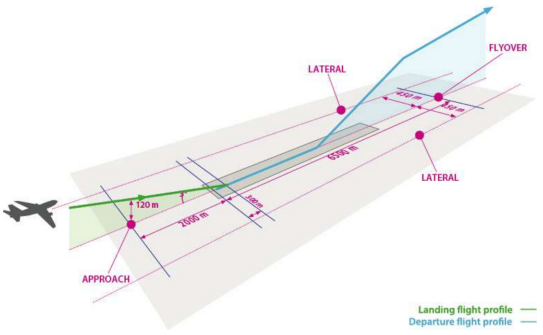

Figure 14.1: Aircraft noise certification positions [54]

14.2.1. Airframe Noise

The method which will be used for the noise analysis is NASA's Aircraft Noise Prediction Program (ANOPP) [54].The noise of each airframe component is calculated using Equation 14.1 where p_e is the effective pressure in $[pa]$. The effective pressure is proportional to several functions, such as the power function, P, the spectral function, F, and the directivity function, D. The term $1/4\pi r^2$ accounts for the accoustic power at a certain distance from the source, and $(1-Mcos\theta)^4$ takes into account the Doppler effect.

$$p_e^2(f,\theta,\phi) = \frac{\rho_\infty cPD(\theta,\phi)F(S)}{4\pi r^2(1-M\cos\theta)^4} \tag{14.1}$$

Using the effective pressure, the sound pressure level (SPL) given in Decibels can be calculated using Equation 14.2 in which p_0 is the reference sound pressure in air 20 $[\mu Pa]$,which is also referred as the threshold of human hearing [1].

$$SPL = 20\log\left(\frac{p_e}{p_0}\right) \tag{14.2}$$

The power function which is given by Equation 14.3, is dependant on several constant for which the values of each airframe component is given in Table 14.1 as well as formulas for the geometry function, G, and length scale, L. For the empennage surfaces the same constants and formulas for the clean wing are used which will also be the case for the spectral function and directivity function.

$$P = KM^aG\left(\rho_\infty c^3 b_w^2\right) \tag{14.3}$$

Table 14.1: Airframe noise source formulas for geometry, length scale and constants[54].

Airframe Noise Source	**Geometry Function, G**	**Length Scale, L**	**Constant K**	**Constant a**
Clean wing, trailing edge	$0.37\frac{A_w}{b_w^2}\left(\frac{\rho McA_w}{\mu b_w}\right)^{-0.2}$	Gb_w	$4.464x10^{-5}$	5
Flaps, trailing edge	$\frac{A_f}{b_w^2}\sin^2(\delta_f)$	$\frac{A_f}{b_f}$	$2.787x10^{-4}$	6
Landing gear	$n\left(\frac{d}{b_w}\right)^2$	d	$4.349x10^{-4}$ (1 and 2 wheels) $3.414x10^{-4}$ (4 wheels)	6

The spectral functions for the airframe components are shown in Table 14.2, which is a function of the Strouhal number.

Table 14.2: Airframe noise source spectral functions[54]

Airframe Noise Source	**Spectral Function, F(S)**	
Clean wing, trailing edge	$F(S) = 0.613(10S)^4[(10S^{1.5}+0.5]^{-4}$	
Flaps, trailing edge	$F(S) = 0.0480S$	for $S<2$
	$F(S) = 0.1406S^{-0.55}$	for $2\leq S\leq 20$
	$F(S) = 216.49S^{-3}$	for $S>20$
Nose landing gear	$F(S) = 13.59S^2(S^2+12.5)^{-2.25}$	
Main landing gear	$F(S) = 0.0577S^2(0.25S^2+1)^{-1.5}$	

The Strouhal number is calculated using Equation 14.4, which is dependant on, f, the centre frequencies of the 1/3-octave bands in $[Hz]$ and the length scale, L. For a certain band number n, the centre frequency is given by $f_n = 10^{n/10}$. The directivity functions for each component can be found in Table 14.3.

$$S = \frac{fL(1-M\cos\theta)}{Mc} \tag{14.4}$$

The directivity function is a function of θ and ϕ which are the polar and azimuthal directivity angles respectively. Since the UCA has a V-tail configuration, the azimuthal angle is assumed to be the same as the dihedral angle of the tail control surfaces, which is 34 degrees.

[1] `https://www3.nd.edu/~atassi/Teaching/ame553/Notes/Sound_power.pdf` [Accessed on:14-06-2021]

Table 14.3: Airframe noise source directivity function[54].

Airframe Noise Source	**Directivity Function, D(θ,ϕ)**
Clean wing, trailing edge	$D(\theta,\phi) = 4\cos^2(\phi)\cos^2(\theta/2)$
Flaps, trailing edge	$D(\theta,\phi) = 3\left(\sin\delta_f\cos\theta + \cos\delta_f\sin\theta\cos\phi\right)^2$
Landing gear	$D(\theta,\phi) = \frac{3}{2}\sin^2\theta$

After having elaborated upon the variables in Equation 14.1 and since the values are now known, the airframe noise of the UCA can be plotted as a function of the 1/3-octave band centre frequencies against the sound pressure level in decibels. The results can be seen in Figure 14.2. The observing point is taken to be the point for approach noise certification at sea level conditions. Thus at a distance of 120 [m] below the approach glide path with a polar directivity angle of 90 degrees and a mach number of 0.2. The maximum noise level caused by the airframe which can be reached is 73.8 [dB] for the 24^{th} band of the 1/3-octave band frequencies. The same analysis have been performed for a Cessna Citation II, the maximum reachable airframe noise is 73.2 [dB] which is sensible due to the difference in size.

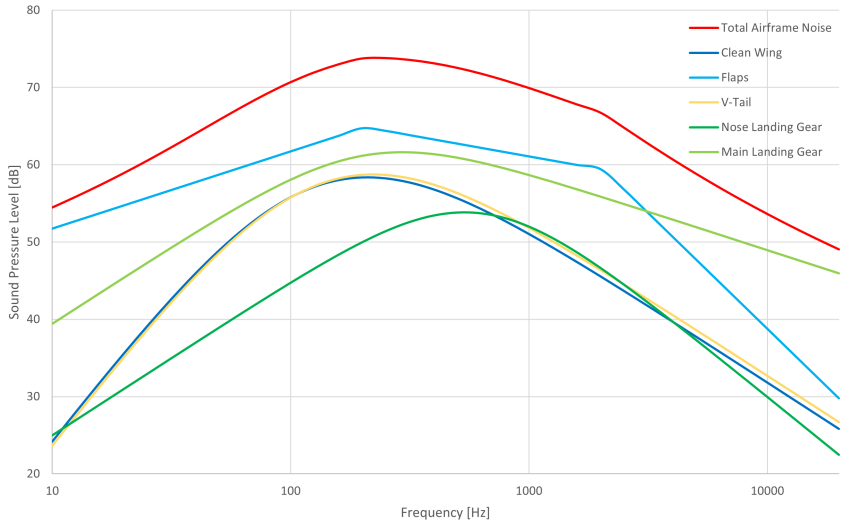

Figure 14.2: Airframe noise of the UCA at approach certification position, sea-level conditions at mach = 0.2

14.2.2. Engine Noise

Noise caused by engines have been decreasing in the past decades due to improving engines designs such as increasing the bypass ratio in turbofan engines. In a turbofan four main noise sources can be distinguished, these are the fan, compressor, turbine & combustor and jet noise. For the engine noise analysis only the fan and jet noise will be assessed since these two sources contribute the most to noise for turbofan engines [54].

The jet noise is mainly caused by the exit jet velocity and the width of the engine, the relation with the effective pressure is shown in Equation 14.5 and the intensity of the acoustic power in relation with distance is once again given in Equation 14.6. Using the exit jet velocities and engine size given by the propulsion department, an effective pressure of 0.01632 [Pa] has been found, which is 58.2 [dB] for the jet noise, measured at the same location for the airframe noise.

$$p_e \sim \frac{\rho V^4 D}{c^2 r} \tag{14.5}$$

$$I = \frac{W}{4\pi r^2} \tag{14.6}$$

Once the jet noise have been found, the fan noise can be determined using Figure 14.3 which shows the relative noise levels of jet noise and fan noise as a function of the bypass ratio. The UCA uses the Rolls Royce ae3007A engine which has a bypass ratio of 5, this results in a relative noise increase of 24.48 [dB] for the fan noise compared to the jet noise. The effective pressure increase is therefore 0.00033 [Pa] leading to an effective pressure of 0.0167 [Pa] for the fan noise. Combining both jet and fan noise results in an engine noise of 64.3 [dB] for the single engine of the UCA, without taking into account any shielding effects of the fuselage.

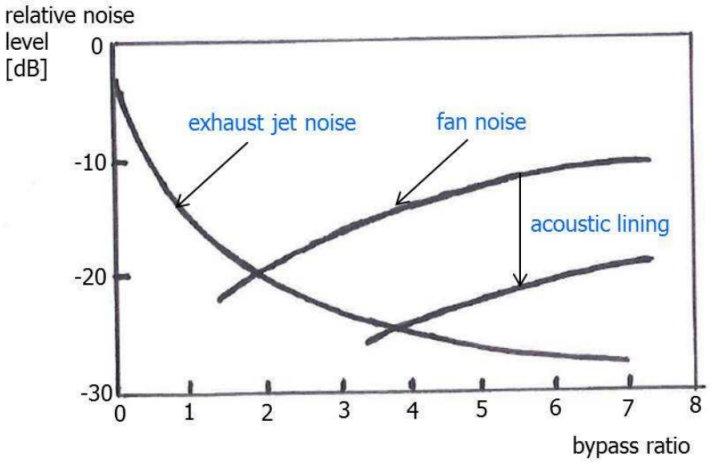

Figure 14.3: Relative noise level of jet noise and fan noise as a function of bypass ratio [54]

14.2.3. A-Weighted Noise Level

The sound pressure levels which have been found in Subsection 14.2.1 and Subsection 14.2.2 are weighted according to the A-weighting curve which is given by Equation 14.7 as a function of frequency. The A-weighting curve is applied to take into account the relative sounds perceived by humans, due to lowered sensitivity to low frequency sound [55].

$$\Delta L_A = -145.528 + 98.262 \log f - 19.509 (\log f)^2 + 0.975 (\log f)^3 \tag{14.7}$$

The overall A-weighted noise can then be calculated using Equation 14.8. A-weighting has a large effect on low frequency noise, allowing for large reduction in decibels, whereas for high frequencies the effects are small and may even increase the noise level [54].

$$L_A = 10 \log \sum_i 10^{\frac{SPL(i)+\Delta L_A(i)}{10}} \tag{14.8}$$

Due to the configuration of the UCA, the engine noise will be partly shielded by the fuselage, introducing lateral attenuation effects. The A-weighted sound pressure level, L_A can be corrected for the effect of lateral sound attenuation ΔL_T which takes into account ground effects and engine noise shielding caused by the aircraft geometry. Assuming that the fuselage will shield the downward propagating sound waves, the elevation angle β will be 0 degrees resulting in Equation 14.9.

$$\Delta L_T = \Delta L_G(s) f(\beta) + g(\beta) \tag{14.9}$$

The ground attenuation ΔL_G for a distance of 120 $[m]$ from the observer is given by Equation 14.10 and the formulas $f(\beta)$ and $g(\beta)$ are given by Equation 14.11 and Equation 14.12 respectively.

$$\Delta L_G = 0.0163 s - 0.815 \tag{14.10}$$

$$f(\beta) = 5.471 \beta^2 - 4.774 \beta + 1 \tag{14.11}$$

$$g(\beta) = 3(1 - \sqrt{\sin \beta}) \tag{14.12}$$

The lateral sound attenuation of the UCA is 4.1 $[dBA]$, which can be deducted from the total A-weighted sound pressure level.

The end result of the combined noise sources from the airframe and engine of the UCA is shown in Figure 14.4 alongside with the noise levels of the Cessna Citation II. The noise levels are given in $[dBA]$ as a function of frequency on a logarithmic scale. The maximum noise levels for the UCA and Cessna Citation II are 72.4 $[dBA]$ and 73.9 $[dBA]$ respectively, showing that the noise level of the UCA is below the noise level of a Cessna Citation II.

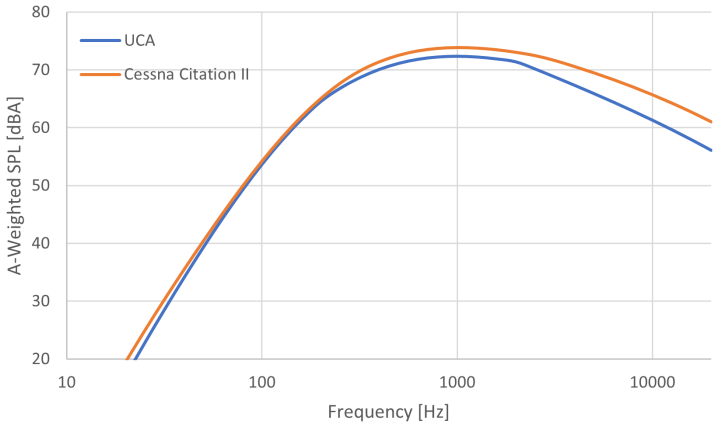

Figure 14.4: Total noise comparison between the UCA and Cessna Citation II

14.2.4. Verification and Validation

For the verification of the noise calculations all calculation have been checked manually for which the error difference is negligibly small and are caused by possible rounding errors. Furthermore, system test are performed to check the behaviour of the calculation due to changes in input values. Doubling the effective pressure would for example increase the sound pressure level with 6 $[dB]$ and an effective pressure which is 10 times stronger has a SPL which is 20 $[dB]$ higher, meaning it follows the logarithmic scale correctly according to Equation 14.2.

For validation, reference data has been used of aircraft which have been analysed on noise based on the same method. The reference aircraft are the Fokker 70 and Airbus 380 during landing and the results can be found in Chapter 9 of the aircraft noise reader from the AE4431 master course thought at the TU Delft [54]. Comparing the data from the UCA to the reference aircraft similar results are found, the main landing gear always produces more noise compared to the nose landing gear and flaps are noisier compared to the clean wing. The noise levels of 72.4 $[dB]$ found for the UCA during approach are considered valid, since according to the CDC noise levels of 75-80 $[dB]$ have been reported during landing of an Airbus 321 [2]

14.3. Sustainable Development Strategy

This section will discuss the sustainable development strategy. Subsection 14.3.1 will give an overview of the CO_2 emissions produced in a life-cycle, Subsection 14.3.2 and Subsection 14.3.3 will discuss the economic and social sustainability of the UCA.

14.3.1. Life-Cycle Analysis

The life-cycle analysis (LCA) gives a general overview of the sustainability of a product. In the midterm-report the main points concerning sustainability in each life-cycle phase, manufacturing, operations and retirement, were given. Now, these points are analysed based on the design and operational decisions of the UCA.

Manufacturing

The first phase which will be discussed is manufacturing, the structure of the UCA will mainly consist of aluminium except for the landing gear which is made from titanium. Using the mass estimation from Section 4.7 the structure and landing gears have a weight of 5527 $[kg]$ and 704 $[kg]$ respectively. The energy needed to produce primary aluminium is 17 $[kWh/kg]$ [56] and for titanium this is 179 $[kWh/kg]$ [3], resulting in needing approximately 94.0 $[MWh]$ and 12.6 $[MWh]$ for producing the material of the structure and landing gears respectively. Assuming natural gas is used to produce the energy needed, a total of 91.7 tonnes of CO_2 will be produced for material extraction alone, since 0.92 pounds of CO_2 is produced per kWh [4].

The parts of the UCA will be assembled in an assembly line in order to increase efficiency. The same crew will be stationed at the same station to reduce production time due to the learning curve and multiple units will be built at the same time to reduce the delivery intervals. This topic is discussed in more detail in Section 18.1. Reducing the production time will save man hours and thus costs, which is beneficial for economic sustainability.

For part manufacturing, the metal sheets are cut in desired sizes using water jet cutting. The equipment cost are relatively high compared to other processes, however water jet cutting is a universal tool including low labour costs.

[2] https://www.cdc.gov/niosh/topics/aircrew/noise.html [Accessed on: 16-06-2021]
[3] https://www.digitalalloys.com/blog/energy-consumption-metal-additive- [Accessed on: 15-06-2021]
[4] https://www.eia.gov/tools/faqs/faq.php?id=74&t=11 [Accessed on: 15-06-2021]

In order to shape the metal sheets, sheet metal forming processes such as bending and rubber forming are applied since they are cheaper compared to other methods, decreasing manufacturing costs[57].

Operations
During flight operations burning fuel is the main contributor to greenhouse gas emissions. At the harmonic range the UCA is able to carry 2542 [kg] of payload and 4425 [kg] fuel. Using synthetic kerosene, which produces 1.33 kg of CO_2 per kg fuel as mentioned in Subsection 7.2.2 the total CO_2 emissions is 5885 [kg] per flight. Assuming that the UCA will do 2 flight per day and has a service life of 20 years, the total CO_2 emissions will be 85916 tonnes.

In order to compare to CO_2 emissions of the UCA to other cargo aircraft during flight operations, a comparison has been made with the B747-400F in Subsection 7.2.2. The results showed that the UCA emits 51.2% less CO_2 per metric tonne compared to the Boeing aircraft. A second comparison is made with the CO_2 emissions produced by air cargo operators which can be seen in Figure 14.5. The FTK of the UCA has been calculated for maximum payload at the harmonic range, resulting in a FTK of 12157 per flight. And knowing that the CO_2 emissions for this point is 2314 kg CO_2 per metric tonne the operations performance of the UCA for cargo transport is 0.484 kg CO_2 per FTK. The UCA is compared to a total of four companies which transport air cargo. Cargolux is a company which only transports air cargo, it currently has a fleet consisting of variants from the B747 freighter family [5] and reported 0.540 kg CO_2 per FTK [6]. Emirates is one of the largest commercial airliners in the world and has a separate fleet consisting of 11 B777F aircraft dedicated to air cargo [7] and has a CO_2 efficiency of 0.556 kg CO_2 per FTK [8]. The last two airlines are KLM and Air France which mainly focus on passenger transport, however if there is left over belly capacity in the aircraft additional freight may be transported. KLM and Air France have reported 0.428 and 0.466 kg CO_2 per FTK respectively [9]. Why the CO_2 efficiency of passenger airlines are lower may be explained by the fact that a smaller portion of the total CO_2 emissions per flight, compared to transporting passengers, is counted towards freight whilst travelling a large distance. From this comparison it can be concluded that the UCA is competitive with aircraft operated by air cargo operations with regard to sustainability.

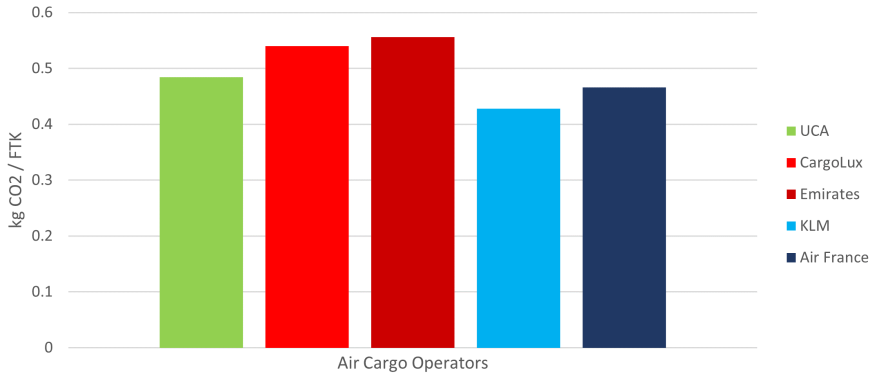

Figure 14.5: CO_2 emissions per freight-tonne-kilometer of the UCA compared to air cargo operators

Retirement
The UCA will enter retirement after its operational lifespan. In order to be as sustainable as possible the goal will be to reduce waste. In Section 9.5 the end-of-life strategy has been discussed in more detail. The main points were to **decommission** the UCA, afterwards reusable parts will be **disassembled** and finally the left over parts are **dismantled** for material recycling. Ultimately, the aircraft will be recycled for at least 90%, the recycled aluminium will not be used for aircraft related structures if the material is not up to par with aviation quality standards due to reduced material properties. Instead, the recycled aluminium could be used in other industries where for example electrical wires or soda cans are produced.

Considering the waste reduction of 90% from recycling aluminium during the retirement phase, 10% of the CO_2 emission from the manufacturing phase is wasted which is 9.17 tonnes of CO_2. And taking into account that recycling aluminium saves up to 90% energy as mentioned in Section 9.2, an additional 8.26 tonnes of CO_2 is added, bringing the total of CO_2 emissions during the retirement phase to 17.43 tonnes. The total CO_2 emissions is 86025 tonnes of which the manufacturing, operations and retirements contribute 0.11%, 99.87% and 0.02% respectively as can be seen

[5] `https://www.cargolux.com/products/Road-Feeder`[Accessed on: 16-06-2021]
[6] `https://www.cargolux.com/about-us/Corporate-Responsibility/environment/Environmental-flyer`[Accessed on: 16-06-2021]
[7] `https://www.skycargo.com/fleet/air-fleet/`[Accessed on: 16-06-2021]
[8] `https://www.emirates.com/english/images/The%20Emirates%20Group%`[Accessed on: 16-06-2021]
[9] `https://www.airfranceklm.com/sites/default/files/universalregistrationdocument2019_20-04-20air_france_klm_1.pdf`[Accessed on: 16-06-2021]

in Figure 14.6. Improvements can be made for the operations phase, however the CO_2 efficiency is already better than current aircraft in the market.

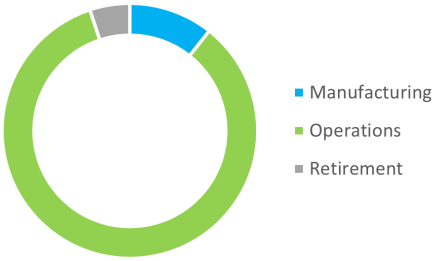

Figure 14.6: Estimated CO_2 emissions from the life-cycle analysis. (Percentages not shown to scale)

In order to give a representation of how sustainable the UCA is, the CO_2 emissions produced in the life-cycle are compared with the the total CO_2 emissions produced by other aircraft. An Embraer 145 and Boeing B737 emit approximately 5.6 and 11 times more CO_2 in their life-cycles respectively, considering the same distances flown [10].

14.3.2. Economic Sustainability

Economic sustainability is about finding and creating new market opportunities with the goal of generating profit. In order to maintain and achieve this, costs should be kept low, ensuring competition to drive innovation and contributing to economic growth.

The UCA will be able to fill a market in the air cargo industry which currently has no competitors, namely the small, high value cargo long range market. And due to the lower freight capacity and flight performance the UCA will also be able to resupply remote communities with goods as mentioned in Subsection 2.2.2. Furthermore, approximately 40% of the of the total air freight will be transported by unmanned aircraft in the coming 40 years, [11] including this UCA. This means other competitors will enter the market which will hopefully lead to improvements and more innovative designs.

The direct operational costs of the UCA is determined to be 9063 euro per flight which will be elaborated upon in Section 15.4. The block hour cost for full cargo aircraft, such as a Boeing 747 can reach up to 24000 euros [12] which is significantly more compared to the UCA. However, if the payload weight is taken into account the cost may be higher as will be discussed in Subsection 15.4.4. In a market with high-value goods a small increase in costs will be less of a problem to customers as the price is relatively inelastic [58] compared to the general cargo industry.

14.3.3. Social Sustainability

Social sustainability addresses the well-being of people in communities, thus their health, happiness and prosperity. A big issue which can have an adverse effect on people's health is noise disturbance as mentioned in Section 14.2. The noise caused by the UCA was therefore kept in mind during the design, and has been kept below the noise caused by the Cessna Citation II.

Other points of concern which may arise from the general public may be because of safety reasons. The first point is that the UCA is unmanned, meaning there is no pilot on board but instead an operator will be able to monitor and control the aircraft from a distance as explained in Chapter 12. Some airports are located in densely populated areas and depending on how many flight movements take place each hour the risk of an accident happening increases. Secondly, the control systems of the UCA may get hacked by group or organizations with harmful intentions in mind. The possibilities of an event such as 9/11 happening may have negative effects on the aviation industry, in particular UAVs.

In order to reassure the general public the UCA is safe to operate and risks of accidents are low, information should be communicated clearly to the public. After analyzing possible risks in Chapter 17, the results should be prepared for communicating it to a specific target group[13].

[10] `https://escholarship.org/content/qt6m5865v5/qt6m5865v5.pdf` [Accessed on: 24-06-2021]
[11] `https://www.platformuca.org/factsheet-1-civil-unmanned-cargo-aircraft/`[Accessed on: 26-04-2021]
[12] `https://www.faa.gov/regulations_policies/policy_guidance/benefit_cost/media/econ-value-section-4-op-costs.pdf` [Accessed on: 17-06-2021]
[13] `https://www.who.int/water_sanitation_health/wastewater/wsh0308chap7.pdf`[Accessed on: 16-06-2021]

14.4. Future Sustainable Development Strategy

Future sustainable development strategies are established to improve the sustainability of the UCA in later development stages or even during operations. Improvements can be made for example during ground operations such as electric taxiing. Decisions can be made to use an on-board system such as a wheel tug, which has a disadvantage since it adds extra weight to the aircraft. And the other option is to use taxibots, test runs are still being made with these vehicles [14], however not all airport will have taxibots available such as on Saint Helena Airport.

In later iteration stages of the design, the aerodynamics of the aircraft may be improved to reduce energy use, the layout can be better optimized to suit the needs various goods and lightweight structures can be implemented in order to reduce weight. Finally, improving the circular economy and minimizing climate effects of the UCA will help in making the aviation industry more sustainable.

[14] https://www.schiphol.nl/en/innovation/blog/what-is-sustainable-taxiing-part-1/[Accessed on: 16-06-2021]

15
Final Design

This chapter will present the outcomes of the performed design process. Throughout this process, multiple technical departments have developed certain subsystems for the UCA which are all implemented to form the final design. In Section 15.1, the features of this final design will be summarised and supported by means of detailed CATIA sketches. After this, the resource allocation and breakdown of the budgets utilised by the technical departments will be discussed in Section 15.2. Furthermore, in Section 15.3 multiple aspects of the aircraft will be considered including Reliability, Availability, Maintainability and Safety. Lastly, a financial analysis will be provided in Section 15.4 where all contributions to the overall cost are regarded.

15.1. Final Design Summary and Technical Drawings

The main technical aspects of the final design will be elaborated upon for the different departments, while all important parameters are also summarised in a table for each subsection. In the end, the technical drawings in CATIA are provided supplying additional dimensions and depicting the final design from different points of view.

15.1.1. Wing Planform

The leading edge at the MAC of the wing is located at 8.90 $[m]$ from the nose. This is determined during the iteration process of the loading diagram, scissor plot and landing gear positioning. The wing is designed using a low wing configuration. A low wing configuration has been chosen because this allows for a better storage of the landing gear during flight. When the project team started positioning the landing gear it was found that a yehudi was needed to store the landing gear, because of the combination of the wing placement, most aft cg position and tip-back angle requirement. The geometry of a SC(2)-0414 airfoil and single slotted flaps are used in the wing design. Furthermore, sweep at quarter chord of 25 $[deg]$ has been added during the wing design, for example to delay drag divergence. In addition, -3 $[deg]$ of wing twist is used to delay stall at the wing tip. Stall at the wing tips has a negative effect on the controllability of the aircraft as the control surfaces are close to the wing tip. Moreover, the dihedral of the wing is 2.5 $[deg]$. The position of the spars, rib and other dimensions of the wing can be found in Table 15.1.

Table 15.1: Wing parameters

Variable	Value	Unit
AR	9.5	$[-]$
b	21.13	$[m]$
c_r	3.39	$[m]$
c_t	1.06	$[m]$
$Dihedral$	2.5	$[deg]$
MAC	2.35	$[m]$
S	46.98	$[m^2]$

Variable	Value	Unit
$Spar_{front}$	15	% chord
$Spar_{rear}$	60	% chord
$Twist$	-3	$[deg]$
X_{LEMAC}	8.90	$[m]$
λ	0.312	$[-]$
$\Lambda_{0.25}$	25	$[deg]$

Table 15.2: Landing gear parameters

Variable	Value	Unit
Tire Diameter	0.686	[m]
LDG Height	1.1	[m]
n_{nw}	1	[-]
n_{mw}	4	[-]
X_{NLG}	2.44	[m]
X_{MLG}	10.25	[m]
Y_{NLG}	0	[m]
Y_{MLG}	1.48	[m]

15.1.2. Landing Gear

The landing gear has been placed in a conventional tricycle configuration. The height of the landing gear is 1.1 $[m]$, determined by the wheel radius, strut length and stroke length. The nose wheel is placed on the centre line of the aircraft at a distance of 2.55 $[m]$ from the nose. The main landing gear has been placed 10.25 $[m]$ from the nose both 1.48 $[m]$ from the centre of the fuselage. The location of the landing gear has been chosen such that the turnover angle, lateral clearance, pitch angle and tip-back angle requirement are met. Furthermore, to meet the loading requirements the nose landing gear design has one wheel and the main landing gear consists of two wheels on each side. Lastly, the landing gear has been placed within the yehudi and not in the wing box structure itself for structural reasons. A summary of the most important landing gear parameters can be found in Table 15.2.

15.1.3. Cargo and Fuel

From the stakeholders preference, a cargo requirement of at least 2000 $[kg]$ was established to be carried by the UCA over a range of 5556 $[km]$. In order to cover this considerable range, relatively large amounts of fuel will have to be

carried by the aircraft as well. All of this fuel will be distributed over 5 fuel tanks in total, located in the centre and aft part of the UCA. Two tanks are located inside the wing boxes, causing a bending stress relief on the wing structure. The other three tanks are located inside the fuselage, where two are hidden under the floor while the last tank is cylindrical and positioned inside the tailcone as explained in Subsection 4.6.4. Together, the fuel tanks can carry up to 7.4 $[m^3]$, which is 25% more than the amount necessary to cover the required range. This was done to contribute towards the mission adaptability of the aircraft, such that it can also cover longer distances while carrying less payload than the desired 2000 [kg]. This cargo will be distributed over three specially selected PYB air cargo pallets with a maximum loading weight of 850 [kg]. These pallets will be loaded into the aircraft sequentially, having a total capacity of 2550 $[kg]$. Similarly to the fuel, the aircraft will also be able to carry more cargo at a shorter range to improve its adaptability. All these fuel and cargo capacities are represented in the table below.

Table 15.3: Cargo and fuel parameters

Variable	Value	Unit
Range	5556	$[km]$
Design payload	2000	$[kg]$
Maximum payload	2550	$[kg]$
Fuel tanks volume	7.4	$[m^3]$

Table 15.4: Propulsion parameters

Variable	Value	Unit
Thrust	38	$[kN]$
Nacelle length	2.92	$[m]$
Nacelle diameter	1.11	$[m]$
Offset	0.2	$[m]$

15.1.4. Propulsion

In terms of the propulsion system, a required thrust level for the single engine of 35 [kN] followed from an extensive performance analysis in Chapter 7. This together with sustainability objectives led to the selection of the AE 3007A engine, with take-off thrust of 38 [kN]. After a few modifications, it will be able to run on synthetic fuel with a reduction in CO_2 emissions. The dimensions of this engine including the nacelle are a length of 2.92 [m] with a diameter of 1.11 [m]. Since the UCA will feature a single-engine configuration, the engine will remarkably be placed on top of the fuselage to remain in the centre line and not generate a net yawing moment. Due to stability and controllability constraints as introduced in Chapter 10, the engine location will start at 9.86 [m] from the nose of the aircraft. Ultimately, the engine will be placed at an offset of 0.2 [m] between the bottom of the engine and the top of the fuselage. This is done to avoid the exhaust stream of the engine to interfere with the empennage as will be described in the next section. All the engine parameters are listed above in Table 15.4. The following figure presents the engine layout:

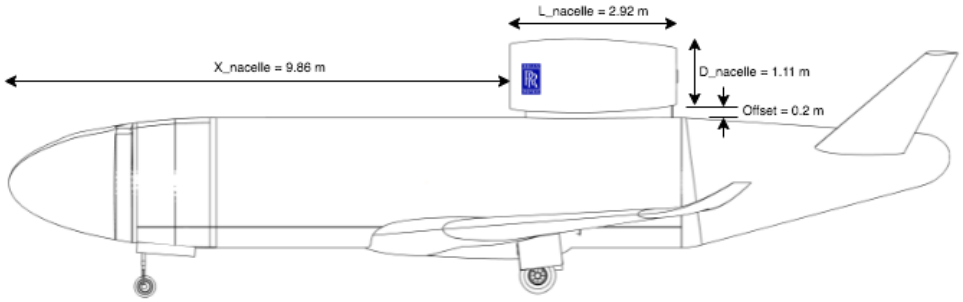

Figure 15.1: Engine positioning

15.1.5. Fuselage design

The fuselage is obviously one of the main components of the aircraft and greatly affects the final design. In Section 4.6, the procedure resulting in the outer dimensions is explained. Eventually, the fuselage length was established at 18.1 $[m]$ with an outer diameter of 2.5 $[m]$. From this, an inner diameter of 2.3 $[m]$ followed while the floor is placed at a height of 0.3 $[m]$. This inner configuration leaves sufficient space for fuel tanks and other electrical systems under the floor, while the cargo pallets still fit in the upper part of the circular fuselage. Moreover, the nose-and and tailcone length were determined to be 3.7 $[m]$ and 6.2 $[m]$ long respectively, leaving a cabin length of 8.2 $[m]$ at full diameter. Regarding the material, the aluminium alloy 7075-T6 was selected for the fuselage in Chapter 9. All these values are listed in Table 15.5, and can also be visualised in the technical sketches in Figure 15.5.

Table 15.5: Fuselage parameters

Variable	Value	Unit
Fuselage length	18.1	[m]
Fuselage outer diameter	2.5	[m]
Fuselage inner diameter	2.3	[m]
Floor location	0.3	[m]
Nosecone length	3.7	[m]
Tailcone length	6.2	[m]
Cabin length	8.2	[m]

Table 15.6: Empennage parameters

Variable	Value	Unit
AR_{vt}	6	$[-]$
$0.5 \cdot b_{vt}$	4.43	$[m]$
c_r	2.28	$[m]$
c_t	0.67	$[m]$
$Dihedral$	34.54	$[deg]$

Variable	Value	Unit
l_h	8.06	$[m]$
S_{vt}	11.00	$[m^2]$
Λ	30	$[deg]$
λ	0.295	$[-]$

15.1.6. Empennage

The final design of the aircraft includes a V-tail configuration. This means that on each side of the fuselage one tail surface is placed. Due to the large dihedral angle of 34.54 $[deg]$, a so-called V shape is created. In order to avoid the vertical tail from being in the exhausts stream of the engine, a V-tail was selected for the empennage. To deal with the exhaust stream of the engine, the engine should either be placed closer to the tail or the dihedral of the tail should be decreased. Furthermore, by means of a small offset of 0.2 [m] between the bottom of the engine and the top of the fuselage, any interference between the jet blast and both the empennage and tail is avoided. This is beneficial since otherwise these elements would demand additional reinforcement and coating since the exhaust stream and acoustics can have a negative impact on fatigue and vibration properties. The jet blast acts as a cone coming out of the engine at a 6 [deg] angle with respect to the longitudinal axis of the engine. This can be visualised in the Figure 15.2. As can be seen in the figure, the current engine placement causes the exhaust stream to perfectly avoid all empennage components. The empennage parameters are shown in Table 15.6.

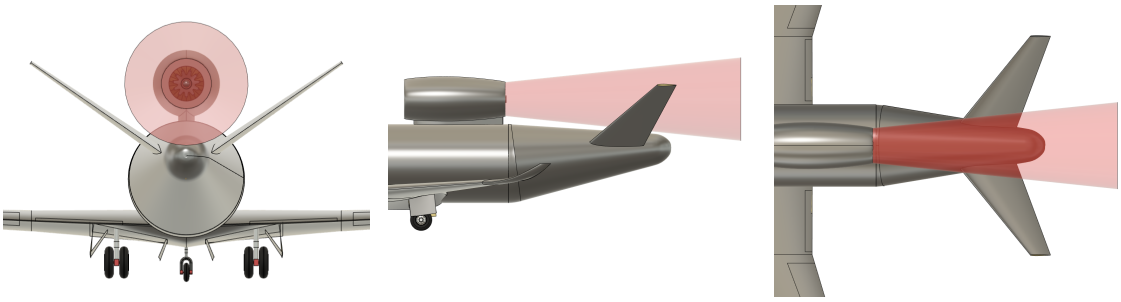

Figure 15.2: Exhaust stream of the engine visualised using a red cone

15.1.7. Aircraft Cargo Door

The cargo door of this aircraft will be located in the front, which is similar to the Boeing 747-400F. The door can be opened within 1 minute in order to decrease turn-around time. The system in place works as follows. One electrical motor will be located in the nose cone, which will drive two flexible shafts. These shafts will lead two to gearboxes. The gearboxes will drive two rods, which can push the door outwards or pull inwards. When closing the aircraft a pin will be located at the bottom to check if the door is closed. If the door is closed, multiple actuators will be used in order to close the cargo hold, which are equally spaced around the circumference of the nose. A redundant number of actuators will be used in order to ensure closure during flight. A monitoring system will be present in order to check if all actuators are closed. The cargo door can only be opened when engine is off, in order to ensure that the cargo door does not open during flight. A side view of the cargo door is shown in Figure 15.3. [1]

[1] `https://youtu.be/qhFsPEtwnVA` [Accessed on: 04-06-2021]

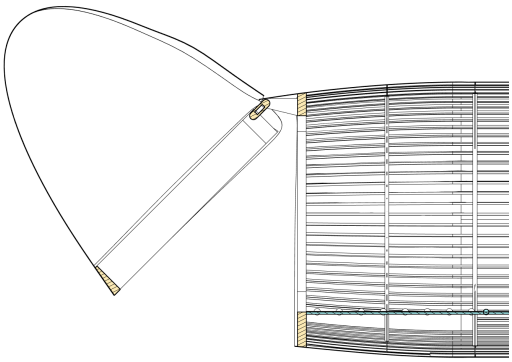

Figure 15.3: Cargo door side view

15.1.8. Unmanned Operations

Important aircraft elements that allow the aircraft to fly autonomous are the FMS, autopilot, flight control software, data busses, and various navigation sensors and air data systems. The UCA flies fully autonomous during all phases of flight. In a GCS a pilot can monitor the UCA and intervene if necessary, however, usually the pilot only exerts direct control over the UCA during taxiing and other ground operations. The pilot can monitor and control the UCA via a C2 link and if necessary a live camera stream can also be relayed. Communications are possible both on short range via 4G and long range via a satellite network. Using the BlackRay Parabolic antenna the required link budget for communication is met. The UCA can also communicate with the ATC and other aircraft via VHF radio and transponders. If contingencies occur the UCA will try to resolve these issues by itself using the contingency management algorithm. If flight has to be aborted the UCA will perform an emergency landing at a remote location possibly with help of the parachute system.

15.1.9. Parachute System

By means of a parachute system, the clients payload will be protected in case of engine failure. This also helps to minimize the damage caused on its nearby surroundings during the impact of the UCA. During a first order estimation of the parachute's dimensions, a total frontal diameter of 32.32 meters was found. Furthermore, the weight was assumed to be 195 $[kg]$. The design of the parachute was driven by a terminal velocity of 11.67 $[m/s]$ at maximum take off weight. The parachute will be deployed in the same way as the parachute of the Cirrus Vision jet, using a little rocket.

15.1.10. Verification and Validation

Just like has been done in all technical departments, later design stages of the final design will also require verification and validation practices to be performed. This will be mostly done in a similar fashion as described in Section 3.2. Namely, firstly unit tests will be performed on all subsystems either using proportional comparison, visual verification, point checks or manual and hand calculations or a combination of these. Afterwards, these subsystems as well as the system as a whole will then be subjected to system tests to examine the behaviour of the aircraft. Ultimately, the final design will also be validated by means of a comparison with reference inputs.

15.1.11. Technical Drawing

To conclude, the aircraft design is shown in Figure 15.4. A technical drawing with the most important dimensions can be seen in Figure 15.5

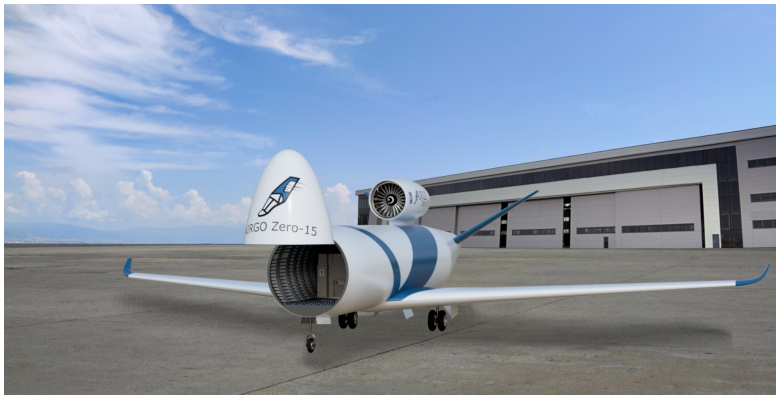

Figure 15.4: Complete render of aircraft with cargo door open, and cargo loaded inside.

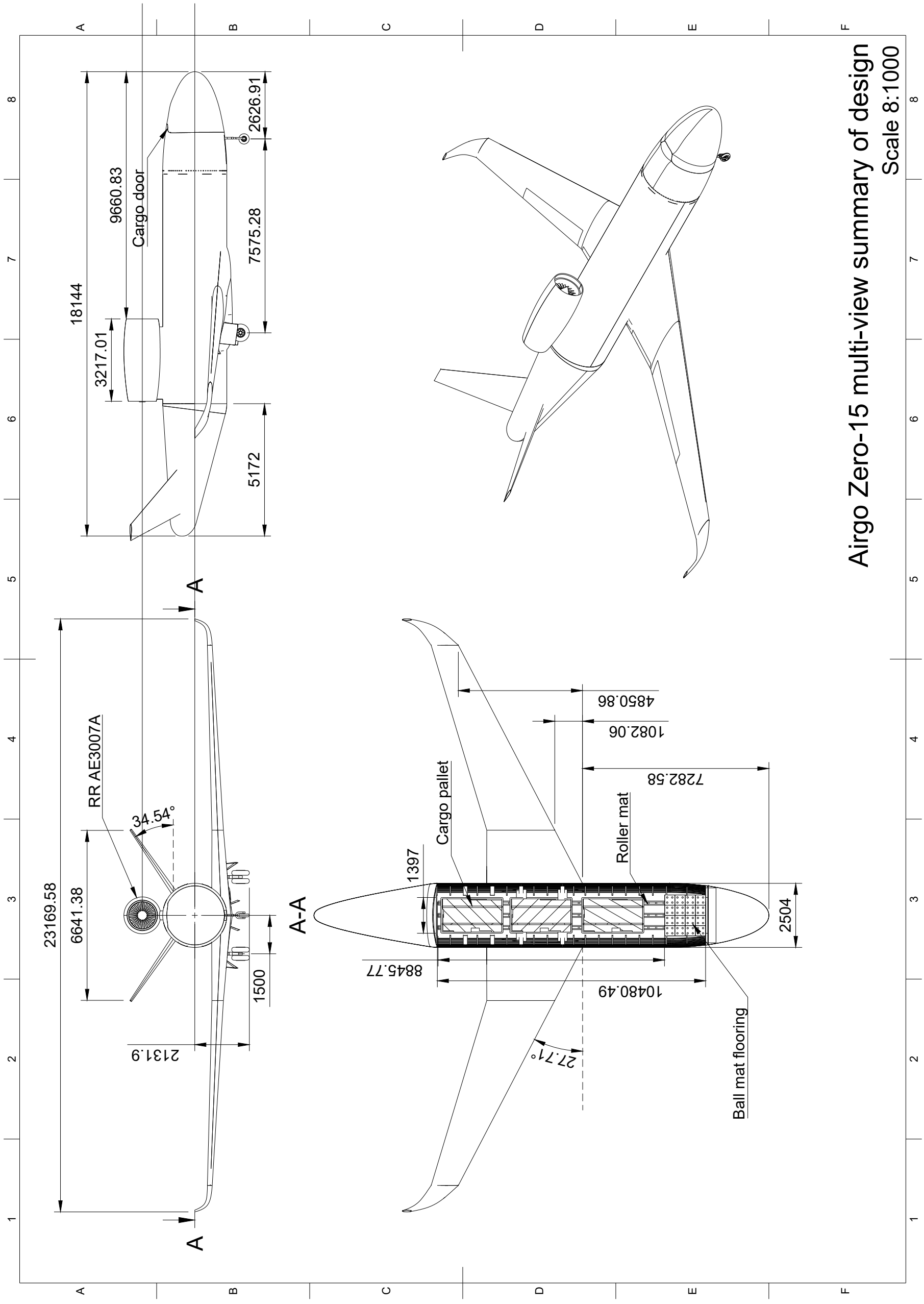

Figure 15.5: Technical drawing summarizing the aircraft's primary dimensions, including isometric view

15.2. Resource Allocation and Budget Breakdown

As explained in Section 3.5, several budgets have been quantified beforehand to guide the technical departments towards a careful implementation of available resources. In the end, four types of resources were identified for which budgets had to be determined; Weight, Power, Cost and Sustainability. However, Sustainability can be divided into CO_2 Emission and Noise Emission, since these both are important to the design and shall thus be treated with sufficient attention.

15.2.1. Weight

During the conceptual design when all four different concepts were considered, an initial estimate was made based on regression of reference aircraft for the economical concept. This led to a MTOW of 10724 [kg], and could be used in further design stages. Namely, from the class I weight estimation a new value of 13198 [kg] was computed. Ultimately, the class II weight estimation concluded the conceptual weight forecast for all subsystems which together amount to a MTOW of 13250 [kg] as explained in Section 4.2. A factor that played a role here was that the empennage is lighter as a result of the V-tail instead of a conventional tail. Assuming that this final value will be within 20% of the eventual obtained value measured on the scale, there is a noticeable convergence of the weight budget during the design phases complying with Subsection 3.5.1. Namely, the conceptual design is 20% off with respect to the detailed design, while the updated conceptual design value is expected to be off by only 15%. Therefore, the initial estimate was already considerably accurate which reduced the number of required iterations while also providing a better target to comply with and accounting for contingencies. In the post-DSE phase, the weight will eventually converge to a definite value throughout the preliminary and detailed design. Here, it is assumed that the preliminary design will be 10% off while the uncertainty of the detailed design will <3% off once more elaborate design techniques are applied.

15.2.2. Power

Next up, another main resource to which a budget was allocated is power. This entails the entire propulsion system, generating sufficient power to propel the UCA. In the early stage, similarly to the weight the required thrust level was derived from linear regression of reference aircraft. This led to a conceptual value of 19.6 [kN] to be generated by the engine. In a later stage, the T/W-W/S diagram from Figure 4.1 imposed a new thrust level to be adhered to which resulted in 35 [kN]. Eventually, mainly resulting from the performance department a final constraint was posed on the required amount of thrust. Also, this thrust level is influenced by a lower experienced drag because of only two surfaces instead of three in a conventional scenario due to the V-tail. This lead to an ultimate take-off thrust value of 38 [kN] from the engine which had been selected in Chapter 7 for the conceptual design. Conclusively, the conceptual design has a contingency factor of approximately 15% while the preliminary design is estimated to be just 10% off the final value. It should be noted that even though the initial estimation was rather poor, appropriate resource management will lead to a high convergence towards the final thrust level that will be obtained for the detailed design with a uncertainty of <5%.

15.2.3. Cost

Another very critical resource that was incorporated in the budget breakdown is cost. Namely, cost will eventually turn out to be one of the most important factors based on which the stakeholder will decide whether to purchase the aircraft or not. Ultimately, all resources are either directly or indirectly related to cost and thus appropriate resource management is of utmost importance here. In the early stage, conceptual analysis concluded a total cost for the customer of approximately 7.8 million euros by means of a top-down approach. Nevertheless, during the a more detailed iteration the sophisticated bottom-up analysis was executed in Section 15.4 once all subsystems were identified and designed. This resulted in a final cost of just under 5 million euros which is assumed to have an uncertainty of less than 35%. The accompanying contingency factors thus were 35% during the conceptual design, 15% during the preliminary design and will be <5% during the detailed design, hence almost satisfying the contingency objectives.

15.2.4. Sustainability

Lastly, sustainability is the final crucial resource to be taken into account for the design of the UCA. As was already discussed above, this can be divided into two main drivers which are CO_2 and noise emission. The CO_2 emission of the aircraft can be expressed as kg of CO_2 emitted per kg of burned fuel. In the conceptual stage, it was found that this value is 1.5 $[kgCO_2/kgfuel]$ for synthetic kerosene during flight. However, this was succeeded by an iteration where the new value was found to be 1.33 $[kgCO_2/kgfuel]$. This had to a contingency factor of 10% during the conceptual design and will have a level of uncertainty of 5% and <1% for the preliminary and detailed design, thus having a gradual convergence.

In terms of noise, the parameters are expressed in $[dB]$ measured at a distance of 300 $[m]$ from the aircraft according to posed regulations by authorities. During the conceptual design a value of 95 $[dB]$ was obtained from a first order analysis on medium-sized aircraft. Afterwards, in Chapter 14 the updated design value was established at 72.4 $[dB]$. Thus regarding the contingency factors, the conceptual design will be off by around 30% hence satisfying the resource management approach as established in Subsection 3.5.1 and accurately guiding the design towards a final result. The preliminary and detailed design are estimated to have an uncertainty level of 20% and 10% respectively due to

contingencies.

Table 15.7: Converging budgets for all resources throughout the design

	Weight [kg]	**Contingency [%]**	**Power [kN]**	**Contingency [%]**	**Cost [M€]**	**Contingency [%]**	**CO_2 Emission [kg CO_2/kg fuel]**	**Contingency [%]**	**Noise Emission [dB]**	**Contingency [%]**
Conceptual Design	13250	20	38	15	4.89	35	1.33	10	72.4	30
Preliminary Design	<TBD>	15	<TBD>	10	<TBD>	15	<TBD>	5	<TBD>	20
Detailed Design	<TBD>	10	<TBD>	<5	<TBD>	<5	<TBD>	<1	<TBD>	10

15.3. RAMS

RAMS stands for reliability, maintainability, availability, and safety. These concepts are discussed in Subsection 15.3.1, Subsection 15.3.2, Subsection 15.3.3, and Subsection 15.3.4 respectively. The RAMS philosophy was used throughout the entire design while making design choices and performing technical calculations.

15.3.1. Reliability

Reliability is the probability of a system to perform its function without failure within a specified time-frame. The reliability of an unmanned aircraft can be discussed qualitatively but also computed analytically. Every component or system of the UCA can be assigned a reliability value. For instance, the propulsion system, flight critical avionics, data links, the GCS and even the GCS pilot. The reliability of a system depends if it is arranged in series or parallel as depicted in Equation 15.1 and Equation 15.2 respectively.

$$R = \prod_{i=1}^{N} R_i \tag{15.1}$$

$$R = 1 - \prod_{i=1}^{N} (1 - R_i) \tag{15.2}$$

The reliability is depended on the incident rate λ, and the time interval t which is the mean time between overhauls (MTBO) as seen in Equation 15.3. Equation 15.4 is shows the incident rate is determined by the mean time between failures (MTBF). The calculated reliability for each of the relevant subsystems is shown in Table 15.8

$$R = e^{-\lambda * t} \tag{15.3}$$

$$\lambda = 1/MTBF \tag{15.4}$$

Propulsion. Propulsion failure is the single largest cause of unmanned aircraft losses [45]. However, this statistic is heavily influenced by small UAV's where reliability is not a driver compared to high power-to-weight and low cost. Fortunately, large turbofan engines are much more reliable.

Avionics and Flight Controls The second largest reliability driver for unmanned aircraft are the avionics and flight controls. These elements are critical for successful unmanned flight as they essentially replace the pilot. Hence for the UCA, redundancy should be provided for these systems. As described in Section 12.6 the FMS, autopilot, and INS will employ a triplex system.

Communication Systems Given the fact that the aircraft is unmanned, the communication systems are also critical for successful flight operations. The communication link might fail due to hardware failure, jamming, or unintentional RF interference. To deal with such events, a contingency management plan was drawn up in Section 12.5. Again redundancy is of high importance here so a backup C2 link is present.

Ground Control Station and Human Operator Although the UCA is unmanned human factors are still of importance in the design. Some human errors may be explained by the lack of situational awareness in the GCS. Unusual vibrations, sounds, smells, or other sensory inputs are not available to the ground based pilot as they would be to the pilot of a manned aircraft. Adequate pilot training and sufficient rest should reduce human errors. Similar to the flight control computers on board the aircraft, the computers at the GCS might also fail. A backup computer will be present for the GCS workstation to ensure redundancy.

Airframe Airframes of large unmanned aircraft are expected to have a high reliability since implementing redundancy is rather challenging in most cases. This high reliability is ensured by applying safety factors to the loads the frame is expected to carry. Both large and small maintenance should help detect cracks and weaknesses early on to prevent the aircraft from structurally failing during flight.

Hydraulic System Hydraulic systems are used for actuating purposes concerning control surfaces, high lift devices, and landing gear and are therefore flight critical. To provide redundancy for the hydraulics, a duplex system is employed as described in Section 13.4.

Table 15.8: Reliability and availability of aircraft subsystems [45] [59] [60]

Subsystem	MTBF [hrs]	MTBO [hrs]	Redundancy	Reliability	Availability
Propulsion	150,000	4,000	[-]	0.9737	0.9836
FMS	10,000	650	Triplex	0.9997	0.9921
Autopilot	10,000	650	Triplex	0.9997	0.9921
INS	10,000	650	Triplex	0.9998	0.9921
Communication Systems	10,000	650	Duplex	0.9960	0.9921
Ground Control Station	15,000	Every two months	Duplex	0.9910	0.9993
Human operator	650,000	8	[-]	0.9999	0.9999
Airframe	200,000	4,000	[-]	0.9801	0.9876
Hydraulic Systems	10,000	650	Duplex	0.9960	0.9921

15.3.2. Maintainability

The degree to which the UCA enables maintenance is known as maintainability. Aircraft maintenance is needed in order to maintain the airworthiness of the aircraft. Otherwise it is not safe to operate the aircraft and accidents may occur. In order to prevent disasters, a variation of maintenance checks will be needed on a regular basis. Maintenance checks are traditionally categorised into "A" checks, "B" checks, "C" checks, and "D" checks, with each check consisting of increasingly heavy maintenance. Contemporary maintenance programs no longer perform "B" checks to improve resource efficiency and reduce downtime[2]. By carefully reviewing scheduling, this has been accomplished while maintaining aircraft safety and reliability[3]. At what point the maintenance checks will take place, their duration in man-hours, and some typical tasks are shown in Table 15.9.

Table 15.9: Maintenance program of the UCA [61]

Check	When	Duration	Tasks (among others)
Daily check	Daily	0.5 man-hours	Visual inspection of the aircraft Checking the fluid levels Checking the functionality of all automation and flight systems Checking the functionality of the landing gear Checking the functionality of control surfaces and high lift devices Checking the functionality of the propulsion system (both engine and fuel)
"A" check	650 FH	70-90 man-hours	Visual inspection of the aircraft's structure Operationally checking emergency lights Lubricating the nose gear retract actuator Extensively testing the landing gear actuator Extensively testing the high lift device subsystem Extensively testing the control surface subsystem Extensively testing the FMS, autopilot, and INS Extensively testing the communication systems General testing the propulsion system (both engine and fuel system) Minor technology upgrades
"C" check	4000 FH	2500 man-hours	Performing "A" check Extensively testing the propulsion system (both engine and fuel system) Extensively testing structural components Major technology upgrades
"D" check	8 years	45000 man-hours	Performing "A" check Performing "C" check Decomposition of entire aircraft for inspection

The lightest maintenance is performed in the form of a daily check, which will be executed during the turnaround

[2] https://www.aviationenthusiasts.org/post/aircraft-maintenance-b-check [Accessed on: 14-06-2021]
[3] https://www.aviationenthusiasts.org/post/aircraft-maintenance-b-check [Accessed on: 15-06-2021]

time of the first flight of the day. The daily check can be performed at the airport by a ground mechanic and a GCS pilot from a remote distance. If during the daily check the airworthiness of the aircraft is determined to be insufficient, the take-off procedure shall immediately be aborted. Afterwards the UCA will be send to the hangar to undergo repairs. A level higher in aircraft maintenance is the "A" check. This check will take place after 650 flight hours (FH) at a designated maintenance station at one of the UCA's hub airports. It will be performed by trained maintenance personnel. Finally, the most heavy maintenance will be performed during the "C" check. In the unlikely event that the aircraft experiences a subsystem failure, or any other form of damage during flight, unscheduled maintenance must be performed. Unscheduled maintenance shall consist of the repair or replacement of the failed or damaged part, and the extensive testing of subsystems related to it.

Certain characteristics of the UCA have an impact on the general maintainability of the aircraft. First of all, since the UCA is unmanned there is no need for windows to be present in the fuselage or nose of the aircraft. This is beneficial for the structural integrity of the UCA as windows are a structural weakness and often one of the first areas where cracks appear. On the other hand the positioning of the engine may pose a challenge to the maintenance crew. Its location on top of the fuselage is not easily reachable. The crew will therefore have to make use of lifters or a maintenance platform.

15.3.3. Availability

To be as efficient as possible it is critical to minimise aircraft downtime. This can be expressed via the term availability. Availability is defined as the probability that the system will be able to operate when called upon at random. Logically, it is in direct relation with reliability and maintainability. The availability can computed with the mean time between failure (MTBF) and the mean down time (MDT) as seen in Equation 15.5.

$$A = \frac{MTBF}{MTBF + MDT} \tag{15.5}$$

Looking at this equation it is evident that to increase the availability, and thereby minimise downtime, the MTBF should be as large as possible and the MDT as small as possible. This is achieved by careful design of aircraft subsystems and efficient maintenance planning. The availability of some of these subsystems is displayed in Table 15.8.

15.3.4. Safety

The safety of the UCA and the ability to not harm the environment or people during the entire life of the system was considered throughout the entire design phase. For example, by designing in accordance with CS-25. Some characteristics of the aircraft specifically impact the aircraft's safety and will be discussed in this section

The fact that the UCA is unmanned may bring about safety concerns. Although the architecture of the unmanned operation avionics is highly reliable as seen in Subsection 15.3.1, there remains a small possibility for a subsystem to fail. Hence a contingency management plan was drawn up in Section 12.5. In the worst case scenario where the aircraft sees failure of critical subsystems and continued flight is no longer possible, a parachute can be deployed. This mitigates damage to the UCA, payload, and environment.

15.4. Financial Analysis

This section calculates and describes all the financial aspects related to the design. In order to compete with the market and to make the aircraft interesting for potential investors the aircraft several financial parameters are calculated. First, the development and production cost are evaluated to come up with the total unit cost per aircraft. After that the direct operating cost is calculated to come up with return on investment. Finally, the cost breakdown structure is given for post-DSE project activities. For the analysis the assumption was made that, following from Chapter 2, 5080 aircraft are produced.

15.4.1. Development Cost

The development cost are all the cost made while developing the actual aircraft. These costs are made before the production and are divided into research, development and testing (RD&T). The development cost are estimated using the DAPCA IV method [62]. This is the latest version of the Development and Procurement Cost of Aircraft. This method will not give the most accurate results, as it is not designed for one class of aircraft, but is will reasonable results for this initial design stage. Following the DAPCA IV method the development costs are divided into several sub cost. Namely, engineering cost, tooling cost, development support cost and flight test cost. All of these cost are explained in more detail below [9] and after that the development cost per aircraft will be calculated.

The engineering hours include the airframe design and analysis, test engineering, configuration control and system engineering. Most of the engineering hours are allocated to the RD&T, but during the actual production of the aircraft there will also be some kind of engineering effort. The engineering effort to integrate the propulsion and avionics systems into the aircraft is included in the engineering hours. However, the engineering hours allocated to the propulsion

and avionics systems itself are not seen as engineering cost. These cost are included in the purchased equipment cost. The engineering support and tooling are included in those cost instead of engineering. The tooling hours includes all the preparation for production. Such as, design and fabrication of the tools and fixtures, preparation of molds and dies, programming of the software for some automated production processes and the development and fabrication of production test equipment. The tooling cost included in the development cost do also include some tooling cost during the production process. Both engineering cost as tooling cost are dependent on the amount of aircraft produced, operational empty weight and cruise speed. The next two costs are only dependent on the empty weight and the cruise speed. Starting with the development support cost. These costs cover all the nonrecurring costs of manufacturing support during the development. Examples of this are the fabrication of mock ups, structural test articles and various other test items used during the development. The final development cost are the flight test costs. The flight test costs cover all the costs to demonstrate the airworthiness for the EASA certification. However, the cost of the test aircraft itself are not included as that cost is part of the production cost. The flight test cost include the planning, instrumentation, flight operations, data reduction and the engineering and manufacturing support during the process of proving airworthiness. To calculate the actual flight test cost the number of flight test aircraft had to be determined. Typically the number of test aircraft is between 2 and 6. A total of 4 test aircraft was selected. As the UCA is a novel concept regarding autonomous flying the aircraft probably needs more testing on this field. In order to do more test 2 extra test aircraft are built.

For engineering and tooling only the required hours are calculated. So in order to calculate the actual cost of those components these hours are multiplied with the labour rates. As the labor rates in the DAPCA IV method are from 1986 these are multiplied with the inflation factor. The same is done with the development support cost and the flight test cost. Using the CPI from 1986 and 2021 an inflation factor of 2.39 was found [4]. The final values of the different components and the total development cost per aircraft can be seen in Table 15.10.

Table 15.10: Breakdown of development cost

Component	**Cost**[10^6**USD**]
Engineering	1026.33
Tooling	909.37
Development support	116.94
Flight test	51.51
Total	2104.15
Total per aircraft	0.41

15.4.2. Production Cost

Besides the development cost, the production cost can also be estimated with the DAPCA IV method. The production cost will be the major part of the total aircraft cost. The production cost is divided into several components. Namely, manufacturing, quality control, material, engine and avionics cost. These components will be explained in more detail and the production cost per aircraft is evaluated.

The manufacturing hours are the hours to fabricate the aircraft. This includes for example, forming, machining, fastening, sub assembly, final assembly, routing of all the wires and hydraulics and the installation of external purchased equipment like the engine and avionics. The quality control is related to the manufacturing of the aircraft, but it is estimated as a separate cost. It includes the inspection of incoming goods, inspection during the production and the final inspection. The quality control also inspect all the tools and fixtures produced by the tooling department. As the UCA will be a cargo aircraft the quality control hours are slightly lower compared to passenger aircraft as the inspection of the cabin itself takes less time. The material cost mostly speak for them self. These costs include the raw materials, hardware and external equipment from which the aircraft is build. Besides those materials it also includes items such as the environmental control system, hydraulic and electrical systems. An example of this could be the electrical motor which is used to operate the nose door. The manufacturing costs include everything expect the engine and the avionics. The engine cost is based on the engine selected by the propulsion department and based on literature the unit cost of one single engine was found [5]. The DAPCA IV method does not estimate the avionics costs. The avionics costs are normally 5-25% of the total aircraft cost. As the aircraft will be autonomous no cockpit is needed. However, it will need more communication systems so this will compensate for the missing cockpit. Therefore a value of 20% was selected for the avionics costs.

The manufacturing and quality control hours were multiplied in the same way as explained in the development section to account for inflation. The total cost of all the different components and the total production cost per aircraft

[4] `https://cpiinflationcalculator.com/`[Accessed on: 16-06-2021]

[5] `https://www.deagel.com/Propulsion20Systems/AE203007/a001710`[Accessed on: 14-06-2021]

can be seen in Table 15.11. It should be noted for both the development and the production cost that the DAPCA IV method is a very preliminary method of cost estimation. So the values shown in both the development table as the production table will not be highly accurate. The integration of the engine on top of the fuselage has not been done before

Table 15.11: Breakdown of production cost

Component	**Cost**[10^6 **USD**]
Manufacturing	9753.63
Quality control	819.69
Material	6726.06
Engine	7112.00
Avionics	3661.71
Total	28073.09
Total per aircraft	5.53

15.4.3. Aircraft Unit Cost

So now both the development cost as the production cost is calculated the actual unit cost of the whole aircraft can be obtained. As stated earlier the assumption was made that 5080 aircraft are produced. So the total development and production cost are added and divided by 5080 to come up with the unit cost of the aircraft in dollar. This resulted in a unit cost of 5.94 million dollar. As the requirement is stated in euros the unit cost is converted from dollars to euros [6]. This resulted in a unit cost of 4.89 million euros. This means that the requirement of aircraft unit cost being lower than 5 million euros is met. With the unit cost in mind the actual selling price of the aircraft can be established. As there is not any similar aircraft on the market, especially no autonomous aircraft, the selling price is difficult to predict. So the selling price is based on comparing the price of various aircraft and dividing the selling price by the range and maximum payload. With this an empirical equation was established based on those reference aircraft. By filling in the range and payload of the UCA a unit price was calculated. The unit price found was 7.6 million dollar.

15.4.4. Direct Operating Cost

The operating costs are split in two different categories, the direct operating cost (DOC) and the indirect operating costs (IOC). The direct operating costs are more important as this is stated in a requirement. The indirect operating costs rely more on the operation of the airline itself instead of the aircraft. The direct operating costs are estimated with the help of a literature study on several cost estimations [63]. This literature study is based on the ATA method [64], the DOC+I method from NASA [65] and AEA method[66].

The direct operating costs can be divided into several components. Namely, fuel cost, maintenance cost, depreciation cost, insurance cost and the landing and navigation fees. Starting with the maintenance costs. The maintenance cost of the aircraft is based on the following parameters. The maintenance cost was dependent on the airframe weight, airframe cost, engine weight, engine cost, take-off thrust, number of engines and the block time. The block time is the time between leaving the gate at the departure airport and arriving at the gate at the destination airport.

- The labour cost for maintaining the airframe and systems
- The maintenance material cost for the airframe and systems
- The labour cost for maintaining the engine
- The maintenance material cost for the engine
- The maintenance burden cost, these costs are defined as labour and material overheads that contribute to overall maintenance costs. Such as the administration, controlling, monitoring and testing.

Next, the depreciation cost is calculated. It is assumed that the resale value of the airframe is 10 % of the market price and the operational life, as discussed in the sustainability chapter, is 20 years. With the cost of the airframe and the engine the depreciation cost per flight was calculated. The insurance cost comes from the fact that the aircraft has to be insured against unexpected events. In case such an unexpected event occurs the potential financial risk is covered by the insurance company. The insurance cost per flight is dependent on the price of the aircraft and the amount hours flown per year. As the UCA will only have one engine, carry high-value goods and flies long distances over oceans it was assumed that the insurance cost will be higher. So the insurance cost per flight was multiplied by a factor of 3 to incorporate the extra risks. The landing and navigation fees is based on the maximum take-off weight of the aircraft. As the aircraft makes use of the facilities and infrastructure of airports these costs has to be covered by the airport. Therefore, every aircraft has to compensate for this with landing and navigation fees. The final cost and biggest contributor to the DOC is the fuel cost. As the UCA uses synthetic fuel this contribution is even higher

[6] `https://www.wisselkoers.nl/dollar-euro`[Accessed on: 16-06-2021]

compared to regular aircraft. The fuel cost per flight is calculated by multiplying the price of one kg of synthetic fuel by the amount of fuel used. In Figure 15.6 the percentage of each component related to the total direct operating cost can be seen. As mentioned before the fuel cost contribution is relatively high and this is conformed by the pie chart.

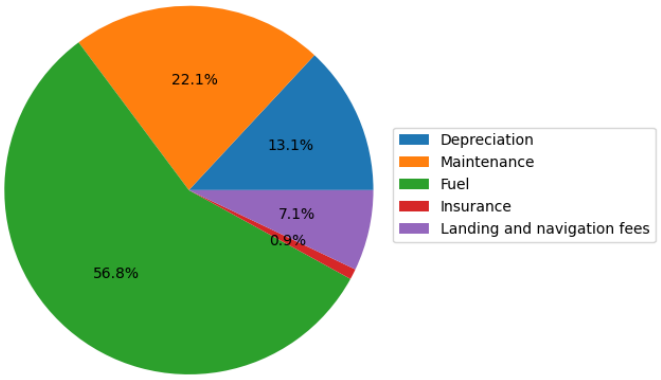

Figure 15.6: Direct Operating Cost divided into the different components

Now all the different direct operating cost per flight are calculated, the cost per tonne can be obtained. This is done by dividing the cost per flight with the payload weight. Doing so gives a DOC of 2450 $\frac{\$}{T}$. As a requirement, the DOC of the UCA compared to the DOC of the Boeing 747-F the DOC had to be obtained. The DOC of the Boeing 747-F was found by some literature research[67]. However the DOC was stated in USD/Available Tonne Mile (ATM) in 1995. The value was converted to USD/Ton and corrected for the inflation. Doing so gave a DOC for the Boeing 747-F of 3256 USD/Ton. This means that only a reduction of 25% is achieved instead of a 50% reduction stated in the requirement. The reasoning why this requirement is not met will be further explained in Section 16.2.

15.4.5. Return of Investment

The Return on Investment (RoI) is a financial metric that is used to measure the probability of gaining a return from an investment. The value is calculated by calculating the total revenue of the program, subtracting the total cost and dividing it by the total cost. Using this definition the RoI is given by Equation 15.6. Where Q is the amount of aircraft produced which is 5080 and UP the selling price per aircraft which was calculated earlier in this section and is 7.6 million dollar. The total cost is the development cost and production cost of the project together. Plugging in all the values gives a RoI of 27.94%. A positive RoI means that the investment is profitable and therefore interesting for potential investors.

$$ROI = \frac{Q \cdot UP - totalcost}{totalcost} \tag{15.6}$$

15.4.6. Cost Breakdown Structure

The Cost Breakdown Structure (CBS) contains all the cost elements of the post-preliminary design project activities. It serves to identify all the elements that contribute to the total costs of the project, after the end of the DSE.

The CBS of the UCA is presented in Figure 15.7, where B stands for a billion and M for a million dollars. For the estimation of the total operating costs, it was assumed that one aircraft does two flights per day, for a total of 20 years. The cost estimations for detailed design, manufacturing, purchased subsystems and testing are directly taken from cost calculations in Section 15.4. This means that not all elements in Figure 15.7 have a calculated cost. Therefore, all shown costs are a lower bound estimation, and the costs may be adjusted in design phase. Furthermore, the marketing costs are to be determined once a marketing campaign is set up, after the end of the DSE.

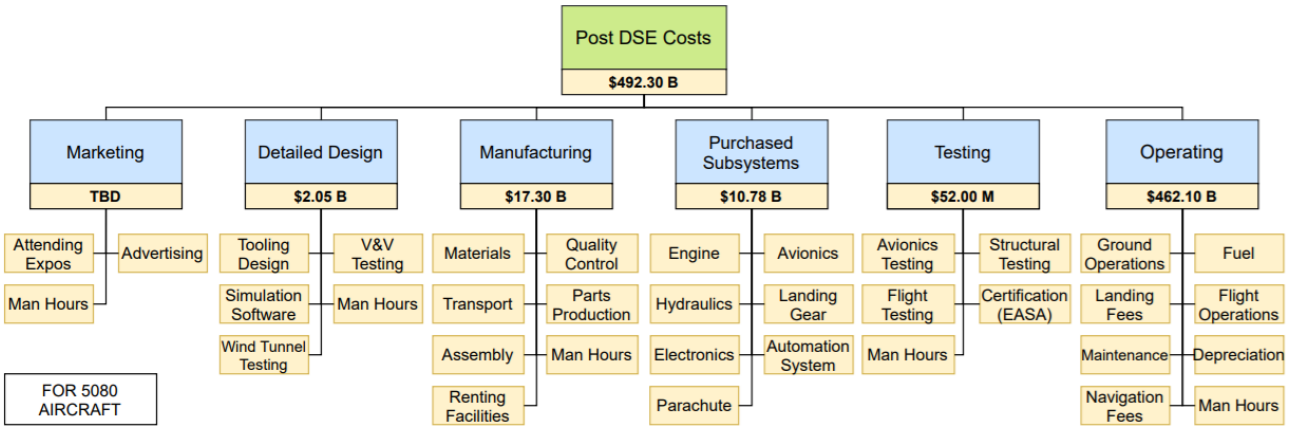

Figure 15.7: Cost breakdown structure for the production & servicing of 5080 aircraft

16
Requirements Compliance

16.1. Compliance Matrix
In order to check if the design meets the requirements, all requirements are displayed in Table 16.1. The full requirement list with all the requirement descriptions can be found in the baseline report [2]. It will be stated whether the requirements are met using a check mark. It is also stated in which section the requirement has been complied. If a requirement is not met this is indicated using an 'X'. It could also be the case that the compliance of a requirement still has to be determined. This is indicated using 'TBD'. For the latter this could occur due to a selection of CS25 requirements, which cannot be determined yet in this phase of the design. In case a requirement has not been met or determined then the rationale, why it is not met or what needs to be changed in order to meet the requirement, will be discussed in Section 16.2.

16.2. Feasibility Study
This section will discuss for every requirement why it still needs to be determined or has not been met.

- **REQ-STK-02:** The UCA shall comply with CS25. This requirement can only be met when the aircraft has been fully tested and qualified by EASA. Up till this point the CS25 regulations have been adhered to as far as possible.
- **REQ-SYS-CST-5.2.00:** The direct operational costs for the UCA shall be less than 50% per metric tonne when compared to a 747-400 freighter. As calculated in Subsection 15.4.4 the direct operational costs for the UCA are reduced by 25% per metric tonne when compared to a 747-400 freighter. The main reason for not meeting this requirement is the fuel choice. The fuel for the UCA will be synthetic kerosene. The main advantage of this fuel is the reduction in emissions. By using synthetic kerosene a CO_2 reduction of 51.2% compared to the Boeing 747-F was achieved. However, the biggest disadvantage is the high cost per kg. So the design choice was made to go for meeting the sustainability requirement instead of the DOC requirement. A sample calculation was made with the price of regular kerosene. The result of this was that the requirement was met by using kerosene. Besides the option of lowering the DOC of the UCA there may also be a change that the DOC of the Boeing 747-F will increase in the future. The European Commission is talking about reducing the emissions from aviation[1]. One option could be introducing a carbon tax. As the Boeing 747-F emits more carbon the DOC will also increase. The other option could be that the synthetic fuel cost will be lowered by subsidies and thus decreasing the DOC of the UCA. Both options will be in the favour of the UCA and therefore there will be a possibility that the requirement is met in the future depending on the regulations.
- **REQ-STK-05:** The UCA shall be relatively cheap to operate when compared to other cargo aircraft. The same rhetoric can be used for this requirement as for requirement **REQ-SYS-CST-5.2.00**.
- **REQ-SUBSYS-CON-1.3.00:** The UCA shall be controllable on the ground with a 90 degrees cross component of windvelocity of at least 37 $[km/h]$ (20 knots) or 0.2VSR0, whichever is greater. Since the ruddervator design is not part of the focus during this design phase, it is not possible to determine whether this requirement has been met. As explained in Section 10.7, during the future design phases the ruddervator will be design. After that it can be checked whether the requirement is met.
- **REQ-SUBSYS-CON-2.3.01:** Any combined lateral-directional oscillations occurring between 1.13VSR and maximum allowable speed appropriate to the configuration of the aeroplane must be positively damped with controls free, and must be controllable with normal use of the primary controls. The same rhetoric can be used for this requirement as for requirement **REQ-SUBSYS-CON-2.3.00**.
- **REQ-SUBSYS-CON-2.3.00:** Any short period oscillation, not including combined lateral-directional oscillations, occurring between 1.13 V_{SR} and maximum allowable speed appropriate to the configuration of the aeroplane must be heavily damped with the primary controls. In this stage of the design not all stability and control derivatives were known, required in order to verify if the aircraft would meet the requirements. However, as discussed in Section 10.4, the aircraft will be both stable and controllable in air, as is shown in the scissor plot. This has been driving for the stability requirements up till this point in the design.

[1] https://ec.europa.eu/clima/policies/transport/aviation_en#tab-0-0[Accessed on: 17-06-2021]

Table 16.1: Compliance Matrix

Requirement ID	Compliance	Section	Requirement ID	Compliance	Section
REQ-STK-01	✓	Chapter 12	REQ-SYS-FLT-2.6.01	✓	Section 13.3
REQ-STK-02	TBD	CS25	REQ-SYS-FLT-2.7.00	✓	Section 12.4
REQ-STK-03	✓	Section 4.6	REQ-SYS-MIS-3.1.00	✓	Section 6.6
REQ-STK-04	✓	Subsection 14.3.1	REQ-SYS-MIS-3.1.01	✓	Subsection 4.6.3
REQ-STK-05	X	Section 15.4	REQ-SYS-MIS-3.1.02	✓	Subsection 4.6.3
REQ-STK-06	✓	Section 6.4	REQ-SYS-MIS-3.1.03	✓	Subsection 4.6.4
REQ-STK-07	✓	Section 14.2	REQ-SYS-MIS-3.1.04	✓	Subsection 4.6.4
REQ-STK-08	✓	Subsection 14.3.1	REQ-SYS-MIS-3.1.05	✓	Subsection 14.3.1
REQ-STK-09	✓	Section 18.2	REQ-SYS-MIS-3.2.00	✓	Chapter 12
REQ-STK-10	✓	Section 18.2	REQ-SYS-MIS-3.2.01	✓	Chapter 12
REQ-STK-11	✓	Section 15.3	REQ-SYS-MIS-3.2.02	✓	Chapter 12
REQ-STK-12	✓	Subsection 15.4.3	REQ-SYS-MIS-3.2.03	✓	Chapter 12
REQ-STK-13	✓	Section 18.2	REQ-SYS-SUS-4.1.00	✓	Subsection 7.2.2
REQ-STK-14	✓	Section 18.1	REQ-SYS-SUS-4.2.00	✓	Section 14.2
REQ-SYS-GRD-1.1.00	✓	Section 18.2	REQ-SYS-SUS-4.3.00	✓	Subsection 14.3.1
REQ-SYS-GRD-1.1.01	✓	Section 18.2	REQ-SYS-SUS-4.4.00	✓	Section 13.2
REQ-SYS-GRD-1.1.02	✓	Section 18.2	REQ-SYS-CST-5.1.00	✓	Subsection 15.4.3
REQ-SYS-GRD-1.1.03	✓	Subsection 11.5.4	REQ-SYS-CST-5.2.00	X	Subsection 15.4.4
REQ-SYS-GRD-1.2.00	✓	Section 18.2	REQ-SYS-SCH-6.1.00	✓	Section 18.4
REQ-SYS-GRD-1.3.00	✓	Chapter 11	REQ-SYS-SCH-6.2.00	✓	Section 18.4
REQ-SYS-GRD-1.3.01	✓	Section 11.5	REQ-SUBSYS-PRP-2.2.00	✓	Section 7.3
REQ-SYS-FLT-2.1.00	✓	Section 12.6	REQ-SUBSYS-PRP-2.5.00	✓	Section 7.3
REQ-SYS-FLT-2.1.01	✓	Section 12.6	REQ-SUBSYS-PRP-2.6.00	✓	Section 7.3
REQ-SYS-FLT-2.1.02	✓	Section 12.6	REQ-SUBSYS-PRP-2.6.01	✓	Section 7.3
REQ-SYS-FLT-2.2.00	✓	Chapter 11	REQ-SUBSYS-PRP-2.6.02	✓	Section 7.3
REQ-SYS-FLT-2.2.03	✓	Section 6.5	REQ-SUBSYS-PRP-4.1.00	✓	Section 7.3
REQ-SYS-FLT-2.2.04	✓	Section 6.5	REQ-SUBSYS-POW-2.6.00	✓	Section 13.5
REQ-SYS-FLT-2.2.05	✓	Section 6.3	REQ-SUBSYS-POW-2.6.01	✓	Section 13.5
REQ-SYS-FLT-2.2.06	✓	Section 6.5	REQ-SUBSYS-POW-2.6.02	✓	Section 13.5
REQ-SYS-FLT-2.3.00	✓	Section 6.6	REQ-SUBSYS-LDG-2.2.00	✓	Section 11.5
REQ-SYS-FLT-2.3.01	✓	Section 6.4	REQ-SUBSYS-LDG-2.2.01	✓	Section 11.3
REQ-SYS-FLT-2.3.02	✓	Chapter 5	REQ-SUBSYS-LDG-2.2.02	✓	Subsection 11.5.2
REQ-SYS-FLT-2.3.03	✓	Section 4.5	REQ-SUBSYS-LDG-2.2.03	✓	Section 11.5
REQ-SYS-FLT-2.4.00	✓	Chapter 10	REQ-SUBSYS-LDG-2.2.04	✓	Section 11.5
REQ-SYS-FLT-2.4.01	✓	Section 10.4	REQ-SUBSYS-LDG-2.3.00	✓	Section 11.4
REQ-SYS-FLT-2.4.02	✓	Section 10.4	REQ-SUBSYS-WNG-2.2.00	✓	Section 5.4
REQ-SYS-FLT-2.4.03	✓	Section 10.4	REQ-SUBSYS-WNG-2.2.01	✓	Section 5.4
REQ-SYS-FLT-2.4.04	✓	Section 6.5	REQ-SUBSYS-WNG-2.3.00	✓	Section 5.2
REQ-SYS-FLT-2.4.05	✓	Section 6.4	REQ-SUBSYS-CON-1.3.00	TBD	Chapter 10
REQ-SYS-FLT-2.5.00	✓	Chapter 8	REQ-SUBSYS-CON-2.3.00	TBD	Chapter 10
REQ-SYS-FLT-2.5.01	✓	Chapter 8	REQ-SUBSYS-CON-2.3.01	TBD	Chapter 10
REQ-SYS-FLT-2.5.02	✓	Chapter 8	REQ-SUBSYS-CON-2.4.00	✓	Section 6.7
REQ-SYS-FLT-2.5.03	✓	Section 13.3	REQ-SUBSYS-CAR-2.5.00	✓	Section 13.3
REQ-SYS-FLT-2.5.04	✓	Section 13.3	REQ-SUBSYS-CAR-2.5.01	✓	Section 13.3
REQ-SYS-FLT-2.6.00	✓	Section 7.3	REQ-SUBSYS-CAR-2.5.02	✓	Section 13.3

17
Technical Risk Assessment

In this report the feasibility of the final design was studied, this required an elevation in the level of detail that many systems and subsystems were designed. In this analysis, many technical risks were identified to the relevant solutions. This chapter will discuss these newly identified risks, and how the project organization plans to mitigate or prevent these risks from triggering. Previously identified risks are still relevant, and can be found in the previous reports.

17.1. Risk identification

Risks were identified on the basis of their likelihood, and the impact they would have on the project. These risks involve anything that would negatively impact the cost, scheduling, quality, and safety of the design, manufacture and operation of the project.

A risk's significance is based on its residual risk, which is the resulting product of a risks likelihood and impact scores. Table 17.1 and Table 17.2 show the scoring system that was used. Using these scales allows for identified risks, however unique, will be comparable based on its residual score. The identified risks and their scores can be found in Table 17.3. As can be seen in the table the risks start at risk 51. This comes due to the fact that in the earlier reports also risk assessment was done. So risk 1-20 can be found in the project plan [68]. These risks are specific to the project team itself and the risk associated with the organisation. Risk 21-39 are discussed in the baseline report [2] and focus on the more general technical risks associated with the project. After that risk 40-50 can be found in the midterm report [6]. These risks are more specific to the different concepts generated.

Table 17.1: Table showing the score that the likelihood represents

Likelihood [%]		
Very low	<5	1
Low	5-29	2
Moderate	30-59	3
High	60-80	4
Very high	>80	5

Table 17.2: Table showing the score that the impact represents (Impact considers [Design Delay, Cost, danger to safety])

Impact		
Very low	Hours	1
Low	Day	2
Moderate	Week	3
High	Weeks	4
Very high	Month	5

17.2. Risk mitigation

Once the Risks were identified, it was crucial to determine the most critical risks that required immediate planning for. These risks would have to have mitigation strategies developed that would reduce the residual risk of the risk to an acceptable range. The mitigation strategies and resultant scores can be found in Table 17.3. Figure 17.1 and Figure 17.2 show the result the mitigation strategies are expected to have on the risk.

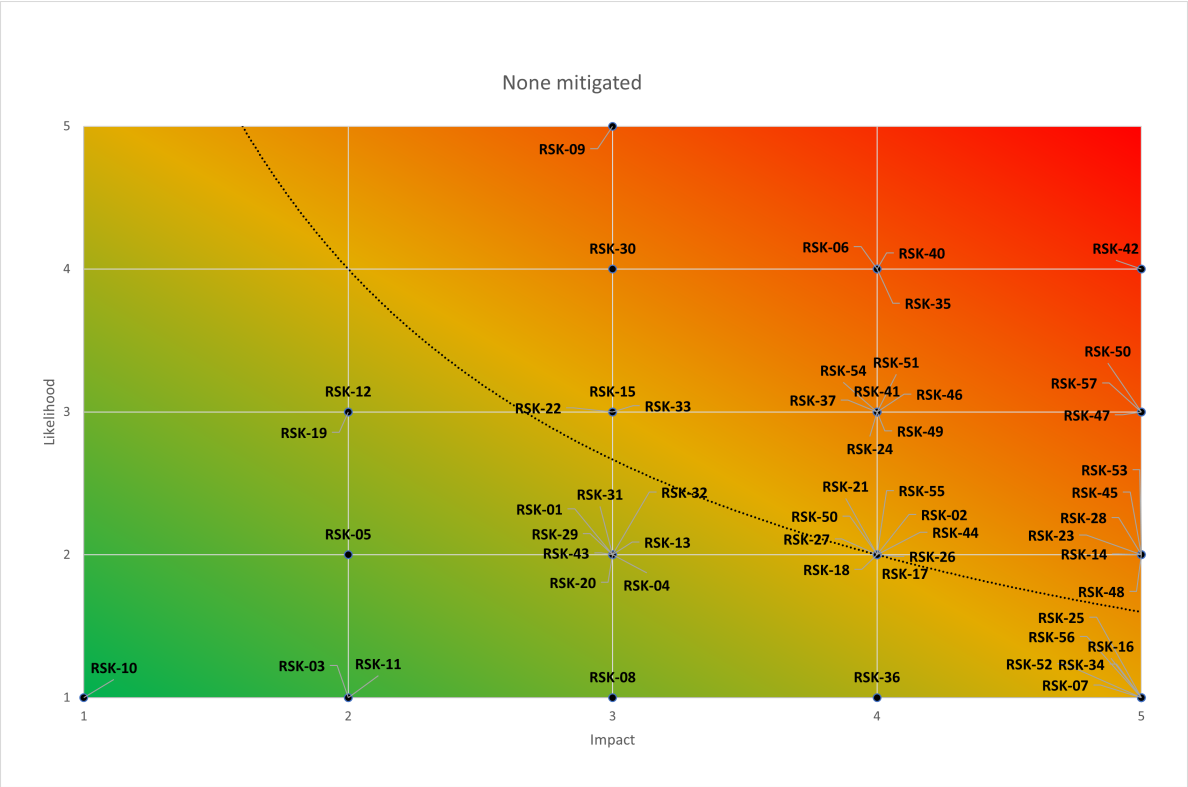

Figure 17.1: Previously mitigated risks combined with current unmitigated risks

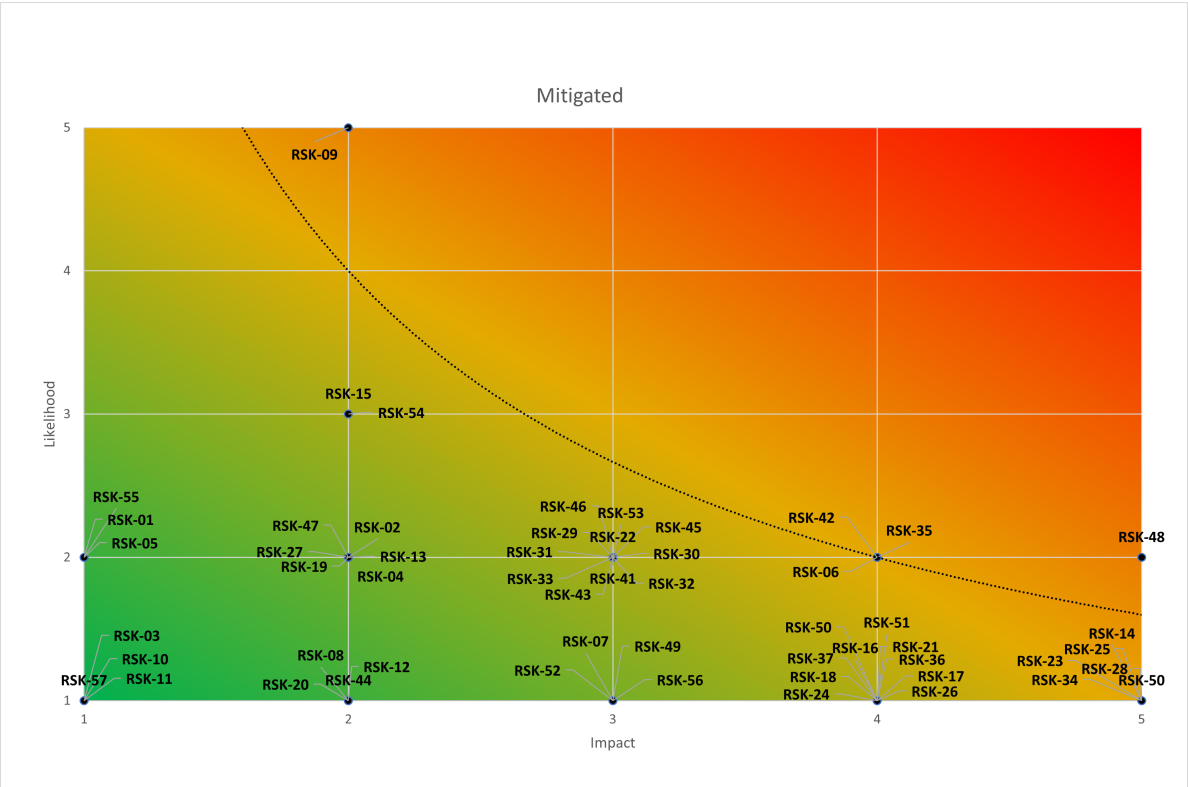

Figure 17.2: All risks after current mitigation revision

Some notable risks in the newly identified batch of risks are two risks which are problematic during the operation of the aircraft, given how long the aircraft service life is expected to be, these risks have a much larger window in which to trigger. These risks were RSK-54 and RSK-55, for the first risk a solution was created to navigate the aircraft back to its last known location where it received data and circle. This mitigation strategy was elaborated on further in Section 12.5.

For the second risk there are actions on an organisation level to prevent damage or loss of goods, but this risk is impossible to fully prevent. For this reason an additional measure will be taken to offload the risk and liability to an insurance company, since both the client and organisation will be handling high value goods, it is in both parties best interest that the goods be insured to maintain healthy relations and prevent significant loss.

Despite these newly identified risks, some of the older risks still posed a threat in this phase of the project. RSK-06, which discussed the effect underestimating deliverable time frames could have on the project was managed exceptionally well. The use of a Gantt chart in combination with regular checkups and oversight allowed the project to run with little delay.

There are many risks to still be identified for the remainder of the project, and many more that will trigger. With reference to RSK-37, which warns of the dangers of not identifying or mitigating risks has on the project, it is important that a continued risk overview is done in the later phases of the project. Circumstances are ever changing and it will be important that project group is prepared for every scenario.

Table 17.3: Table of newly identified risks as well as the mitigation strategy and the resulting residual risk [UM-Unmitigated;M-Mitigated;I-Impact;L-Likelihood;RR-Residual Risk]

Risk ID	Risk Title	Effect	UMI	UML	UMRR	Mitigation	MI	ML	MRR
RSK-51	Global chip shortage continues	Price or availability of chips negatively affects production	5	3	15	Create binding contractual agreements when making the initial purchase. In this way the supplier is obligated to deliver or to pay a fee if this is not possible.	5	1	5
RSK-52	Fuel prices increase	Price or availability negatively impact the profit margin of aircraft	4	3	12	Binding contractual agreements with certain fuel suppliers to make sure that the fuel price stays between a reasonable margin	4	1	4
RSK-53	Aircraft crashes	Loss of reputation, potential threat to safety and lives	5	1	5	By the use of a parachute in case of an emergency the impact is reduced. Besides of that the insurance paid for the aircraft is higher, so the financial consequences remain limited	3	1	3
RSK-54	Aircraft losses communication to controller	Aircraft is unable to be monitored or controlled, large safety hazard	5	2	10	Navigation protocol to fly back to location of last contact	3	2	6
RSK-55	Clients payload is lost/-damaged/destroyed	Compensation to the payload must be made, loss of profits, and reputation	4	3	12	A higher insurance fee is paid, so in case of a loss/damage of the payload the client can be paid via the insurance company.	2	3	6
RSK-56	Cargo door jams	Unable to access interior of aircraft, or payload	4	2	8	Implement internal and external access hatch for manual opening	1	2	2
RSK-57	Failure of hydraulic system	Aircraft is unable to control its control surfaces	5	1	5	Implement redundant hydraulic systems to minimize the effect of the failure	3	1	3
RSK-58	Jet stream stalls tail	Aircraft flight performance could be bad, aircraft crashes	5	3	15	By doing a literature study and geometric check the problems were solved and should not be an issue	1	1	1

18
Development

This chapter will discuss the development of the aircraft in the Post-DSE phase. First the manufacturing processes in Section 18.1 will be discussed including the reason for assembly, production plan, manufacturing of different components and integration of different subsystems. Afterwards the operations and logistic concept will be discussed in Section 18.2. Next, the project design and development logic will be analysed in Section 18.3, including a diagram to show all post-DSE tasks. These tasks will be planned out in Section 18.4

18.1. Manufacturing

After designing the aircraft, it is also important to investigate the manufacturing process. First, the reason for assembly will be given. Afterwards, the production plan will be shown. Next manufacturing processing of different elements will be briefly discussed. Lastly, the most interesting subsystem integrations will be analysed.

18.1.1. Reason for Assembly

After designing the aircraft, it is also important to determine how the aircraft is going to be build. The aircraft will be constructed using several sub assemblies. The assembly will take place orderly by joining different elements into sub assemblies. These parts will be assembled into larger sub-assemblies up till the final assembly, which is the entire aircraft. The main reasons for assembly are production efficiency, ease of production, maintenance, and structural reasons. The product efficiency is depended on how the overall production line is organised. Splitting up the assembly into different work-packages and planning them, will decrease the overall production time. Moreover, using assembly strategies, the ease of production can be increased. Different structures will be more difficult to manufacture if their size is too large. For instance an entire wing structure can not be made out of one piece of aluminium. Also during operations, replacement of different structures is more easily realised if the aircraft consist of sub-assemblies. Lastly, sub-assemblies will stop crack division, making the aircraft structure more robust.

In order to increase the efficiency, the manufacturing will make use of an assembly line. All assembly lines will be presented in the Production Plan, described in Subsection 18.1.2. Regarding the work force, the same crew will always perform the same tasks in order to develop routine. This will decrease the production time, which can be described by the learning curve. The learning curve and therefore the time needed to produce an aircraft is given by Equation 18.1. Where K is the effort to produce the first aircraft, N is the aircraft number and s is the slope constant.

$$E_N = K \cdot s^N \tag{18.1}$$

It is assumed that a reduction of 20 percent in production time is achievable when the number of aircraft is doubled. Assuming the aircraft manufacturing would take 2 years, it would be a total of 3200 hours (assuming 8 working hours per day, and 200 working days per year). This means that for aircraft number 2, 2560 hours are needed, and for aircraft number 4 2048 hours are is needed. This is shown in Figure 18.1. As described in Section 2.3, a potential market volume of 5080 aircraft exist. In order to increase the production multiple aircraft will be built at the same time in order to reduce the delivery interval. After the production of the first couple of aircraft, it could be possible that the overall production time is massively decreased. This is a rough estimation of the manufacturing time. During the post-DSE phase, the manufacturing process will be planned out in more detail. When more information is available, a better indication of the manufacturing time and its decrease can be given.

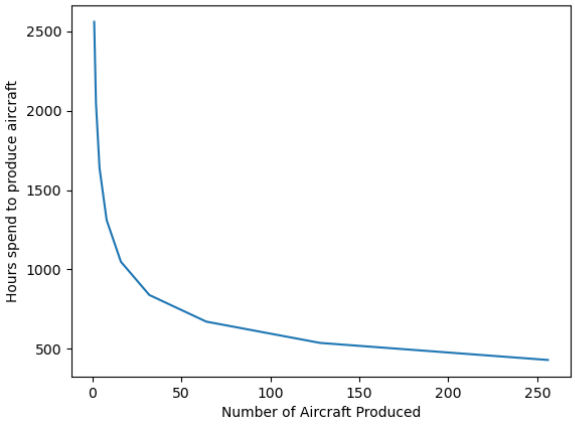

Figure 18.1: Learning Curve Plot, indicates production time

18.1.2. Production Plan

The production plan shows the overall lay-out of the line production in a chronological order. The diagram is shown in Figure 18.2. The diagram is divided into smaller sub categories. A loop has been created as for retired aircraft, subsystems as well as materials will be reused as much as possible, as discussed in Section 9.5. This will be the input for the manufacturing cycle. For a better understanding all quality controls in middle stages are not given. However, between all manufacturing and assembly flows, quality control and testing will take place. Also during sub-assembly itself, these test will take place. Moreover, it can be noted that the parachute, electrical systems, hydraulic systems, avionic systems, flight systems, and engine can be either be ordered new or reused from retiring aircraft. These systems could also come from different retiring aircraft. A comprehensive quality control will take place before implementing recycled or reused products in order to assure its quality. Lastly, hydraulic and electrical systems will be used for all sub-assemblies, but for more clarity, this has been added as onboard integration. More details regarding different subsystem assemblies can be found in Subsection 18.1.4.

To conclude, most structural elements will be made in-house or reused from retiring aircraft. Raw and recycled materials will be bought from suppliers. All electrical and hydraulic systems will be bought from suppliers, such as Hader Industries Inc [1]. Avionics and automation systems will also be bought from external suppliers. The engine supplier will be Rolls-Royce, and the engines will be partly bought and partly leased. This is done in order to decrease maintenance cost on the engines.

18.1.3. Manufacturing

This section will briefly touch upon the general manufacturing methods for different main structures. For all structures, the cheapest or most suitable method has been chosen using the reader of AE3211 Production of Aerospace Systems.

For both fuselage and wing skin, it will be made of different panels, which will be produced using bending. Most parts will be single curved parts, with large bend radii. From aluminium plates, the desired thickness can be achieved using mechanically separating. The correct sizes can be cut using water jet cutting. The correct form can be obtained using bending. For the nose and tail cone the same procedure will be used, except stretch forming will be used instead of bending, as large and slightly double curved sheets are needed. After stretch forming, heat treatment will be needed in order to remove the effects of work hardening.

Wing ribs and fuselage frames will be made using rubber forming, in the case that the initial sheet thickness is between 0.5 and 3 $[mm]$ and the length is not longer than the forming machine. This process is most suitable for single and double curved parts with small bend radii. Heat treatment beforehand is needed to increase the formability. For wing ribs, punching and/or separating is needed to obtain all correct dimensions and cut-outs.

Stringers and longerons can be produced using bending as well, due to their significant length. However, after the bending process, one should use other processes in order to account for the spring back at the flanges itself. Lastly, forging can be used for the production of highly stress parts, which are not thin-walled and have no large variation in thickness. The benefit of forging over casting and machining is a fibrous grain structure, which is favourable for corrosion and fatigue resistance.

[1] `http://www.haderind.com/index.html` [Accessed on: 12-06-2021]

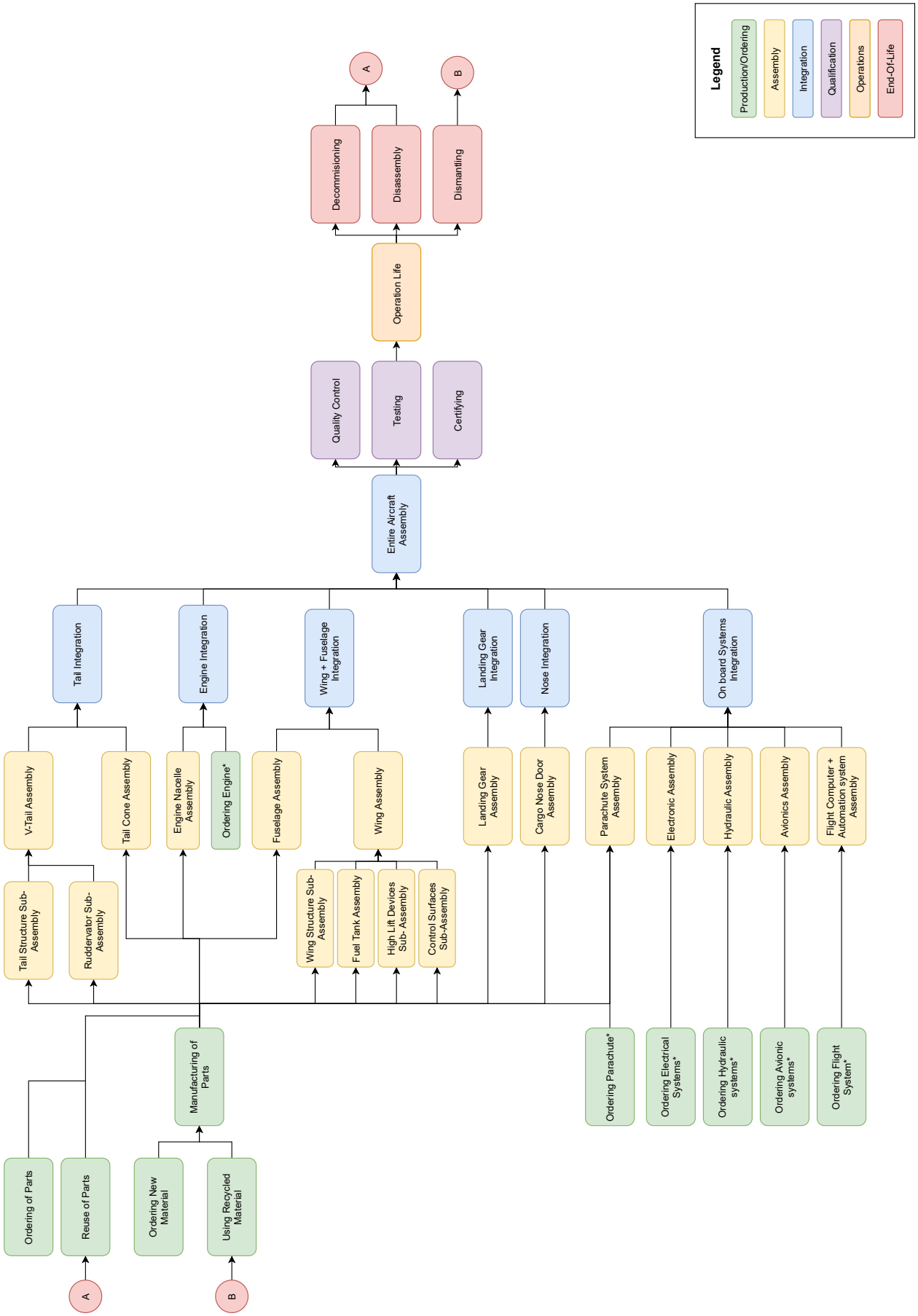

Figure 18.2: Production Plan, * indicates that this part can also be reused from retired aircraft

18.1.4. Subsystem Integration

This section will discuss the most critical assembly and integration processes of the aircraft, which are the engine and fuselage connection, the fuselage and wing connection and the tail integration. The landing gear is discussed in Section 11.4.

Engine and Fuselage Integration

The carrying structure needed for the engine has been designed in Subsection 8.3.2. This section will discuss the connection between the engine and the fuselage itself, mainly on a conceptual level. The structure will be similar to pylons of fuselage mounted engines. The engine will have three connection points at which a frame can be connected. This frame is shown in Figure 18.3. A top view of the structure is shown in Figure 18.4. The front frame will be a U-form in order to carry the engine. The main benefit of this frame is that it does not allow the engine to deform a vibrate. For fuselage mounted engines this structure is designed for bending stresses. For this aircraft the structure must be designed for compressive stresses as well. In the post-DSE phase, a more detailed analysis is needed in order to check the feasibility of this structure. The rear connection point is needed to counteract the moment. The fairing will be shaped like an airfoil to reduce drag. The pylon itself can easily be removed for maintenance purposes. As the engine has only three connection point it is fairly easy to remove the engine. A motor hoist or a similar lifting device will be needed to place and remove the engine [69].

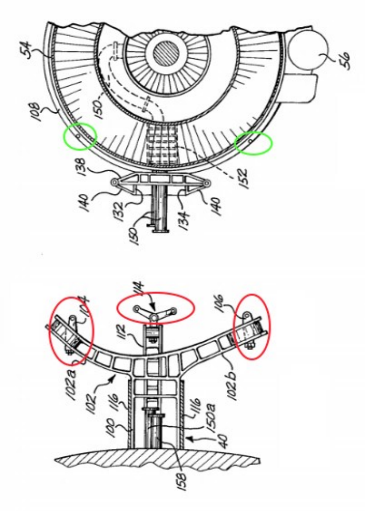

Figure 18.3: Engine Integration Frame, red circles indicate assembly points structure, green circles indicate assembly points engine [69]

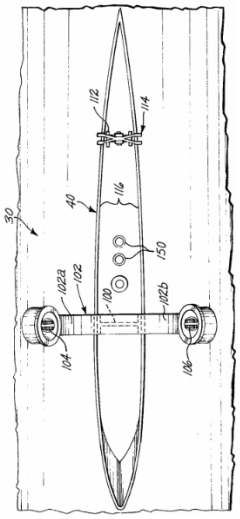

Figure 18.4: Engine Integration Frame, top view [69]

Fuselage and Wing Integration

The fuselage and wing will be integrated using a lug attachment, as it easy to assemble and more economic. The wing box structure will be connected to a bulkhead within the fuselage in order to transport all loads. Heavy concentrated loads are received through lug joints, as it should be able to transport both the aerodynamic bending moment and shear loads due to torsion. Four lugs will be used for the wing box, two at the front spar and two at the rear spar. An additional two lugs will be needed to attach the yehudi spar to the fuselage frame. A representation of this connection is shown in Figure 18.5. A isometric view of the lug is shown in Figure 18.6 [2]

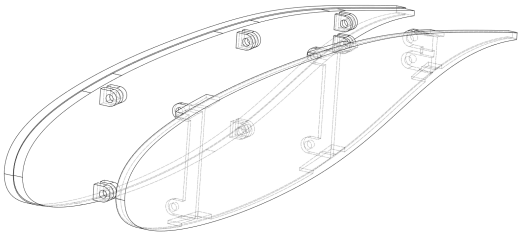

Figure 18.5: Fuselage and wing lugs isometric view

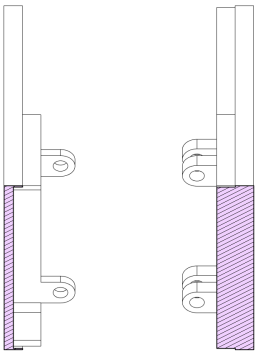

Figure 18.6: Wing lug isometric view

[2] https://www.highskyflying.com/how-are-airplane-wings-attached-to-the-fuselage/ [Accessed on: 15-06-2021]

Tail integration
The tail will be joint in a similar manner as the wing to the fuselage. Lugs will be used in order to connect the V-tail to the rear bulkhead. Per wing 4 lugs will be used, 2 for the front spar, 2 for the rear spar.

18.2. Operations and Logistic Concept

Operations and logistics can be divided into three main branches, which are ground operations and logistics, flight operations, and end-of-life operations. End-of-life operations have been discussed in Section 9.5. Ground operations and logistics, and flight operations will be discussed below.

18.2.1. Ground Operations and Logistics

As discussed in Section 2.4, ground support will be outsourced to Swissport on all main hubs. Local companies will be used on non-hub airports. The main ground handling aspect for the UCA will be loading and unloading. A pallet loader will be used to (un)load all cargo pallets. The pallets are moved into the cargo bay using built-in rollers, situated in the floor. This equipment is present at hub and secondary airports, and therefore no specialised equipment is needed to (un)load the aircraft. This will mean that the aircraft can be loaded and unloaded in a fast manner. Regarding the loading time, for a 747 the typical loading and unloading time per container is below 2 minutes. Opening and closing of the aircraft nose door would take a total of 2 minutes as well. This means that in theory the aircraft could be loaded in 8 minutes. This is very positive estimation, but shows that loading could be done within 30 minutes. [70]

Next, the aircraft must also be fueled. The aircraft will be fueled using synthetic kerosene. As discussed in Section 7.2 synthetic kerosene can be transported in a similar manner as kerosene, both being from a centralised production site. In the case that no synthetic kerosene is available at the regional airports, normal kerosene can also be used, due to the engine and fuel system changes, as discussed in Subsection 7.2.3. Synthetic kerosene can be fueled in the same manner as normal kerosene, and therefore no special training is needed for ground personnel. The aircraft has a fuel tank volume of 7400L. The aircraft can be refueled with a rate of 900L/min[71]. This shows that the aircraft can be fueled within the required time.

Lastly, maintenance will mainly take place on the hub airports or secondary hub airports. Four different kinds of maintenance exist, as is discussed in Subsection 15.3.2. Daily checks can take place on all airports, even on local airports. All aircraft main systems can be checked by the remote pilot, before flight. "A" check will take place on both the main hubs and the secondary hubs. More specialised personnel is needed for "A" checks compared to daily checks. "C" and "D" maintenance will only take place on main hubs, as this will require specialised equipment and personnel. The exact location of these maintenance hubs can also differ, depending on the customers. If FedEx Express, DHL aviation and UPS airlines would buy the aircraft, "D" checks could take place at Memphis, Frankfurt, Bahrain, and Narita only, as facilities are already present.

18.2.2. Flight Operations

Flight operations can be divided into two main parts, LOS operations and BLOS operations. For take-off, climb, descent and landing LOS operations will be used. On hub airports GCS will be present including flight operators. They will operate the aircraft during these four phases. During cruise BLOS of will be used, where the flight operator will send way points to the aircraft. This was more extensively discussed in Chapter 12.

18.2.3. Operational and Logistic Flow Diagram

The operational and logistic flow diagram can be found in Figure 18.7. The diagram is divided in a flight operations part and ground operations part.

As explained in Subsection 18.2.2, the flight operations part can be divided as well. The line-of-sight operations and beyond-line-of-sight operations. More about the BLOS and LOS operations is explained in Chapter 12. Note that during LOS operations ATC clearance is needed for taxi, take-off and landing operations. Furthermore, during BLOS operations there is continuous communication between the satellite and GCS.

The ground operations are divided in ground handling and maintenance procedures. The ground handling procedures exist of refueling and the cargo handling. Fuel is provided by the fuel supplier and the steps before the actual cargo handling are shown in the grey boxes. If the aircraft needs maintenance, the aircraft will be moved to the hangar where maintenance will be done. Before the maintenance can start, the type of maintenance needed needs to be determined. Four types of maintenance are possible. Those types of maintenance are explained in Subsection 15.3.2. Note that when "D" Check maintenance is needed "C" and "A" maintenance are executed as well.

The end-of-life operations have not been included in this diagram, but can be found in Figure 1.3 and Section 9.5.

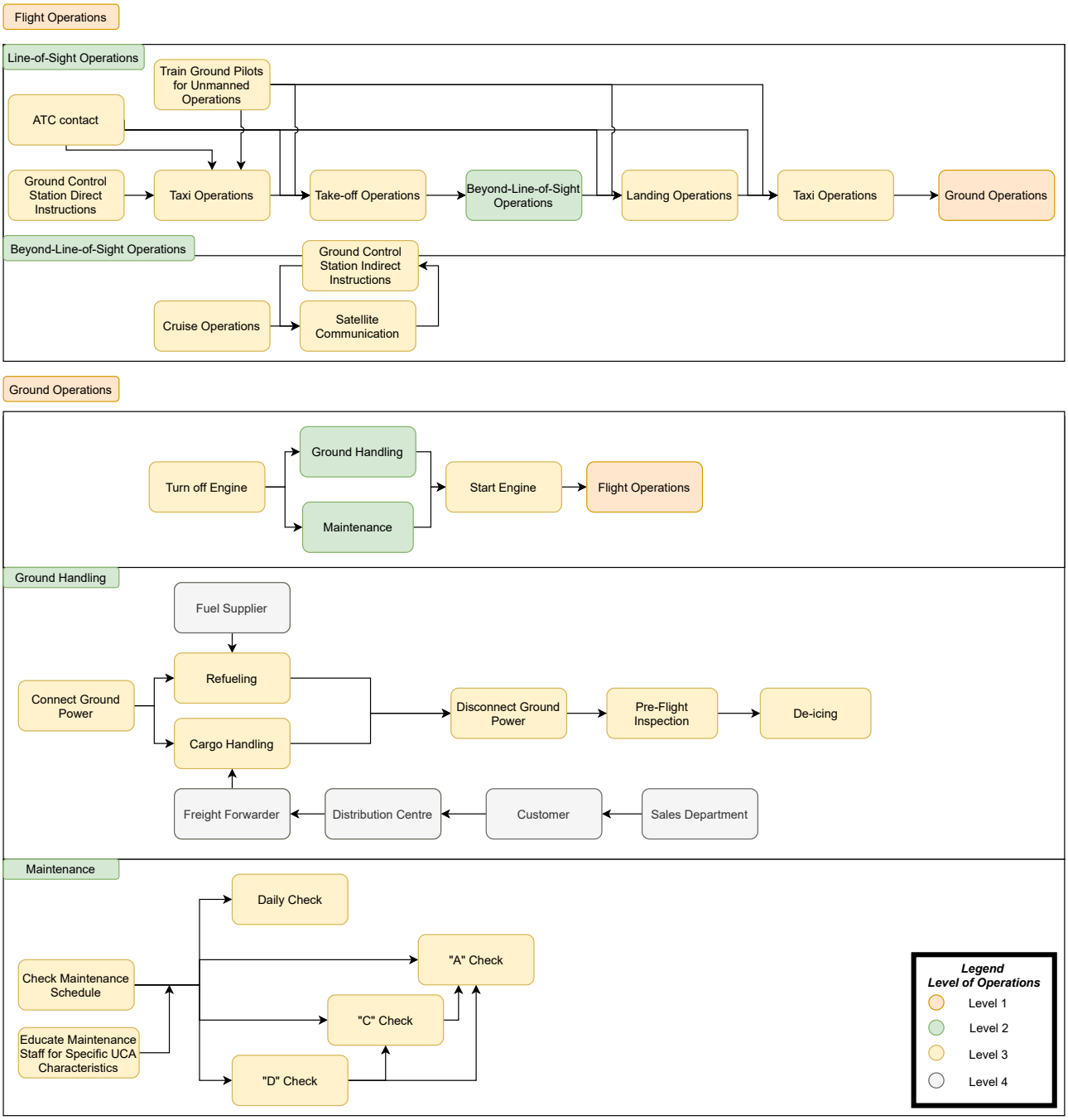

Figure 18.7: Operations and Logistic Flow Diagram

18.3. Project Design and Development Logic

This section discusses the plan for the post-DSE phase, where a diagram with the flow of activities is shown in Figure 18.8. The overall planning exist of 4 main phases, which are planning, design, certification & testing, and manufacturing & delivery. In the first phase, the DSE project will be evaluated. Afterwards, a business plan, including a detailed market analysis will take place to verify the market feasibility of this aircraft. In this phase also a team will be hired in order to successfully design the aircraft.

The next phase is the design. In this phase iteration will take place on the preliminary design and at the end a detailed design will take place. Also the first two steps towards aircraft certification will take place. First, the project will be presented to the EASA. An EASA certification team will establish the rules that apply to this aircraft. After this is established, the manufacturer and EASA will define and agree how compliance will be demonstrated.

After designing the aircraft, a prototype will be build for testing purposes. This will include setting up the manufacturing and testing facilities. As addition this aircraft will require extra test flights in order to test all flight and automation systems. This will include feedback from pilots on the ground as well. During testing, the compliance of the aircraft will be shown by testing all structures and systems. This is the longest phase in the certification process. For large

aircraft this can take up till 5 years. The last certification procedure is issuing the certificate. This will also include verification from other aviation agencies, such as the FAA. [3]

The last phase will include the mass manufacturing of aircraft and delivering all aircraft. Marketing will also take place during this stage, but will start already during the certification and testing phase, after a prototype is present.

This diagram does not include the end-of-life strategy, which is discussed in Section 9.5. However, if the aircraft would retire, the recycling itself would be outsourced. The products obtained will be implemented in the manufacturing.

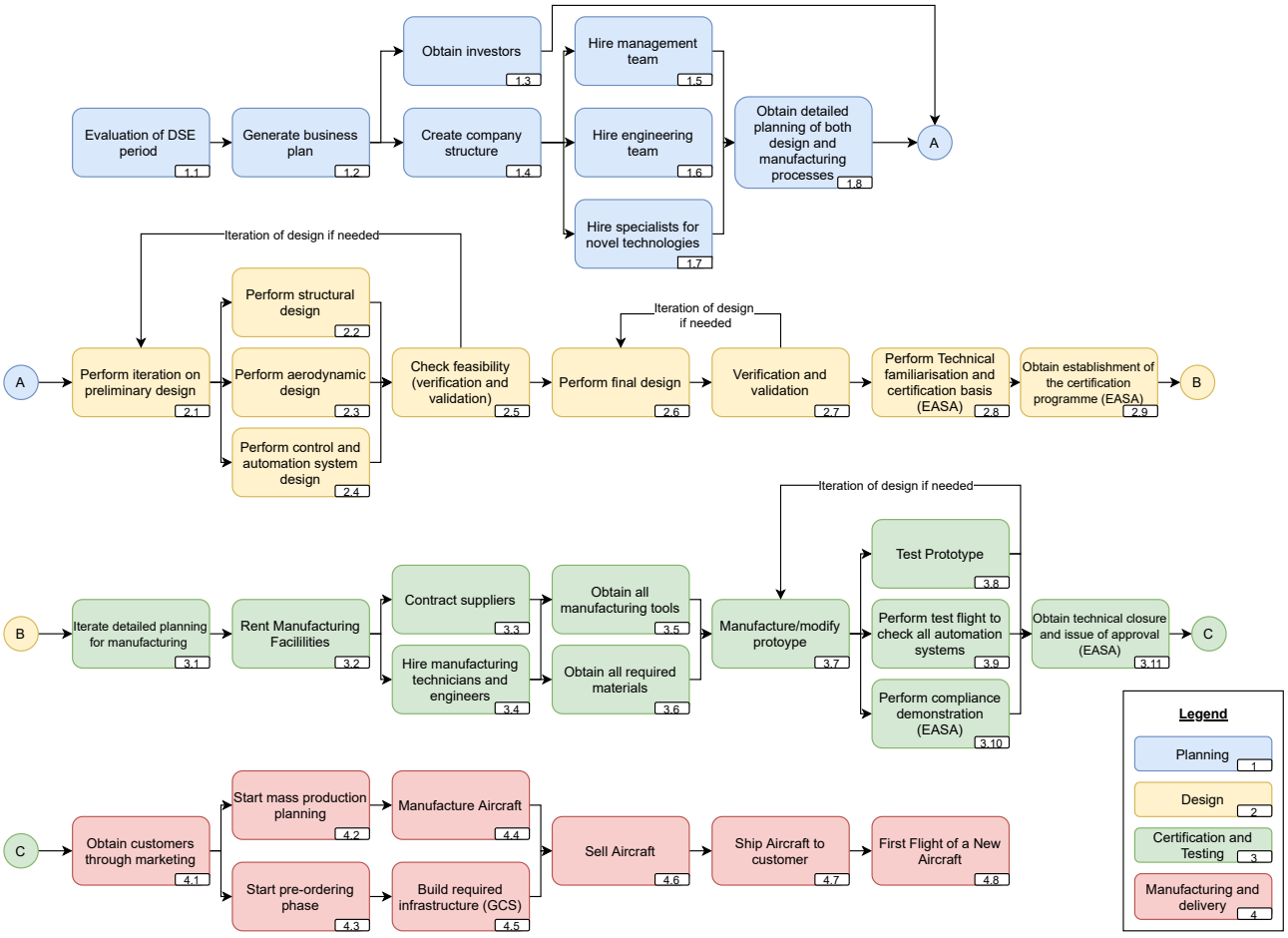

Figure 18.8: Project Design and Development Logic Diagram

18.4. Project Gantt Chart

Following from the project design and development logic, a project Gantt chart has been made to include all activities up till the delivery of the first aircraft. The Gantt chart is shown in Figure 18.9, and it assumes that the business plan will show a positive market analysis and enough investors and funds can be raised. The first aircraft should be delivered before the year 2035. Using this initial planning at the end of 2032. This means a 2 year buffer is created if delays occur. Regarding 3.10 Perform compliance demonstration, a duration of 4 years has been chosen, as it will take more time to test all relevant flight and automation systems. Obtaining customers will at least take 2 years, but will be a continuous process after a prototype has been made. Beforehand also marketing activities will take place to check the feasibility of bringing the product to the market. After producing the first couple of aircraft, evaluation will take place. This will be to make sure that the break-even point will be reached and if it would be possible to extent the market by increasing the adaptability of the aircraft.

[3] `https://www.easa.europa.eu/domains/aircraft-products/aircraft-certification` [Accessed on: 08-06-2021]

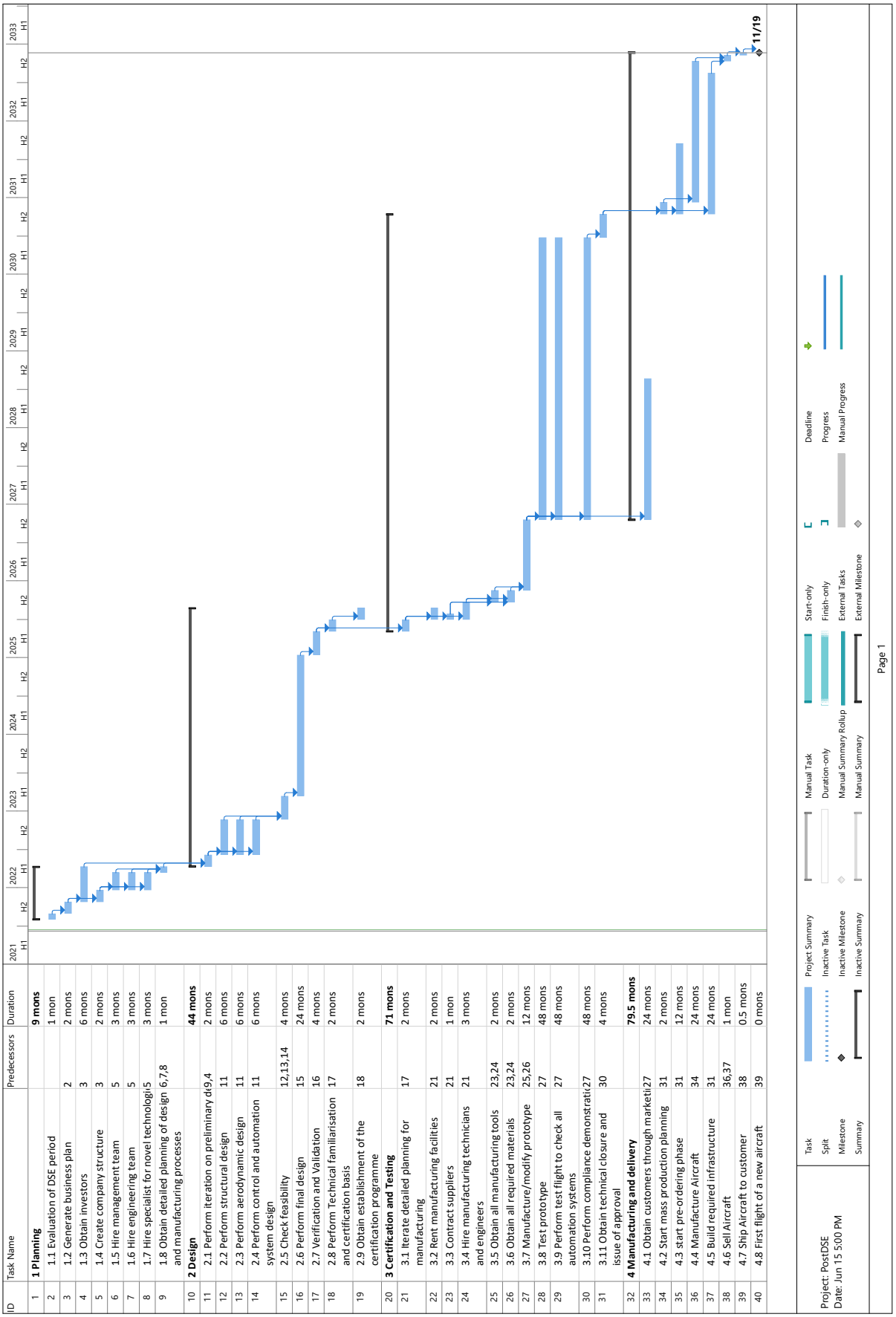

ID	Task Name	Predecessors	Duration
1	**1 Planning**		**9 mons**
2	1.1 Evaluation of DSE period		1 mon
3	1.2 Generate business plan	2	2 mons
4	1.3 Obtain investors	3	6 mons
5	1.4 Create company structure	3	2 mons
6	1.5 Hire management team	5	3 mons
7	1.6 Hire engineering team	5	3 mons
8	1.7 Hire specialist for novel technologi	5	3 mons
9	1.8 Obtain detailed planning of design and manufacturing processes	6,7,8	1 mon
10	**2 Design**		**44 mons**
11	2.1 Perform iteration on preliminary d	9,4	2 mons
12	2.2 Perform structural design	11	6 mons
13	2.3 Perform aerodynamic design	11	6 mons
14	2.4 Perform control and automation system design	11	6 mons
15	2.5 Check feasibility	12,13,14	4 mons
16	2.6 Perform final design	15	24 mons
17	2.7 Verification and Validation	16	4 mons
18	2.8 Perform Technical familiarisation and certification basis	17	2 mons
19	2.9 Obtain establishment of the certification programme	18	2 mons
20	**3 Certification and Testing**		**71 mons**
21	3.1 Iterate detailed planning for manufacturing	17	2 mons
22	3.2 Rent manufacturing facilities	21	2 mons
23	3.3 Contract suppliers	21	1 mon
24	3.4 Hire manufacturing technicians and engineers	21	3 mons
25	3.5 Obtain all manufacturing tools	23,24	2 mons
26	3.6 Obtain all required materials	23,24	2 mons
27	3.7 Manufacture/modify prototype	25,26	12 mons
28	3.8 Test prototype	27	48 mons
29	3.9 Perform test flight to check all automation systems	27	48 mons
30	3.10 Perform compliance demonstrati	27	48 mons
31	3.11 Obtain technical closure and issue of approval	30	4 mons
32	**4 Manufacturing and delivery**		**79.5 mons**
33	4.1 Obtain customers through marketi	27	24 mons
34	4.2 Start mass production planning	31	2 mons
35	4.3 start pre-ordering phase	31	12 mons
36	4.4 Manufacture Aircraft	34	24 mons
37	4.5 Build required infrastructure	31	24 mons
38	4.6 Sell Aircraft	36,37	1 mon
39	4.7 Ship Aircraft to customer	38	0.5 mons
40	4.8 First flight of a new aircraft	39	0 mons

Figure 18.9: Post DSE Project Gantt Chart

19
Conclusion

In conclusion, the CoViD-19 pandemic has exposed the dependency of the air cargo industry on passenger aircraft. This lead to the idea to design an unmanned cargo aircraft, to both reduce the dependency on passenger aircraft and accommodate for the rapid transportation of high value goods with a low volume. Over a period of 10 weeks, 10 aerospace students have been working on this assignment to finalise their bachelor's programme.

After an extensive trade-off process, the economical concept was selected to form the basis for the final design. This final design is characterised by a single-engine configuration, placed on top of the fuselage. This also lead to the implementation of a remarkable V-tail with respect to the empennage configuration. Moreover, the cargo pallets can be loaded into the aircraft by means of an opening nose mechanism and rollers integrated in the floor. To contribute towards sustainability, the propulsion system, consisting of a single Rolls Royce AE 3007A engine, will run on synthetic kerosene to lower the CO2 emission by more than 50% in comparison to a B747-400F. In the mean time, the emitted noise levels are comparable to those of a Cessna Citation II, partially as a result of the engine placement with respect to the tail. As an additional safety feature, an integrated parachute system is installed to account for the occurrence of an engine failure. In the end, the aircraft has a design payload of 2000 kg at a range of 3000 nautical miles. However, the aircraft is also adaptable to fly at longer ranges carrying less payload or the other way around. Ultimately, the maximum take-off weight is established at 13250 kg, with a cruise speed of 667 km/h. The unmanned cargo aircraft will have a unit cost of 4.89 Million Euros, while the direct operating costs amount to approximately 5200 Euros per flight. Some proposed applications for the aircraft are transporting seafood from Canada to different continents, or delivering CoViD-19 vaccines and other medical supplies to remote areas such as Saint Helena island.

As the final product at this stage of the design is still preliminary, more research has to be done. The main recommendations on the AirGo Zero-15 are to perform more in-depth analysis on the various subsystems. This includes evaluating the aerodynamic characteristic via CFD analysis and the sizing of the complex ruddervator control system. Also the effect of adverse yaw coupling must still be considered. The regulations on the unmanned control of aircraft are also still in the development phase, and need to be considered in greater detail. In order to fulfill this, the EASA has to be contacted to work out the setup of autonomous aircraft in more detail. Finally, a more accurate cost estimation of the AirGo Zero-15 should be performed. For now the estimation is mainly based on manned reference aircraft and the expectation is that, due to the fact that the aircraft is unmanned, the final cost may differ from conventional aircraft.

Figure 19.1: Render of the final design in-flight

Bibliography

[1] Boeing, "World air cargo forecast 2020-2039," Boeing, 2020.

[2] DSE Group 21, Unmanned Aerial Cargo Delivery Van for High Value Goods - Baseline Report Version 2. Delft University of Technology, Delft, Netherlands, 2021. Unpublished.

[3] World Bank, "Air freight: A market study with implications for landlocked countries," tech. rep., The World Bank Group, 2009.

[4] G. Tzimourtos, "Air freight transport: A strategic modelling approach on a global scale," master thesis, TU Delft, jun 2015.

[5] European Union Aviation Safety Agency, "Certification specifications and acceptable means of compliance for large aeroplanes cs-25," Tech. Rep. Amendment 26, EASA, 2020.

[6] DSE Group 21, Unmanned Aerial Cargo Delivery Van for High Value Goods - Midterm Report Version 2. Delft University of Technology, Delft, Netherlands, 2021. Unpublished.

[7] E. Torenbeek, Synthesis of Subsonic Airplane Design. Martinus Nijhof Publishers, P.O.B.566, 2501 CN The Hague, Holland & Delft University Press, Mijnbouwplein 11, 2628 RT Delft, Holland: Martinus Nijhoff & Delft university press, 1982.

[8] B. Z. R. Vos and M. Hoogreef, "Aerospace design and systems engineering elements i - ae1222-ii," 2021.

[9] D. Raymer, Aircraft Design: A conceptual approach. 370 L'Enfant Promenade, S.W., Washington, D.C. 20024: American Institute of Aeronautics and Astronautics, Inc., 2nd ed., 1992.

[10] F. Oliviero, "AE2111-II Aerospace Design and Systems Engineering Elements II; Aircraft aerodynamic analysis: Fundamentals," 2021.

[11] F. Oliviero, "AE2111-II Aerospace Design and Systems Engineering Elements II; Aircraft aerodynamic analysis: Lift & Drag Estimation," 2021.

[12] R. Finck, "Usaf (united states air force) stability and control datcom (data compendium)," tech. rep., MCDONNELL AIRCRAFT CO ST LOUIS MO, 1978.

[13] R. Faye, R. Laprete, and M. Winter, "Blended winglets for improved airplane performance," Aeromagazine Boeing, vol. 17, 2002.

[14] D. Howe and G. Rorie, Aircraft conceptual design synthesis. Professional Engineering Publishing London, UK, 2000.

[15] T. Ahmed and T. Amin, "Computational study of flow around a naca 0012 wing flapped at different flap angles with varying mach numbers," Global Journal of Researches in Engineering General Engineering, vol. 13, pp. 1–15, 2013.

[16] F. Oliviero, "Aerospace design and systems engineering elements ii - ae2111-ii," 2021.

[17] P. Roling, "Flight & orbital mechanics - ae2230-i," 2020.

[18] R. Martinez-Val, E. Perez, and J. Palacin, "Historical perspective of air transport productivity and efficiency," 43rd AIAA Aerospace Sciences Meeting and Exhibit, 2005.

[19] J. Melkert, "Propulsion and power ae2203:gas turbines.," 2019.

[20] P. Rompokos, S. Kissoon, I. Roumeliotis, D. Nalianda, T. Nikolaidis, and A. Rolt, "Liquefied natural gas for civil aviation," Energies, 2020.

[21] G. L. M. Vonhoff, "Conceptual design of hydrogen fuel cell aircraft," Student Thesis TU Delft, 2021.

[22] D. K. Bryngelsson and K. Lindgren, "Why large-scale bioenergy production on marginal land is unfeasible: A conceptual partial equilibrium analysis," Energy Policy, 2013.

[23] R. A. Lee and J.-M. Lavoie, "From first- to third-generation biofuels: Challenges of producing a commodity from a biomass of increasing complexity," Animal Frontiers, 2013.

[24] A. Meurer and J. Kern, "Fischer–tropsch synthesis as the key for decentralized sustainable kerosene production," Energies, 2021.

[25] HanaâEr-rbib, C. Bouallou, and F. Werkoff, "Production of synthetic gasoline and diesel fuel from dry reforming of methane," Energy Procedia, 2012.

[26] F. T. Jane, Janes All the World's Aircraft. Janes Group UK, 2012.

[27] E. Roux, Turbofan and Turbojet Engines. Elodie Roux, 2007.

[28] B. Warwick, I. Y. Kim, and C. Mechefske, "Substructuring verification of a rear fuselage mounted twin-engine aircraft," Aerospace science and technology, vol. 93, 2019.

[29] A. Murphy, C. Lynch, M. Price, and A. Gibson, "The computational post buckling analysis of fuselage stiffened panels loaded in compression," Thin-Walled Structures, vol. 42, no. 10, pp. 1445–1464, 2004.

[30] J. T. Eylem Asmatulu, Michael Overcash, "Recycling of aircraft: State of the art in 2011," Journal of Industrial Engineering, vol. 2013, p. 8, 2013.

[31] J. Ribeiro and J. Gomes, "Proposed framework for end-of-life aircraft recycling," Procedia CIRP, vol. 26, pp. 311–316, 12 2015.

[32] O. Takeda and T. H. Okabe, "Current status of titanium recycling and related technologies," JOM, vol. 71, 2019.

[33] B. Björkman and C. Samuelsson, "Chapter 6 - recycling of steel," in Handbook of Recycling (E. Worrell and M. A. Reuter, eds.), pp. 65–83, Boston: Elsevier, 2014.

[34] D. Radford and E. Teghtsoonian, "Fracture toughness of carbon fibre/epoxy composites," in TEQC83 (T. Feest, ed.), pp. 27–35, Butterworth-Heinemann,

1983.

[35] S. A. Resetar, J. C. Rogers, and R. W. Hess, "Advanced airframe structural materials: A primer and cost estimating methodology," tech. rep., RAND CORP SANTA MONICA CA, 1991.

[36] A. P. Mouritz, "3 - materials and material requirements for aerospace structures and engines," in Introduction to Aerospace Materials, pp. 39–56, Woodhead Publishing, 2012.

[37] M. F. Ashby, "Appendix b - useful solutions for standard problems," in Materials Selection in Mechanical Design (Fourth Edition), pp. 525–558, Oxford: Butterworth-Heinemann, fourth edition ed., 2011.

[38] M. H. Sadraey, Aircraft Sesign: A Systems Engineering Approach. Daniel Webster College, New Hampshire, USA: Wiley, 1st ed., 2012.

[39] B. Z. R. Vos and J. Melkert, "Aerospace design and systems engineering elements i - landing gear and empennage design," 2019.

[40] J. Roskam, Airplane Design - Part II: Preliminary configuration design and integration of the propulsion system. DARcorporation, 1985.

[41] F. Oliviero, "AE3211-I Systems Engineering and Aerospace Design; Design for Lateral-directional aspects, Design for ground operations," 2021.

[42] F. Oliviero, "AE2111-II Aerospace Design and Systems Engineering Elements II; Aircraft aerodynamic analysis: Mobile surfaces of the wing," 2021.

[43] B. Z. R. Vos and J. Melkert, "Aerospace design and systems engineering elements i - wing positioning, landing gear and empennage design," 2019.

[44] P. Sforza, Commercial Airplane Design Principles. Butterworth-Heinemann, 2014.

[45] J. Gundlach, Designing unmanned aircraft systems: a comprehensive approach. American Institute of Aeronautics and Astronautics, 2012.

[46] M. Zolanvari, R. Jain, and T. Salman, "Potential data link candidates for civilian unmanned aircraft systems: A survey," IEEE Communications Surveys & Tutorials, vol. 22, pp. 292 – 319, 2019.

[47] K. P. Valavanis and G. J. Vachtsevanos, Handbook of unmanned aerial vehicles, vol. 1. Springer, 2015.

[48] J. Emond, F. Mercier, and M. Nunes, "In-flight temperature conditions in the hold of a widebody aircraft," Proc. of 20th IIR/IIF. Sydney, Australia, pp. 19–24, 1999.

[49] M. J. Izadi and M. Dawoodian, "Cfd analysis of drag coefficient of a parachute in a steady and turbulent condition in various reynolds numbers," in Fluids Engineering Division Summer Meeting, vol. 43727, pp. 2285–2293, 2009.

[50] S. Singh, J. Singh, J. Stallings, G. Burgess, and K. Saha, "Measurement and analysis of temperature and pressure in high altitude air shipments," Packaging Technology and science, vol. 23, pp. 35–46, 2010.

[51] G. Baxter and K. Kourousis, "Temperature controlled aircraft unit load devices: The technological response to growing global air cargo cool chain requirements," Journal of technology management & innovation, vol. 10, no. 1, pp. 157–172, 2015.

[52] S. Wang, M. Tomovic, and H. Liu, Commercial Aircraft Hydraulic Systems: Shanghai Jiao Tong University Press Aerospace Series. Academic Press, 2015.

[53] P. Roling, "Airport planning, design and operations - ae3502-14," 2020.

[54] D. Simons and M. Snellen, "Course ae4431 aircraft noise and emission part a: Introduction to general acoustics and aircraft noise," 2020.

[55] Meyer-Bisch, Christian, "Les chiffres du bruit," Med Sci (Paris), vol. 21, pp. 546–550, may 2005.

[56] P. A. Claisse, "Chapter 32 - alloys and nonferrous metals," in Civil Engineering Materials (P. A. Claisse, ed.), pp. 361–368, Boston: Butterworth-Heinemann, 2016.

[57] J. Sinke, "Production of aerospace systems (ae3211-ii) - reader," 2019.

[58] A.Bombelli, "Air transportation - ae3501-19," 2020.

[59] J.-C. Mare, Aerospace Actuators 1: Needs, Reliability and Hydraulic Power Solutions. Iste Ltd And John Wiley & Sons Inc, 05 2016.

[60] I. Moir, A. Seabridge, and M. Jukes, Civil Avionics Systems. John Wiley & Sons Inc, 2013.

[61] H. A. Kinnison and T. Siddiqui, Aviation Maintenance Management. The McGraw-Hill Companies, Inc, 2 ed., 2013.

[62] R. W. Hess and H. Romanoff, "Aircraft airframe cost estimating relationships: All mission types," tech. rep., RAND CORP SANTA MONICA CA, 1987.

[63] R. Ali and O. Al-Shamma, "A comparative study of cost estimation models used for preliminary aircraft design," Global Journal of Research In Engineering, 2014.

[64] E. Thomas, "Ata direct operating cost formula for transport aircraft," tech. rep., SAE Technical Paper, 1966.

[65] R. H. Liebeck, D. A. Andrastek, J. Chau, R. Girvin, R. Lyon, B. K. Rawdon, P. W. Scott, and R. A. Wright, "Advanced subsonic airplane design and economic studies," 1995.

[66] A. of European Airlines, Short medium range aircraft: AEA requirements. 1989.

[67] J. P. Johnson and E. M. Gaier, "Air cargo operations cost database," tech. rep., 1998.

[68] DSE Group 21, Unmanned Aerial Cargo Delivery Van for High Value Goods - Project Plan. Delft University of Technology, Delft, Netherlands, 2021. Unpublished.

[69] "nacelle assembly and mounting structures for a turbofan jet propulsion engine," Aug 1977.

[70] W. Beelaerts, R. Huijser, R. Stahls, and S. Santema., "Future airport turnaround ground handling processes: How to reduce the turn around time of aircraft at the airport," Master's thesis, TU Delft, 2008.

[71] Clean Sky 2 and FCH 2 JU, "Hydrogen-powered aviation. a fact-based study of hydrogen technology, economics, and climate impact by 2050," 2020.